DASH

Distributed Asteroid Surveying Herd

Final Report

AE3200: Design Synthesis

Group 23

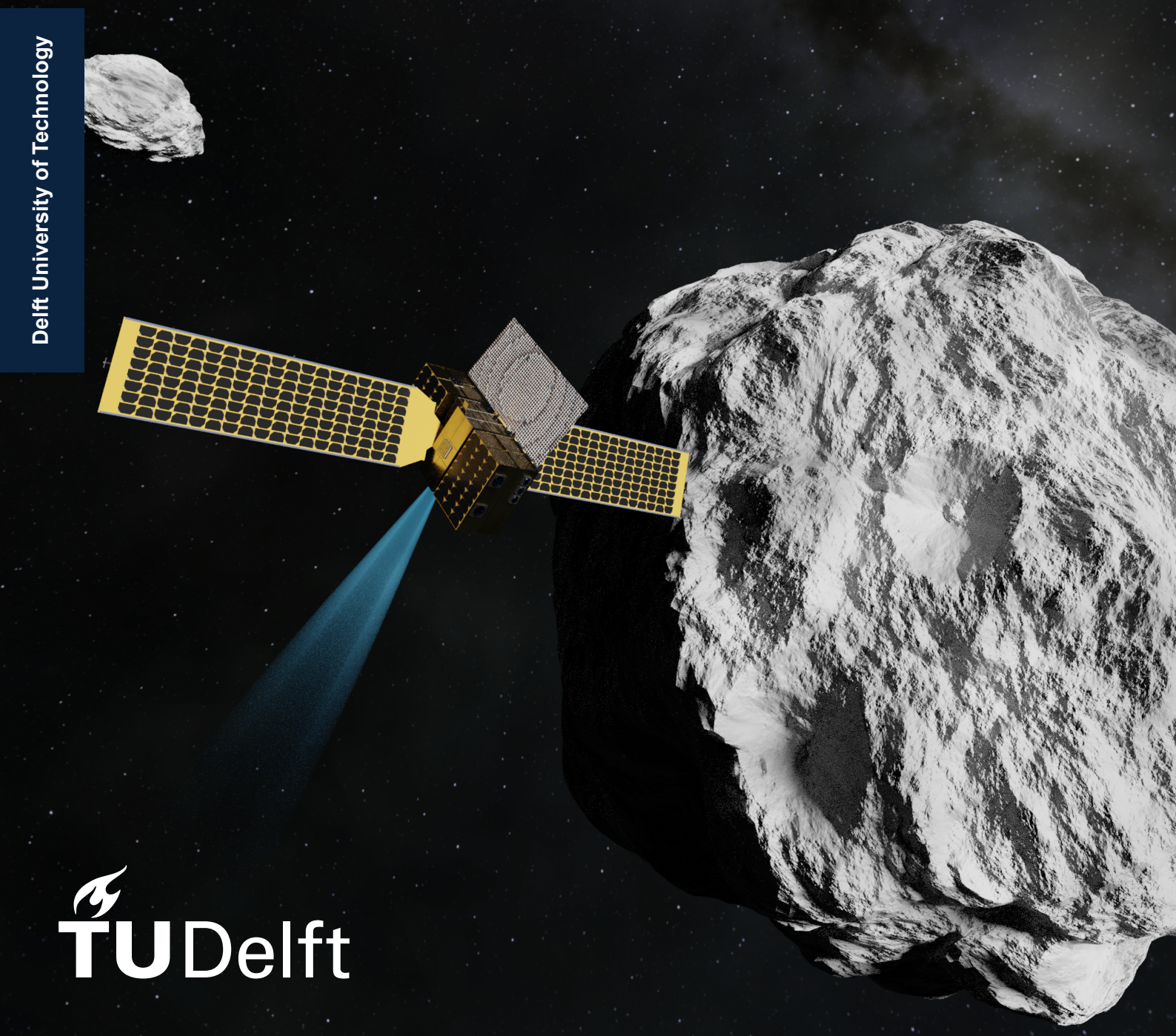

Delft University of Technology

TU Delft

This page is intentionally left blank

DASH

Distributed Asteroid Surveying Herd

Final Report

by

Group 23

Alessandro Battegazzore	4994221
Juan Sebastian Calberto Muñoz	5030730
Siddharth Dixit	5028205
Tamim Doozandeh	5029236
Timo Kramer	5038944
Kyoungeun Lee	4843320
Jeremy Lems	4826493
Anibal Luciano Pastinante	5010276
João Rodríguez	4993578
Simon Van Hulle	4998006

Version 1.1

Submitted: June 21, 2022

Tutor:	Dr. ir. Prem Sundaramoorthy
Industry Partner:	ir. Piotr Perczynski
Coaches:	ir. Mahdi Noorafza & ir. Stefano Casini

Project Duration:	April, 2022 - June, 2022
Faculty:	Faculty of Aerospace Engineering, Delft

TU Delft

Acknowledgement

We would like to express our sincere gratitude to our tutor and coaches, Prem Sundaramoorthy, Stefano Casini, and Mahdi Noorafza, without whose guidance and support this exercise would not have been possible. For his invaluable expertise and feedback, we are also very grateful to our industry partner, Piotr Perczynski. Many thanks to our Teaching Assistant, Katharina-Inés Janisch, for all her feedback on systems engineering and insights from having recently done the DSE as well.

In addition, we want to thank the professionals in the aerospace industry who have contributed to the design:

- ISISPACE's Juan Miguel Peiro Garcia and Ralph Slootweg for their technical expertise and consultancy related to their deployers
- Aurora Propulsion Technologies' Timo Mustonen and Perttu Yli-Opas for their enthusiastic help and technical data regarding their cold gas propulsion unit
- DAWN Aerospace's Rob Hermsen and Fabio Kerstens for their helpful insights and advice
- ESA's Dario Izzo for his advice on the use of trajectory propagation software
- ExoTerra's Michael Vanwoerkom and Alex Seidcheck for the information they provided on the Courier
- Momentus' Alex Drossler and Negar Feher for the information on the performance of the Vigoride

We would also like to acknowledge all the companies who have provided us with technical data on their products over email. These are AAC Clydespace, Dragonfly Aerospace, EBAD, Epson Electronics, GomSpace, Hexagon, Inertial Labs, Jenoptik, Memsense, RFA, Simera Sense, Space Micro and Terma.

Finally, we would be remiss in not mentioning the OSCC, without whom there would have been no DSE, and the OSSAs, who have helped organise the DSE.

Contents

Nomenclature

Acronyms

△-DOR	Delta-Differential One-way Ranging
ADCS	Attitude Determination and Control Subsystem
AGE	Aerospace Ground Equipment
AIM	Asteroid Impact Mission
AOCS	Attitude and Orbit Control Systems
AU	Astronomical Unit
BC	Boundary Condition
BER	Bit-Error-Rate
CAD	Computer Aided Design
CDHS	Command and Data Handling Subsystem
CG	Centre of Gravity
CMG	Control Moment Gyroscope
COPV	Composite Overwrapped Pressure Vessel
COTS	Commercial Off-The-Shelf
DART	Double Asteroid Redirection Test
DASH	Distributed Asteroid Surveying Herd
DOT	Distributed Observation Tool
DSN	Deep Space Network
EBAD	Ensign-Bickford Aerospace & Defense
ECSS	The European Cooperation for Space Standardization
EOL	End Of Life
EPS	Electrical Power Subsystem
ERM	Eejctor Release Mechanism
GSD	Ground Sample Distance
GSE	Ground Support Equipment
HDRM	Hold Down & Release Mechanisms
HWBD	Hardware Block Diagram
HY2	Hayabusa2
ISL	Inter-Satellite Link
JPL	Jet Propulsion Laboratory
LDC	The Large Diameter Centrifuge
LiAISON	Linked, Autonomous, Interplanetary Satellite Orbit Navigation
LOS	Line-Of-Sight
LSIB	Life Support Interface Board
M-ARGO	Miniaturised-Asteroid Remote Geophysical Observer
MAC	Mass Acceleration Curve
NDT	Nondestructive Testing
NEA	Non-Explosive Actuators
PSE	Peculiar Support Equipment
RCS	Reaction Control System
RIRO	Rubbish In, Rubbish Out
RMSE	Root Mean Squared Error
S/C	Spacecraft
SDG	Sustainable Development Goals
SMAD	Space Mission Analysis and Design
SNR	Signal-To-Noise Ratio
SPENVIS	Space Environment Information System
SWBD	Software Block Diagram
TCS	Thermal Control System
TRAM	Technical Risk Assessment Methodology
TRL	Technology Readiness Level
TSP	Tracking Solar Panels
TT&C	Telemetry, Tracking & Command
UKF	Unscented Kalman Filter

Executive Overview

The economic and holistic incentives of asteroid exploration have sparked an increased interest within the space industry. Missions like Hera and M-ARGO have taken steps towards said exploration, each with its own concept, but both using CubeSats due to the versatility they add. Thus, an interesting question arises on whether adopting a distributed, deep space system approach will reduce the costs and increase the versatility of the mission. To answer this query, the DASH mission takes Hera's goals as its own to propose an innovative distributed framework that can match current asteroid exploration missions at significantly lower cost. As a result, this report deals with the design of the system and subsystem elements of the DASH mission, short for Distributed Asteroid Surveying Herd. Consequently, it is fitting to first analyse the current state of the market and then proceed with the mission-dependent elements.

Market Analysis

The global space industry market is young and growing, with a projected market cap of 630 B USD within the next decade. The rapid growth of the space is greatly attributed to the seemingly infinite commercial applications of space. In the last few decades, launch costs have become significantly lower in comparison to the early days of space exploration. This trend can be expected in the asteroid market, which the DASH mission is aiming to expand upon. With the Hera mission planned to launch soon to study the impact of DART, DASH will be using the Hera mission as a baseline from which to build up upon. DASH's architecture allows for it to accompany Hera or be launched at a later date to assist Hera in its objectives. This has the potential of increasing the amount of data collected at a relatively smaller cost in comparison to purchasing an entire dedicated mission. With such a modular design, DASH is able to comply with many missions of varying scales, allowing for entities with less funding to still be able to explore deep space. While futuristic applications such as asteroid mining and planet protection are far and beyond, the potential of asteroids is seemingly endless. DASH is ultimately providing a product and a service, facilitating space exploration, in anticipation of the future of the asteroid exploration market.

Mission Overview

The DASH mission to explore the asteroid Didymos is subdivided into several mission phases, each describing different segments of the overall operations. These phases and the associated timeline is presented below in Table 1.

Table 1: Mission phases, their duration and start time with respect to the mission clock

Mission Phase	Expected time frame	Mission clock [days]
Launch	2 hours	- 32.1
GTO Loitering	1 - 4 weeks	- 32
Ejection	4 days	- 4
Commissioning	1 day	+ 0
GTO to Didymos	650 - 750 days	+ 751
Arrival at Didymos	1 - 2 weeks	+ 765
Pre-Operational	2 - 3 days	+ 768
Scientific Phase	6 months	+ 954
End-of-life Phase	1 week	+ 961

The DASH mission consists of three groups, called TRIADs, each made up of three physically interconnected CubeSats. Each TRIAD acts as a single spacecraft for the initial mission phases until it arrives at the target. Each TRIAD is composed of a SHEPHERD, providing the transfer propulsion and serving as a long range communication node, and two DOTs, focused on maximizing the payload fraction available to the customer.

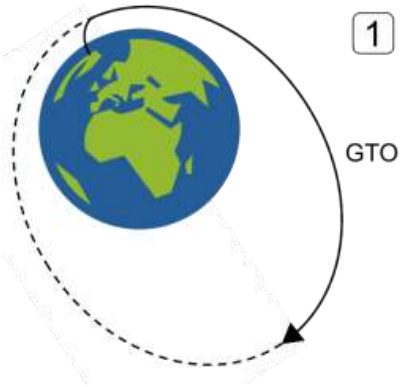

Beginning with assembly, SHEPHERDs and DOTs are assembled into TRIADS and installed onto the high energy Photon kick stage, and subsequently, onto the RFA One launch vehicle. The DASH mission will perform three launches, each delivering one TRIAD and its kick-stage to a highly elliptical Geostationary Transfer Orbit (GTO). This first phase **(1)** can be seen in the figure on the left.

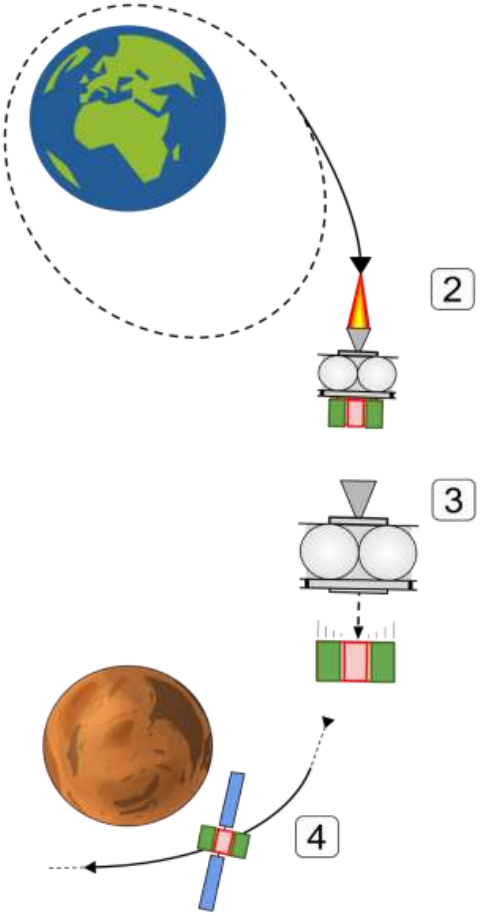

After a loitering period in GTO, the Photon kick stage begins the Earth escape burn to send the TRIAD it's carrying into an escape trajectory **(2)**. The TRIAD is released from its containerised deployer when the desired trajectory is achieved **(3)**. From there, SHEPHERD, responsible for propulsion and telecommuni-cations, deploys its antennae and solar panels. Electric-ion propulsion aboard SHEPHERD provides the necessary velocity change during the transfer to the target asteroid. DASH's trajectory will exploit a Mars gravity assist to match the asteroid body's orbital inclination during the 900-day transfer phase to the target **(4)**.

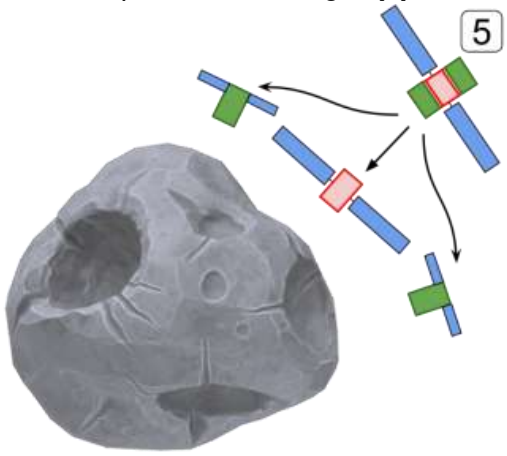

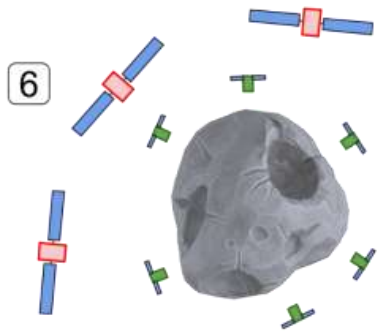

As each TRIAD arrives to Didymos, the two dots separate from the central SHEPHERD, leaving three free-flying CubeSats around the target asteroid **(5)**. When separated, both DOTs will extend their own low-power antennas and start distributing around the target. Once all DASH mission elements arrive at Didymos the scientific phase of the mission com-mences with SHEPHERDs providing a deep-space capable communication network to the distributed sensor array the DOTs compose **(6)**.

Design Overview

DASH Design Factsheet

Astrodynamics and Propulsion

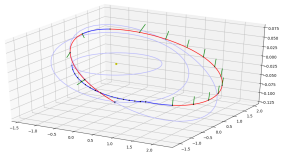

- Launch in October 2024 on RFA One rocket
- 894 day transfer with Mars gravity assist
- Nominal operations from January 2027 onwards
- Transfer thrust by ion engine on SHEPHERD (M-ARGO engine)
- 1.95 kg of compressed Xenon fuel
- Orbit maintenance at asteroid is provided by the ADCS thrusters on every CubeSat

Electrical Power System

- $2 \times 0.44\,\mathrm{m}^2$ rotating solar panel on SHEPHERD
- $2 \times 0.20\,\mathrm{m}^2$ rotating solar panel on each DOT
- SHEPHERD uses ExoTerra EPS
- Separation connector for power and data transfer during transfer
- Battery capacity of 92.2 W h and 46.1 W h for SHEPHERD and DOTs, respectively

Structures

- SHEPHERD structure provided by ExoTerra, including deployable solar panels.
- DOT structure off-the-shelf from ISISPACE
- ISISPACE custom containerised deployer
- Novel separation mechanism to hold and release DOTs from SHEPHERD

Thermal Control

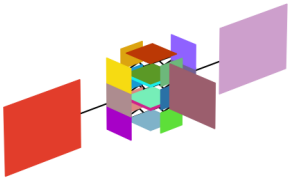

- No active systems required
- Thermal straps for conductive link between engine and walls.
- Passive thermal louvers for autonomous adjustment of effective surface properties
- Internal temperature range between −20 °C and 50 °C

CDHS and telecommunication

- COTS command and data handling system
- physical power and data link between CubeSats during transfer
- Inter-satellite link between the satellites at asteroid
- High gain antenna on SHEPHERD for earth link
- Downlink data rate of 1000 bit s^{-1}

ADCS and Navigation

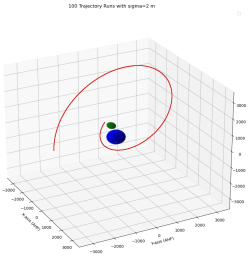

- Use of autonomous navigation through optical and radiometric measurements, with verification through ground station tracking.
- Unscented Kalman Filter for multi-spacecraft data fusion strategy.
- Model Predictive Control paired with Sequential Convex Programming to provide for the guidance and control laws for collision avoidance and reconfiguration.

Subsystems Integration

The internal layout of each CubeSats is set up by allocating a space on the bus for each subsystem and its components. Once the architecture is known the centre of gravity is estimated and a detailed mass budget presented.

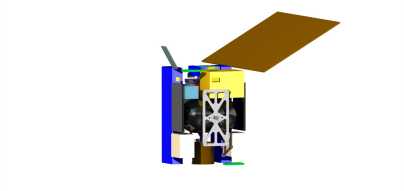

Figure 1: SHEPHERD Internal view of components

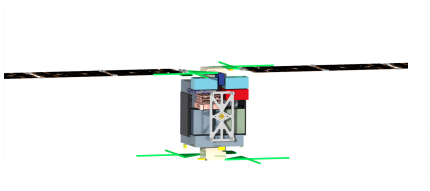

Figure 2: DOTs Internal view of components

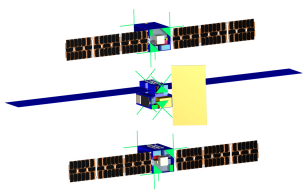

Figure 3: TRIAD Separation configuration

Performance Analysis

Meeting all mission requirements, the comparative performance of the system is evaluated primarily through the cost budget, as this is the main determinant of the performance of the distributed system in comparison to other missions. Additionally, the mass, volume and power budgets are also considered within the performance to characterise the system even further. A summary of these budgets is shown in Table 3. More detail on the margins is provided within chapter 18.

	Mass [kg**]**	**Volume [**U**]**	**Cost [**MEUR**]**
DOT	8.8	12	0.674
SHEPHERD	18.9	12	2.57
TRIAD	36.5	36	24.4

Table 3: Budget Summary

Design & Development

Having defined all subsystems, structures and components to be used in the entirety of the DASH mission, it is imperative to define the complete life-cycle of the mission, including the design, manufacture and testing of each element in the mission, where requirements are verified and validated. Furthermore, sustainable approaches can also be defined for every phase of the mission, which must be adhered to in order to reduce the negative impact of the mission operation. These approaches are derived from the United Nations' Sustainable Development Goals, and from ISO requirements on space debris.

As for the design and development approach for the mission, a modified spiral model for systems engineering was adopted with concurrent engineering for the development of DOTs, SHEPHERDs and TRIADs. This essentially means that DOTs and SHEPHERDs are tested continuously up to a subsystem level during the preliminary design phase and at a system level during the detailed design phase. Thus, the knowledge gained during the testing of each of the components, modules, subsystems or CubeSats can be used to improve the design of the overall system for the next iterations. Additionally, the models (whether preliminary or detailed) for the CubeSats can be tested for integration within the TRIAD development. This process is iterated until the design converges to produce the TRIAD flight model.

1 Introduction

In the current day and age, the market for space exploration is at an all-time high interest. The number of startups in the aerospace industry has drastically increased, especially in the CubeSat and SmallSat sector. This brings an exponential growth to space technology and a reduction in cost as a result of the heavy competition. On top of this, many universities around the world are starting to do more research into the possibilities of these technologies and are striving to deliver a new and innovative design. This fact relates to the goal of the Distributed Asteroid Surveying Herd (DASH) mission, which is to show the feasibility of a distributed CubeSat system for deep space asteroid exploration. Next to this, the group also is aiming to show that the costs of current Small Sattelite missions, for instance the Hera[1] can be optimised further with an alternative mission concept.

This report outlines the systematic process of designing the DASH mission from the high-level goals above. The subsystem components were chosen based on calculations, simulation models, trade-offs, and other more methods. Afterwards, the final design was visualised by appending all the subsystems. Lastly, the mission concepts were proven to be feasible as well.

The structure of the report is as following. Firstly, the current space market will be analysed in chapter 2. Next, the concept of operations during the mission phases will be elaborated in chapter 3. Following the concept of operations is the functional analysis, which includes the functional flow diagram and the functional breakdown structure, which will be done in chapter 4. The sustainable development strategy will be discussed in chapter 5. Next, the risk analysis has to be done. In chapter 6, all the risks are identified, assessed, and after on the mitigating strategies and contingency plans are made for each risk. After this, the trajectory optimisation is made in chapter 7, where all the astrodynamics calculations will be explained. After these chapters, the subsystem design will be explained in detail. Firstly, the propulsion subsystem, the EPS, and the structure of the CubeSats will be elaborated upon in chapter 8, chapter 9, and chapter 10, respectively. The thermal control, the command and data handling subsystem, the TT&C system, the ADCS, the navigation subsystem, of the S/C will be discussed in chapter 11, chapter 12, chapter 13, chapter 14, and chapter 15, respectively. Lastly, regarding the different systems, the payload will be discussed in chapter 16. After all these subsystems have been designed, their integration is discussed in chapter 17. This is followed by the performance analysis in chapter 18, where the budget breakdown and cost breakdown will be established. In chapter 19 the requirement verification will be done, and all the verification and validation methods will be discussed. Finally, the design and development logic will be done in chapter 20, which will also include the project Gantt chart.

There is a lot of future potential in the space industry. For our mission, different stakeholders can be identified. This includes, among others, the scientific community, space agencies, aerospace companies, educational institutes and governments. All the stakeholders have been more thoroughly analysed in the Baseline Report [4].

1.1. Mission Overview and Requirement

The mission overview can start with deriving the MNS (Mission Need Statement) and POS (Project Objective Statement) of the whole project. These define the need to be satisfied by the DASH and the aim of the project in total.

Mission Need Statement

Given the scientific and societal significance of asteroid research, improving mission execution needs an increase in S/C versatility and scalability while simultaneously delivering cost savings.

[1] URL https://www.Heramission.space/ [cited 10 June 2022]

Project Objective Statement

DSE team 23, composed by 10 students, shall design in 10 weeks a price competitive, distributed space system with commercial off-the-shelf components for deep space investigation of asteroids within a budget of € 100M.

Based on these two statements, it can be determined that the project gives the opportunity to prove that distributed space systems can be applied to CubeSats for deep space missions, which is not a conventional option for previous missions. The project also aims at showing the versatility and scalability of the S/C in the sense of being able to be used for other applications as well as including asteroid exploration. Furthermore, it also aims to demonstrate that tremendous reduction in cost of space missions is possible due to many factors including CubeSat standardisation, new technology and many other factors. The user requirements, that were used as the basis for the design of the mission, are given in Table 1.1.

Table 1.1: User requirements

Identifier	Description
R-USR-01	The mission shall perform payload operations at the asteroid 65803 Didymos.
R-USR-01	The payload operations shall be performed at a distance of less than 30 km from the asteroid.
R-USR-03	The payload operations shall be performed for at least six months
R-USR-04	The mission shall accommodate at least 9 individual payloads.
R-USR-05	The mission shall accommodate the individual payloads with a form factor of at least 2U.
R-USR-06	The mission shall downlink to Earth at least 130 Gb of payload data.
R-USR-07	The mission shall achieve the performance objectives with at least 70% probability of success.
R-USR-08	The mission shall comply with “Space debris mitigation requirements ISO 24113:2019”.
R-USR-09	The S/C shall adhere to the CubeSat standard.
R-USR-10	The individual S/C volume shall not exceed 16U.
R-USR-11	The mission shall begin payload operations no later than December 2026.
R-USR-12	The total cost of the mission, including launch and operations, shall not exceed 100 million EUR.
R-USR-13	The mission shall consider Deep Space Network for communications.

One of the main drivers for the design of the project is what constitutes the success of the mission. The success will be determined based on the following parameters; demonstrating the distributed space system, reaching the target asteroid, delivering the payload to the target objective, reaching the target within a scheduled time frame, and performing valuable scientific measurements. Table 1.2 shows the criteria in order to consider success of the mission in the big scope.

Table 1.2: DASH mission success criteria

ID	Criterion
DASH-SCS.01	Successfully demonstrate deep space autonomous navigation with at least 3 CubeSats, independently of a mothership or any other parent-children equivalent systems
DASH-SCS.02	Successfully deliver at least 3 CubeSats to the target asteroid
DASH-SCS.03	Successfully deliver at least 3 operational payloads to the target asteroid
DASH-SCS.04	Perform relevant scientific measurements and collect data
DASH-SCS.05	Successfully reach the target asteroid within the time frame allocated

2 Market Analysis

More space agencies and private sector companies, for instance NASA, ESA, and SpaceX are planning large projects such as lunar bases and planetary explorations on earth neighbouring celestial bodies. While the size of asteroids is smaller in comparison to planets like Earth and Mars, there is still a variety of commercial and scientific opportunities to be gained from studying them further. Future uses such as asteroid mining for precious metals, asteroid depots and bases, and trajectory alterations for Earth-threatening asteroids are just a few of which apply to today's society. Many private companies and projects have realised this and are planning launches with large space agencies, such as the Hera mission. DASH aims to provide a lower cost and more versatile platform to fulfil those very same scientific goals and commercial objectives. This drives the need for a thorough market analysis to ensure the right product or service is designed. It aims to describe how the mission as a whole could inspire and fit within the current and future market.

This chapter focuses on several aspects of the market analysis. As stakeholders were mentioned in the DASH baseline report [4], they will not be presented in this chapter. Starting with Section 2.1, the future market projection are described. Section 2.2 discusses DASH's marketing aspects and compares DASH with Hera as the baseline. Finally, Section 2.3 deals with the commercial and scientific applications of the DASH mission from a commercialisation point of view.

2.1. Market Trends

Over the last decades, the cost to launch hardware to orbit has decreased drastically. Figure 2.1 shows the cost evolution of launching a kilogram of payload into Low Earth Orbit and projects this trend towards the future. It is worth noting that the vertical axis has a logarithmic scale. Over the last forty years, the price has been reduced by two orders of magnitude, and it is expected to keep dropping.

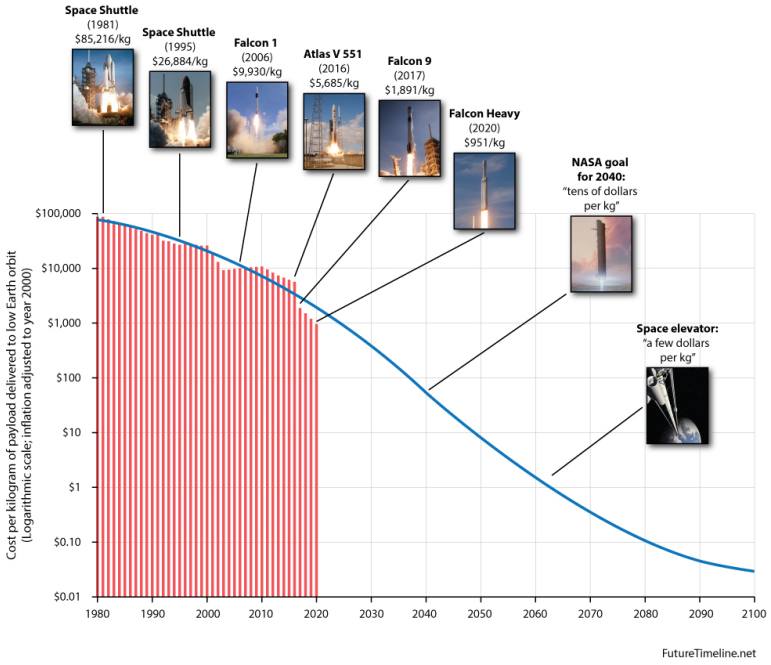

Figure 2.1: The trend of decreasing launch cost per kilogram and the future projection for 2023 and beyond[1]

[1] URL https://www.futuretimeline.net/data-trends/6.htm [cited 26 April 2022]

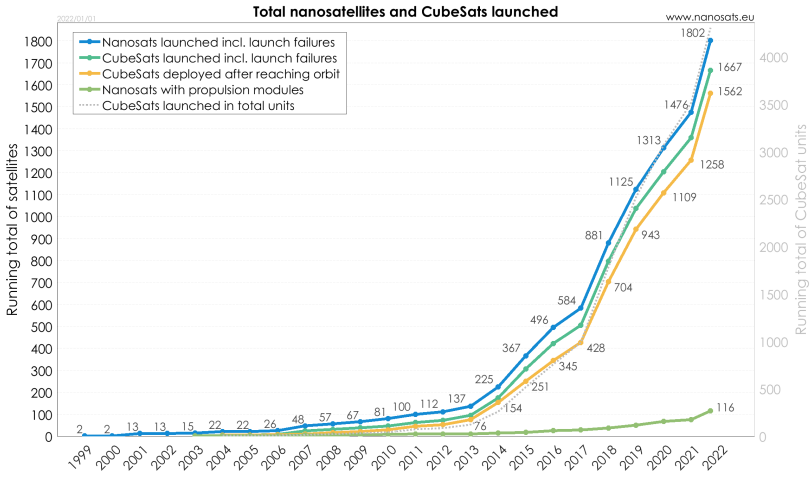

Figure 2.2: Accumulated nano-satellite and CubeSat launches over time

Another relevant trend to consider is the cumulative number of nano-satellites and CubeSats launched over the years starting from 1999 to 2022 for various categories (Figure 2.2 [2]). Note that these trends are also increasing exponentially, which indicates consistent growth of the industry and the market.

2.2. Mission Market Aspirations

The scientific community strives to be on the cutting edge of technological and research advancements, and as of late, they have set their sights on asteroids. The growing demand for asteroid resources mining and exploration has resulted in numerous missions planned to launch between 2024 and 2026. The satellites designed for these missions are planned to be mostly CubeSats, which better suit investigations of asteroids with significantly smaller size compared to planets or different celestial bodies in space. Although packed in a small form factor when compared to preceding spacecrafts, these new-space missions aim to generate similar amount of scientific data through more cost-effective and versatile architectures. A similar approach, in addition to a distributed mission architecture, is what will allow DASH to accomplish its ambitious scientific objectives. These small-form factor missions allow for comparable performance to much more expensive traditional spacecrafts at a fraction of the cost. With DASH, low cost, high versatility, and distributed systems are to be provided for use on a wide range of asteroid categories. By designing a mission able to operate in any asteroid environment, the cost of adapting the spacecraft to a specific asteroid and payload is significantly reduced, making DASH more flexible and versatile independently of the desired scientific target.

2.2.1. Hera Baseline

The Hera mission is seen to be the mission with the most overlap and alignment with DASH's goals and objectives. As such, the market analysis research performed will be aimed at competing directly with Hera in terms of cost and potential scientific gains. An outline for the desired research outcomes is given in Table 2.1.

[2] URL https://www.nanosats.eu/img/fig/Nanosats_total_2022-01-01_large.png [cited 26 April 2022]

Table 2.1: Desired research outcomes in comparison to the Hera program obtained from DASH goals and methodology

Hera mission	Desired outcomes from research
Cost of 129.4 million EUR	Cost reduction to 94.5 million EUR including launch
Mothership concept with two spacecrafts (Milani and Juventas)	Distributed system with independent spacecrafts
Asteroid properties and dynamics characterisation	Comparable performance in smaller form factor

As can be seen in Table 2.1, the desired outcomes can be categorised into 3 main categories: a reduction in cost, use of distributed systems, and a smaller form factor. Decreasing spacecraft cost and form factor while achieving performance comparable to that of a larger spacecraft significantly increases the scientific capabilities of the mission. This, in combination with a distributed system capable of performing observation with higher spatial and/or temporal resolution, means that asteroid exploration becomes more accessible and productive to those without government sized budgets. The scientific community stands to gain greatly, paving the way for future asteroid exploration without needing to pay extraordinary sums of money upfront.

DASH's proof of concept for the applicability of distributed space systems can allow for increased redundancy, extendability, and replaceability of deep space related missions. As one of the main objectives of this research is to provide low-cost distributed systems, the low-cost and distributed aspect of the mission allows for high versatility. A distributed system allows for increased redundancy as there are many spacecraft working together, and in the case of failure, the remaining spacecrafts can adjust and prevent a single point of failure. This in combination with low-cost allows for more risky operations to be performed as the spacecrafts are easily replaceable for the cost. Such low-cost spacecrafts sent at once to perform a singular mission also means that parallel observation are a reality, providing more data points from different locations on the asteroid body with the same time stamp. The research can also show the possibility of extending mission duration by utilising the DASH distributed swarm for supporting larger missions already in deep space.

Due to the small form factor, the versatility of the spacecraft cannot be undermined. A smaller form factor can allow for piggyback swarms to accompany larger deep-space spacecrafts during launch. The piggyback swarm can perform risky manoeuvres and check areas well ahead of the main spacecraft to protect it from unsuspecting danger. The size of each individual spacecraft in the swarm also entails that it is more manoeuvrable at a lower propellant cost, making it able to go to places requiring a more tight fit.

While DASH will have a predetermined payload onboard the spacecraft to demonstrate its capabilities, the allocated payload space is essentially still interchangeable for other types of scientific equipment. Hereby allowing for individual specialisation of the spacecrafts in the distributed systems, each with specific tasks. Also entailing that one customer or organisation that has purchased the distributed system can perform a wide range of operations ranging from close to surface measurements to large scale asteroid scanning.

On top of the point of view mentioned above, there are also improvements in the perspective of production and funding possibilities. The DASH also proves that shorter time period and faster production and certification processes are available. Hence, shorter development and manufacturing cycles are available. The main reason is due to the fact that the size of an individual satellite has decreased significantly compared to the past missions. The reduction in size, shorter development time, and better certification also leads to the fact that the possibilities of getting financial sponsoring can grow as well. The reason is that the mission budgets demanded is going to decrease, as well as fewer compromises will be necessary. This will in hence lead to more opportunities for future asteroid exploration with fewer constraints compared to the past.

2.2.2. DASH contribution to Hera

The DASH architecture can also be used to assist and build up upon the Hera mission that is scheduled for 2024. This, however, does not entail that the architecture of DASH is only able to compliment Hera's architecture. The discussion here serves as a way to describe the potential and possibilities with respect to Hera but can also be applicable to future planned missions. As the DASH has a very versatile configuration, simply scaling it up or down to meet the requirements of a specific mission is possible with ease.

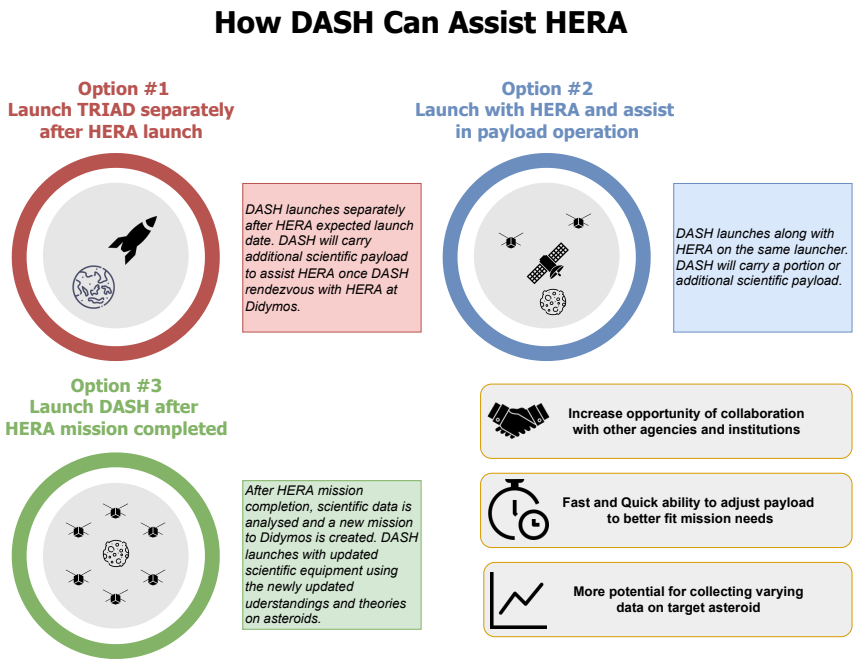

Figure 2.3: A few examples of ways that the DASH mission can be used to further Hera

From Figure 2.3, three options were provided for using the DASH architecture to supplement the Hera mission objectives. As Hera also makes use of an inter-satellite link, smooth integration with DASH is very feasible as all satellites will be able to communicate using pre-existing architecture. The main concession from these options are the timeframe in which the DASH is integrated into the mission. Both options 1 and 2 are able to support the Hera mission as it is still operational, with option 1 being able to take different payloads to Didymos at a later stage of the Hera mission. Option 1 can be seen as an advantage if there are some payload instruments which are experiencing some delays in development but the Hera launch cannot be delayed further, DASH will be able to allow for such flexibility in mission design. Option 3 is an entirely dedicated mission which takes the findings of Hera and uses them to refine upon the mission profile and adjust the payload to be carried for the new mission accordingly. As Hera aims to study the DART impact, findings may suggest new theories which may realise new instrumentations to be taken to Didymos to verify those theories and findings.

2.3. Return On Investment

While the cost of the mission is calculated based on launch and recurring costs, actual total mission costs presented to the client can be expected to be higher. This is to cover development costs and personnel costs to be accounted for potential expansion and under-developed technologies research and development to be done by DASH. With more capital and investments, the current architecture can be further improved upon, lowering DASH and client side costs while maintaining a high profit margin. In the space industry, technological advancements happen rapidly and as such high external investments will be needed to keep up with research and development of new and potentially novel technologies with higher future potential.

The applications of DASH can be categorised into two parts; commercial and scientific applications. The commercial applications deal with how the mission can be used for business opportunities and

profitability related aspects. The scientific side of the applications is more focused on providing valuable data to further the understanding and assumptions surrounding asteroid dynamics, composition, and properties. The potential to monetize such data will also be discussed.

2.3.1. Commercial Applications

The commercial opportunities within the DASH mission stem mainly from potential deep space technological advancements. Distributed space systems have long been in the works, and one stands to gain a lot from being the first to successfully implement it at an affordable cost. A private company with such technology can easily compete for government grants and funds to support further research on distributed systems development. The lower costs add an entire new level of accessibility to scientists, unprecedented in the old days of expensive space programs. As such, advertising the lower costs will bring in previously untested customers simply due to the more affordable costs in comparison to other deep space related missions.

As the asteroid exploration sector is considered niche in deep space exploration, more funds will have to be allocated for advertising and reaching to the interested parties. However due to the low cost of the DASH mission, these costs can be made up for in the initial stages of the business. Once the mission has been sufficiently pushed to the public and scientific community and orders have been lined up, advertising funds can then be diverted to research and development for the next iteration of the DASH mission. The importance of advertising in such a niche market cannot be emphasised enough as the survival of DASH as a whole will be placed on future interest and potential of asteroid exploration and market.

With reusable rockets beginning flight and increase privatisation of the space sector, increasing competition leads to lower costs to have an edge over the rest. The race to be the first on the moon may have ended, but the race to be the first to commercialise asteroid exploration is still underway. It must not be forgotten that cost is the main barrier to space exploration and not human curiosity, and providing more or even the same science for lower cost immediately places one well ahead of the pack.

2.3.2. Scientific Applications

There are still many theories and questions lingering about asteroids in the scientific community. Missions such as the DART and Hera have already been dispatched or are in the works with the objective of answering those questions. DASH also aims to provide the scientific community with tools and data to help answer some of these questions. Investigating the internal and external structure of asteroids to better understand asteroid composition and analysing what effects of asteroid orbits and dynamics are some of the main scientific goals to be covered.

The low-cost driver of the project allows for entities such as educational institutions to be more involved in asteroid exploration. Costs can be lowered even further for the individual entity by ride-sharing opportunities due to the versatility and small form factor of the spacecraft. As more launches are done to different location in the solar system, more data is obtained and thus more research can be done to investigate future asteroid uses and potential with regard to the human species.

3
Concept of Operations

The concept of operations is used to outline the general mission timeline expected for DASH. Here it is given from DASH's perspective, and as such external factors which have an effect on the mission are not taken into account. This is also because there would be many variations in the mission timeline, which cannot be fully covered in this report. Things such as unexpected launch vehicle delays or delays in payload provisions from client side are not taken as they are too variable. Only a representative mission scenario is given in this chapter.

Starting from Section 3.1, the entities involved are discussed and then the general terminology and architecture is defined in Section 3.2. Next the operational modes are discussed followed by the mission operations in Section 3.3 and Section 3.4, respectively. Mission logistics are then discussed in Section 3.5, and finally the hardware and software block diagrams in Section 3.6.

3.1. Involved Parties

The involved parties in the concept of operations are all entities which are actively working together with the DASH team. This includes the client, the launcher/kick-stage provider, ground stations operator, and third parties involved in assembling the spacecraft. Their involvement in the specific phases of the mission will be outlined as they are discussed in Section 3.4.

Table 3.1: Involved Parties and Roles

Party	Role
DASH	Provide mission architecture and assist in operations
Client	Purchases DASH services, provides payload onboard the DOT
Launch vehicle provider	Provides launch vehicle to be used and assists in integration
Kick stage provider	Provides kick stage and assists in integration
Ground stations operator	Provides the facilities and interface to communicate with the DASH mission
Third parties	Assist in qualification testing and integration of DOT CubeSat

From Table 3.1, it can be seen that there are many involved parties in the DASH mission. It is important to note that the launch vehicle provider and kick stage providers are involved at the early stages of the DASH mission before transfer has begun. The involvement of third parties also depends on the number of components which need to be flight qualified, this includes both payload provided by the client and DOT and SHEPHERD components provided by DASH.

3.2. Mission Architecture Definition

To understand the DASH mission configuration, terminology for naming the specific elements within the architecture needs to be defined. The mission is named DASH, which stands for *Distributed Asteroid Surveying Herd*. This reflects the very essence of what the mission is trying to achieve and how it will do so: survey and characterise asteroids using a distributed network (or herd) of spacecraft. The mission, or DASH, is made up of three groups called TRIADs. Each of these groups is launched as a single payload on its own launch vehicle and constitutes a single spacecraft when it comes to the launch and transfer phases of the mission. Each of these TRIADs is then further made up of three individual 12 U CubeSats which, for more efficient use of the mission budgets, specialise either on maximising payload capacity, or on propulsion and telecommunication capabilities. These

two variations of the CubeSats are named SHEPHERD, referring to the propulsion and deep space communication node, and DOT for the payload spacecraft. These names are summarised below in Table 3.2. Do note that both an S-DOT and an N-DOT variation of the DOT spacecraft are presented in the table. These do not refer to structurally different variations, rather simply denote their mounting location with respect to the central SHEPHERD spacecraft. N and S-DOT stand for north and south DOT mounted on the positive or negative Z direction with respect to the TRIAD coordinate frame introduced in Section 3.2.1.

Table 3.2: Mission elements names and designations

Element Name	Definition and designation
DASH	Mission name, acronym standing for *Distributed Asteroid Surveying Herd*. Made up of three TRIADS
TRIAD	Assembled group of three CubeSats, made up of one SHEPHERD and two DOT spacecraft.
SHEPHERD	Propulsion and deep space communication specialised CubeSat.
DOT	General nomenclature for a payload specialised CubeSat.
S-DOT	South DOT, in the negative Z direction from the central SHEPHERD
N-DOT	North DOT, in the positive Z direction from the central SHEPHERD

3.2.1. Relative Reference Frames

In order to have a consistent representation and relation between positions and orientations within each TRIAD, a coordinate system is defined as follows. Starting from an assembled TRIAD, the origin is placed at the geometric centre of the central SHEPHERD 12U bounding box (20x20x30 cm). The positive X axis is then defined as up, or parallel and away from the ion engine thrust, which can be considered the bottom of the TRIAD. The positive Z axis is defined as pointing directly towards one of the two DOTs. More specifically, the DOT mounted on the SHEPHERD side not hosting the stowed solar arrays, see Figure 3.1 where the stowed solar array bounding box is clearly indicated by their hatched cross-section. Lastly, the positive Y axis is defined with the right-hand rule and the positive X and Z directions.

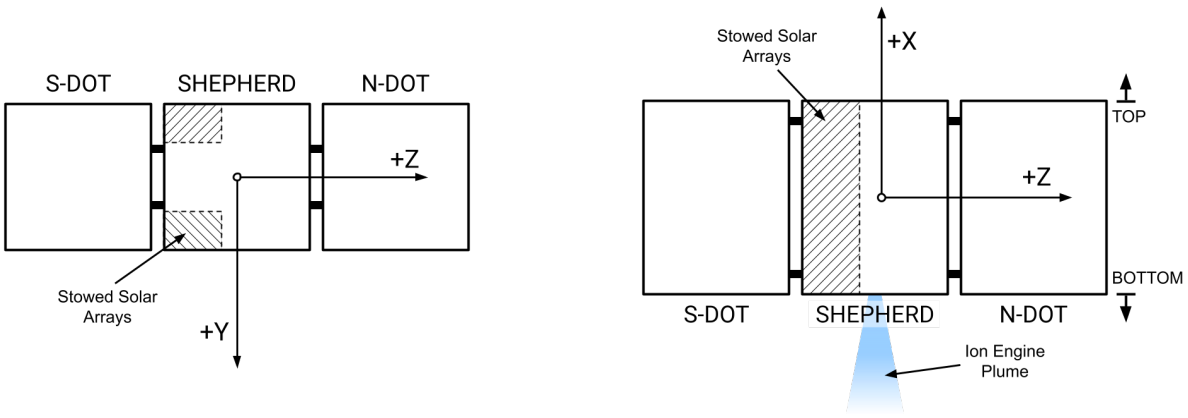

(a) Top view **(b)** Side view

Figure 3.1: TRIAD right-handed coordinate frame

Figure 3.1 shows the physical relations of the mission elements outlined in Table 3.2 making up a TRIAD. Note the difference between the N-DOT and S-DOT spacecraft, although structurally identical, they differ based on their mounting orientation with respect to the central SHEPHERD propulsion

module. To easily remember their nomenclature, the south DOT, or S-DOT, can be remembered as the DOT mounted on the same side as the solar arrays while the north DOT, or N-DOT, not on the side of the arrays.

3.2.2. Mission Configuration

Using a somewhat unique mission architecture, DASH's configuration varies over the mission phases. The entire DASH mission is made up of nine 12 U CubeSats. These are delivered by three individual launch vehicles, each sending a single TRIAD towards the target asteroid. On each of the three launch vehicles, a TRIAD is mounted within a single custom deployer atop of a kick-stage which provides some of the delta-V required for the initial deep space transfer ejection burn. A diagram of a TRIAD in launch configuration can be seen in Figure 3.2.

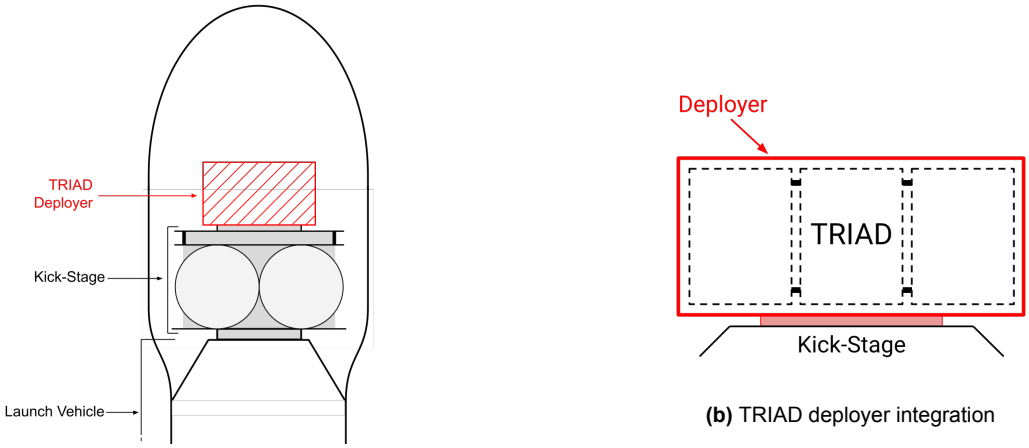

(a) Launcher fairing configuration

(b) TRIAD deployer integration

Figure 3.2: One TRIAD in launch configuration

The launch vehicle and kick-stage accelerate the TRIAD with enough energy to escape Earth's sphere of influence and send it on a deep space trajectory with some excess velocity, roughly aimed at the target asteroid. Once the kick-stage has completed its burn and has sent the payload on its deep space trajectory, it deploys the TRIAD from its containerised deployer. The TRIAD is now on its own power and propulsion and can begin commissioning, deploying its solar arrays and long range communication system. The TRIAD will remain in this configuration for the entirety of the transfer mission phase and will act as a single spacecraft. A diagram of the TRIAD in the transfer configuration can be seen in Figure 3.3.

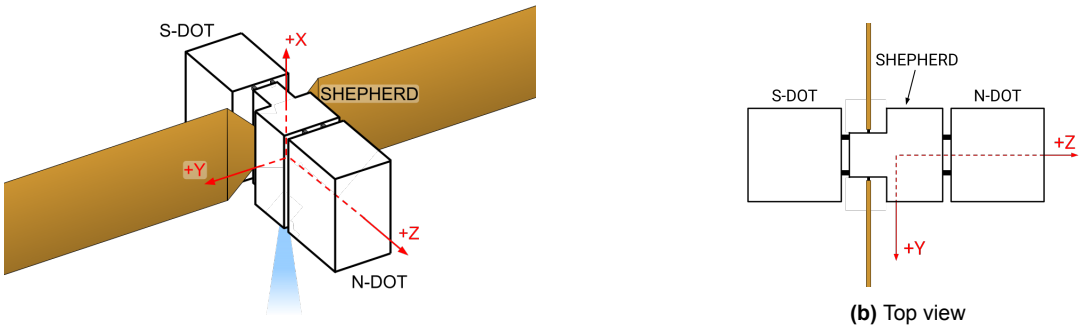

(a) Isometric view

(b) Top view

Figure 3.3: TRIAD transfer configuration with deployed solar arrays

Lastly, as the TRIAD reaches the target asteroid, its configuration changes one last time before beginning the operational scientific mission phase. The three 12 U CubeSats separate from each other, leaving two DOTs and one SHEPHERD in orbit around the asteroid. From here, the DOTs, carrying the mission payload and instrumentation, will spend the entirety of the operational mission phase

collecting data on the mission scientific target. The SHEPHERD will instead switch to serving as a long range communication node, the DOTs sending the collected data to the SHEPHERD through low power transponders, while the SHEPHERD uses its long range communicator to relay the same data back to the DSN on Earth. Both the DOT and SHEPHERD operational configurations can be seen in Figure 3.4.

(a) SHEPHERD spacecraft **(b)** DOT spacecraft

Figure 3.4: DASH operational configuration

3.3. Operational Modes

The operational modes of the DASH mission are presented in this section. There are different operational modes for the DOT and SHEPHERD spacecraft respectively based on the mission phase CubeSats status. Modes are divided based on whether they are pertinent to DOTs or SHEPHERDs to more accurately reflect the functions and entry/exit conditions for each mode. The SHEPHERD and DOT operational modes are introduced and defined in Section 3.3.1 and Section 3.3.2 respectively. Then, the TRIAD modes will be introduced, which are combinations of the modes of its individual constituents, two DOTs and a SHEPHERD.

3.3.1. SHEPHERD Modes

The SHEPHERD module has five key operational modes. In this section, they are described with reference to the specific functions performed in each one of them, as well as when and how the vehicle transitions into and out of each mode. A summary of the modes is presented below in Table 3.3.

Table 3.3: SHEPHERD vehicle modes

Mode	Description
Sleep	Used when stowed until the transfer phase begins
Thrusting	Describes the mode used for ion propulsion transfer burn
Transfer Communication	Entered for communication back to Earth and trajectory adjustments
Nominal Operational	Mode for nominal operations at the asteroid, SHEPHERD serves as a communication node in service of the DOTs
Safe	Utilised once problems are detected

The operational modes introduced in Table 3.3 are now described in more details.

Sleep Mode
During this mode the ion engine is powered off, and the entire spacecraft is operating at low power. Communication with the ground station occurs less frequently and with lower bandwidth. As spacecraft health is still relevant during all phases of the mission, regular health checks are still sent to the DSN. When in sleep mode but still inside its deployer, SHEPHERD is directly interfaced to the deployer and then to the kick-stage. This allows using the kick-stage/launcher hardware to communicate with ground stations when the SHEPHERD antennas are not deployed yet.

Additionally, both during transfer and operations, health data is also relayed back for the DOTs given

they are not capable of communicating to Earth ground stations on their own. During transfer, health data is received through the physical connection with the DOTs while after TRIADs separate and the physical connections are severed, health data is received through the ISL.

The SHEPHERD remains in sleep mode mostly during the initial phases of the mission. During pre-launch operations, launch, and all the way through kick-stage ejection burn, the SHEPHERD is in sleep mode. It exits sleep mode when ejected from the deployer and begins commissioning. Sleep mode is also used to save power between data downlinks back to Earth during nominal operations. Sleep mode is also entered between long low-thrust burns as the SHEPHERD (while still within a TRIAD) coasts in deep space.

Thrusting Mode
Thrusting mode defines operations when the SHEPHERD is actively using its ion propulsion system. While in this mode power is directly channelled from the EPS system into the ion propulsion module and most of the power usage is allocated for thrusting. The solar arrays are thus tracking the sun for optimal power generation. When thrusting during transfer, power is only delivered to the propulsion system aboard SHEPHERD. Although having the DOTs physically connected, minimum power is delivered to them while thrusting, just enough to receive regular health checks. Communication with the ground stations is limited, as there are not enough degrees of freedom to guarantee both the long range antenna and the panels are oriented in the right direction while the engine is operational.

SHEPHERD transitions to this mode automatically both during transfer and nominal operations whenever the onboard computer required a velocity change. When actively changing its trajectory, the SHEPHERD spends 13 days out of 14 in thrusting mode (duty cycle of 93%). The remaining time is dedicated to navigation and long range communication. See Section 3.4.6 for a more detailed description of the thrust-navigation cycle.

Transfer Communication Mode
This SHEPHERD mode complements the thrusting mode during transfer. While actively changing its trajectory, transfer communication mode makes up the remaining one day out of 14 of the 93% thrusting duty cycle. This mode is responsible for receiving and processing navigational data from the DOTs, communicating health and/or scientific data from DOTs to DSN, receiving data from DSN and providing the DOTs with power to perform navigation functions. It is important to note that, during this phase, the ion engines will not be firing as power is now diverted to navigation and communication functions. This mode is entered once trajectory adjustments have to be made during transfer. Once trajectory adjustment and calculations have been completed, transfer communication mode is exited and thrusting mode is re-entered to switch back to active thrusting

Nominal Operational
Once a TRIAD has reached the target asteroid and it has separated into two DOTs and one SHEPHERD, the SHEPHERD CubeSat switches from being a propulsion module, to serving as a long range communication relay for the DOTs. Through the inter-satellite link (ISL), the SHEPHERD receives data from the DOTs to be sent back to DSN ground stations through its long range transponder. While in this mode, the SHEPHERD uses the majority of its power budget to supply the long range communicator. The SHEPHERD enters nominal operations once it has separate from the two DOTs it is mounted to during transfer and the scientific operational mission phase begins.

Safe Mode
As all spacecraft, SHEPHERD needs to be able to deal with unexpected contingencies without damage to its critical components. In the case a critical system malfunctions, SHEPHERD enters safe mode. During this mode, the engine is turned off, and all systems which are not essential to the survival of the spacecraft are turned off or operated at minimum power. This helps in decreasing the load on the EPS and CDHS. The SHEPHERD module will attempt to fix the underlying issues autonomously, whilst relaying health data more frequently to the ground station.

3.3.2. DOT Modes

Similarly to the SHEPHERD modes, the DOTs share some similarities in their modes of operations, namely the sleep and safe mode. It is important to note that DOT modes are the same for both S-DOT and N-DOT spacecraft, as position in the TRIAD does not entail separate modes to be allocated. All principal operational modes are listed in Table 3.4.

Table 3.4: DOT modes and descriptions

Mode	Description
Sleep	Used at initial stages of mission and during transfer burn
Transfer Navigation	Activated for trajectory corrections during transfer
Operational	Describes the scientific aspect once in close proximity to Didymos
Safe	Activated in case of an encountered issue

Sleep Mode
Sleep mode is used mainly to reduce loads and switch to only collecting housekeeping data. DOTs are placed in sleep mode from the moment the spacecraft is assembled and integrated into the launch vehicle until transfer trajectory adjustments are needed. During transfer, when the ion engines are burning and the SHEPHERD is in thrusting mode, the DOT will also remain in sleep mode. Only housekeeping data collection and regular health checks are performed while the DOTs are in sleep mode.

Transfer Navigation Mode
During transfer, trajectory adjustments will have to be made to ensure proper thrust vector heading. As mentioned in the SHEPHERD operational modes, thrusting and navigation is performed in a 93% duty cycle of 14 days thrusting to one day navigation and trajectory adjustments. During the one day of adjustments, the DOT switches to transfer navigation mode. In this mode, power is received from the central SHEPHERD through a physical connection and is used to power the onboard navigation equipment. Depending on the distance to the target, either close range or far range navigation is performed. The mode is exited once trajectory calculations and measurements have been performed after which the ion engine is re-engaged by the SHEPHERD and the DOTs are switched to sleep mode.

Operational Mode
Operational mode for the DOTs describes the scientific operations and navigation functions to be performed during the data collection phases at the target asteroid. Once at Didymos, swarm navigation will be performed using specific orbits for optimal data collection, see more about navigation in chapter 15. Data collected from the payload and onboard instruments is also transmitted to the SHEPHERD to be relayed back to Earth. This mode is entered once the DOTs separate from their TRIAD and close navigation sensors are activated at close proximity to Didymos. It is then exited once the mission has been completed and the end-of-life phase has begun for proper disposal of the DASH mission.

Safe Mode
DOT safe mode is designated great importance due to the swarm nature of the DASH mission. Any slight interference can cause catastrophic failure if not handled properly. As such, during safe mode, interference with the nominal operations of other CubeSats is limited. Non-critical systems such as the payload is turned off and health checks are performed more frequently. This is of course entered once an issue has been detected throughout the duration of the mission. Additional measures are also implemented in the form of a manual override by the ground station. This is in the case that the failure imposes a danger to other CubeSats and the DOT may have to be disposed of before imposing a greater threat to mission success.

3.3.3. TRIAD Modes

Now that the operational modes for both the SHEPHERD and DOT spacecrafts are defined, the modes for the TRIAD can be specified. As described in Section 3.2.2, a TRIAD simply consists of a two DOTs mounted onto a SHEPHERD. Operational modes of a TRIAD are then simply combinations of DOTs and SHEPHERD modes, a summary of which can be found in Table 3.5.

Table 3.5: TRIAD modes and descriptions

Mode	Description	SHEPHERD mode	DOT mode
Sleep	TRIAD operating at lower power, hibernating non-critical subsystems	Sleep	Sleep
Safe	Troubleshooting identified operational issues	Safe	Safe
Cruise	Actively changing course with the onboard ion propulsion	Thrusting	Sleep
Pilot	Performing deep space navigation and updating global trajectory	Transfer communication	Transfer navigation

The operational modes presented in Table 3.5 are now described in more details. Refer back to Table 3.3 and Table 3.4 for a thorough definition of the SHEPHERD and DOT modes respectively.

Sleep Mode
As rather self-explanatory, sleep mode for the TRIAD is essentially just about placing both the SHEPHERD and the DOTs in sleep mode. Both operate at lower power, and health data for the entire TRIAD is relayed back to ground stations at a reduced frequency. While in the deployer, health data is transferred to the launch vehicle/kick-stage through a physical connection while during transfer, the long range transponder aboard SHEPHERD is responsible for relaying health data back to earth. Health data is transferred from the DOTs to the central SHEPHERD for relaying through physical connections at the mechanical interface between them.

Safe Mode
Similarly to the TRIAD's sleep mode, safe mode simply entails switching both the SHEPHERD and two DOTs to safe mode when a fault in a critical system is detected. The TRIAD as a whole, just as its constituting elements, can be manually forced to enter or exit safe mode from mission control.

Cruise Mode
Cruise mode defines the operations of the TRIAD when in powered flight. During cruise mode, the SHEPHERD propulsion system is actively thrusting and the DOTs are switched to sleep mode. See *Thrusting* and *Sleep* mode for the SHEPHERD and DOT for more details.

Pilot Mode
Pilot mode defines the TRIAD operations when in unpowered flight. During pilot mode, the SHEPHERD shuts down its ion thruster and receives navigation data from the sensor arrays mounted on the side DOTs which are operating in transfer navigation mode. The DOTs receive power from the SHEPHERD to operate their navigational sensor suite. Measurements are sent to the SHEPHERD who's responsible for updating the trajectory estimations and correcting the burn vector for the next thrusting cycle. For a complete description of SHEPHERD and DOT operations during this TRIAD mode see the *Transfer Communication* and *Transfer Navigation* modes respectively.

3.4. Mission Operations

The mission operations section presents the DASH mission, modes and configurations in chronological order from initial assembly of the CubeSats and launcher integration to the final disposal. This allows for a timeline to be given to provide an idea as to the time frame expected for each phase

and which ones are contributing the most to the DASH mission timeline. It is important to note that the timeline described will not include unexpected delays caused by any entity other than DASH. As each phase is described and outlined, the parties which are directly involved and their role will also be touched upon.

Table 3.6: Mission phases, their duration and start time with respect to the mission clock

Mission Phase	Expected time frame	Mission clock [days]
Assembly & Integration	40 - 52 weeks	- 396
Launch	2 hours	- 32
GTO Loitering	1 - 4 weeks	- 32
Ejection	4 days	- 4
Commissioning	1 day	+ 0
Transfer	650 - 750 days	+ 751
Arrival	1 - 2 weeks	+ 765
Pre-Operations	2 - 3 days	+ 768
Scientific Phase	6 months	+ 954
End-of-life Phase	1 week	+ 961

Table 3.6 shows the expected timeline of the DASH mission and the duration of the phases. Do note that when defining the mission phase's start time, the longest expected time frame is used to avoid being over-optimistic with the mission timeline. Furthermore, the mission clock is assumed to start at zero as the TRIAD is deployed from its containerised deployer and begins initial commissioning.

Important values to note in Table 3.6 are the time frames expected for Assembly and Integration, GTO Loitering and Transfer. Assembly and Integration is assumed to take a maximum of 52 weeks, 1 year, as most of the DASH mission constituents are off-the-shelf components which only necessitate qualification and acceptance tests to be performed before being flown. Specialised components instead, such as release mechanisms, while not commercially available, are simple in design requiring little development and as a result are easy to test and can fit within the allocated time frame. Loitering in GTO is estimated to last 1 to 4 weeks to accommodate for potential launch delays or just managing provided launch cadence. This is seen as a fair assumption due to the rapidly increasing launch frequency seen in the space market, as such, procuring the few launches to be scheduled so soon is feasible within the DASH mission launch window. Finally, the transfer phase's time frame is addressed. A large expected time frame is given due to uncertainties at this design stage in regard to the transfer burn and the necessary correction and orbital adjustments during such a long time frame.

An extra consideration is made regarding the scientific phase of the DASH mission. The current expected operational phase duration is 6 months as designed for from the mission requirements. As some deep space mission can have extended operational lifetimes, this possibility is not ignored while designing the DASH mission. Rather, DASH will guarantee 6 months of scientific operations with the entirety of the distributed system operational at the target asteroid. Any increase upon this time frame is then seen as a bonus both to DASH and all stakeholders involved, especially the client. Thus, 6 months will be assumed for when referring to the scientific phase.

Each mission phase is now described. The relevant entities, configurations, modes of operations and general timeline are presented for each phase. These are the same primary phases highlighted by the functional analysis performed earlier in chapter 4.

3.4.1. Assembly and Integration

The assembly and integration of the DASH mission is the first phase which will have to be passed before launch. During this phase, many entities are directly involved such as the client, launch vehicle provider, kick stage provider, third parties, and DASH. The client, third parties, and DASH will assemble the payload into the DOTs which are subsequently attached to the SHEPHERD to form a TRIAD. Qualification tests are performed in the relevant steps during this process. Once the DASH architecture is integrated with the payload, each TRIAD is fitted into its deployer and onto the kick

stage, which is then fitted onto the launch vehicle itself. As can be inferred, the involvement of the kick stage provider and launch vehicle provider is very essential to ensuring the interfaces during the initial stages of the DASH mission are without fault. Flight qualification tests on the launcher and kick stage are also performed during this phase.

The total time frame for this phase is estimated as 52 weeks as many of the DASH mission components are off-the-shelf. The launcher itself is assumed to be able to be built in 6 months and fully flight qualified in 9 months. This number was obtained using the Falcon 9 build time of 4-6 months [1] and is seen to take the biggest portion of time in this phase. Using COTS components reduces development time and makes the testing and qualifications process easier due to the higher technical readiness of the technology used. Qualification tests are performed all the way up until the TRIAD is integrated on the launch vehicle and launch day has arrived. Once activated close to the launch windows, The DOTs and SHEPHERD will be in sleep mode to conserve power, but still capable of communicating health data. Below an expected chronological order of this phase of the design is described from DASH's perspective.

1. Customer and DASH go into talks about specifics of mission and payload
2. DOTs and SHEPHERDs ordered to be made
3. Commercial off the shelf components are ordered from various manufacturers
4. A launcher and kick stage is ordered from private manufacturers
5. The payload is integrated into the DOTs and tested
6. All mission constituents are transported to assembly space near launch location
7. DOTs and SHEPHERDs are assembled into TRIADs
8. Each TRIAD is assembled and placed in a deployer
9. TRIAD deployer is placed on kick stage and tested
10. Kick stage is integrated with launch vehicle

3.4.2. Launch

launch is one of the shortest phases and most critical in the DASH mission. During this phase, the same entities as from the assembly and integration phase are involved. This is because pre-launch checks will have to be performed on all constituents of the mission. Once launch begins, telemetry data from the launcher, kick stage, and TRIAD will still be taken requiring continuous involvement from all entities in case of issues during launch. This means that in the event that a specific component such as the kick stage experiences an issue, the responsible entity will be present to assist in troubleshooting the issue. As the chosen rocket is the PSLV, there will be four total stages of separation before the launch vehicle is spent. Once the DASH mission is placed in a GTO transfer orbit, 45 minutes after rocket ignition [2], the TRIAD and kick stage will only remain in orbit with the final stage of the PSLV properly disposed off. The SHEPHERD and DOTs are still in sleep mode, and safe mode can be engaged in case of complications.

1. Pre-flight checks
2. Start of telemetry data collection
3. Main engine ignition
4. Exhaustion of first to start of second stage
5. Fairing separation
6. Exhaustion of second stage
7. Separation of kick stage and TRIAD from second stage of RFA-1
8. Final orbit placed in highly elliptical GTO orbit with apogee of 250 km

[1] URL https://www.mcnallyinstitute.com/how-long-to-assemble-rocket-engine/ [cited 7 June 2022]
[2] URL https://www.isro.gov.in/pslv-c25-mars-orbiter-mission/pslv-c25-brochure-0 [cited 8 June 2022]

3.4.3. GTO Loitering

During GTO loitering, the TRIAD and kick stage will remain in GTO orbit anywhere from 1 to 4 weeks. 1 week is chosen on the lower end in anticipation of a one-week consecutive launch window, with 4 weeks being a maximum interval between launches. This four-week time interval is chosen to use Didymos as the reference target, different target bodies may have varying viable launch windows. The launch vehicle provider is no longer involved at this stage, as the launcher has already placed the DASH mission in GTO. During this time period, data is sent to the kick stage to then be communicated back to the ground station and batteries are kept at optimal conditions. As the transfer stage hasn't begun yet, both the SHEPHERD and the DOTs are still in sleep mode. In the event that there are many launches to be made, and unexpected delays occur, it can still be decided by the client to only send mission elements already in orbit rather than wait for the complete mission to be in GTO and then wait even longer for the next transfer window to open. During this phase, multiple functions can occur at once and as such a chronological order cannot be determined, rather a list of simultaneous functions to be performed is presented.

- Keep battery power in optimal performance range
- Maintain designated elliptical orbit
- Communicate position and health status of DASH mission at consistent intervals
- Perform constant checks and undergo preparation phase for kick stage ignition in anticipation of next phase of DASH mission

3.4.4. Ejection

Ejection is when the kick stage is activated and burns to provide the remaining required delta-V to escape Earth's sphere of influence and be injected into transfer trajectory. The kick stage provider is heavily involved in this stage as the burn duration is a significant factor to take into account for effective burn and any issues faced by the kick stage during burn must be fixed with haste. Once the burn is completed, the deployers are then brought into play and the TRIAD is released. At this stage, the SHEPHERD is still in sleep mode and the DOTs are also in sleep mode. The duration of this phase is a couple of days due to the low thrust and long burn time expected. Some time is also allocated for pre-ignition checks that may take longer than expected due to the low technical readiness of the kick stage used. The order of operations for this phase can be illustrated below. After this stage, the kick stage providers are no longer involved in the DASH mission as their task is completed at successful separation of TRIAD. At this stage, the TRIAD is travelling with an excess velocity of 6000 meters per second outside the sphere of influence of Earth.

1. Green light given by ground station to signal all mission constituents are in orbit
2. Determine position and attitude of kick stage
3. Adjust attitude and determine thrust vector needed for ejection burn
4. Ignite engines and begin continuous burn
5. Burn completed, signal TRIAD of beginning of next phase
6. release TRIAD from kick stage in designed trajectory and inclination

3.4.5. Commissioning

During the commissioning mission phase, TRIADs will perform the initial subsystem setup procedures to prepare for the transfer and cruise towards the target asteroid. Only DASH, the client, and third parties will be involved at this stage as other entities will have had their job completed by this point in the mission timeline. Third parties here refers to producers and operators of TRIAD's components, such as the off-the-shelf solar panel deployment mechanism used on the SHEPHERD, it is critical for proper deployment to occur with no issues before transfer begins. The solar panels of the SHEPHERD will be deployed first, followed by the high gain antenna and a system level calibration of the sensors and transfer-critical equipment. The ion engine is warmed up at this phase and the SHEPHERD will be in thrusting mode once the start up process is complete and all necessary checks have been

performed. The DOTs will have their system equipment checked and will be in the navigational mode until trajectory calculations are done and sent to SHEPHERD. After that, the DOTs will be back in sleep mode and the SHEPHERD will begin transfer burn, entering thrusting mode. A step-by-step process is outlined below.

1. DOTs and SHEPHERD exit sleep mode and undergo warm up process
2. SHEPHERD solar panels and high-gain antenna are deployed and EPS systems is operating at higher capacity
3. DOTs calibrate navigational data and onboard instruments
4. DOTs enter navigational mode and are feeding data into the SHEPHERD for transfer trajectory burn
5. SHEPHERD performs subsystem level checks to ensure propulsion system, thermal system, TT&C system, and EPS are nominal
6. SHEPHERD uses DOTs data to determine required thrust vector
7. SHEPHERD adjusts TRIAD attitude
8. SHEPHERD prepares for ion thruster engagement

3.4.6. Transfer

It is important to note that once the ion thrusters are turned on, ready to begin transfer, and thrusting, then the DASH mission is officially in the transfer phase. During transfer, a 93% duty cycle is assumed, this means a 13-day burn accompanied by a 1-day trajectory adjustment. During the 13-day burn, the ion propulsion module continuously burns, and the SHEPHERD is in thrusting mode with the DOTs in sleep mode. During the 1-day trajectory adjustement period, the DOTs are in far-range navigation mode given that they are in the interplanetary regime at this phase. Furthermore, the SHEPHERD enters communication mode in this time period. DOTs gather navigation data and refine the burn vector to be fed into the SHEPHERD. Data is also transferred to the ground station, with health checks and trajectory data being received by the ground station. The inter satellite link is not used for communication, as there is a physical connection used to transfer data. During this phase, as can be seen, when the SHEPHERD is in thrusting mode, the DOT is in sleep mode. And when it is time for trajectory adjustments, the SHEPHERD is in communication mode with the DOT in navigation mode. This phase will continue until the TRIAD is close to Didymos and is the longest part of the DASH mission. The process outlined below is a 14-day cycle, which will occur continuously during transfer and repeat itself until in close proximity to the target asteroid. During the entirety of the transfer burn, the solar panels of the SHEPHERD will be pointing to the sun for optimal power generation.

1. SHEPHERD ion engines switched off
2. SHEPHERD enters communication mode
3. DOTs enters short-range navigation mode
4. SHEPHERD diverts power to DOTs and for communication
5. DOTs perform navigation functions and feed data to SHEPHERD
6. Data is sent back to ground station along with health checks
7. SHEPHERD adjusts attitude according to new required thrust vector
8. DOTs enter sleep mode once trajectory adjustments are completed
9. SHEPHERD goes through ion engine warm up process
10. SHEPHERD enters thrusting mode
11. Power used mainly for 13 day continuous thrust
12. Excess power stored in battery

3.4.7. Arrival

The arrival phase of the mission begins once the DOTs' cameras are able of identifying Didymos visually with the TRIAD's onboard cameras. This essentially means the Arrival mission phase begins as soon as the target is visible to the TRIAD's visual sensors, even if in just one pixel of the taken images. During this phase, as the TRIAD is in the local navigation regime, the short-range navigation techniques are employed. The ion engine will also be used more frequently with a lower duty cycle as long continued thrust burns will not be used, rather short bursts for small adjustments in trajectory. This can be on the order of a few hours or days. In this example, it will be one or two days. Communication and health checks will still be possible, and communication to Earth occurs more frequently as a result of the proximity to the target asteroid and need for constant ground station updates. The uncoupling mechanism will undergo multiple checks as well as many more system level checks before the commission phase of the mission begins and the DOTs separate from the TRIAD. The purpose of this phase is to reduce the duty cycle and keep the ground station more up to date as the mission nears the start of the scientific phase.

1. SHEPHERD ion engines switched off
2. SHEPHERD enters communication mode
3. DOTs enter short-range navigation mode
4. SHEPHERD diverts power to DOTs and for communication
5. DOT cameras identify asteroid target body
6. DOTs perform navigation functions and feed data to SHEPHERD
7. Data is sent back to ground station along with health checks
8. Ground station informed of close proximity to asteroid body
9. SHEPHERD adjusts attitude according to new required thrust vector
10. DOTs enter sleep mode once trajectory adjustments are completed
11. SHEPHERD goes through ion engine warm up process
12. SHEPHERD enters thrusting mode
13. Power used mainly for 1 or 2 day continuous thrust.
14. Excess power stored in battery

3.4.8. Pre-Operations

The pre-operation phase of the mission occurs once DASH is sufficiently close to the Didymos asteroid system. At this phase, the separation mechanisms to release the DOTs from the TRIAD into specific orbits are initiated. The release mechanism separates into four parts, with 1 part on each DOT and two parts on the SHEPHERD. At the end of this manoeuvre, the DOTs are both released into the same orbit, trailing each other with the SHEPHERD module at an orbit altitude higher than those of the DOTs. As the scientific phase follows immediately after the completion of this phase, it ensures that all TRIAD elements are in the designated orbits around Didymos before payload operations start and the SHEPHERD acts as a communication node to the DSN.

1. TRIAD approaches Didymos
2. SHEPHERD enters nominal operational mode
3. TRIAD oriented with N-DOT to be released in designed trajectory
4. DOTs enter operational mode
5. DOTs deploy ISL antenna systems and establish links with SHEPHERD
6. N-DOT released at $3\,\mathrm{cm\,s^{-1}}$
7. SHEPHERD relays data with N-DOT release time stamps and DOT orbit data
8. SHEPHERD assembly rotates 180° to release S-DOT into trailing orbit with N-DOT
9. S-DOT released into trailing orbit 125 m behind N-DOT

10. SHEPHERD relays data with S-DOT release time stamps and DOT orbit data
11. SHEPHERD enters into designated orbit
12. SHEPHERD and DOTs run system checks before scientific phase start

A more detailed separation logic sequence is further developed in Section 10.1.5.

3.4.9. Scientific Phase

Nominal operational during this phase is designed to last for 6 months, with this phase of the DASH mission representing where all the scientific payload data is generated for the client. Collected data is relayed to the SHEPHERD to be sent to the ground station along with health checks and telemetry data. The inter satellite link plays a major role at this stage, with the DOTs communicating to each other about their individual orbit and performing adjustments where necessary to stay in the designated formation around Didymos. The DOT's autonomous navigation ability is put to the test at this phase where the swarm is fully functional and performing payload operations. Functions such as changing between formations, will be performed during this phase. Care has to be taken in the event that one DOT experiences critical failure and will be initiate safe mode. When such DOT is in safe mode, the DOT shall not pose a threat to the other DOTs and the ground station must take the necessary steps to ensure that is indeed the case. An example scientific phase is shown with a formation change to demonstrate the order of operations to be taken. The order described is starting from the DOTs collecting and storing scientific data and relaying health data to SHEPHERD. At the same time, SHEPHERD is managing its own battery, thermal conditions, and relaying DOT health data to ground station. Then the DOTs have collected enough science data to be sent to Earth. This triggers the large data transfer to Earth process and an additional level of complexity is added with an order for formation change before the process ends.

1. DOTs in operational mode and SHEPHERD in nominal operational mode
2. DOTs collect scientific data
3. DOTs use ISL to communicate and adjust orbit formation
4. DOTs relay health checks to SHEPHERD
5. SHEPHERD enters nominal operational mode
6. SHEPHERD transmits health data to ground station
7. SHEPHERD keeps adjusting solar panel angle and attitude depending on power availability and thermal conditions
8. DOTs collect scientific data and store it until a sufficient amount has been gathered
9. DOTs relay collected data and telemetry to SHEPHERD
10. SHEPHERD receives data from DOTs and sends it to Earth
11. SHEPHERD (potentially) receives commands from Earth to change formation of DOTs
12. SHEPHERD send order of formation change to DOTs
13. DOTs stop payload operations and adjust trajectory as necessary
14. Individual DOTs confirm completion of respective orbital adjustments
15. DOTs use ISL to confirm global formation change is completed and send confirmation message to SHEPHERD
16. SHEPHERD sends confirmation of formation change to ground station upon completion
17. Ground station green lights resuming of payload operations
18. SHEPHERD relays ground station order to resume payload operations
19. DOTs start payload operation again and begin collection of new set of scientific data

3.4.10. End-of-life Phase

The end-of-life phase signifies the completion of the DASH mission as a whole. The ground station gives the command to SHEPHERD to be relayed to all DASH constituents to prepare for proper disposal. Final checks are made, all remaining data is sent and the DOTs and SHEPHERDs undergo a disposal process outlined by deep space regulations, sustainability standards, and DASH itself. The entire process is outlined below chronologically. The end-of-life trajectory is such that any future mission to Didymos will not experience interferences caused by remaining DASH elements that are no longer in operation. As such, all elements will be placed in an end-of-life trajectory away from Didymos. This distance away will be defined as the distance from which the close proximity sensors can no longer be used for tracking the Didymos asteroid body.

1. SHEPHERD receives order of disposal confirmation from ground station
2. All remaining scientific data collected from DOTs and sent to ground station via SHEPHERD
3. The DOTs and SHEPHERDs are placed in end-of-life trajectory
4. Final confirmation of all elements no longer in proximity of Didymos sent by SHEPHERD before decommissioning
5. Ground station confirms mission termination

3.5. Mission Logistics

The operation concept outlined earlier takes certain liberties to outline the prescribed process. Such elements to take note of are the launch frequency, loitering times, and kick stage ejection period. These elements and their assumption will be discussed in greater detail.

Starting with launch frequency, it is assumed to be a 1-week interval using the recent achievement of SpaceX of 3 launches in under 14 days [3]. Though the PSLV rocket is not as in demand in comparison to SpaceX rockets, once the rockets have been ordered, multiple launches in a comparable time frame as SpaceX is feasible. The upper limit of intervals that can be done is 4 weeks due to the tight launch windows due to the precise trajectories needed.

Loitering times are also heavily dependent on launch intervals. Due to the highly elliptical GTO orbit, a long orbital period is also expected. As such, in combination with a 4-week window to get into transfer trajectory, the position of the kick stage and TRIADS in this elliptical orbit plays a role in determining when to ignite the kick stage. This loitering period influences when ejection starts, and how long the DASH mission elements already in GTO can afford to wait for their launches and mission elements to also be placed in GTO. Finally, given that the kick stage actually produces low thrust over a long period of time, the duration and start time of the ejection will be crucial to insert the TRIADs into the designed trajectory. The loitering time will also have to take this time period into account, as the TRIAD may not be in the optimal position in GTO to start the transfer burn.

3.6. Hardware and Software Block Diagrams

In order to facilitate the design and production of DASH, its components and their interactions are visualised in the Hardware Block Diagram (HWBD) and the Software Block Diagram (SWBD).

3.6.1. HWBD

The HWBDs of the SHEPHERD and the DOTs are shown in Figure 3.5 and Figure 3.6, respectively. In these diagrams, it can be seen that the distribution unit is connected to all the components that need power and the OBC is connected to all the components that need or produce data. Additionally, there is a wireless connection between the ISL antennae and the ISL receivers of the SHEPHERD and the DOTs. Note that the components that make up the thermal system are not connected to anything else, as these are passive components.

[3] URL https://www.nasaspaceflight.com/2022/05/spacex-2500th-starlink/ [cited 8 june 2022]

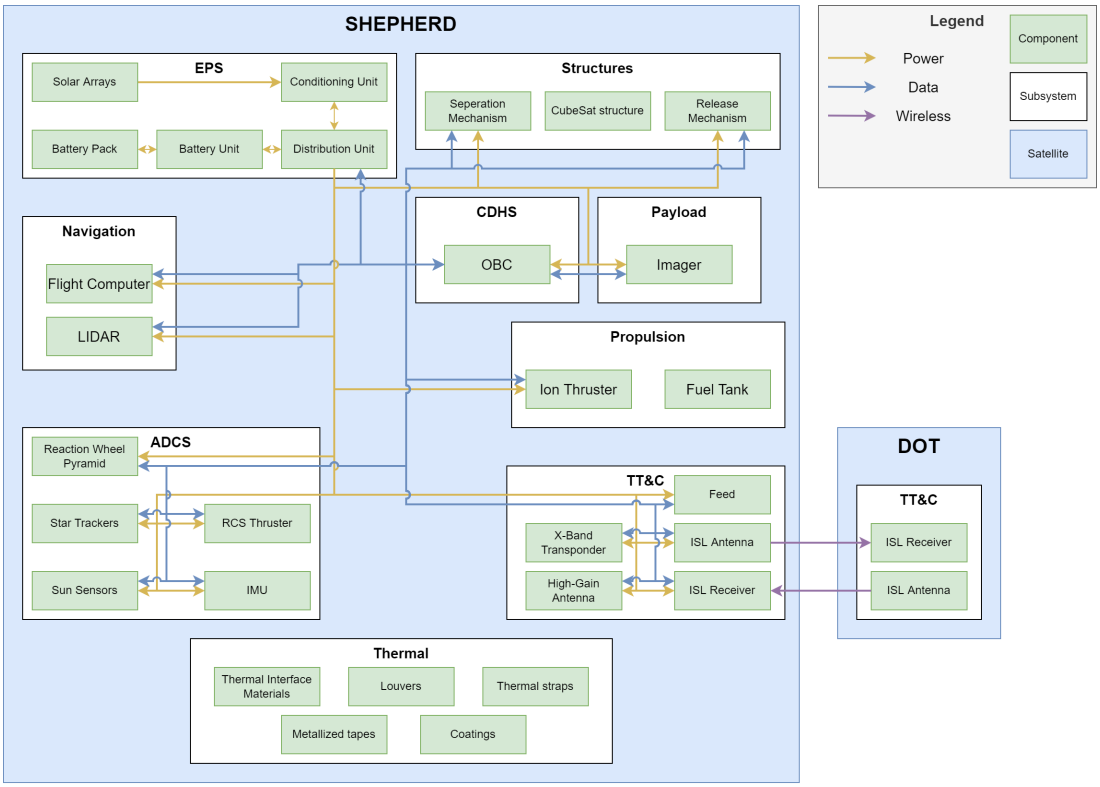

Figure 3.5: Hardware Block Diagram of the SHEPHERD

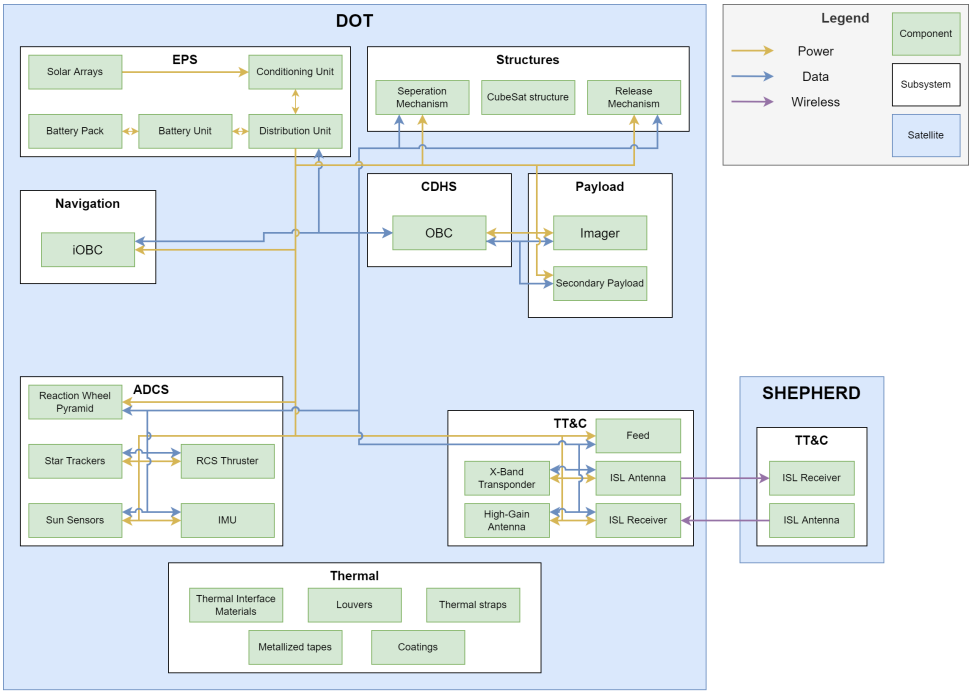

Figure 3.6: Hardware Block Diagram of the DOTs

3.6.2. SWBD

The SWBD is shown in Figure 3.7. The flight computer takes care of all the guidance, navigation and control algorithms, which runs in a loop and provides control input for the ADCS and propulsion systems to control the trajectory. Additionally, data is sent to the inter-satellite link antennae to send to the other satellites. The OBC runs the rest of the algorithms.

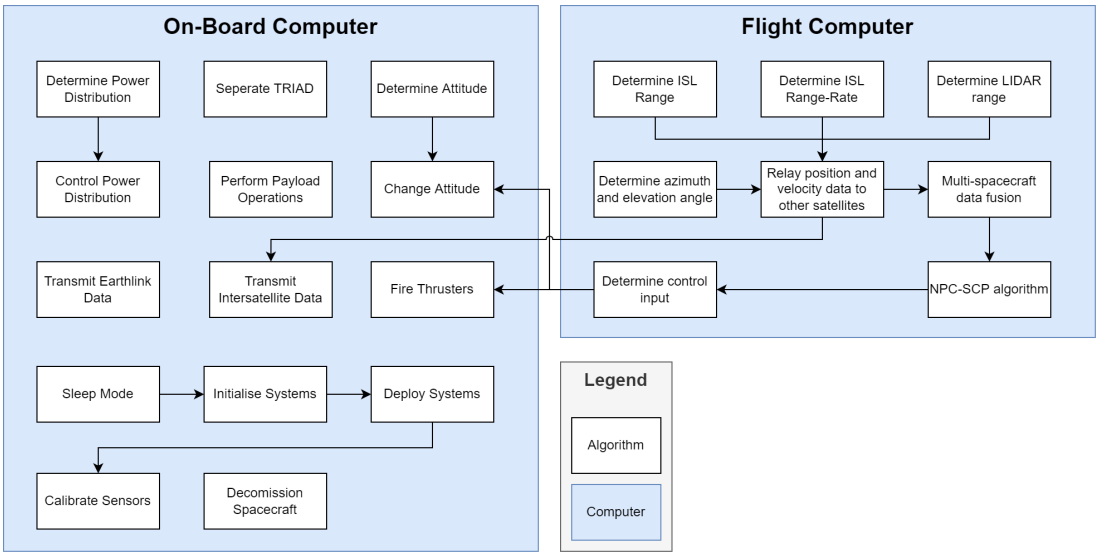

Figure 3.7: Software Block Diagram of the DASH spacecraft

4 Functional Analysis

DASH's functional analysis focuses on determining and explicitly defining a coherent, and most of all complete, set of functions the mission systems have to perform. The first iteration of DASH's functional analysis was performed in the team-written Baseline report [4] but is here updated to encapsulate the new design elements and more detailed mission phases defined for DASH. Two diagrams are provided in this chapter: a functional flow block diagram, or FFBD, and a functional break down structure, or FBS. The former include all defined functions presented preserving their temporal structure, while the latter provides the same functions organised in a hierarchical manner to display the relation between phases, functions, and sub-functions.

Refer back the Baseline report [4] for an overview of the structure and organisation of the FFBD. The entire block diagram can be found below in Figure 4.1.

Similarly, as for the FFBD, refer back to the Baseline report [4] for an overview of the structure of the diagram. The full block diagram can be found below in Figure 4.2.

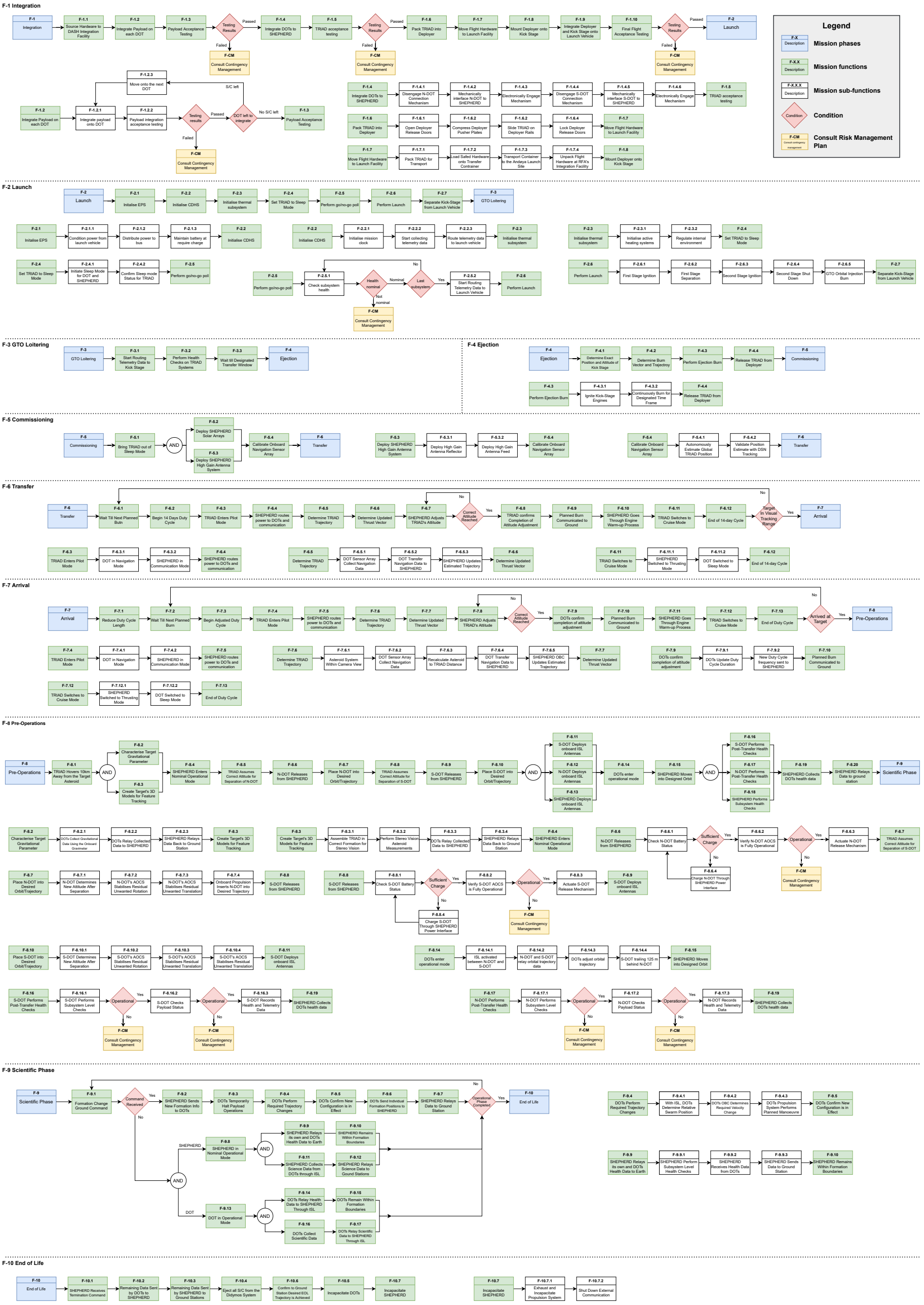

Figure 4.1: Functional flow block diagram (FFBD)

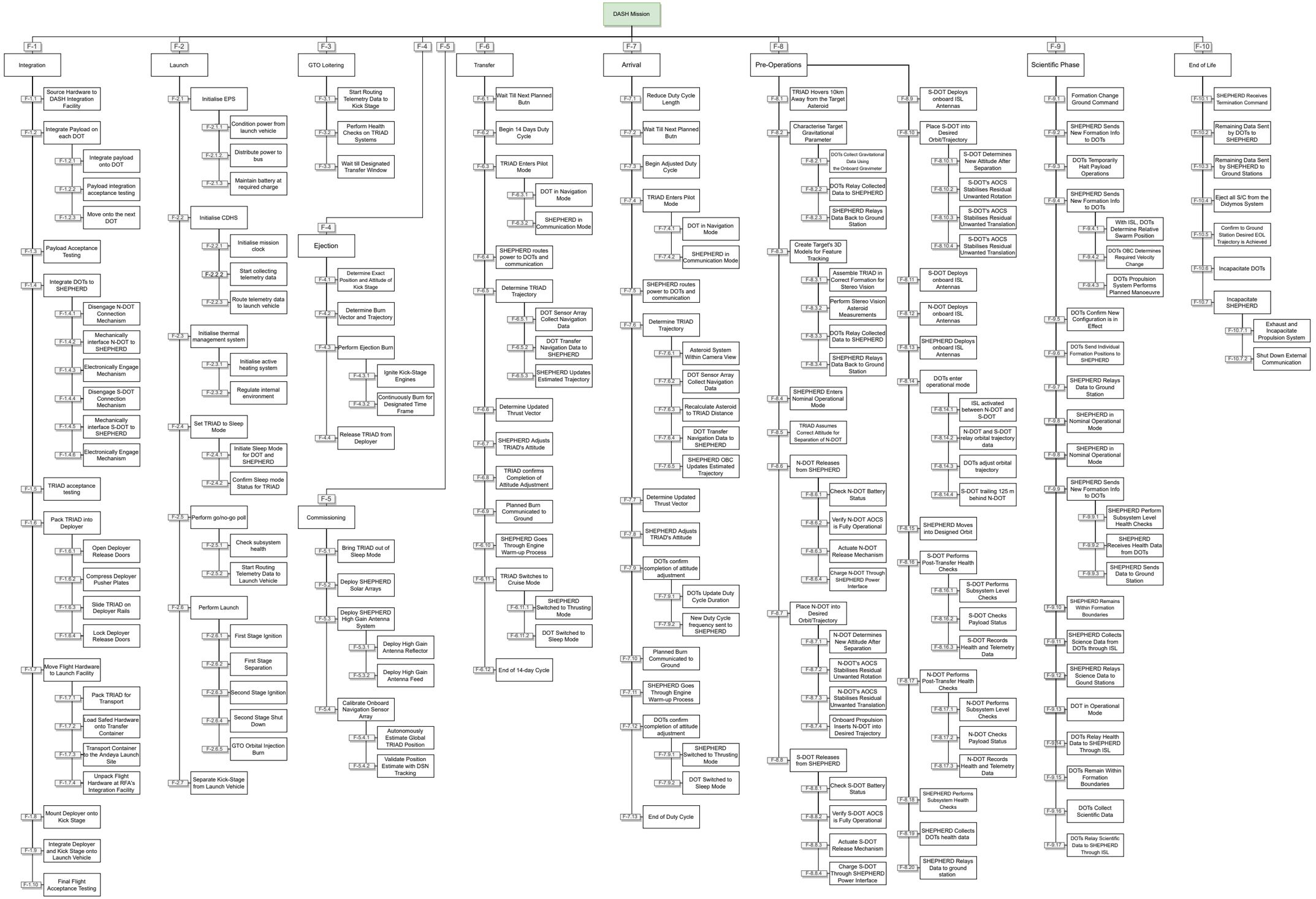

Figure 4.2: Functional breakdown structure (FBS)

5 Sustainability Strategy

The DASH team strives for a bright, clean future, and shares the sustainable vision of TU Delft. The decision to increase the weight of the sustainability score to the maximum in the mission concept trade-off reflects the team's commitment to designing a mission that preserves the needs of future generations as well as those of the planet. This chapter details all the strategies and guidelines used to make DASH as sustainable as possible, so that it does not have lasting adverse consequences. In these strategies and guidelines, all stages of the system development are considered, from definition to EOL.

5.1. UN Sustainable Development Goals

The 2030 Agenda for sustainable development, adopted by all United Nations Member States in 2015, defines 17 sustainable development goals (SDGs). A few of these goals addressed by the DASH mission have been identified and outlined in this section.

SDG 3 - Good health and well-being

The DASH team aims for the well-being and good health of all members and staff. As previously presented on our modus operandi in [5], team members must be able to keep doing their work while maintaining a healthy work balance. This means that the members must take their breaks, they cannot be expected to work late into the evening to avoid fatigue and decreased productivity in future work sessions. The completion of the design is a group effort, and therefore the group well-being is of utmost importance for a successful mission.

SDG 4 - Quality of Education

A successful mission brings great educational benefits. The scientific results obtained from the DASH mission will positively contribute to humanity's body of knowledge. With the generated knowledge from this mission, more about asteroid composition and exploration will be known. This knowledge will be carried for generations to come, enabling the future batch of engineers to develop more in depth missions that can contribute for human kind advancement. DASH is a space mission, and NEA exploration enabler.

Moreover, by bringing costs down and allocating a fraction of payload room on the DOTs for different mission needs, potential higher education projects can finally get access to deep space by piggybacking on future DASH missions or by funding their own entire mission once costs are low enough.

SDG 7 - Affordable and Clean Energy

The use of clean energy, including transportation to launch site, is preferred over less clean alternatives. To minimise the use of fossil fuels, clean alternatives are considered first, for instance the use of water plasma propulsion for the kick stage. When the use of fossil fuels can't be avoided, like for the launcher, other sustainability factors play a role in the decision-making, like the possibility of reusable parts for the launch vehicle or the origin and how the build materials were processed.

SDG 8 - Decent Work and Economic Growth

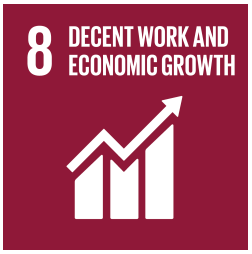

DASH is a NewSpace mission that brings together commercially available technologies and makes deep space exploration more available to the private sector. This creates employment opportunities and stimulates the economy, increasing

prosperity.

SDG 9 - Industry, Innovation and Infrastructure

The DASH mission seeks innovation and the widespread distribution of this information. The generated knowledge during this feasibility study will be properly documented and open sourced for ease of access in case repeatability is needed, or the project is transferred to a different team. The code developed in-house by the team will also be designed to be easily adapted for future similar applications.

DASH aims to demonstrate autonomous navigation and distributed space systems, and develop these technologies for use in the space flight industry. This stimulates growth for the industry and provides a starting point for further innovation in deep space exploration.

SDG 11 - Sustainable Cities and Communities

During the development phase, the DASH team will selectively choose sustainable communities and infrastructure over less sustainable options. This can be taken into account for instance when selecting testing facilities. A sustainable assessment shall be performed based on environmental impact to ensure the facilities vision on sustainability aligns with the sustainable goals established for DASH.

SDG 12 - Responsible Consumption and Production

When outsourcing any design parts or purchasing COTS parts from different manufacturers, a previous sustainability study shall be performed to ensure that the supplier's vision on sustainability aligns with the sustainable goals established for the DASH mission. Assessment can be based on supplier's environmental impact, for instance whether the material used for their product was sustainably processed with minimal social and environmental impact.

For in-house produced parts, the team must adhere to certain sustainability standards. A lean manufacturing philosophy is adopted where waste is reduced and value created. Measures such as, but not limited to, recycling chips from machined parts and other materials in general, reducing transportation of parts and assemblies, just in time production shall be adopted. The launcher environmental impact is considered based on the sustainability vision from supplier and reusability possibility, and the mass of the S/C is minimised to reduce the use of fuel. On an organisational level, reducing the team's footprint is also considered by not printing documents or report on paper and bring mugs to prevent use of single-use cups.

DASH's research is partially aimed at determining the interior of asteroids. This information can be used to support efforts to make asteroid mining a reality. The potential high concentration of rare metals in asteroids can provide a solution to resource depletion on Earth, and DASH will therefore contribute to the procurement of rare resources for future generations.

SDGs 14 & 15 - Life Below Water and On Land

The mission and its development's effect on the biosphere will be minimised. Therefore, no toxic fuels will be used during launch, as these may bring harm to animals or plant-life. Manufacturing and testing facilities will be placed in locations where they will have no impact on the local ecosystem. Toxic fuels such as liquid caesium and hydrazine, as well as nuclear materials for power generation, are discarded as they will produce toxic or nuclear waste. The launch will be performed in a location where the noise will minimally affect the local wildlife.

DASH will do research on the dynamics of Near Earth Asteroids, the data of which will be used to design planetary protection protocols in case an asteroid ever threatens to collide with Earth. In doing so, DASH is contributing to the protection of the Earth's ecosystems and wildlife, as well as human civilisation.

5.2. Sustainable Space Exploration

A highly important additional consideration for the sustainability of space mission is the prevention and mitigation of space debris. The importance of this lies in the preservation of the space environment for the needs of future missions.

This is of primary importance in Earth orbits, where many new missions will be planned and space is running out. The mission's main source of space debris in this environment are the first stages of the launchers, which will break off from the later stages in Earth orbit. Two options for the sustainable disposal of these stages are available: firstly, there is deorbiting the stage and allowing it to burn up in the atmosphere, and secondly, there is the option of making the stage reusable and returning it to Earth. Launch providers that provide either of these options are acceptable for performing a launch for DASH.

Table 5.1 gives an overview of the technical requirements from the ISO standard [33], as taken from the baseline report of the DASH mission [4], and the strategies that will be implemented to meet these requirements.

Table 5.1: Strategies to meet ISO sustainability requirements

ID	Requirement Summary	Strategy
DASH-ISO.01	No space debris released into earth orbit during operations.	Reentry of launcher stages or use of reusable launchers.
DASH-ISO.02	No more than two launch vehicle stages left in Earth orbit.	Reentry of launcher stages or use of reusable launchers.
DASH-ISO.03	No debris larger than 1 mm from pyrotechnic devices in Earth orbit.	Use of launchers that conform to this standard.
DASH-ISO.04	Probability of accidental break-up in Earth orbit less than 10^{-3}.	Robust design of interface between satellites and launcher.
DASH-ISO.05	Accidental break-up probability includes quantitive assessment of all relevant risks.	Comprehensive risk analysis for earth orbit phase.
DASH-ISO.06	Spacecraft and orbital launch stages that won't be re-entered into Earth orbit must be passivated at end of life.	All launcher stages will be re-entered.

The EOL strategy of the CubeSats must also be considered. There are three options: land the satellites on the asteroid, leave them in orbit around the asteroid, or send them into an escape trajectory from the asteroid. The first option minimises space debris, but this is of much less importance in deep space, given the sheer size of it. The drawback of this option is that it pollutes the asteroid and possibly inhibits future missions. The second option is similar to the first one in the sense that it is likely that eventually the satellites will collide with the asteroid and pollute it. Perhaps in orbit even more so than on the surface, they are likely to inhibit future missions. An even greater risk with this strategy is that the satellites may collide with each other, get damaged, and produce more space debris. The last option creates debris in deep space, but leaves the asteroid free of residue of the mission. As the removal of space debris from Didymos is deemed more important than from deep space, the last option is opted for. Additionally, the spacecraft will be passivated at the end of life to prevent cluttering of communication bands.

6
Risk Analysis

Once the mission concept of operations is determined, a technical risk analysis can be performed based on it. In this chapter, the risk types are identified and analysed, mitigation strategies are discussed for the risks and possible contingency management plans are performed. The technical risk varieties are presented in Section 6.1. After that, the risk assessment is shown in Section 6.2. Lastly, the mitigation strategies and contingency plans are shown in Section 6.3 and Section 6.4, respectively. In the third and fourth section, there are also risk maps which assist in visually representing the risks before and after mitigation strategies have been applied.

6.1. Risk Identification

It is possible to derive the types of risks by classing them in categories presented in this section. In this way, it is more convenient to manage those risks and to provide a mitigation and contingency plan for certain risks later in the process.

6.1.1. External Risks

External risks are related to risks that are introduced due to external factors of the project. There could be many examples of external contributions to the DASH mission specifically, which are introduced.

DASH-RISK.01 DSN causes problem with communication: There are possibilities that the DSN prioritises missions other than the DASH mission. This will cause scheduling issues such as unexpected changes in mission timeline, which will in hence alter the final launch date as well.

DASH-RISK.02 Launch failure: The launch profile itself could fail to reach the target orbit as well as the launch vehicle and launch vehicle payload failure which will result in failure of the launch as a whole. Launch failure could also happen elsewhere such as the upper stage or kick stage failing to initiate or activating at the wrong time, ultimately causing the escape trajectory to never be reached. This will also result in failure of the mission which is why launch failure is considered a risk.

DASH-RISK.03 Communities or media objecting the space mission: Even though the DASH objectives are clear and meaningful in regard to researching deep space asteroids in depth, there might be certain communities or media outlets objecting the space mission for a certain reason. It could be a factor related to the environment, in case it is an environmental organisation, among many other reasons. Even though they have a less influence on the confirmation of launch date in comparison to the more political organizations, which are introduced in the next risk, they could be a factor to hinder the mission timeline in general. This leads to them being a risk to the DASH mission.

DASH-RISK.04 Political Objections: For every launch made to outer space, it is necessary to get permission from government branches such launch date confirmation, the use of a certain orbital trajectory during launch, and many other factors. There are possibilities that these certifications could not be confirmed on the certain date range of launch planned by the group. In this case, the launch date will have to be done earlier or postponed. This will result in needing to modify the orbital calculations of the mission during launch which is a risk, especially if this occurs during the final phase of the design when all the verification and validation processes have been executed already.

DASH-RISK.05 Payload operation failure at the target asteroid: The main aim of space missions are to successfully operate the payloads at the target destination. The payload of the DASH mission is provided. Even though sufficient enough testing would have been done by the companies or entities providing the payload, there are still chances that failure of the payload would occur at the target asteroid. This is a risk that would bring failure to the mission.

DASH-RISK.06 COTS products: Most of the subsystem components for the Dash mission utilise

COTS products. Once the company and product is decided, request has to made to the company in order to order those products. In this process, it might be that the company is unable to fulfil the group's demands or that the manufacturing process of it takes longer than expected. In this case, delays in the mission happen, which leads this to being a risk towards the mission.

DASH-RISK.07 Manufacturing and Assembly Delay: After the design is completed, and the satellite itself has to be manufactured and assembled by a third party, risks might occur in this process. There could be delays in this process due to external factors imposed on the manufacturing segment, such as the COTS products not arriving in the scheduled time, insufficient amount of employees allocated to manufacture the product, and many more reasons. This is a risk to the DASH mission in the sense that it could result in delays to the launch date, and subsequently the mission timeline.

DASH-RISK.08 Provide of software: During the process of the design phase, verification and validation process, the use of external software might be demanded by the group. However, the software itself or the licence necessary to run the program might not be accessible within the scheduled time constraints. This will also cause delays at the design stage.

DASH-RISK.09 Test scheduling delay: Even though the verification and validation processes are planned in advance, certain delays might occur. They could be such that understanding the software documentation provided by the company could be more complex than expected, taking more time to be able to implement it with the design. Due to certain reasons, as the one mentioned previously, it could cause delay in the scheduling of the test which is also considered a risk to the entire mission design.

6.1.2. Environmental Risks

Environmental risks comprise every risk that is related to environmental situations. In the case of the DASH mission, it includes space environment as well, unlike missions done on Earth only.

DASH-RISK.10 Micro-impacts: During the transfer of the S/C from Earth to the target asteroid, there will be a time period present where the TRIAD will be exposed to space debris in LEO. When the craft is impacted by these particles, severe damage could occur to it depending on the size and impact velocity. Such damage will lead to failure in the mission even before reaching the targeting asteroid, which is why it is considered a risk.

DASH-RISK.11 Celestial impacts: During the computation of the trajectory calculation, considerations of celestial bodies will be made. However, there are chances where certain ones were not taken into account on accident. This, similarly to the micro-impacts, but the impact being way worse, will direct the mission to failure immediately.

6.1.3. Technical Risks

Technical risk is related to the technical aspects of the mission such as the design itself, the structure and many other factors.

DASH-RISK.12 Structural design insufficient: Insufficient structural design could happen if there are errors in the calculation of structural loads applied to the S/C structure. On top of that, not stiff and strong enough elements such as truss and beam structures could have been used as well. These could lead to risks such as the structure not being able to survive the launch loads or other severe load conditions that could emerge during the mission.

DASH-RISK.13 Error in trajectory calculation software: The DASH mission aims for the S/Cs accomplishment of autonomous transfer and trajectory adjustment during the transfer and at the target orbit. In order to do so, calculations of certain phases of the mission have to be programmed in. In this process, calculation mistakes might occur or wrong feedback loops could be implemented that could cause errors in the mission. This leads to this being a risk.

6.1.4. Operational Risks

Operational risk is the broadest concept among the categories used in this section. It includes the risks that can occur during the mission phase. It is also considered to be one of the most important risks to be handled, which means that thorough mitigation strategies should be introduced later on in the process.

DASH-RISK.14 Failure in separation of TRIADs from kick stage: The DASH mission is designed to piggyback on a selected launcher. After the launcher has reached the determined orbit, the TRIADs are planned to separate from the kick stage. In this process, failure might occur, such as the TRIADs separating prematurely or that the only one separates, that would result in failure of the mission.

DASH-RISK.15 Failure of solar panel deployment: After the TRIADs have been deployed successfully, the solar panels mounted on the SHEPHERD have to be deployed in order to provide sufficient power in order for the S/C to operate. In this process, failure might occur that would result in failure of the mission.

DASH-RISK.16 Failure of antenna deployment: After the TRIADs have been separated successfully, the antennas on the DOTs have to deployed in order to communicate with the SHEPHERD down and uplink to provide and gather information used to determine the housekeeping of the S/C, in order to ensure if the S/C is proceeding with the intended trajectory and many other aspects. If failure happens in the deployment of antennas, all these necessary processes can not happen, which will lead to failure in the mission.

DASH-RISK.17 Failure in propulsion module during transfer to target asteroid: After the deployment of the TRIADs, ion engines mounted on the SHEPHERD are used to transfer to the target asteroid. In this procedure, failure might happen due to reasons such as inaccurate thrust level management, the engine itself not switching on and off at the proper time, propellant not injected at the intended time, the entire mission. This will lead to failure of the entire mission, which is why it is considered a risk.

DASH-RISK.18 Loss of power during transfer: During transfer, a lot of situations can cause loss of power. One is the solar panel disconnecting or unexpected degradation rate due to unpredictable thermal environment of deep space. Apart from this, there are many more considerations that can be made. Therefore, this is considered a risk to the mission.

DASH-RISK.19 Loss of communication between SHEPHERD and DOTs during transfer: During transfer, communication is necessary among the DOTs and the SHEPHERD. The DOTs will collect required data for the navigation decisions. This data is relayed to the SHEPHERD using a physical connection. Furthermore, the thermal control system of the DOTs has heaters to manage the cold situations. If this communication fails on one DOT, this results in loss of power on that CubeSat, such that any active heating options are eliminated. This could be fatal for the DOT, but since navigation has redundancy over the DOTs, a critical mission failure would only result if both links are defective.

DASH-RISK.20 Insufficient pointing accuracy during transfer: During transfer, sufficient pointing accuracy is necessary in order to transmit housekeeping data to the DSN via downlink and obtain information about adjustments in the orbital trajectory of the TRIAD via uplink. In this process, failure could happen due to reasons such as navigation and ADCS failure. This will lead to failure of the entire mission, thus categorizing it as a risk.

DASH-RISK.21 Failure in DOT solar panel deployment: Once the TRIAD reaches the target asteroid, it separates into two DOTs and one SHEPHERD. In this situation, it is important that the two DOTs now have their own solar panels deployed in order to generate power to maintain in the asteroid orbit. If failure in deployment of the panels occur, it will lead to one or both DOTs failing to proceed in the mission.

DASH-RISK.22 Failure in DOT antenna deployment: Once the TRIAD is separated into two DOTs and one SHEPHERD, the DOTs send information which is collected data of the payload via short range communication nodes to the SHEPHERD. In this process, the present of antennas deployed for each DOT is necessary. If the failure of the antenna deployment occurs, it will lead to failure of

that DOT to succeed in transmitting payload data to the Earth.

DASH-RISK.23 Insufficient pointing accuracy of the DOTs and SHEPHERD during asteroid operations: Sufficient pointing accuracy is necessary in order to transmit collected payload data from the DOTs to the SHEPHERD or from the SHEPHERD to Earth using long range communication nodes. If failure happens for instance due to navigation and telecommunication failure, it will lead to failure of transmitting valuable data back to Earth which is one of the requirements of the mission and hence failure of the mission.

DASH-RISK.24 Loss of power of SHEPHERD or DOTs during asteroid operations: There are possibilities that the power system can fail during asteroid operations. It could be due to solar panel disconnection or unexpected degradation rate of it due to unpredictable thermal environment of deep space. However, the battery, which stores power to be used during when the Sun is not visible, could fail as well due to reasons such as circuit failure and excessive degradation. Lastly, failure of the power management and distribution system could fail as well, which means that each subsystem in the S/C would not be able to use the demanding amount of power during operation. In these cases, failure will occur in which insufficient amount of power is provided to either the SHEPHERD or DOT, or both, which will lead to failure of the mission.

DASH-RISK.25 Failure of command and data distribution to each subsystem: The CDHS is the subsystem that is in charge of distributing commands and data to different subsystems. However, failures such as microcontroller, flash memory and data storage might occur that leads to the failure in the subsystem. This will lead to the mission in a whole or partially failing, which is a risk.

DASH-RISK.26 Subsystem interface failure: The interface between the subsystems should be done as planned, with the inputs and outputs applied to a certain subsystem in order for the S/C to work as a whole. However, issues such as subsystem feedback loop error, input or output of each subsystem non-readable and code errors could cause this to fail. If this occurs, it will bring failure to the mission, which is why it is considered a risk.

DASH-RISK.27 TRIAD separation exceeds $5\,\mathrm{cm\,s^{-1}}$**:** During the separation of the SHEPHERD and the DOTs, the speed of the separation should not exceed $5\,\mathrm{cm\,s^{-1}}$ in order to stay in the capture orbit of Didymos, and also stay within ISL range of the DOT and the SHEPHERD. If this speed were to be exceeded, the DOT would not be able to be retrieved, which results of partial failure of the mission. Which is why it is considered a risk.

DASH-RISK.28 Failure of cold gas thrusters: During operations of all the CubeSats, one of the cold gas thrusters could fail. This would mean that keeping the correct orbit would not be able to be held, and the attitude and orientation of the CubeSat would no longer be able to be adjusted. Since this would mean failure of one of the CubeSats, it's considered a risk.

DASH-RISK.29 ISL communication loss after separation: After separation of the TRIAD into one SHEPHERD and two DOTs, ISL communication has to happen among them or even between the 9 CubeSats the DASH mission possesses. Throughout this process, payload, housekeeping and navigation data can be relayed to Earth in a convenient matter. If ISL communication is loss, which could be caused for instance due to inaccurate pointing accuracy between the 2 satellites communicating, it could result in failure for transmitting information to Earth which is one of the main aims of this mission. Therefore, this is considered a risk.

6.1.5. Regulatory Risks

Regulatory risks are related to regulations settled upon by certain organisations such as the government or the UN which is obligatory for the group to comply with.

DASH-RISK.30 Space debris regulations change: Certain space debris regulations exist that have to be followed when the mission is conducted. The design of the systems are also made based on these regulations. However, if there is a possible space debris regulation change, this will cause delays in the finalising of the design, which is considered a risk.

6.2. Risk Assessment

Now that the risks have been identified, they have to be assessed. For the main method in order to carry out the assessment of technical risk analysis, a method called Technical Risk Assessment Methodology (TRAM) [37] is used. Each risk has been given a method of assessment, a probability, and the severity of the impact. Regarding the method of assessment, there are four methods considered; comparison to other missions, decomposition of the risk, theoretical modelling and mock-up construction. For the probability, this is divided in four levels; almost no chance, unlikely, likely and very likely. Regarding the risk severity, this is also divided in four levels; negligible, moderate, critical and catastrophic. The table containing all the information related to these are shown in Table 6.1.

Risk Type	Assessment Method	Risk probability	Risk severity
DASH-RISK.1	Comparison	unlikely	critical
DASH-RISK.2	Comparison	unlikely	critical
DASH-RISK.3	Decomposition	almost no chance	moderate
DASH-RISK.4	Decomposition	unlikely	moderate
DASH-RISK.5	Decomposition, Theoretical Modelling	unlikely	critical
DASH-RISK.6	Comparison	almost no chance	moderate
DASH-RISK.7	Decomposition	likely	moderate
DASH-RISK.8	Decomposition	unlikely	moderate
DASH-RISK.9	Comparison	likely	moderate
DASH-RISK.10	Theoretical modelling	almost no chance	critical
DASH-RISK.11	Theoretical modelling	almost no chance	catastrophic
DASH-RISK.12	Theoretical modelling	unlikely	critical
DASH-RISK.13	Theoretical modelling	unlikely	critical
DASH-RISK.14	Theoretical modelling	unlikely	catastrophic
DASH-RISK.15	Mock-up construction	unlikely	catastrophic
DASH-RISK.16	Mock-up construction	unlikely	catastrophic
DASH-RISK.17	Theoretical modelling	unlikely	critical
DASH-RISK.18	Theoretical modelling	unlikely	critical
DASH-RISK.19	Theoretical modelling	likely	critical
DASH-RISK.20	Theoretical modelling	likely	critical
DASH-RISK.21	Mock-up construction	unlikely	catastrophic
DASH-RISK.22	Mock-up construction	unlikely	catastrophic
DASH-RISK.23	Theoretical modelling	very likely	critical
DASH-RISK.24	Theoretical modelling	unlikely	critical
DASH-RISK.25	Decomposition, Theoretical modelling	unlikely	critical
DASH-RISK.26	Decomposition, Theoretical modelling	unlikely	critical
DASH-RISK.27	Theoretical modelling	likely	critical
DASH-RISK.28	Mock-up construction	unlikely	critical
DASH-RISK.29	Theoretical modelling	very likely	critical
DASH-RISK.30	Comparison	unlikely	moderate

Table 6.1: Risk Analysis assessment

The assessed risks can also be shown in a risk map in Figure 6.1. In this, there are four colours presented. For clarification, the red box indicates risks that have to compulsory be mitigated. Without any mitigation strategy for these risks, the DASH mission can not be continued on the launch plan date and have to be delayed, or in the worst case scenario, terminated. For the research and inspection boxes, during the mitigation process, they should be examined and strive to mitigate if strategies exist. Lastly, for the green boxes, they are considered acceptable without any mitigation's necessary.

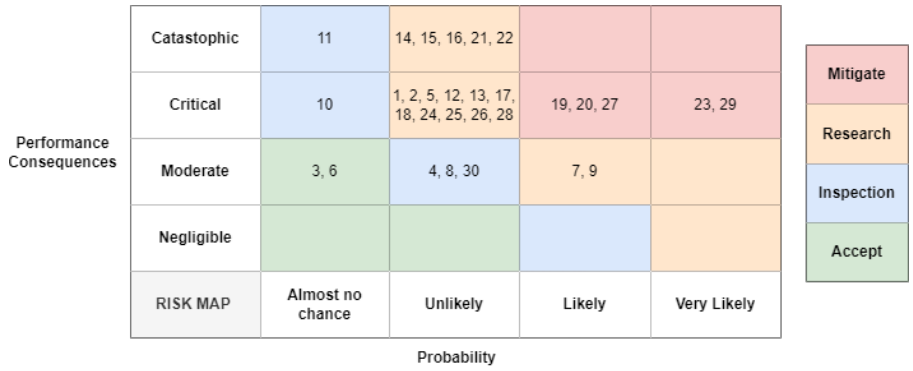

Figure 6.1: Risk Map of Risks before risk mitigation measures

6.3. Mitigation Strategies

Once the risks have been assessed, mitigation strategies must be provided, which is the main goal of this chapter. Mitigation strategies can be grouped into four categories: accepting and monitoring, avoiding and reducing, transferring, and removing. Risk acceptance occurs when the risk occurrence probability is not effected much by actions taken by the DASH mission. Examples of risk avoiding are modifying or constraining software requirements in order to reduce the risk. The involvement of a third party is considered transferring the risk, as the responsibility for ensuring compliance is either shared with third parties and the DASH group or completely given to them. Using COTS is a risk transferring strategy as well, as the manufacturer, which is also considered a third party, will have to ensure component specification and performance. Lastly, removing is used when the risk assessed seems to be inapplicable in a later stage. In the situation of the DASH mission, most risks will be considered accepted than removed. The Table 6.2 shows the mitigation strategies for each risk assessed.

Table 6.2: Risk mitigation strategies

Risk Type	Mitigation Strategy
DASH-RISK.01	Transfer by outsourcing the verification and validation
DASH-RISK.02	Transfer by outsourcing the verification and validation
DASH-RISK.03	Accept and monitor
DASH-RISK.04	Accept and monitor
DASH-RISK.05	Transferring by outsourcing the verification and validation
DASH-RISK.06	Transfer to the company the responsibility to provide the COTS in the scheduled time
DASH-RISK.07	Transfer by assuring the companies to finish this process in the scheduled time
DASH-RISK.08	Transfer by to the company the responsibility to provide the software in the scheduled time
DASH-RISK.09	Avoiding by giving applicable constraints to the software
DASH-RISK.10	Accept and monitor
DASH-RISK.11	Accept and monitor
DASH-RISK.12	Avoid and reduce by ensuring sufficient review of the structural load calculation
DASH-RISK.13	Avoid and reduce by ensuring correct trajectory calculation
DASH-RISK.14	Avoid and reduce by ensuring the separation mechanism is properly installed
DASH-RISK.15	Avoid and reduce by ensuring the panel deployment mechanism is properly installed
DASH-RISK.16	Avoid and reduce by ensuring the antenna deployment mechanism is properly installed
DASH-RISK.17	Avoid and reduce by ensuring the propulsion module is properly installed
DASH-RISK.18	Avoid and reduce by ensuring the power supply is properly installed
DASH-RISK.19	Avoid and reduce by ensuring the telecommunication components are properly installed
DASH-RISK.20	Avoid and reduce by ensuring the telecommunication and ADCS components are properly installed
DASH-RISK.21	Avoid and reduce by ensuring the panel deployment mechanism is properly installed

Table 6.2 continued from previous page

Risk	Mitigation Strategy & Explanation
DASH-RISK.22	Avoid and reduce by ensuring the antenna deployment mechanism is properly installed
DASH-RISK.23	Avoid and reduce by ensuring the telecommunication and ADCS components are properly installed
DASH-RISK.24	Avoid and reduce by ensuring the power supply is properly installed
DASH-RISK.25	Avoid and reduce by ensuring the CDHS components are properly installed
DASH-RISK.26	Avoid and reduce by ensuring the interface system is properly installed
DASH-RISK.27	Avoid and reduce by ensuring the separation mechanism is stably installed
DASH-RISK.28	Avoid and reduce by ensuring the cold gas thrusters are properly installed
DASH-RISK.29	Avoid and reduce by ensuring ISL communication is properly installed
DASH-RISK.30	Accept and monitor

Based on the mitigation strategies introduced above, the new risk map is shown in Figure 6.2. It can be shown in the figure that all the risks that were initially in the red box, the mitigation necessary section, have been moved to a different colour. This states that the risks have been mitigated. On top of that, there are risks that were moved as well to a less probability box.

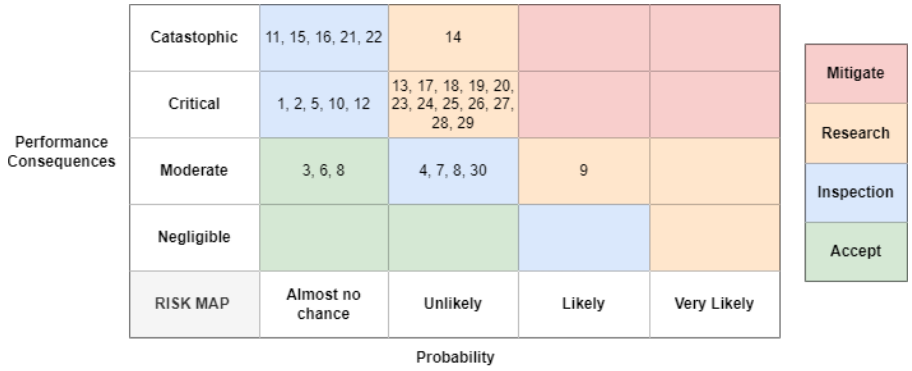

Figure 6.2: Risk Map of Risks after risk mitigation measures

6.4. Contingency Plan

Now that the mitigation strategies have been introduced, one last step, which is introducing the contingency plans must be done. Eventhough mitigation strategies have been applied to risks, they might not have a significant effect on it. When the risk reappears in this situation, contingency measures are demanding in order to reduce the impact of the risk and probability of occurrence. This might also lead in removing the risk totally, which is the best scenario. In Table 6.3, the contingency actions to be taken with respect to each risk is described. In the big sense, all the contingency plans have been implemented by decreasing uncertainty in the design, change the specification values or modify the design partially in order for improvement. Future adjustments could be made in this once more detailed investigation of the mission has been made, in which a better solution could be determined.

Table 6.3: Risk Contingency plans

ID	Contingency Strategy
DASH-RISK.01	Consult with the DSN in order to check the availability during the mission.
DASH-RISK.02	Assure reliability of the launch vehicle with the provider company normally.
DASH-RISK.03	Provide statements will convince the communities and media to agree with the mission.
DASH-RISK.04	Prepare statements that will convince the political objections once a certification.

Table 6.3 continued from previous page

Risk Type	Contingency Strategy
DASH-RISK.05	Keep track of the payload which failed and determine the extent of functionality loss.
DASH-RISK.06	Come up with at least one alternative of COTS product for each subsystem.
DASH-RISK.07	Consult with the manufacturing company to assure the process is going as planned.
DASH-RISK.08	Make sure to come up with at least one alternative software type that could be used.
DASH-RISK.09	Assure theoretical understanding of the software is thoroughly done by all the groups for their own subsystem.
DASH-RISK.10	Test all components to analyse the impact of the space debris. Analyse potential subsystem shut-off due to critical damage.
DASH-RISK.11	This would be a catastrophic failure, no contingency possible.
DASH-RISK.12	Investigate which structure parts has issues and analysis if it is acceptable.
DASH-RISK.13	Test the software of the subsystems affected, check potential for software fixes.
DASH-RISK.14	This would be a catastrophic failure, no contingency possible.
DASH-RISK.15	This would be a catastrophic failure, no contingency possible.
DASH-RISK.16	This would be a catastrophic failure, no contingency possible.
DASH-RISK.17	Investigate which component in the module causes an error and try to implement fixes.
DASH-RISK.18	Test all power components suffering issues, assess the damage, implement the power diversion or subsystem shut-off.
DASH-RISK.19	Try re-establishing communication within a 10-minute time interval by sending a signal to the calculated position of the SHEPHERD and DOTs.
DASH-RISK.20	Investigate additional power applied in order to operate the ADCS or navigation subsystem to adjust the pointing accuracy and apply.
DASH-RISK.21	This would be a catastrophic failure, no contingency possible.
DASH-RISK.22	This would be a catastrophic failure, no contingency possible.
DASH-RISK.23	Investigate additional power applied in order to operate the ADCS or navigation subsystem to adjust the pointing accuracy and apply.
DASH-RISK.24	Test all power components suffering issues, assess the damage, implement the power diversion or subsystem shut-off.
DASH-RISK.25	Update software with better algorithms if possible or place processing limiters.
DASH-RISK.26	Investigate normally which subsystem is not receiving or transmitting signals to other ones and try to implement fixes.
DASH-RISK.27	Determine course adjustment ΔV required and implications.
DASH-RISK.28	Investigate which component in the propulsion unit causes an error and try to implement fixes.
DASH-RISK.29	Try re-establishing communication within a 10-minute time interval by sending a signal to the calculated position of the S/C.
DASH-RISK.30	Keep track on the modifications of the regulations normally.

7

Trajectory Optimisation

Determining an optimal trajectory is an integral part of the design of a space mission. The DASH architecture specifies the use of ion propulsion during the transfer from Earth to the target asteroid. This requires a deep dive into the astrodynamics aspect of the DASH mission during transfer to be able to completely characterise and optimise the trajectory that will be taken.

As the initial trajectory devised by the DASH mission used an impulsive burn to get to Didymos, and corresponding array sizing based on preliminary calculations, it must be noted that impulsive burns are not feasible with current ion engine technologies. Thus, the need for a simulation which takes into account continuous thrust and adjusts the thrust vector based on a varying trajectory becomes of paramount importance at this stage of the design. The trajectory optimization done by DASH in this chapter will lead to a fully defined trajectory which takes into account factors such as panel size available, fuel mass, the specific ion thruster characteristics, and the wet mass of the TRIAD.

Starting from Section 7.1, the simulation methodology and assumptions are documented. Though there are two simulations that were run for the DASH mission (one used to determine general engine characteristics to look for, and the other used a specific engine with Mars gravity assist), the underlying assumptions remain the same and methodologies still remain the same. Then the trajectories are simulated, and a final one is chosen with the best performance. Finally, in Section 7.2, the verification and validation of the simulation is discussed.

7.1. Astrodynamics Optimisations

The optimisation simulation is discussed in this section. Starting with the assumption followed by the methodology prescribed, the flow of information throughout the simulation is adumbrated. Once all the data has been collected, the best engine and best trajectory for that engine is taken and refined for use as the final DASH transfer trajectory. The engine parameters which must be adhered to are discussed in Section 7.1.2, a list of feasible engines are procured and then one chosen in Section 8.2.2. This allows for the optimal trajectory simulations, in Section 7.1.3, to be run for only the one engine due to the high computational effort required. Found trajectories are then screened and the best one chosen in Section 7.1.4. Though the simulation is run without a Mars gravity assist at the beginning for engine selection, the general assumptions and methodologies are still applicable to the more complex simulation which includes a Mars gravity assist.

In summary, the trajectory simulation is used as a simplified version, with no Mars gravity assist, to first aid in determining general engine characteristics, and then to compare the list of procured engines, found using the aforementioned general characteristics as criteria. Once an engine is chosen, the RIT-μX, Mars gravity assist is implemented and multiple possible trajectories are found. From all found trajectories, one is chosen and fully characterised.

7.1.1. Assumptions

The simulation performed for finding the optimal trajectory has limitations which have to be acknowledged in order to correctly interpret and use the results generated. Furthermore, understanding the model assumptions is key to identify the limits and applicability of the conclusions drawn. The assumptions taken for the simulation model are described and subsequently their effects on the final generated results are explored. The assumptions taken are shown below.

- Only the gravitational attraction between the spacecraft and the Sun is considered.
- The simulation starts just outside the sphere of influence of the Earth.
- No degradation of the solar array cells over the simulation epoch.
- Thrust levels do not change in between simulations segments, rather only at the start and end

of each segment.
- No Mars Flyby considered at this stage

Gravity effects of other planets are present in the actual mission, however such effects are assumed to be negligible as the sun is a major contributor in comparison. Similarly, as the simulation starts outside the sphere of influence of the Earth, it is assumed that the launch vehicle will be able to provide the required Delta-V to leave this sphere of influence in the first place. As such, excess velocity outside the sphere of influence of the Earth and used in the program added will have to be taken after complete depletion of the launch vehicle tanks. In regard to the segments selected for simulation, thrust levels do not vary once the segments have been made and as such, thrust remains constant during the time frame of the respective segment. The effect of this assumption is directly relevant to simulation accuracy and precision, and is addressed by using course meshes early on and using finer meshes once only a few trajectories need to be simulated. This is seen as an advantage in terms of time and computing power efficient as t allows for many iterations in a short period of time. The last assumption is of the lack of a Mars flyby at this stage of the design. As Mars is more than likely to be in the path of the Shepherd to Didymos, a potential gravity assist will be considered once engine selection has been performed and an engine with favourable characteristics is chosen. A gravity assist is seen to be very beneficial and only stands to improve upon estimated values obtained from ion trajectory optimisation.

7.1.2. Methodology

The program used to determine the optimal trajectory for the DASH mission is primarily derived from an M-ARGO mission simulation for ion engine thrust burns during transfer. The inputs to the code have also been adjusted accordingly, as shown in Table 7.1. The changes implemented were including adding multiple engines for thrust and Isp calculations, adjusting the constraints, and adding more variables to the decision vector. Multiple engines were simulated by running iterations on each of them separately. All engines had power-thrust and power-Isp relations, with lower and maximum limits set on performance based on specification sheets found. The lower and upper bounds used in the simulation are outlined below in Table 7.2 with reference to the variable being constrained.

Table 7.1: Simulation inputs and descriptions

Input Variable	Variable Name	Description
Target	target	Didymos system is the target for DASH
Number of segments	n_seg	Number of discretization used for Taylor propagation
Departure timeframe	t0	range of days from which departure from Earth is done
Time of flight ranges	tof	how long the spacecraft s allowed for flight
Final mass	m_f	Final dry mass excluding panel mass of the propulsion unit
Power efficiency	eff	Chosen as 90%
Grid type	grid_type	Chosen as a uniform grid for segments
Panel specific mass	specific_mass	Chosen as 2.8 kilograms per square meter of panel area
Engine chosen	engine_num	an integer input that selects which engine to use for calculations

Table 7.2: The upper and lower bounds of the trajectory simulation variables

Variable	Lower	Upper
Departure date from 1 Jan 2000 (days)	8900	9200
time of flight (days)	200	1096
Panel Area (m^2)	0	9
Propellant mass (kg)	0	10
Relative velocity at Earth ($m\,s^{-1}$)	-5000	5000

In Table 7.2 the relative velocity at Earth is determined by the excess velocity that can be provided by the launcher and kick stage. This also depends on the initial mass of the DASH mission in

the launch vehicle, as such some iteration and fine-tuning will be necessary to adjust the allowable excess velocity. The variables in the table also compose the decision vector used in the simulation. There are a total of 7 decision variables, as the relative velocity variables have an x, y, and z component. Additionally, depending on the total number of segments and additional 3 variables are added for every segment which determines the thrust component in the x, y, and z axis. Initial runs of the program allow for an expected range of values with regard to engine performance to be procured. Things such as expected order of magnitude for thrust level, power level, and I_{sp} were determined. Off the shelf ion engine selection from various companies was then done by filtering out engines which do not fit the expected performance during transfer. A summary of the orders of magnitude expected for engine performance is shown in Table 7.3. Dimensional limitations are also included if present at this stage. A more detailed look into the specific engines chosen for simulating is presented in chapter 8.

Table 7.3: Expected orders of magnitude for Engine performance

Engine Specification	Lower	Upper
Isp [s]	750	4500
Power [W]	0	800
Thrust [mN]	0.5	25
Engine Bounds Radius [cm]	0	20

The program starts by randomly choosing the variables to be selected, with a focus on the objective variable of the initial mass being minimised as the goal. With every iteration of the program. Once the objective value has converged and the change is minimised to below the threshold set, it is repeated for a set number of times to get a substantial data set to represent the engine's performance adequately. Once this is done, the data sheet is saved and the whole process repeated for the remaining engines. Once all the simulations have been run, the data is filtered out for anomalies, the best engine is selected, the bounds adjusted, and a finer mesh is used to find the final trajectory for the DASH mission. This process is outlined in greater detail in Section 7.1.3.

7.1.3. Optimal Trajectory

The optimal trajectory is chosen by compiling all engine data and their respective successful trajectories. The data is sifted through to find the engine with the best combination of initial mass, propellant volume, and panel area. These factors will be used to determine which engine is to be simulated again with finer meshes to get a more accurate and precise delta-V estimates. Additionally, at this stage, a Mars gravity assist is implemented.

Similarly to Section 7.1.1, the assumptions all hold, except for the lack of a Mars flyby. Instead, a lower limit of the viable distance from the surface of Mars for flyby is used, this limit is 169 km from the surface of Mars or 5% of the radius of Mars. The simulation inputs are also adjusted to include a Mars flyby, with additional inequalities provided to restrict free variables.

Table 7.4: Additional simulation inputs and descriptions for MArs gravity assist

Input Variable	Variable Name	Description
Flyby Planet	flyby	Mars planet used for gravity assist
Power transfer efficiency	eff	Chosen as 90%
Relative velocity at Mars	fb_rel_vel	Relative velocity magnitude limit at Mars to restrict flyby
Initial at Earth	initial_vel	Initial velocity magnitude limit at Earth imposed by rocket and kick stage

Due to the way the Mars flyby was coded, an additional inequality was added, which restricted the combined total fuel mass used during transfer to Mars from Earth and to Didymos from Mars to 5 kilograms total.

The decision vector in this case is much larger with 6 needed for Mars flyby velocity parameters, 3 for earth velocity parameters, 2 for time of flight, 2 for propellant, one for initial departure time, and one for panel area. This brings the total to 15 elements in the decision vector, more than double what is used in the simple model with no Mars flyby considerations. This, as expected, takes much longer to run and find feasible trajectories to the tighter imposed bounds. As such, Mars gravity assist is only used once engine selection has been narrowed down.

Table 7.5: The updated and additional upper and lower bounds of the trajectory simulation variables

Variable	Lower	Upper
Departure date from 1 Jan 2000 (days)	9000	9130
time of flight (days)	240	910
Panel Area (m^2)	0	1.2
Propellant mass (kg)	0	5
Relative velocity at Earth ($m\,s^{-1}$)	-6000	6000
Relative velocity at Mars ($m\,s^{-1}$)	-14000	14000
Lowest allowable altitude for Mars flyby (km)	170	-

For the optimal trajectory simulations, the M-ARGO RIT-μX engine was chosen, as can be seen in Section 8.2.3. To provide more varying trajectory options, the arrival time was also extended from December 2026 to June 2027,an addition of 6 months. The compiled trajectories can be seen below in Table 7.6.

Table 7.6: Optimal trajectories and their arrival data

Departure	Arrival	Transfer	Panel Area	Fuel Mass	Engine Delta-V	Flyby Gain
30 Oct 2024	12 Apr 2027	894 days	1.06 m^2	1.77 kg	917.74 $m\,s^{-1}$	561.74 $m\,s^{-1}$
20 Oct 2024	09 May 2027	930 days	1.17 m^2	1.58 kg	807.54 $m\,s^{-1}$	726.78 $m\,s^{-1}$
30 Oct 2024	03 Mar 2027	854 days	1.16 m^2	1.73 kg	931.90 $m\,s^{-1}$	529.80 $m\,s^{-1}$
22 Sept 2024	27 May 2027	977 days	1.18 m^2	2.62 kg	1306.94 $m\,s^{-1}$	1513.57 $m\,s^{-1}$

As can be seen in Table 7.6, all launches which occur in October have similar fuel masses and panel areas found. This also corresponds to a similar range of Delta-V used by the ion engine. The notable exception is the trajectory with a launch which occurs near 2 months prior to those in October, 22 September 2024. A Delta-V increase of 499.4 $m\,s^{-1}$ is seen as a result of this earlier launch window. Another factor to take into account is that the bus to be chosen has a maximum fuel capacity of 2.1 kg. With a 10 % margin of fuel[72], total fuel mass comes to 1.738 kg taking the trajectory with the least amount of fuel used, which is well less than the limit. An additional observation is that, by looking at the launches in October 2024, a larger Delta-V gained from the Mars gravity assist results in a lower Delta-V provided by SHEPHERD and subsequently a lower fuel mass used to get to Didymos. This entails that future advances of the trajectory code are recommended to improve upon the gravity assist to find one which maximises the flyby Delta-V gained.

7.1.4. Chosen Trajectory

The chosen trajectory will be done by selecting that with the lowest initial wet mass of the TRIAD. The dry mass of the TRIAD excluding the solar panel is kept at a constant of 53 kg for all trajectories. Once the trajectories produce a corresponding panel area and fuel mass, the total wet mass can be calculated and the best trajectory chosen.

Table 7.7: Transfer trajectories and initial mass

Arrival Date	Fuel Mass (kg)	Panel Mass (kg)	TRIAD Wet Mass (kg)
12 Apr 2027	1.77	2.96	57.74
09 May 2027	1.58	3.27	57.85
03 Mar 2027	1.73	3.26	58.08
27 May 2027	2.62	3.31	58.93

From Table 7.7 it can be seen that the trajectory with the lowest mass is the trajectory which arrives on April 2027, highlighted in green. An additional condition which greatly helped in choosing this trajectory is the size of the solar panel. The trajectory's power model use conservative estimates for the power model of the SHEPHERD. As the courier bus panels are more efficient, once these efficiencies have been accounted for, panel areas calculated can be decreased by 16.7%. With the courier bus being able to provide a solar panel area of 0.8 m^2 (customisable depending on customer requirements) and the April trajectory panel area decreasing to 0.883 m^2, this represents an increase of 10.3% upon the courier solar area.

Table 7.8: Optimal trajectory Timeline and relevant parameters

Trajectory Parameter	Date/Velocity	Time from transfer start
Earth Departure date	30 Oct 2024	+0 days
TRIAD Earth Velocity	5998.15 m s^{-1}	+0 days
Mars Flyby	18 Mar 2025	+138.42 days
TRIAD Flyby Velocity	8796.12 m s^{-1}	+138.42 days
Mars Flyby Gain	561.74 m s^{-1}	+138.42 days
Arrival Date	12 Apr 2027	+893.66 days

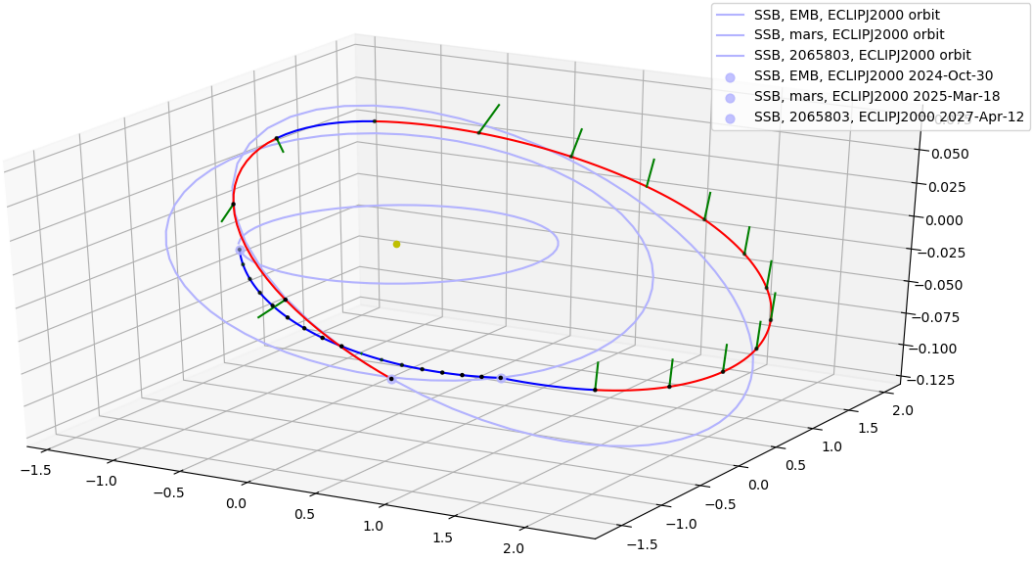

Figure 7.1: Mars gravity assist trajectory for arrival at April 2027 with the lowest panel area found. Red trails represent segments with thrust and blue represent segments with no thrust. It should be noted that the axes are not to scale, which especially causes the inclination to be highly exaggerated

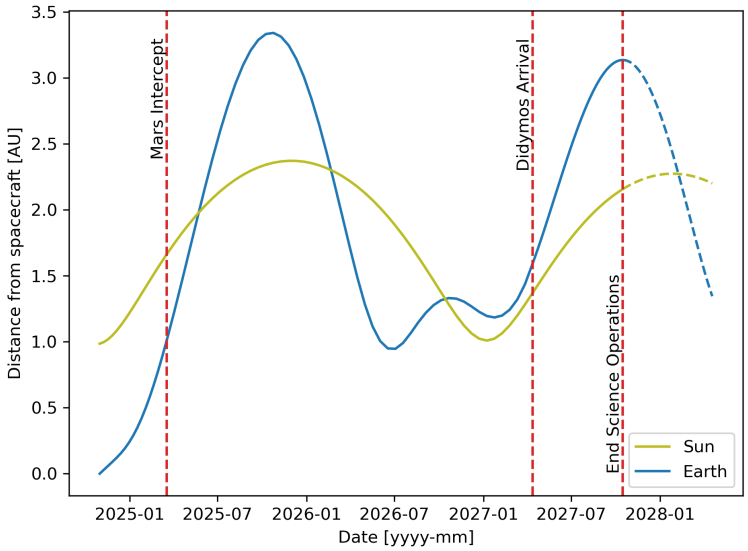

Figure 7.2: Distance to Earth and Sun during the mission

Figure 7.1 shows the trajectory for arrival date of April 2027. The corresponding distances to the Earth and Sun are shown in Figure 7.2. It can be seen that the ion engines are not operational to a large extent during transfer until the TRIAD performs the Mars gravity assist. This occurs as the initial Delta-V given is in a specific orbital plane to the TRIAD, such that transfer to Mars occurs without needing much thrust from the ion engines. Once at Mars, an additional Delta-V is obtained due to flyby. From Table 7.8, the TRIAD velocity is stated as 8796.12 m s^{-1}. The absolute velocity does not change before and after the gravity assist has been performed. Rather, as can be seen in Figure 7.1, the velocity components are altered at Mars causing the aforementioned orbital plane change and resulting in a Delta-V gain of 561.74 m s^{-1}. The change in the individual velocity components can be seen in Table 7.9. This orbital plane is now more aligned with the trajectory of Didymos. Additionally, once Mars flyby has occurred, the thrust vectors from the ion engine become more prominent. By summing the burn segment durations, red trails in Figure 7.1, the total thrust on time is determined to be 660.84 days in total. This means that the thruster model is operational for 74% of the entire transfer duration. Summing the engine Delta-V of 917.74 m s^{-1} for the chosen trajectory and the Mars flyby gain brings the total trajectory Delta-V to 1479.48 m s^{-1}.

Table 7.9: Velocity components for Mars gravity assist

	Initial Velocity (m s^{-1})	**Final Velocity (m s^{-1})**	**Change (m s^{-1})**
X component	6434	6612	+ 178
Y component	-5997	-5769	+ 228
Z component	-134	-615	- 481

The final fuel mass, panel area, and initial wet mass for the TRIAD is provided below in Table 7.10. All of these values are, including a margin, and will be used from here on for further calculations in other relevant subsystems. With further iterations and more refined bounds, a better trajectory can be potentially found given a large enough population sample for the algorithm to run optimization on.

Table 7.10: Trajectory optimisation DASH budgets

SHEPHERD

Parameter	**Value**	**Unit**
Panel Area	0.883	m^2
Panel Mass	2.472	kg
Fuel Mass	1.947	kg
Dry Mass	15.472	kg
Wet Mass	17.419	kg

DOT

Parameter	**Value**	**Unit**
Total Mass	20	kg

TRIAD

Parameter	**Value**	**Unit**
Dry Mass	55.472	kg
Wet Mass	57.419	kg

7.2. Verification and Validation

The trajectory simulation program, as all other code, needs to undergo proper verification and validation procedures. In this section, procedures which were performed for this report will be discussed and potential for improvement will also be explored. The methods will be covered in a qualitative manner, to describe the process of verifying adequately.

Starting with verifying the results, each of the optimal trajectories ran were checked to ensure that there are no discontinuities present. As the program is designed to run a forward and backward segment to ensure convergence of generated trajectories, while the masses and solar panel area may match, the trail left by the TRIAD may not connect. The trajectory solutions with these ”jumps” during transfer were filtered out, both by automatic checking and manual checking of the trajectory plot. Checks were also performed to ensure that solutions are near the theoretical limitations of Delta-V.

Simulations with too low of a Delta-V were checked to ensure the correct engine parameters and power model has been implemented. This includes producing graphs for the thrust-power and I_{sp}-power curves for each engine to be verified individually to be within the bounds specified by each

engine specification sheet.

Another aspect of code testing that was performed was setting the lower and upper bounds to extreme conditions and analysing the behaviour of the algorithm. As expected, bonds which were not set properly or had their signs flipped automatically yielded failed optimisations. Additionally, when unrealistic permitted values of fuel, such as 0 kg upper and lower bound were used, the trajectory failed to converge as expected even whilst maintaining feasible solar panel areas and initial velocities. This extreme value test applied to panel area, initial velocity, allowed Mars flyby velocity, and most importantly the thrust vectors. Setting the thrust vectors to only point in a specific direction, represented in a 3 dimensional vector, led to completely unfeasible trajectories as the engine would not be able to adjust its direction. In short, all variables that were altered, and expected to yield unfeasible results, did so as intended when checking the implementation of the changes upon the original M-ARGO trajectory simulation.

An added layer of verification was that the simulation program was derived from the M-ARGO ion propulsion trajectory model. This allowed the DASH team to implement minimal changes, using the provided documentation, to the code as the underlying process and core calculation should already be verified and validated for the M-ARGO mission. The team's task was to mainly alter the performance characteristics and inputs of the model to better fit the DASH architecture. This is also applicable to the Mars trajectory code, as the underlying procedures and equations to include a gravity assist were already implemented in the library used.

The gravity assist is a key aspect of the trajectory of this mission and was also verified manually. Given the in and out velocity vectors chosen by the optimiser, the angle between asymptotes is determined to be, 176.3° which means a 3.66° change in the trajectory. The total effective Delta-V provided is 562 m s^{-1} at an eccentricity of 31.32 and semi-major axis of -553.5×10^3 km. This results in a periapsis of 16 782 km which is far more than necessary to avoid Mars's atmosphere. These calculations are done using the following equations.

$$\theta_\infty = 0.5 \arccos\left(\frac{-\vec{\boldsymbol{v}_{\infty,1}} \cdot \vec{\boldsymbol{v}_{\infty,2}}}{\left|-\vec{\boldsymbol{v}_{\infty,1}}\right| \left|\vec{\boldsymbol{v}_{\infty,2}}\right|}\right) \tag{7.1}$$

$$e = \frac{1}{\cos\theta_\infty} \tag{7.2}$$

$$a = \frac{-\mu_{mars}}{\left|-\vec{\boldsymbol{v}_{\infty,1}}\right|^2} \tag{7.3}$$

$$r_p = -a(e-1) \tag{7.4}$$

A final layer of verification and arguably the most crucial still needed to be performed on the DASH code, and that is to compare the results with that of another independent program. Even with high confidence in the current obtained result due to the strong foundation of using M-ARGO code as a base, verifying convergence of results using other simulations is yet to be done. It is recommended to use an open source deep space continuous thrust model, if that can be procured, or talk with individual entities and organisation with experience in designing deep space missions. As long as the results from both DASH and the third party match to with the acceptable margins and limitations of the code, it is acceptable.

8

Propulsion

This chapter discusses all the propulsion used in the DASH mission including the launcher, kick stage, and CubeSat propulsion. Section 8.1 details the method used to determine the launcher and kick stage option. Section 8.2 and Section 8.3 present the propulsion systems of the SHEPHERD and DOT respectively. Section 8.4 summarises the propulsion budget design. Finally, Section 8.5 performs a sensitivity analysis on the propulsion of DASH.

8.1. Launch and Orbit Insertion

The launch segment is one of the main elements driving the mission cost, as the price per launch quickly rises depending on the propulsive needs of the mission. It is important to first consider the trade-off performed previously, the propulsive elements selected are comprised of ion engines with large Delta-V contributions using continuous, low-thrust. Considering the constrained size of the propulsive module (SHEPHERD) of 5 kg, the amount of Delta-V that can be delivered by the module is severely limited, which requires a launcher and kick-stage combination to put the TRIAD into a specified orbit. Several feasible launcher and kick-stage options are compiled in Table 8.1 and Table 8.2 respectively. Only launchers from countries which European space agencies and companies are known to have worked with and that are presently politically feasible are considered. It should also be noted that several launchers are currently under development which may be feasible for the DASH mission; however, these will not be available for a 2024 launch. These are further discussed in Section 20.3.

Table 8.1: Viable launchers within the 2024 launch date and cost constraints. Note: other launchers were also considered

Launcher	Class	Payload to LEO [kg]	Payload to GTO [kg]	First-launch year	Successful Launches	Cost per launch [kEUR]
PSLV-XL [58]	Low-end MLV	3800	1300	1993	22/23	28750
Falcon 9 [60]	High-end MLV	16250	5500	2018	100/100	62780
GSLV Mk.III [34]	MLV	10000	4000	2017	4/4	50820
Ariane 6 [40]	MLV	10350	5000	2022	0/0	75000
RFA One [1]	SLV	1600	450	2022	0/0	3000

Table 8.2: Viable kick-stages within the 2024 launch date (where cost is not available, it is estimated using the relation of 0.655 kEUR per m/s)

Kick-stage	Delta-V [m/s]	First launch year	Successful launches	Cost per launch [kEUR]
Photon [20] (HP: High Performance)	50 to 4000	2020	2/2	Estimated: 2450
Astris [59]	$\sim$400	2024 (HERA)	0/0	Unknown
Vigoride [47]	max 1600	2022	0/0	1310

The propulsive module design makes use of the assumption incorporated within the trajectory optimisation (see chapter 7): the TRIAD begins its transfer outside the sphere of influence of Earth with an excess velocity of 6000 m s^{-1}. However, it should be noted that excess velocity was constrained concurrently with launcher and kick-stage selection and it was determined that excess velocity less than 5000 m s^{-1} likely makes the mission in its current concept infeasible.

[1] URL https://www.rfa.space/launcher/ [cited 14 July 2022]

The total wet mass for the TRIAD of 57.5 kg and an additional 18 kg is taken for the TRIAD deployer. This means that a total wet mass of 75.5 kg per TRIAD must be given sufficient excess velocity at the correct inclination. The correct escape inclination is achieved by launching directly to the orbital inclination needed within the designated launch window. Since the angle between the plane of the ecliptic to equatorial plane (Earth's axial tilt) is 23.5° while only an 11.5° inclination to the ecliptic is required as shown in Section 7.1, all launchers are capable of achieving their maximum GTO performance for the required range orbits of the DASH mission.

The kick-stage mass must be added to the 80 kg to determine the amount of mass that is to be taken to GTO by the launch vehicle, which depends on the kick-stage chosen, but wet mass data is quite restricted considering the early design stages of commercially available kick-stages. Given the cost and ΔV constraints, it was determined that two options can be considered to achieve the required escape trajectory. These are the large single launch and several small launch options.

For the purposes of keeping a distributed mission architecture with a low minimum viable mission, it is desirable to choose to launch on a small launcher several times. This allow for a much more scalable mission to be devised while further distributing the launch mission segment. Furthermore, a sustainability goal of this mission is to not use any toxic fuels, which eliminates the PSLV and GSLV launchers. However, it should be noted that the PSLV is otherwise an extremely favourable launch option, capable of launching two TRIADs with each launch at minimal costs. Considering the capabilities of such a class of launcher to GTO, only the high performance (HP) Photon kick stage is capable of giving the additional required amount of Delta-V from GTO as determined by Figure 8.1. Conservative estimates with values from [20] show that the propellant mass fraction of the high performance photon varies from approximately 0.55 to 0.72 depending on the mission profile. Given DASH's performance requirements, with all margins included as described in chapter 7, a propellant mass fraction of 0.67 is required, which falls well within photon's capabilities. This is also determined to be feasible since many of photon's high performance subsystems such as ADCS, EPS, TT&C, and others are either not required, or can be scaled down for the DASH mission. Assuming a standard 5 % margin on the stated required excess velocity of 6000 m s^{-1}, hence 6300 m s^{-1}, the total mass to GTO required to be delivered by the launcher is at least 420 kg.

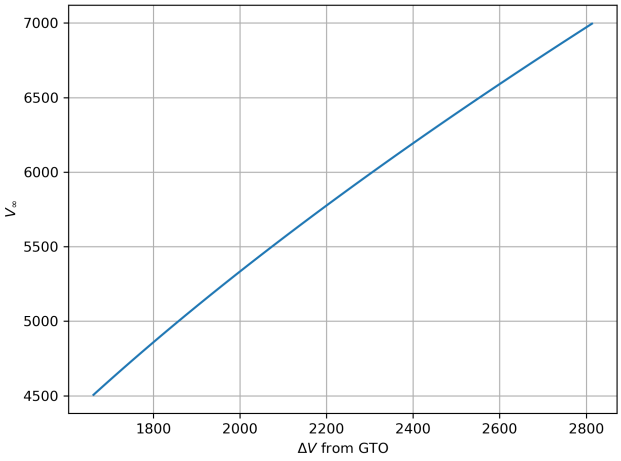

Figure 8.1: Delta V from GTO vs Excess velocity from Earth

Given these choices and constraints, the only small launcher which remains cost feasible, available by 2024, and sustainable with sufficient capacity to GTO is the RFA One. Another option may be a rideshare launch to GTO on a larger launcher. However, these are not considered at the moment due to the low frequency of such rideshare possibilities. Some key parameters of the final chosen concept are highlighted in Table 8.3.

Table 8.3: Final launcher and kick stage choice summary

Parameter	Value
Chosen launcher	RFA One
Launcher performance to GTO	450 kg
Chosen kick stage	High Performance Photon
Assumed kick stage propellant mass fraction	0.67
Resulting kick stage mass	340 kg
DASH required kick stage payload	80 kg
Launcher mass margin to GTO	30 kg
Photon hyperbolic excess velocity performance	6.3 km s^{-1}
TRIAD traj. opt. required hyperbolic excess	6.0 km s^{-1}

8.2. SHEPHERD

As introduced in the Concept of Operations in chapter 3, the SHEPHERD is the propulsion module in each TRIAD in charge of the trajectory velocity to reach the target asteroid. The engine first turns on after the kick stage has completed the initial transfer burn and is ejected from the group. SHEPHERD utilises ion propulsion and as such, a specific engine from a list of potential engines will be selected in accordance to the findings for the optimal trajectory of the DASH mission.

8.2.1. Potential Engines

The Shepherd will be using an electric propulsion module as means of propulsion. For this, a list of potential engines is procured. The selection criteria to generate a list of viable engines are provided in Table 7.2 in Section 7.1. The engines which are compatible with the general expected trajectory of the DASH mission are provided in Table 8.4 with their specific impulse, power and thrust performance characteristics.

Table 8.4: The upper and lower bounds of the trajectory simulation variables

Engine	**Isp range** (s)	**Max Thrust** (mN)	**Max Power** (W)
RIT-EVO10 [2]	1900 - 3100	25	760
Tile 3 [3]	1625	15	667
BHT-100 [4]	947 - 1274	9.19	165
Aurora [5]	950 - 1370	19	305
RIT-μX (M-ARGO) [67]	1900 - 3200	2.45	120
Halo Micro Electric Thruster [6]	780 - 1200	25	456
ST25 Hall effect thruster [7]	845 - 1250	15	272

As discussed in Section 7.1.3, all these engines are used in the trajectory simulation software to generate a set of possible trajectories. Once the data points have been collected, the best engine according to the relative performance is filtered out. With an engine chosen, the respective trajectory is further refined by tightening the simulation bounds around the desired solution and running the simulation software over much finer meshes. The reasoning behind choosing many engines with

[2]URL https://satcatalog.s3.amazonaws.com/components/915/SatCatalog_-_ArianeGroup_-_RIT_10_EVO_-_Datasheet.pdf?lastmod=20210710015124 [cited 1 June 2022]

[3]URL https://satcatalog.s3.amazonaws.com/components/1299/SatCatalog_-_Accion_Systems_-_TILE_3_-_Datasheet.pdf?lastmod=20220216045341 [cited 1 June 2022]

[4]URL https://satcatalog.s3.amazonaws.com/components/1281/SatCatalog_-_Busek_-_BHT-100_-_Datasheet.pdf?lastmod=20211014054617 [cited 1 June 2022]

[5]URL https://satcatalog.s3.amazonaws.com/components/993/SatCatalog_-_Orbion_Space_Technology_-_Orbion_Aurora_-_Datasheet.pdf?lastmod=20210710024345 [cited 1 June 2022]

[6]URL https://satcatalog.s3.amazonaws.com/components/953/SatCatalog_-_ExoTerra_Resource_-_Halo_Micro_Electric_Thruster_-_Datasheet.pdf?lastmod=20210710020654 [cited 1 June 2022]

[7]URL https://satcatalog.s3.amazonaws.com/components/918/SatCatalog_-_Space_Electric_Thruster_Systems_-_ST25_-_Datasheet.pdf?lastmod=20210710015254 [cited 1 June 2022]

varying performances is to have a variety of options that are still feasible in the event that one engine is seen to contain unforeseen issues further along in the development cycle of the DASH mission. Trade-offs such as I_{sp}, thrust and power requirements are incorporated in the simulation software, which only concerns itself with minimising the total TRIAD mass. The final engine selection and characteristics can be found in Section 8.2.2.

8.2.2. Best Performing Engines

Once all the potential engines are compiled, their characteristics and performance curves are implemented in the trajectory simulation. From each engine's data sheet, relations between power and thrust as well as between power and I_{sp} are found and integrated within the trajectory optimisation software.

The trajectory simulation is run for each engine in the order of 100 iterations or greater to get a sufficient number of data points. This is also done to take into account the varying performances of different engines, as some may have less possible trajectories than others given their inherent performance with respect to the mission. Once the simulations are complete, key parameters for all trajectories can be plotted to compare them quantitatively and make an informed decision on the best engine for the mission.

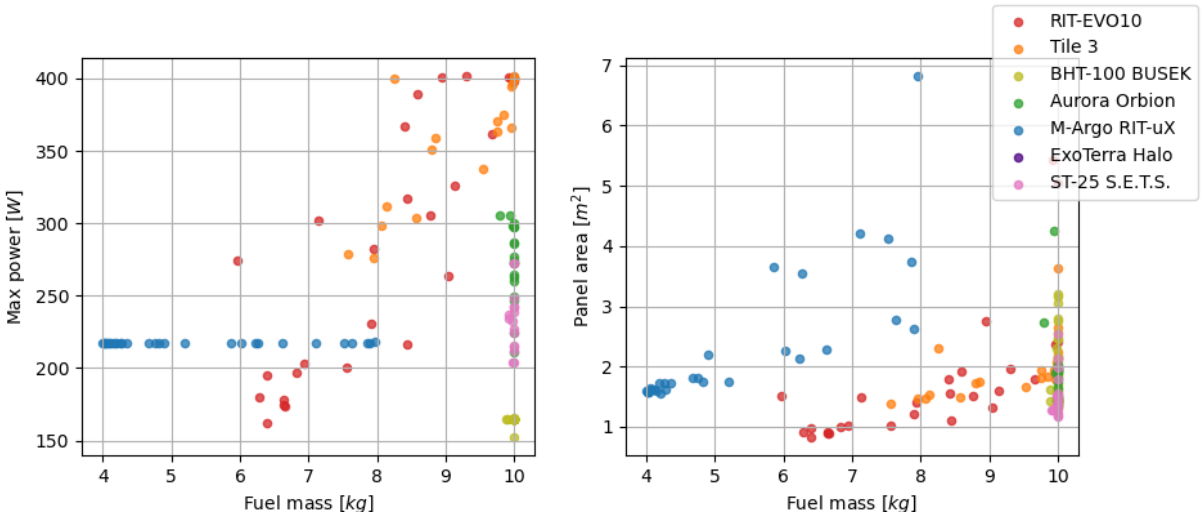

Figure 8.2: All trajectories calculated for the different engines and combinations of fuel mass, panel area, and maximum power observed

Figure 8.2 presents the required fuel mass, panel area and peak power for many possible trajectories for each of the considered engines. In order to understand the conclusions drawn from these plots, it is important to note a few things.

Firstly, notice how the transformation from max power and required panel area is not a linear scaling operation as perhaps expected. This is due to the change in solar flux throughout the trajectory of the spacecraft around the Sun. A maximum required power of for example 100 W may translate to different required panel areas depending on the trajectory phase the maximum power is required at.

Secondly, from the distribution of some engine's performances, some of the bounds within the trajectory simulation and optimisation software become evident. For example, notice the sharp line of viable trajectories at a fuel mass of 10 kg in both plots in Figure 8.2. This reflects some of the upper bounds set on simulation parameters, in this case maximum power set here at 400 W, maximum fuel mass set at 10 kg, and maximum panel area set at 7 m^2.

Lastly, although hard to see for most engines, some internal performance parameters can be observed coming in play limiting the viable design space engine by engine. As most evident for the M-ARGO RIT-μX ion engine in the left plot in Figure 8.2, internal maximum operating power was set at about 215 W as per engine specifications. This is directly reflected in the sharp horizontal line of points forming in the left plot in Figure 8.2 at a max power of 215 W.

More stringent bounds for both maximum fuel mass and maximum panel area are now introduced to weed out the worse performing engines. The bounds are set at a maximum fuel mass of 8 kg and a maximum panel mass of 2 m^2. Do note that the trajectory points as well as the bounds at this stage of the selection process are not final, but should be seen more as way to quantify the engines' relative performance. Based on the exact final system mass, launcher capabilities and internal layout, different required panel area or required fuel mass may be reached. This does not though change the relative performance of each engine hence leaving conclusions drawn from Figure 8.2 and Figure 8.3 valid with respect to any updated design. Figure 8.3 shows these updated bounds overlaid over the same engines' required panel area and fuel mass.

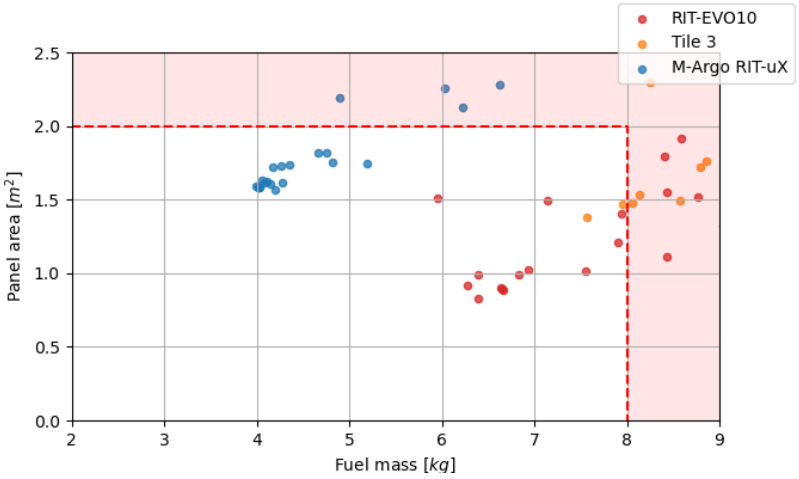

Figure 8.3: Panel area versus fuel mass with introduced upper bounds

As evident from Figure 8.3, three engines stand out as significantly better than the rest, these are the RIT-EVO10, the Tile3 engine system, and the RIT-μX engine used on the upcoming M-ARGO mission.

8.2.3. Final Engine Choice

From the analysis performed in Section 8.2.2, three engines stand out as superior when it comes to suiting DASH's performance requirements. These are the RIT-EVO10, the Tile3 engine system, and the RIT-μX engine used on the upcoming M-ARGO mission. From the data plotted in Figure 8.3, the Tile3 system performs worse or similar to the other options, both in terms of required panel area and required fuel mass. Furthermore, the Tile3 system as of 2022 has no flight heritage and, given the low thrust per unit, would require a relatively large volume aboard the SHEPHERD to achieve the desired thrust levels. For more reliability and lower costs, propellant is stored at low pressures aboard the integrated Tile3 system[8], This results in a very large required tank volume in order to meet the mission delta-V requirements. It is hence considered as an inferior option and discarded as a possible engine for the mission.

Lastly, relative performance between the RIT-EVO10 and RIT-μX is comparable, with the RIT-μX thruster achieving much a lower required fuel mass for a slight increase in panel area. Although perhaps similar in performance in this specific scenario, the RIT-EVO10 is a much larger and more powerful engine, and consequently, has a much larger bounding box which would make integration with the SHEPHERD challenging. See Figure 8.4 for the bounding boxes for these two engines to scale compared to the bottom of the SHEPHERD where they would have to be mounted to.

In addition to the much smaller form factor, as visible from the relative performance in Figure 8.3 the RIT-μX thruster manages to propel the mission to the target with much smaller mass of required fuel at the cost of a very small increase in panel area. The panel area increase from the RIT-EVO10 to the RIT-μX is deemed more than acceptable given the solar array technology used for DASH (see chapter 9) so a greatly reduced fuel mass is preferable. Hence, in conclusion, given the much smaller

[8]URL https://accion-systems.com/tile-propulsion/ [cited 9 June 2022]

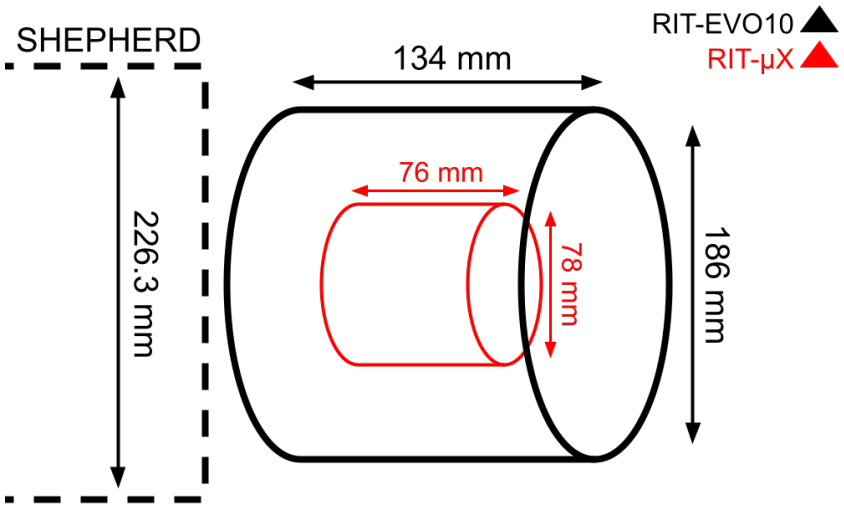

Figure 8.4: RIT-EVO10 versus RIT-μX thruster bounding box next to the SHEPHERD mounting plate

form factor as well as the smaller required fuel mass to achieve the same end goal, the RIT-μX is chosen as the thruster to power the SHEPHERD vehicle.

8.2.4. Tanks and Fuel Feed System

Although being the main design choice to be taken, choosing an engine is not everything required to fully define the SHEPHERD's propulsion system. To complete the ion-electric propulsion system definition, an appropriate tank and fuel feed and management system must be sized. As later discussed regarding the COTS bus chosen for SHEPHERD, see Section 10.2.1, both the propellant storage tanks and feed system will be purchased by ExoTerra as COTS components. These components come as part of the pre-made customisable Courier 12 U satellite bus. The propulsion system aboard ExoTerra's Courier module is very similar to the one which will be provided by DASH which makes compatibility a non-issue. The tank aboard Courier will be scaled up/down to fit DASH's performance requirements, ExoTerra's capability of doing so has been verified through direct personal communication with company employees.

Starting from the tank parameters aboard the standard Courier bus module, the specific fuel density for ExoTerra's tank can be calculated. Starting from the given specifications for Courier, its tank is designed to hold 2.06 kg of xenon fuel in a cylindrical tank with spherical bulkheads. Given the tank dimensions (from personal communications and the Courier specification sheet [17]), the internal volume can be calculated to be equal to 2036 cm^3 or about 2.04 U which yields a round final relation of propellant mass to stored propellant volume of about 1:1. This reference value of 1 U/kg will be used throughout the report to relate the fuel mass to its stored volume.

As not directly provided by ExoTerra, the fuel tank mass is estimated using a statistical relation between comparable pressurised xenon tanks for similar space applications. Furthermore, given ExoTerra makes use of titanium-lined COPVs to store their xenon propellant [17], only tanks built with similar technologies were used to derive the relation between tank volume and tank mass. Table 8.5 presents a list of tanks with their respective relevant properties used. Based on this information, a statistical relation is estimated using a power curve. This is to encapsulate the decrease in

Table 8.5: Comparable xenon fuel tanks specifications

Tank name	Volume	Dry mass	Source
S-XTA-60	60	11.7	[9]
ETS VIII	50	7	[65]
XS-XTA	7	3.5	[10]
Harvard Tank	70	10.5	[42]
HS 601	32	6.35	[64]

[9] URL https://satcatalog.s3.amazonaws.com/components/813/SatCatalog_-_MT_Aerospace_AG_-_S-XTA-60_-_Datasheet.pdf?lastmod=20210709221237 [cited 10 June 2022]

[10] URL https://satcatalog.s3.amazonaws.com/components/836/SatCatalog_-_MT_Aerospace_AG_-_XS-XTA-7L_-_Datasheet.pdf?lastmod=20210709222241 [cited 10 June 2022]

tank mass efficiency as the tanks get miniaturised. The relation derived is presented below in Equation 8.1.

$$m_{tank} = 1.3067 \cdot V_{prop}^{0.4822} \tag{8.1}$$

Where m_{tank} and V_{prop} represent the tank mass and propellant volume respectively. Using this relation and the value relating propellant mass and propellant volume, the tank mass required to house DASH's required 1.95 kg (see Table 7.10) of fuel can be calculated. DASH's fuel tank mass is hence equal to 1.80 kg.

Lastly, the propellant management and feed system mass is determined based on reference values found for similar missions. 0.50 kg is a reasonable estimate given the engine and tank size aboard SHEPHERD [12]. Furthermore, this coincides with the estimate reached in Section 10.2.1 for the Courier bus with a very comparable propulsion system.

8.3. DOT

Differently from the SHEPHERD vehicle, the DOT's propulsion system only needs to provide the required velocity changes to perform DASH's operational mission after the target asteroid is reached. This essentially means the Delta-V required from each DOT is in the range of a few tens of meters per second, instead of being in the thousands as for SHEPHERD. Specifically, each DOT has to provide a total of 20 m s^{-1} throughout the 6 month operational mission [25]. Given the much relaxed requirements for DOTs in comparison to SHEPHERD, a very different propulsion system architecture is used. A COTS cold gas thruster system is used to provide both the required velocity changes and momentum dumping for attitude control. Given the wide commercial availability of such a system, a COTS options is chosen as superior from both a cost and performance perspective. The *Aurora Propulsion Technologies ARM-AO* system is selected to meet both the propulsion and attitude control energy requirement. The system's performance and specifications can hence be found in the chapter discussing the DOTs ADCS (chapter 14), more specifically, in Section 14.6.

8.4. Propulsion Budgets

As the entire propulsion segment for the DASH mission is defined, this section aims to summarise the main decisions taken as well as the mass distribution across TRIAD's propulsion systems. Differently from other subsystems, most of the work went into calculating and optimising the low-thrust trajectory and iterating engine choices to reach a global optimum with respect to cost, launch mass, as well as overall mission performance. This means iterating over the propulsion segment as a whole, not just from the SHEPHERD or DOTs perspective, but taking into account the launch and kick-stage segment of the mission. Table 8.6 presents the chosen launch vehicle, commercial kick-stage, and TRIAD's delivered Delta-V, while Table 8.7 instead presents the individual components mass budgets and quantities within each TRIAD's propulsion system.

Table 8.6: Propulsion system segments sourcing and performance

Propulsion segment	Chosen option	Commercial provider	Delivered performance
Launcher	RFA One	Rocket Factory Augsburg (RFA)	Delivers kick-stage and stowed TRIAD to GTO
Kick stage	High Performance Photon	Rocket Lab	Delivers TRIAD on escape trajectory with characteristic energy $C_3 = 36$ km^2 s^{-2}
TRIAD	In-house development	DASH team and commercial partners	Delivers SHEPHERD and two DOTs within Didymos' sphere of influence

Table 8.7 presents the mass budget for the components relevant to both SHEPHERD's and DOT's propulsion systems.

Table 8.7: Propulsion system mass budget breakdown

Propulsion element	Chosen Option	Quantity	Total mass [kg]
	SHEPHERD		
Ion Thruster	M-ARGO RIT-μX Thruster	1	0.44
Propellant	Xenon propellant	N.A.	1.95
Propellant tank	ExoTerra Courier onboard 2.06 kg COPV xenon tank	1	1.80
Propellant management system	ExoTerra Courier onboard propellant management system	1	0.50
	DOT		
Combined ADCS and propulsion	Aurora Propulsion Technologies ARM-AO all-in-one system (thrusters mass)	2	0.20
Propellant	ARM-AO all-in-one system (propellant mass)	N.A.	1

From Table 8.7, the dry mass and wet mass of the propulsion system onboard SHEPHERD can be determined to be 2.74 kg and 4.69 kg respectively. For the DOTs instead, the dry and wet mass of the onboard propulsion is 0.2 kg and 1.20 kg respectively.

Table 8.8: Caption

	Mission Components		**Mass (**kg**)**	
Mission phase	***Phase start***	***Phase end***	***Phase start***	***Phase end***
Launch	• Launch Vehicle • Kick-stage • Deployer • TRIAD	• Kick-stage • Deployer • TRIAD	76500	415.5
Ejection	• Kick-stage • Deployer • TRIAD	• TRIAD	415.50	57.42
Transfer	• TRIAD	• SHEPHERD (x1) • DOT (x2)	57.42	55.47
Scientific operations	• SHEPHERD (x1) • DOT(x2)	• SHEPHERD (x1) • DOT(x2)	55.47	52.47

8.5. Sensitivity Analysis

There is a heavy dependency between the selected launcher (and kick stage combination) and the ion engine selection. This is because in the trajectory simulations, the TRIAD starts outside the sphere of influence of Earth with an initial excess Delta-V relative to earth of 6000 m s^{-1}. With such a high initial excess velocity to be provided, the launcher and kick stage combination must be more than capable of providing this in mission scenario lest the risk of running out of fuel during transfer is to be avoided.

Increasing the initial Delta-V to be provided to the TRIAD for transfer results in a decrease in the required engine performance as less Delta-V will have to be provided by the ion engine during transfer. On the other hand the much more severe alternative of a decrease in initial Delta-V can prove detrimental to the mission. A less powerful launcher and kick stage combinations, while cheaper in cost, means less excess velocity and the requirement of a more powerful engine. More trajectory adjustments will have to be made to meet the transfer and start of operations time. As such this will result in a higher thrust needed for longer durations of time, especially in the early stages of transfer.

Using the engine at a higher capacity requires more power and fuel, which is already severely limited in the SHEPHERD. Consequently, fewer engines will be feasible and able to comply with the new trajectory requirements, with low I_{sp} engines taking a heavier loss due to the fuel capacity limitations on the courier bus.

The mass of the TRIAD also plays a role though not as large as it may seem due to the presence of an effective ratio in Equation 10.1. Increasing the mass of the DOTs from 20 kg each to 25 kg, a 25% increase, results in a decrease in Delta-V of 15% during transfer. And the Delta-V difference due to this increase in mass for the kick stage burn phase is observed to be less than 4%. This loss in Delta-V becomes more minimal during launch as the mass of the launcher takes a majority of portion and the addition of 10 kg does not affect reaching GTO. As can be seen, Delta-V and mass does not scale proportionally and depending on the ratio and phase of the mission its effects can vary from low, when the kick stage burns, to significant enough, for transfer burn.

As was previously shown in Figure 8.2, engines with low I_{sp} tend to maximise the fuel mass allowable and vary in panel size. To understand why this is, it must be noted that the time of flight which the simulations were run through is also a parameter of the DASH mission. Increasing the transfer duration allows engines to be run on lower power settings for longer, which especially helps engines with low efficiency in comparison.

The filtered engines, shown in Figure 8.3, are essentially those engines which operate very fuel efficiently and have favourable ion engine power usage relations. The limits set by the courier fuel capacity and panel area make it such that engine which are unable to meet the transfer window are unfeasible. Increasing the allowed transfer time indefinitely can bring those engines such as the BUSEK BHT-100 back into play due to its low power consumption but low I_{sp} characteristics. It must be understood that the Delta-V provided by the engine is heavily influenced by the I_{sp} and time constraint, the possible trajectories all require similar Delta-V, and it is then up to the engine to not use more fuel than what can be housed.

A final consideration for the propulsion system is the thrust capabilities of the engines. Engines which are capable of providing smaller thrust are more likely to be feasible, as the efficiency of ion engine and its properties does not scale well as the power is dramatically increased. Power availability also played a large role in ion engine performance. With the maximum ion engine power being capped by the solar panel area, engines with higher thrust capabilities lose their advantage as not enough power is supplied to provide such high thrust. The combination of low-thrust and high-I_{sp} engines are thus found to be ideal as they are usually more efficient engines that are able to throttle down significantly to reduce the fuel used and power into the system.

9 Electrical Power System

A preliminary EPS sizing was provided in the midterm report [25]. This included several assumptions which resulted in the over-designing of several parts of the EPS. Therefore, the EPS design was reiterated during trajectory optimisation and in regular iterations. The result of these changes are presented in this chapter. Firstly, solar cell degradation over mission lifetime will be estimated. Then, the DOT's EPS system will be designed, followed by the SHEPHERD. After that, the interface between the SHEPHERD and the DOTs is specified. This is followed by the electrical block diagram, and finally the sensitivity analysis.

9.1. Solar cell degradation

The Space Environment Information System (SPENVIS) interface was used to determine the degradation of solar cells for the mission. Several assumptions were made when using this software. The main ones are highlighted below.

- The spacecraft spends 31 d in GTO
- The spacecraft spends 2.8 yr in a 1AU interplanetary orbit
- CREME-96 solar minimum model was used to simulate the galactic cosmic ray flux (solar minimum corresponds to cosmic ray maximum)
- The SAPPHIRE solar particle model is used to determine solar ion radiation.
- Solar particle fluences not exceeding a confidence interval of 95 %
- AZUR 3G30 cell is used to determine 1 MeV
- SiO_2 coverglass with density of 2.32 g cm^{-3} is used

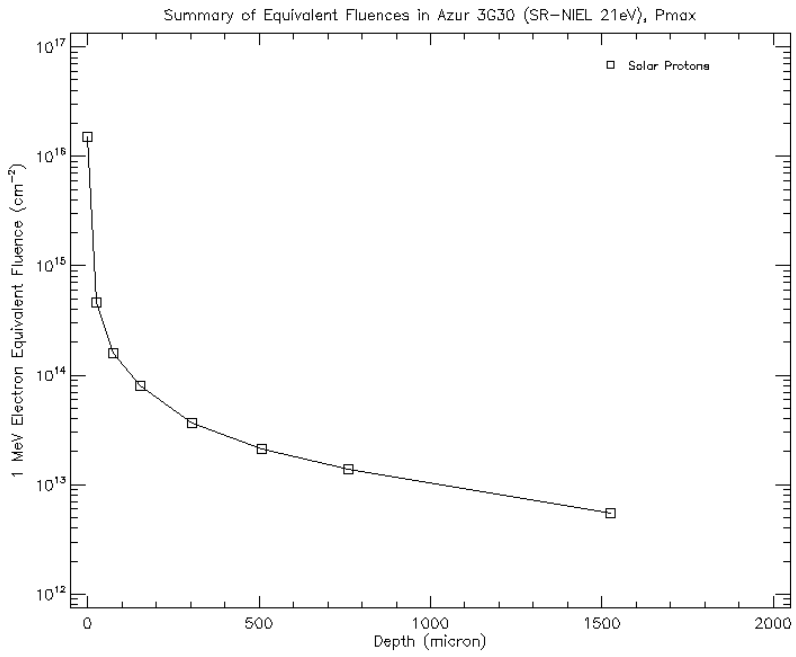

Figure 9.1: Equivalent fluence vs coverglass thickness

This method resulted in Figure 9.1. From this figure, a cover glass thickness of 50 µm was chosen which results in less than 2.5×10^{14} MeV electrons per cm^2 equivalent fluences. This results in a factor of approximately 0.97 degradation due to radiation fluences [1]. This thickness of coverglass results in

[1] URL http://www.azurspace.com/images/0003429-01-01_DB_3G30C-Advanced.pdf [cited 14-07-2022]

approximately 0.1 kg of coverglass weight for the panels of SHEPHERD. It should be noted that this weight is not used further in EPS sizing since COTS components are used for which the coverglass thickness is not known. Rather, this analysis is only used to estimate the degradation due to solar electron fluences.

Additional degradation is expected due to a variety of factors such as outgassing, thermal cycling, micrometeoroid strikes, etc. This is estimated to be 1.25 % per year [75]. This results in total estimated degradation of 0.935 over the mission lifetime.

9.2. DOT

This section describes the EPS of the DOTs. The method used to design the EPS is detailed in Section 9.2.1. The power system design is described in Section 9.2.2. The chosen solar panels are presented in Section 9.2.3. Finally, an estimate for the wiring mass is given in Section 9.2.4

9.2.1. Design methodology

For the EPS of the DOTS, only commercial off-the-shelf (COTS) components were used as options due to the relatively small development time remaining until launch.

Several other key constraints which drive the EPS design are highlighted in Table 9.1. The average and peak power consumption is determined by summing the idle and peak power consumption of all other components during nominal operations. The maximum average power usage occurs due to the ASPECT payload. The MultiScape100 payload is a part of the bus power, since it is constant for all DOTs.

For battery sizing, the most constraining situation is the slew manoeuvre. The next most constraining situation is the momentum dumping manoeuvre, but that uses approximately half as much total energy. In the midterm report [25] it was assumed that slew power consumption remained the same as during nominal operations and slew occurred for 0.667 h. This assumption was refined so that only relevant subsystems are assumed to be running, and it was determined that a 180° slew manoeuvre will not take longer than 300 s. Using the same method as in the midterm report [25], the resulting battery sizing is 1.56 W h which is far lower than that offered by most COTS battery packs.

Table 9.1: Key parameters in EPS design

Parameter	Value	Unit
Bus average power consumption	14.4	W
Bus peak power consumption	32.6	W
Payload maximum average/-peak power consumption	7	W
Slew power usage	7.4	W
Slew time	300	s
Largest distance to Sun	2.15	au

9.2.2. Power conditioning, distribution, and storage

There are a multitude COTS EPS components available for CubeSats which are capable of meeting the EPS requirements of the DOT [2] [3]. Furthermore, most COTS power distribution, conditioning, and storage components have similar mass, volume, and performance. Therefore, only two COTS EPS suppliers (GomSpace and ISISPACE) were considered in this preliminary design stage due to time constraints and the lack of availability of complete datasheets from all EPS suppliers. It is recommended for other EPS suppliers and components to be considered in future design of this system. Nevertheless, the performance of these components should not vary if the requirements on the EPS remain similar. The relevant constraints on the EPS are highlighted in Table 9.2. The solar panel peak power production is determined

Table 9.2: Key parameters in power conditioning, distribution and storage design

Parameter	Value	Unit
Energy storage	1.56	W
Peak power consumption	39.6	W
Solar panel peak power production	90	W

[2] URL https://satsearch.co/products/categories/satellite/power/eps [cited 14-06-2022]
[3] URL https://www.cubesatshop.com/product-category/nanosatellite-power-systems/ [cited 14-06-2022]

in Section 9.2.3 which was designed concurrently.

From these parameters, power systems were chosen using GomSpace and ISISPACE parts. The results and key differences are highlighted in Table 9.3. All components are approximately 10 cm by 10 cm in length and width, so only height is compared in Table 9.3.

Table 9.3: Comparison between ISISPACE and GomSpace power systems

Parameter	ISISPACE	GomSpace
Mass [g]	416	731
Height [mm]	54	81
Battery heater power [W]	2.5	6.0
Energy storage [W h]	46.1	86.4
Battery configuration	4S1P	8S1P
Idle power consumption [W]	0.526	1.378
Maximum allowed solar panel power [W]	156	330

From the table it is clear that while the GomSpace components are better performing, that performance is largely not needed by the DOT and the smaller and lighter ISISPACE components can be used. The configuration from ISISPACE which is used has one distribution unit, conditioning unit, battery unit, and battery pack each. The datasheet for this configuration is available on the ISISPACE website [68].

9.2.3. Solar panels

As mentioned in the midterm report [25], the solar panels must be able to track the sun. This will be done by rotating the spacecraft in the roll direction while being able to rotate the solar panels along their axis. Preliminary research provided only one COTS tracking solar panel with sufficient performance for this mission, which are the GomSpace tracking solar panels (TSP). While it would be possible to use regular solar panels and attach them to a custom-made deployment and tracking mechanism, this was not chosen as an option because of the little development time until launch and the ready availability of the GomSpace TSP which should gain flight heritage on similar missions such as M-ARGO and HERA. Several key parameters of the panel are highlighted in Table 9.4.

Table 9.4: Parameters of GomSpace 6U TSP

Parameter	Value	Units
Wing mass	650	g
Hold down release mechanism (HDRM) mass	30	g
Z cover close out parts mass	40	g
SADA-50 mass	80	g
Stowed volume	330x208x9	mm^3
Deployed length	990	mm
BOL power production at 1 au	45	W
BOL power production at 2.20 au	15	W

It should be noted that the values stated in Table 9.4 are for a single wing. To satisfy the power requirements of the DOT, each DOT must have at least two such wings. Assuming an inverse square law variation of the solar flux with distance from the sun and 0.935 solar cell power degradation, the total power generation at EOL is estimated to be 29.4 W. It should be noted that the degradation of the DOTs may be less since they are stowed for a large majority of the transfer, protecting the inner cells from radiation and micrometeoroids. Still, the degradation is assumed conservatively to be 0.935.

9.2.4. Wiring

Wiring is estimated to be 10 % of the total EPS mass according to [75] which results in a mass of 0.2 kg. This is a rough estimate, and an accurate estimate will likely occur much further in the design process.

The EPS for SHEPHERD is the same as used in ExoTerra's Courier. Relatively little data was available about the details of the EPS because of this.

9.3. SHEPHERD

As mentioned earlier, no specific component breakdown is provided for the Courier subsystems. Solar panel sizing occurred during trajectory optimisation in Section 7.1. The remaining EPS component masses are therefore estimated based on a generic EPS architecture and similarly performing COTS components at the same power level as provided by Courier's bus [17]. A component break down with masses is given in Table 9.5 where numbers are based on specifications provided by ISISPACE for their modular CubeSat EPS system [4]. These estimations and some performance values are highlighted in Table 9.6.

Table 9.5: Estimated Courier EPS components and mass

Component	Quantity	Total Mass [kg]
Distribution Unit	3	0.172
Conditioning Unit	2	0.116
Battery Pack	2	0.504
Battery Management	1	0.049

Table 9.6: Performance/constraint estimations of SHEPHERD EPS supplied by ExoTerra

Parameter	Value	Units
Solar panel area	0.88	m^2
Solar panel mass	2.47	kg
Estimated power production at 1 au	325.6	W
Estimated power production at 2.2 au	67.3	W
Maximum average power required from EPS	129	W
Estimated power system mass	0.841	kg
Estimated battery capacity	92.2	W h
Distribution and conditioning unit power capacity	>296	W

9.4. Interface between SHEPHERD and DOTs

As described in Section 10.1, the CubeSats will be connected to each other during the transfer by means of a release mechanism. When the groups are in transfer, the CubeSats will have an electrical connection, which interfaces the DOTs with the SHEPHERD. This connection will be similar to the connection used on the HERA mission, connecting the HERA mothership with the Milani and Juventas CubeSats [43]. To reduce the risk of failure propagation from the DOTs to the SHEPHERD, the first interface between the CubeSat is the so-called Life Support Interface Board (LSIB). Each CubeSat will have an LSIB, which provides power and data from the SHEPHERD to the DOTs. Vice versa, the DOTs will send housekeeping data to the SHEPHERD, which then will be relayed to the ground. The difference of DASH with HERA is that our mission does not use deployers for the separation of the CubeSat, so where HERA connects the LSIB to the umbilical of the deployers, our LSIB is directly connected to the DOTs. It should however be noted that the physical position of the LSIB is not yet finalized. This connection will be based on the CarboNIX electrical connection from Exolaunch[5], see Figure 9.2 as a reference.

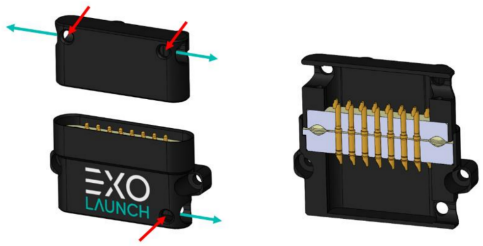

Figure 9.2: CarboNIX Separation Connector.

9.5. Electrical block diagram

The electrical block diagram is presented in Figure 9.3.

[4] URL https://www.isispace.nl/product/modular-electrical-power-system/ [cited 12 June 2022]
[5] URL https://satcatalog.s3.amazonaws.com/components/528/SatCatalog_-_Exolaunch_-_CarboNIX_15in_-_Datasheet.pdf?lastmod=20210813204912 [cited 13-07-2022]

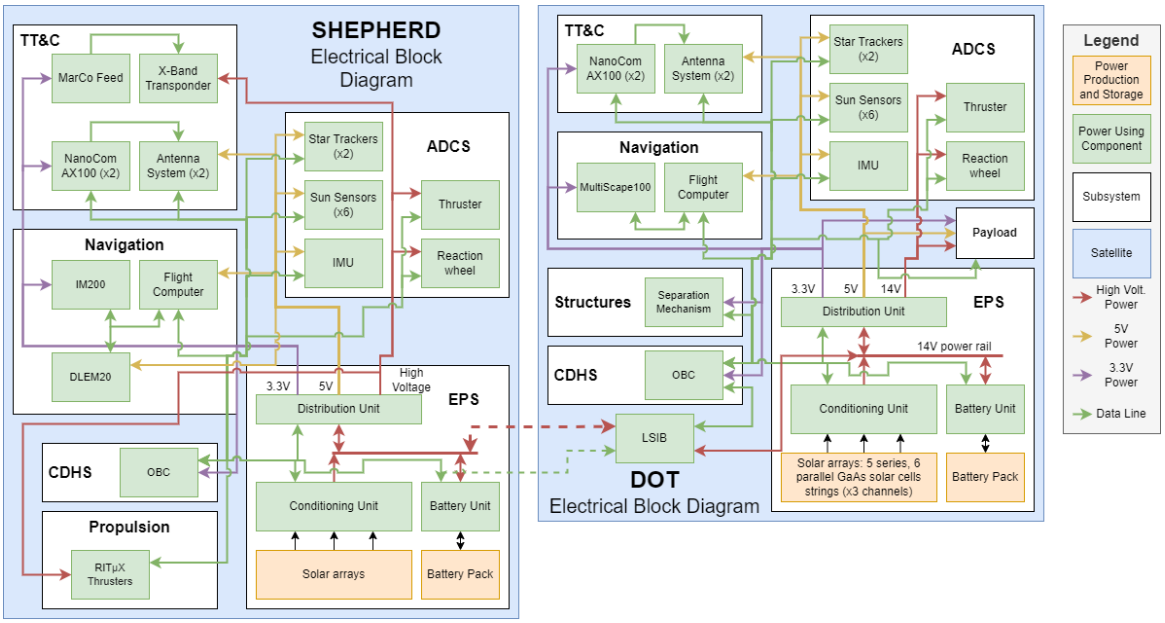

Figure 9.3: Electrical block diagram for DOTS and SHEPHERD. It should be noted in this diagram the SHEPHERD is only connected to one DOT while it is actually connected to two. Furthermore, the physical position of the LSIB is not finalized as mentioned in Section 9.4. Also, the several voltages are not known at this time; it is possible that some voltage converters may be required for certain components.

9.6. Sensitivity Analysis

The EPS sizing is not likely to change significantly if changes occur in the average or peak power requirements.

If the peak power requirements are increased, another battery pack can be easily added to each CubeSat since these components are modular. It would however result in an increase of the power system mass and volume in steps corresponding to a single battery pack. If peak power requirements are decreased, it is likely not feasible to decrease the size of the battery pack since the smallest COTS components are already chosen.

If average power requirements are changed, the solar panel sizing can be incremented by a single panel, which is about 4.9 W. Although, if the size is not incremented at two panels at a time, it will result in asymmetries. Mass and volume of the solar panels will scale proportionally.

10
Structures

This chapter is divided into two parts, *Release Mechanism* and *COTS Structure Elements*. In the first part, a design for the release mechanism is proposed, followed by a structural analysis. Then, recommendation and testing is presented alongside possible mechanism alternatives in case the current selection does not perform as expected. Finally, an operational logic for the separation event is shown. For the second part, the COTS components are presented, these parts constitutes the bus of SHEPHERD and DOT, and the outsourced TRIAD containerised deployer.

10.1. Release Mechanism

In this section, the design of the release mechanism will be developed. Aspects such as the hold down & release mechanisms (HDRM) selection, manufacturability considerations, and recommendation and testing are addressed. The release mechanism is of great importance for the mission since it ensures joint transfer to Didymos and separation once the TRIAD has arrived. This mechanism will maintain the DOTs connected to the SHEPHERD and separate it once scientific operation starts, assuring one of the distribution aspect of the mission which is a core aspect of DASH, making part of our mission objective (DASH-OBJ.02).

First, the structural analysis of the CubeSats release mechanism is presented. A static analysis is performed to guarantee that the mechanism can withstand the launch loads. On top of that, a modal analysis is simulated to assure the structure natural frequency is above the limit of the one specified on the payload user guide of the launch vehicle. Next, recommendation and testing is presented, and possible alternatives are discussed. Finally, the operational logic is developed.

The following analyses were performed to show design feasibility of the release mechanism in accordance to the key subsystem requirements, referred below. These analyses, however, do not show requirement compliance and tests still need to be developed and performed to verify and validate this mechanism.

- Static Analysis - Performed to ensure DASH-LVP.01-MI.34-SYS.68-STR.01 and DASH-LVP.01-MI.34-SYS.69-STR.02 is met
- Modal Analysis - Performed to ensure DASH-LVP.01-MI.34-SYS.70-STR.03 is met.

The use of an Ejector Release Mechanism (ERM) is considered as a possible solution to release the CubeSats. This is considered based on a recommendation in [29]. Moreover, it is easier to manufacture a structure to interface with the ERM while still performing the desired function. Furthermore, this mechanism also allows for reusability given its manual reset capability, with a minimum life of 50 cycles specified by the manufacturer. The ease of manual reset can also bring additional benefits, such as non-destructive testing (NDT) on ground to verify and validate this mechanism.

A few ERM solution offered by Ensign-Bickford Aerospace & Defense (EBAD) is shown in Table 10.1. EBAD is a well known company in the aerospace industry to provide release mechanisms. Its EBAD's TiNi™ products have previously offered solutions to many deep space missions such as Juno, Rosetta and Mars Surveyor to name a few. EBAD has also provided the James Webb Space Telescope (JWST) with 178 release mechanisms responsible for all critical release events of that mission, characterised by a complex deployment sequencing from its stowed position. Given the level of development and its flight heritage, the ERMs provided by EBAD are considered as an option for the DASH mission.

Table 10.1: Possible COTS ERMs from EBAD

	Mass [g]	Power [W]	Kick-off force [N]	Max Release load [lbf]
ERM E250	75	1.9W@0.75A	6.7	250
ERM E500	100	5.0W@1.00A	28.9	500
ERM E1000	160	8.1W@2.25A	42.3	1000
ERM E2000	300	11.1W@2.25A	37.8	2000
ERM E4000	530	12.7W@2.25A	80.1	4000

As a first design option, to separate two 16U CubeSats, two ERM E250, one for the top half and another one for the bottom half, is considered. This may later be changed based on the sizing and mass budget of the SHEPHERD and DOTs to ensure an adequate separation velocity. The current choice is based on the size and mass estimates performed on [25]. This current solution poses an additional challenge, namely firing both mechanism at the same time.

The lowest kick-off force out of all options was chosen since ideally no force is desired to separate the CubeSats. A higher kick-off force implies a higher separation velocity, which for this application is critical given that the escape velocity of Didymos is approximately 24 $cm\,s^{-1}$ [79]. Assuming a function time of the actuator to be 100 ms, as stated by EBAD on their product details, a kick-off force of twice 6.7 N, to account for the two ERM, and a mass of 21.7 kg, for the DOTs, an approximate separation velocity of 6.18 $cm\,s^{-1}$ is found. Comparable past application such as the release of MASCOT from Hayabusa2 shows a separation velocity of 5 $cm\,s^{-1}$ [24]. If desired, due to a decrease in mass or excessive reaction control requirement after separation, the separation velocity can be halved by going with one separation mechanism only instead of two, this would also eliminate the challenge of firing both actuator concurrently. This will be addressed later in the design phase.

To ensure concurrent separation, with little to no delay, it is recommended that both ERMs be kept at about the same temperature and supplied with the same current at the release phase to ensure simultaneously separation and to minimise rotational motion. Possible mitigation strategies to avoid rotational motion when separating the two release mechanism is to evenly space the release mechanism from the DOTs centre of gravity and providing a lower arm with respect to the centre of gravity in case firing happens with some delay. The position of the mechanisms may be revisited later based on the mass distribution of the DOTs and outcomes of testing. Testing is recommended to be performed at low temperature and low current, which would illustrate a critical condition as shown in Figure 10.1. This figure also shows a need for thermal control and power management during the separation phase for a successful operation.

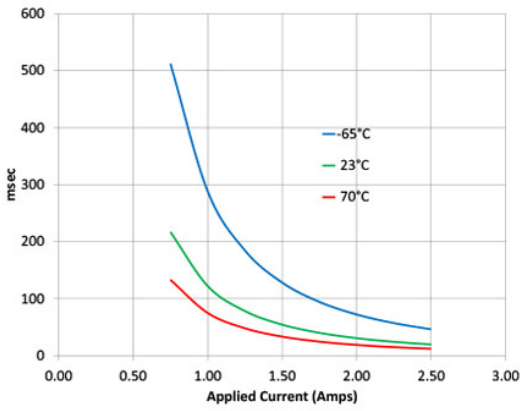

Figure 10.1: Function Time at Various Temperatures

Figure 10.2 shows the assembled design proposed to interface with the COTS ERM from EBAD. The mechanism consists of 5 parts, as shown in the Bill of Material in the top right corner of the drawing, namely: ribs, cups, cones, a plate, and the ERM. Excluding the ERM, the remaining parts will be manufactured in house. Therefore, they were designed to be easy to manufacture with none of them posing any manufacturing challenges except for the cups which may require some manual labour on a lathe and may be difficult to manufacture with a low tolerance. Alternatively, some casting method could be considered as opposed to machining for this specific part to meet tolerance requirements. The plate part will also act as an adaptor in case a bigger clearance is needed between SHEPHERD and DOTs.

The first material chosen to perform the structural analysis of this design was aluminium. Aluminium is

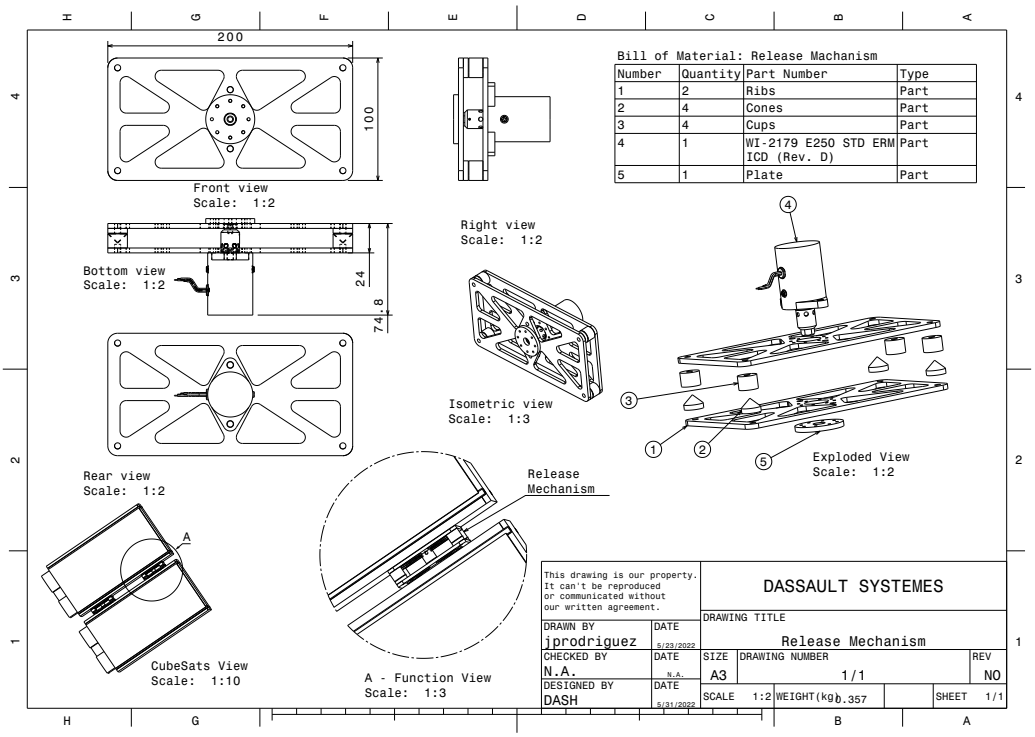

Figure 10.2: Assembly drawing of the Release Mechanism

lightweight, easy to work with, abundant and cheap. A mass estimate based on 3D Design software estimates the frame (ribs, cups, cones and plate) to be 0.282 kg. EBAD specifies the mass of the E250 at 0.075 kg, amounting to a total mass per mechanism of 0.357 kg. It should be noted that the weight of the bolts are not considered in this estimate. Bolts are often made of stronger material than what they are joining, common materials are steel and titanium which has considerably higher density than aluminium. Depending on the number of bolts, nuts, and washers in the mechanism, this may have a significant contribution to the mass budget of the structure.

A preliminary cost estimate was executed to determine how financially viable the use of COTS ERM from EBAD would be and whether an in house solution would be beneficial. When contacted on pricing, EBAD stated that it depends on the quantity and model of the components, with prices ranging from $9k to $14k for the ones displayed at Table 10.1. For 16 E250, the unit price amounts to $9210.

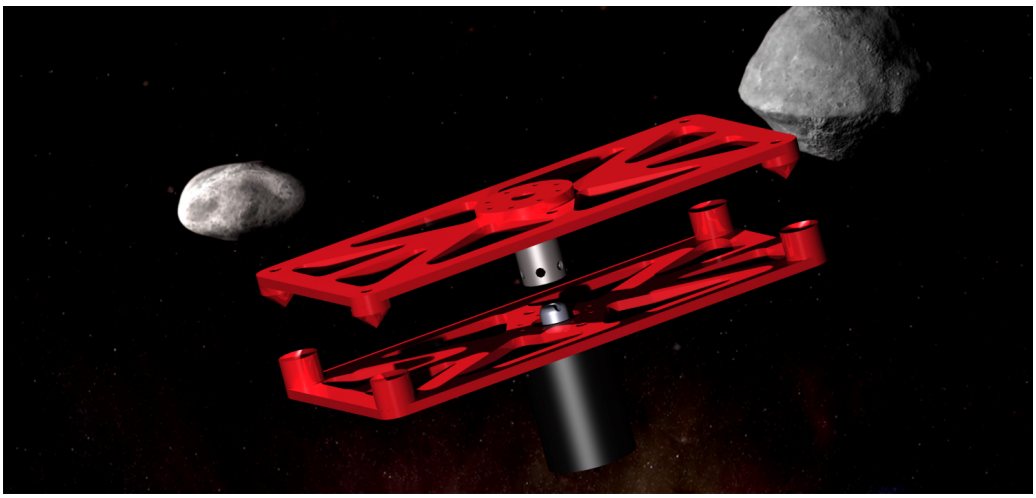

Figure 10.3: Render of the Release Mechanism

Figure 10.3 shows a render of the release mechanism. Note that the colour is merely illustrative and was chosen for visualisation purposes only. Both frames are connected to each other by the ERM

through the middle. A bolt is used to attach the ERM to both frames, by tightening the top bolt against the plate part, the cups and cones will be pressed against each other, facilitating these components to take the shear, bending and compressive loads. Once the ERM is activated, the 6 pins keeping both frames attached will retract and the spring-loaded mechanism will separate the two. The pin release and separation moment is illustrated in the render.

10.1.1. Static Analysis

A static analysis of the release mechanism assembly is performed to estimate the peak stresses and concentrations under certain loading conditions. This is done to ensure that the structures subsystem requirements are met, namely DASH-LVP.01-MI.34-SYS.68-STR.01 and DASH-LVP.01-MI.34-SYS.69-STR.02. Moreover, the g loading was applied on all 3 axis to guarantee structural integrity regardless of mounting direction.

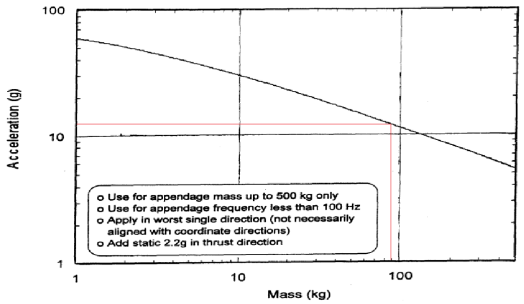

Figure 10.4: Mass Acceleration Curve [11]

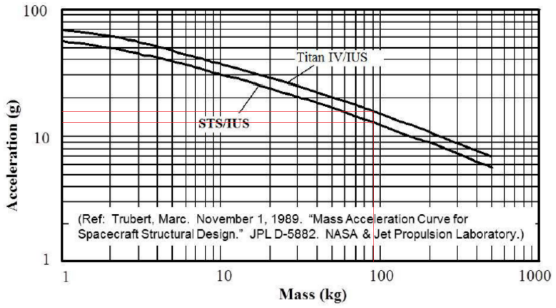

Figure 10.5: Mass Acceleration Curve for specific LV [29]

The mass acceleration curve (MAC) method, depicted in Figure 10.4 and Figure 10.5, was developed by JPL to perform preliminary structural sizing. From the preliminary mass budget presented in [25] each DOT CubeSat was estimated to have 21.7 kg and the SHEPHERD one 46.5 kg. In total, the group mass, constituted of 2 DOTs and 1 SHEPHERD, is approximated to be 89.9 kg.

Following the mass estimate, a load case can be extracted from the MAC plots. Figure 10.4 leads to a reading of 14g. Nonetheless, literature seems to diverge on the MAC plot, some taking a more conservative approach depending on the launch vehicle. Figure 10.5 for instance varies between 14g and 17g depending on the launch vehicle. Adding the recommended 2.2g margin on the launch direction for Figure 10.4 a figure closer to 16.2g is found. Given that a lower mass leads to a higher g loading in this plot and that the mass estimate performed was preliminary, and conservative, the highest of the 3 was taken, namely 17g. This loading case is more critical than the ones formulated at DASH-LVP.01-MI.34-SYS.68-STR.01 and DASH-LVP.01-MI.34-SYS.69-STR.02 and hence if the structure can withstand the 17g in all direction, then it will also fulfil these key requirements.

As a first analysis, it is useful to identify peak stresses in highly loaded components and stress concentrations. For that, 3 simplified static analysis were performed based on the different cases listed below.

- Case 1 - Cups and Cones take all the load
- Case 2 - ERM takes all the loads
- Case 3 - Both take the loads

In reality, the structure is designed such that the cups and cones take the shear, bending and compressive loads while the ERM takes the tensile loads. In all cases the rib face that will be in contact with the SHEPHERD was constrained as a fixed support and an acceleration of 166.77 $m\,s^{-2}$, equivalent to 17g, was applied to all elements. Different fixed constraints were considered, namely fixing the cups only instead of an entire rib surface, but results were fairly similar.

The outcomes of the performed analysis are presented below. This was executed using the default mesh size for a qualitative analysis to identify possible stress concentrations, the following is found:

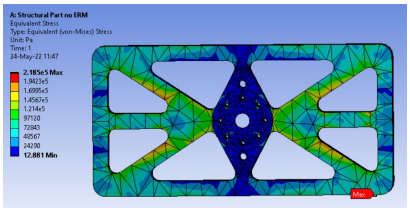

Figure 10.6: Case 1-Stress analysis on structure without ERM

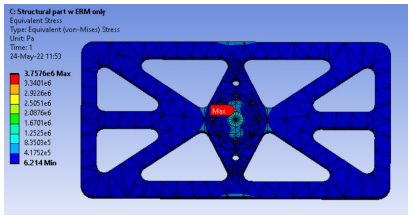

Figure 10.7: Case 2-Stress analysis on structure without cups and cones

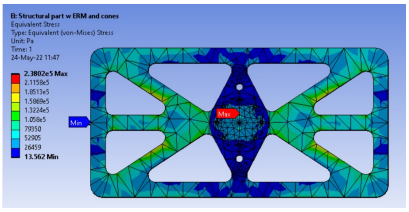

Figure 10.8: Case 3-Stress analysis on structure with ERM and cups and cones

Note the increase in stress from case 1 to case 2, this is expected since now the only load path is through the ERM as opposed to the 4 cups and cones. Case 3 shows how the cups and cones alleviate the stresses on the ERM by reducing the peak stress at that part. From this analysis possible stress concentrations were identified, namely on the joining of cups and cones, and at the ERM. The cups and cones also showed to be functioning as intended.

Unfortunately, a mesh could not be generated over the CAD file provided by the COTS supplier for the ERM, hence a replacement ERM part, similar in size and geometry, was designed to perform a stress analysis over the whole assembled structure.

As the previous default mesh size was too coarse to provide reliable numerical values, a finer mesh was considered. With the peak stresses identified, a mesh refinement in those locations was performed. Figure 10.9 and Figure 10.10 show a finer mesh at the bottom rib for a critical configuration at that part, structure with no ERM.

Similarly, a mesh convergence study was performed for the full assembly to assess the peak stress at the structure. To show convergence, the software kept refining the mesh until the percentage difference between the current iteration and the previous iteration was below 1%. The convergence trend is shown in Figure 10.12, this plot is based on a refinement depth of 2. The refinement depth defines how aggressive the mesh refinement is from iteration to iteration, ranging from 1 to 3 where 3 is the most aggressive one. The converged result is shown in Figure 10.11.

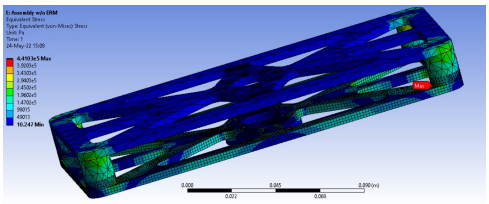

Figure 10.9: Full Assembly with connected parts and no ERM

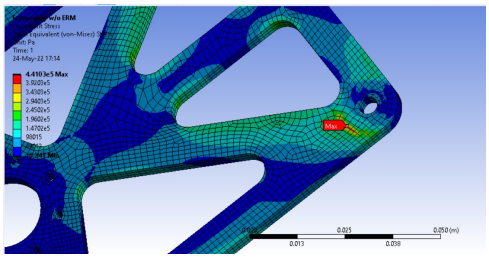

Figure 10.10: Close-up look on bottom rib

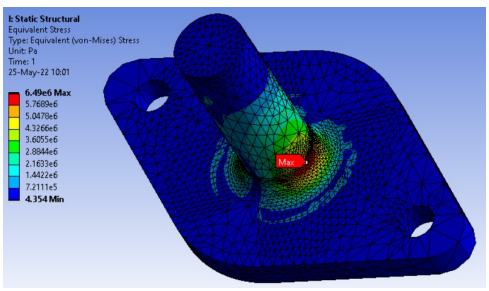

Figure 10.11: Improved geometry

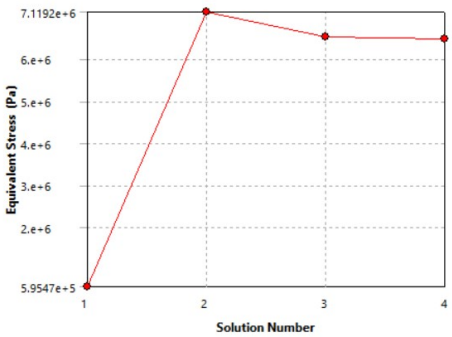

Figure 10.12: Mesh convergence

It should be noted that bolts have not been considered in this analysis. Bolt preload introduce additional stresses to areas where there is already a high stress concentration due to the holes to accommodate the bolts. In this simulation, the parts were connected with a contact constraint that distributes

the stress equally along the contacted area, as opposed to locally at the bolted region. Given that the maximum stress in the structure is far below the yield stress of the material, below 10 MPa, it is assumed that even with a high stress concentration factor along the bolted region the peak stress would not damage the structure.

As a possible point of improvement on a manufacturing point of view, the frame design could have the cups, cones and ribs machined from a single block of aluminium to avoid the need for a bolt to connect the cups/cones with ribs. This would lead to two different frame designs, a male and female that would connect with each other with the ERM in the middle, which is more similar to what the FEM is actually modelling with the contact constraints. Alternatively, welding it on top of bolting could also bring benefits since the added material might help given the stress concentration region identified in the FEM analysis. Another point of improvement identified is to remove sharp tips from the cones to avoid high stresses and even damaging the cups. When modelling with a purely compressing acceleration at the frames, a stress singularity arose due to the infinitely small area in the tip of the cone.

Although cups and cones are meant to carry the shear and bending loads, there is quite some stress on the ERM itself. This, however, should pose no problem given the material property, titanium and nickel, and the magnitude of this stress, never exceeding 10 MPa. Moreover, the 17g was tested on all 3 axis, this is more critical than the required 7g axially and 2.4g laterally dictated by the structure subsystem requirements. Making sure the structure withstand that loading in all directions guarantees that the separation mechanism can be mounted in any direction, if desired, on the LV while still meeting the requirements.

It is worth mentioning that the assembly model does not perfectly simulate the structure, but it sufficiently models it to show that the design would meet the requirements. Modelling the full assembly with a high fidelity, including part connections and bolts, is highly complex, if not impossible, and given the margin between peak and yield stress, an attempt to do so might just lead to inefficient allocation of human resources, especially on such a short design project.

10.1.2. Modal Analysis

A modal analysis of the release mechanism assembly is performed to estimate the structure natural frequency. This is done to ensure that the low frequency mode is higher than 25 Hz as specified by DASH-LVP.01-MI.34-SYS.70-STR.03. As expected the eigenmodes of the structure is quite sensitive to the BC, because of that the mechanism was modelled with fixed constraint in several different configurations. This was executed to show that regardless of how the structure is fixed, the main natural frequency is well above the required 25 Hz.

The Tables and Figures below show the frequency of the first 6 modes of the structure depending on how the mechanism is fixed, from most to least critical.

Table 10.2: Release Mechanism fixed on side surfaces

Mode	Frequency [Hz]
1	196.06
2	535.66
3	710.95
4	1218.00
5	1379.60
6	1419.40

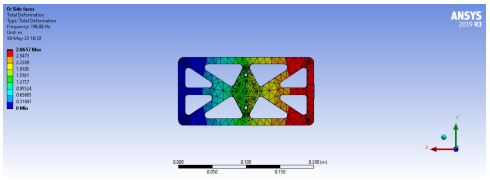

Figure 10.13: Main eigenmode for fixed side surfaces

Table 10.3: Release Mechanism fixed on bottom surfaces

Mode	Frequency [Hz]
1.	523.05
2.	642.98
3.	1127.80
4.	1714.70
5.	2145.10
6.	2237.00

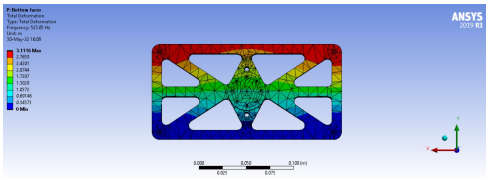

Figure 10.14: Main eigenmode for fixed bottom surfaces

Table 10.4: Release Mechanism fixed on the cone surfaces

Mode	Frequency [Hz]
1	538.73
2	1264.60
3	1394.60
4	1866.60
5	1905.50
6	2004.90

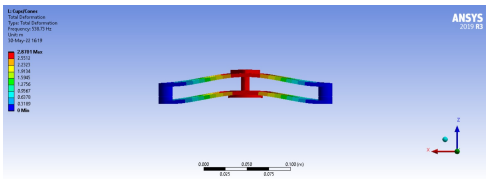

Figure 10.15: Main eigenmode for fixed cone surfaces

Table 10.5: Release Mechanism fixed on rib surface

Mode	Frequency [Hz]
1	1331.00
2	1841.10
3	1959.70
4	2477.20
5	2671.10
6	2894.00

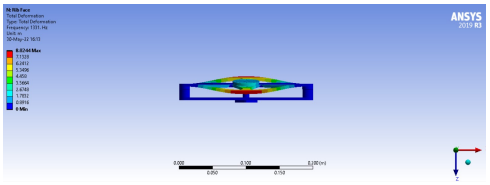

Figure 10.16: Main eigenmode for fixed rib surface

A material sensitivity analysis was also checked by changing the material of the part from aluminium to titanium, in case later iterations require this adjustment. The changes in the lowest natural frequency remained above the required 25 Hz.

From literature, the eigenfrequencies of a thin plate with lumped mass in the centre depends on the aspect ratio of the plate [21]. This roughly represents the assembled structure, so if future resizing of the mechanism is required to mount on the CubeSat structure, it is recommended to keep the 2:1 aspect ratio investigated here.

10.1.3. Recommendation and Testing

According to the MAC, the maximum acceleration is inversely proportional to the square root of the mass ($acceleration \propto \frac{1}{\sqrt{mass}}$), therefore a recommendation is made for repeating the analysis, once the mass budget is more precise, and in case there is a decrease in mass, since a decrease in mass leads to a higher maximum acceleration which in turns means higher stresses. Although the wide margin identified from the stress analysis, a more detailed analysis, with bolt constraints instead of contact constraint, is also recommended to better model the problem if human resources allow.

To show design feasibility in terms of requirement agreement, the key requirements that concern this particular structure have been considered. It is important to mention that The FEM analysis does not show proof of compliance, and proper testing must still be performed. As previously mentioned, the manual reset feature of this actuator allows for non-destructive testing to be performed on ground for verification purposes.

Given that such separation mechanism has not been used before for deep space separation of CubeSats, proper testing must be performed to ensure mission success. Following the ECSS standards

[16], the in house developed structure would be classified as a Category D, requiring a full qualification test programme to be performed whereas the COTS from EBAD would be classified as Category A and further qualification testing need not be performed.

A set of qualification testing, representing non-recurring costs, is required for the designed structure. For the quasi-static structure testing, generally two types of approaches are used, namely whiffle tree tests, and centrifuge tests. For the unidirectional launch loads testing of smaller parts, centrifugal tests are recommended, despite its high cost and large test facility requirements. At European level, the Large Diameter Centrifuge from ESA is able to simulate hypergravity condition of up to 20g and would be suitable to perform these sorts of tests not only for the qualification tests of the release mechanism but also at acceptance level for the complete CubeSats structure. At qualification level the goal is to test for ultimate load with the purpose of verifying structural adequacy, whereas for acceptance tests the flight limit loads are not exceeded.

For vibration testing, the use of a shaker to verify the modal analysis performed is recommended. The test shall show proof of compliance that the structure natural frequency is sufficiently greater than 25 Hz in accordance to DASH-LVP.01-MI.34-SYS.70-STR.03. Moreover, a random vibration and sine vibration test is also recommended to ensure the durability of the assembly. The use of accelerometers and strain gauges is prescribed for line load calculation, as explained in [76].

To validate the calculations performed for the separation velocity, an air table test is proposed. In such test, a frictionless surface is simulated, and the separation event can be replicated. Both linear and rotational velocity can be determined and the concurrent firing for simultaneous separation of both mechanism can be verified.

10.1.4. Alternatives

According to NASA space vehicle design criteria [23], most of the time and effort in structural acceptance testing is spent at the component and subassembly level. Designing the entire separation solution in house may amount to high levels of human resources allocation that could lead to delays and be used elsewhere. Therefore, outsourcing this design was also considered as an alternative solution. Companies such as ISISPACE have vast experience in the design of release mechanisms, and their Micro Satellite Separation System (M3S) have shown to be promising. This solution would vastly decrease the need for validation and verification, and delegating the work would unclutter the human resources of the DASH team.

Possible alternative actuators have also been considered in case the ERM from EBAD is not available or does not perform its function as planned, i.e. too high separation velocity, significant deployment delay etc. ARQUIMEA offer several hold and release mechanism, but their release load was comparably high to the ones offered by EBAD. Another promising solution with flight heritage is the non-explosive actuators (NEA) Model 9100 from EBAD used for similar purposes on releasing MASCOT from Hayabusa2 [24].

CarboNIX from EXOLAUNCH has also been considered as a possible solution with flight heritage. Not only does this mechanism provide a separation mechanism, but also an electrical connection between the connected CubeSats. Nonetheless, their smallest microsatellite separation system, 8 inches in diameter, was deemed too big to interface with the side surfaces of the DOTs and SHEPHERD.

10.1.5. Configuration and Operations

Because the design was performed concurrently, the full mission architecture was not known when the release mechanism was first designed. At a later stage of the design, more information was known and the solution updated. Figure 10.17, Figure 10.18 and Figure 10.19 shows how the release mechanism is expected to be mounted on the CubeSats and how it would look like during transfer and after separation.

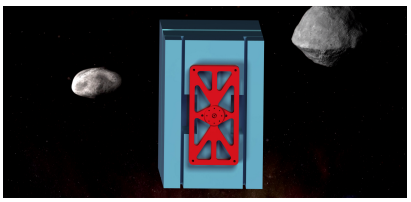

Figure 10.17: Mounted mechanism

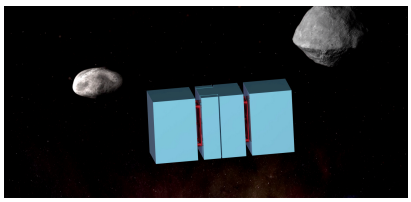

Figure 10.18: TRIAD configuration

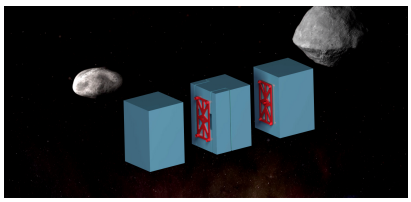

Figure 10.19: Separated

An architecture modification, from 16U to 12U, was performed which lead to a reduction from two to one separation mechanism per DOTs. Moreover, the decrease in volume would likely lead to a decrease in mass which in turn would mean a higher separation velocity, so maintaining the two separation mechanism would lead to a higher separation velocity than previously estimated. Another constraining reason was the allocated volume for the stowed solar panels. This led to mounting the mechanism 90° from it's previously planned position and the reduction from two to one mechanism per connection.

Based on the similarity with the release mechanism from previous missions, some functions that this mechanism need to comply with during mission operation, were derived based on the ones previously established for the release of MASCOT from Haybusa2 [24].

Functions adapted from MASCOT

- Secure and lock the CubeSats during transfer
- Deploy the system in a dedicated direction and with a defined velocity
- Provide deployment status information

Following the functions' definition, a possible separation logic sequence is defined. This is to be done in accordance to the previously defined operation modes in Section 3.3.

- SHEPHERD enter nominal operation mode
- DOTs enter operational mode
- Check DOTs battery status to deliver power to ERM
- DOTs AOCS fully operational
- Separation
- Attitude determination
- Control rotational motion
- Control translation motion
- Insert DOTs into desired operational orbit

Once the TRIAD has arrived in the Didymos system, the separation procedure needs to be performed. The sequence presented above will be further developed and what happens at each phase explained. First, the SHEPHERD will enter nominal communication mode, the engines will be shut down and as a result there will be a power surplus. At this phase, the SHEPHERD will be ready to relay information including separation status by ISL to the DSN.

Following that, the DOTs will enter operational mode, from this point onward DOTs will have control to separate from SHEPHERD. A consideration was made on whether the ERM should be fired from the SHEPHERD or DOTs, and due to size constraint it was decided that they would go into the DOTs, this means that the DOTs are responsible for their own detachment to the SHEPHERD. The downside is that it increases the difficulty of separating both DOTs simultaneously and in case of a malfunction of a DOT the SHEPHERD wouldn't be able to detach the defective unit. A potential benefit is that each DOT can separate from the SHEPHERD at different locations, allowing to insert each into their desired orbit around Didymos.

Before separation, the battery status in the DOTs must be checked to ensure enough power can be supplied to the separation mechanism. If there is insufficient power, transfer shall happen from the SHEPHERD to the DOTs before separation. The AOCS shall also be fully operational before separation happens to ensure it can react within reasonable time to counteract disturbances and undesired motions introduced by the separation mechanism. After that, the separation phase starts,

power is no longer transferred through the electrical connection and information is shared through ISL between the DOT to be separated and the SHEPHERD.

Finally, the ERM is ordered to be fired from the ground station. Once separated, the AOCS shall determine the attitude, followed by correcting for rotational and translational motion using the RCS on board each DOT, respectively. The RCS will ensure that separation velocity is kept within reasonable bounds and perform the desired orbit insertion. Next, deployment status information, including electrical separation status, will be relayed to the DSN through the SHEPHERD.

In about 10 to 12 minutes, the separation status should be received at the ground station on Earth. Assuming a separation velocity of half the one estimated on Section 10.1, to account for the removal of one mechanism, a speed of $3.09\,\mathrm{cm\,s^{-1}}$ is used for calculations. After 12 minutes, maintaining that separation velocity, the DOT will have moved 22.25 m from it's released position. Similarly, the remaining DOT + SHEPHERD will be moving in the opposite direction with a speed of approximately $0.98\,\mathrm{cm\,s^{-1}}$ having moved 7.08 m in the opposite direction, assuming the full wet mass for the SHEPHERD.

As previously presented in Section 3.4.8, it was decided that the N-DOT would separate first. The remaining two CubeSats, will have to perform a manoeuvre once the separation is successfully carried out and the ground station has received the separation status for the N-DOT. A 180° turn is commanded by the ground station to be performed to position the S-DOT into the correct separation direction. Once the manoeuvre is completed, both CubeSats can stand by for some time to ensure enough separation between the N-DOT and S-DOT. A 125 m trailing orbit is proposed requiring a total wait of 51 minutes assuming no influence of the AOCS so that the separation velocities between N-DOT and S-DOT + SHEPHERD remain as estimated previously.

Once the standby period is over, the same logic sequence is followed for the separation of the S-DOT. It should be noted that a different separation velocity might be expected if the translational speed from the S-DOT + SHEPHERD, due to the separation of the N-DOT, is not dumped. This can be used to further decrease the separation velocity of S-DOT with respect to Didymos or if desired the RCS could actuate to ensure a different separation velocity. Either way, the use of the RCS for the trailing orbit insertion will be required. Another consideration is that the resistance of the electrical separation has not been taken into account in these calculations. If, however, qualification tests show that the current ERM is not powerful enough to separate the CubeSats and disconnect the connection with the desired separation velocity, the actuator can be easily interchanged with a bigger one from EBAD while making little to no modification on the release mechanism interface structure.

10.2. COTS Structure Elements

A selection based on COTS components was considered and chosen for the main structure body of the CubeSats. This section will be split into the SHEPHERD and DOT bus since these CubeSats are so intrinsically different and thus require a different layout and hence a different COTS structure.

For the SHEPHERD, a 12U COTS structure from ExoTerra was selected. This is a particularly interesting part given this COTS product also comes with an integrated EPS and propulsion. For the DOTs bus, a 12U COTS unit from ISISPACE was selected. Considering the entire TRIAD configuration, a custom-made containerised deployer by ISISPACE is chosen.

10.2.1. SHEPHERD Bus

For the SHEPHERD bus, the ExoTerra Courier 12U platform is chosen[1] (see Figure 10.20). This bus module is typically delivered to customers already as a semi-complete spacecraft. The customer is allotted a payload volume, power, and mass which they have available to fill with the mission specific payload. For the DASH mission, much of the internals that can be provided by ExoTerra are not needed and will be replaced by custom hardware. The very appealing aspect of the bus is the very mass and volume efficient solar array folding technology, as well as the integrated ion engine gimbal, feed, and propellant tanks. The rest of the systems aboard SHEPHERD will be provided by the

[1] URL https://exoterracorp.com/products/solar-electric-propulsion-modules-and-bus/ [cited 12 June 2022]

DASH mission; this includes the ADCS, telecommunication, CDHS, thermal control, and navigation. To summarize, DASH will only use Courier's structural components, EPS and parts of ExoTerra's propulsion system. The rest will be developed in-house to suit the specific mission performance requirements. The key reason to choose this bus options over others, is how ExoTerra manages to provide a very capable solar array while remaining within the 12U bounding box of the stowed configuration.

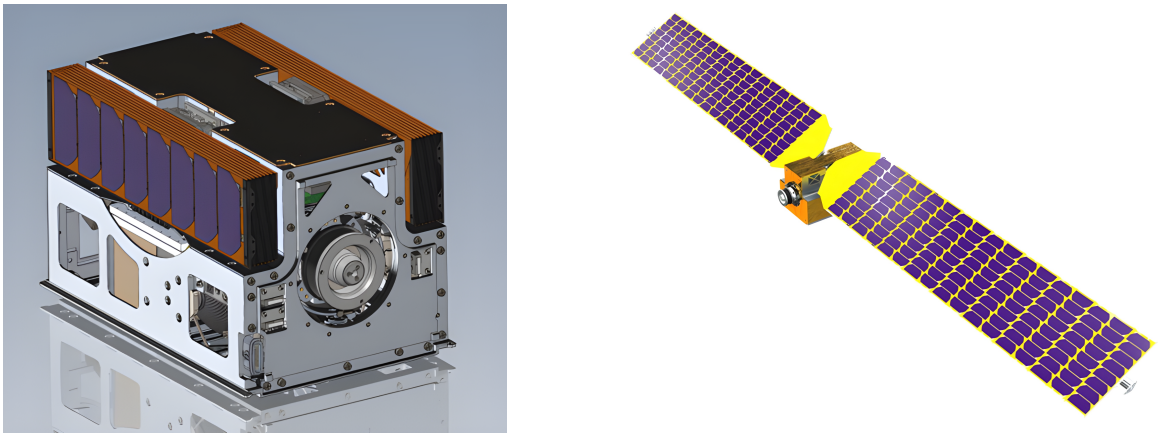

(a) Stowed configuration **(b)** Deployed configuration

Figure 10.20: COTS 12U Courier bus from ExoTerra for SHEPHERD

Through direct interviews with employees working at ExoTerra, the feasibility of using the Courier bus for the DASH mission was established. Specifically, ExoTerra's capability to provide modified versions of their standard 12U module was verified. Given the modular design of the solar arrays used on the Courier bus, ExoTerra confirmed that it is possible to scale/resize their panels to meet modified mission performance requirements in-line with those of the DASH mission. Although ExoTerra did provide a general performance overview for the Courier bus, the group was not able to obtain a detailed mass and power breakdown for all subsystems and components present aboard the pre-made module.

In order to perform a sensible mass budget for the SHEPHERD spacecraft, it is hence critical to know the mass distribution of the subsystems within the Courier bus. This allows the team to subtract components which are not going to be purchased usually part of the package, and add the extra equipment specific to the DASH mission. Both a bottom-up and a top-down mass distribution estimates are performed to verify the approximate validity of the results reached. This adds the additional layer of verifying that the masses in both approaches converge to within the allowed margin of errors when estimating such numbers with lacking initial data. So essentially, assuming (as specified directly by ExoTerra) that the specifications provided for the 12U Courier bus are those for a complete spacecraft minus the payload, a mass budget is done for all the subsystems aboard the completed COTS bus.

Bottom-Up Courier Mass Estimate

The mass distribution between subsystems is estimated with a bottom-up approach first, excluding payload from the bus dry mass. This is done to match SHEPHERD's zero payload design within DASH's mission architecture, see the mission configuration in Section 3.2.2. As ExoTerra does not provide a detailed mass breakdown for all components within the Courier bus, masses for each subsystem are taken where found and estimated otherwise. Specification sheets provided by ExoTerra are used whenever possible. Where no data is provided, estimates based on statistical relations as well as DASH's mission design are used to paint a complete picture of the Courier bus' mass distribution.

Starting with propulsion, three main components are considered, the ion engine, fuel tanks and propellant management system. The engine used aboard Courier, Halo, is also provided by ExoTerra and masses at 790 g [18]. The propellant management system mass is estimated by comparison to a similarly sized propulsion system masses at approximately 500 g [12]. To estimate the remaining element

mass, the fuel tanks, a more detailed statistical analysis has to be performed. Relations to correlate fuel volume, fuel mass and tank mass have already been found and described in Section 8.2.4 within the propulsion system definition. Using those relations and the directly provided (through personal communication with ExoTerra employees) Courier fuel capacity of 2.06 kg, the fuel tank mass can be estimated at 1.85 kg. Adding the masses of the tanks, engine and propellant management system yields an estimate for the mass of the propulsion system aboard Courier massing at an estimated 3.14 kg

Next is the electrical power system (EPS). The courier bus solar arrays are able to provide 300 W with a total panel area of, 0.8 m^2 separated into two deployable wings [17]. Using an assumed conservative specific power of 2.8 kg m^{-2} [57], a total panel mass of 2.24 kg is estimated. This means a mass of 1.12 kg per wing. The EPS mass of SHEPHERD was estimated in Section 9.3 to be 0.841 kg.

The rest of the subsystems, namely the thermal, CDHS, TT&C, ADCS, and structure, will have their mass estimated based on the requirements imposed by DASH on mission architecture as those will be highly comparable to Courier's performance requirements. As such, the same components and budgets derived for SHEPHERD are applied to Courier to estimate the masses of the remaining subsystems, see the respective chapters for a more detailed breakdown and analysis. This yields the Courier total dry mass breakdown by subsystem provided in Table 10.6. See the bulleted list below for a general overview of the assumed sources of mass within the remaining Courier subsystems.

Assumed Courier Remaining Subsystems:

- **Structures:** ISISPACE 12 U off-the-shelf structure
- **Thermal:** Heating elements including louvres, straps, and tapes
- **CDHS:** Onboard computer system
- **TT&C:** Transponder, High gain antenna, feed system, and transponder; inter-satellite link antennas and transponders
- **ADCS:** Reaction wheels, thrusters, and sensors
- **Navigation:** Lidar, camera, and avionics

Table 10.6: Bottom-up Courier bus mass estimate

Subsystem	Mass [kg]
Propulsion	3.14
EPS	3.08
Structures	1.50
Thermal	0.50
CDHS	0.10
TT&C	2.49
ADCS	2.67
Navigation	0.19
Wiring & margins	2.35
Total	16.02

Combining the masses of the individual subsystem leads to a total estimated Courier dry mass of 16.02 kg, excluding any potential payload.

Top-Down Courier Mass Estimate

To verify the mass estimate generated from the bottom-up is reasonable, a quick top-down estimate can be performed using the known Courier bus performance. From personal communications with ExoTerra, the bus is rated to provide a maximum delta-V of 800 m s^{-1} using 2.06 kg of xenon fuel when carrying a 1 kg payload mass. Furthermore, the standard on-board engine operates with a specific impulse between 715 s and 730 s. Using the rocket equation, the these parameters can be linked to the Courier's dry mass as follows.

$$\Delta V = I_{sp} \cdot g_0 \cdot \ln\left(\frac{M_{dry} + M_{fuel} + M_{payload}}{M_{dry} + M_{payload}}\right) \tag{10.1}$$

Plugging in the known values, the equation can be re-arranged and solved for the dry mass. With the provided range in specific impulse, Courier's dry mass can be estimated to be between 16.04 kg and 16.44 kg. This estimate is at most about 2.6% greater than the estimate reached using a bottom up approach, which indicates the validity of the subsystem mass distribution presented in Table 10.6.

Final SHEPHERD Bus

With the mass breakdown presented above, the general parameters for the COTS bus to be used for the SHEPHERD spacecraft can now be outlined. As introduced above, the Courier structure and bus is to be used for SHEPHERD. In addition to the structural elements, the EPS and propulsion system (except for the engine) is provided by ExoTerra. For clarity, the following distinction is made between components ExoTerra will provide for SHEPHERD and the ones DASH will provide instead.

Provided by ExoTerra as a single package:
- 12U Courier bus structure
- Propellant tanks, capable of storing 2.06 kg of Xenon
- Propellant management system
- Integrated ion engine gimbal mechanism
- Complete EPS (Panels, and conditioning and distribution electronics)

Provided by DASH:
- Ion engine
- Thermal management system
- CDHS
- TT&C
- ADCS
- Navigation system
- Interfaces to side-mounted DOTs

Note that being rated at similar power levels, ExoTerra's ion engine and the chosen DASH thruster are both expected to be compatible with the provided EPS. Furthermore, given the nearly identical cylindrical bounding boxes of the two engines and the DASH's lower engine thrust, compatibility with the gimbal mechanism is expected not to be an issue. Key parameters for the two ion engines are provided in Table 10.7, see chapter 8 for more details on DASH's engine selection and performance.

Table 10.7: ExoTerra Courier bus original thruster versus DASH's chosen replacement thruster

Parameter	**ExoTerra Courier Bus Thruster** [18]	**DASH replacement** [73][74]
Thruster name	Halo Hall-Effect Thruster	RIT-μX M-ARGO
Bounding box length	74 mm	76 mm
Bounding box diameter	76 mm	78 mm
Thruster mass	0.79 kg	0.66 kg
Max Thrust	8 mN	2.45 mN
Max Power	175 W	120 W

10.2.2. DOT Bus

For the DOT bus, the DASH mission will go with a COTS 12U structure from ISISPACE. This was chosen given the close contact with ISISPACE during the design phase of this project. The manufacturer confirmed the possibility of adapting the COTS structure to fit our mission and perhaps more importantly, the fact that the containerised deployer will also be outsourced to this company, integrating their own COTS structure may facilitate the entire design, and avoid extra costs and delays if a COTS structure from a different manufacturer was chosen. Table 10.8, provided by ISISPACE, shows the main properties of this component.

Table 10.8: 12U COTS structure description from ISISPACE

Property	**Value**	**Unit**
Primary Structure Mass	1500	gram
Primary + Secondary Structure Mass	2000	gram
Outside Envelope (l x w x h)	226.3 x 226.3 x 340.5	mm
Thermal Range (min – max)	-40 to +80	°C

A few considerations were made when selection of this COTS component. The main ones are presented below.

- Cutouts to integrate the separation mechanism
- Folding panels integration
- Physical connection between TRIAD configuration and containerised deployer

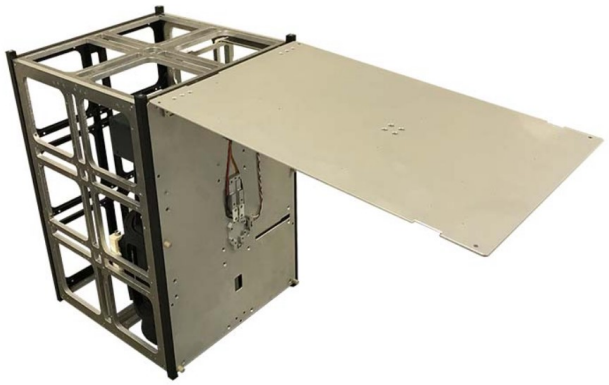

Figure 10.21: COTS 12U structure from ISISPACE (DOTs)

The COTS structure seem to perform sufficiently well to fulfil the considerations identified. Furthermore, the manufacturer itself also communicated the ability to customising this component if required to fit specific parts such as the ERM for the release mechanism. For the reasons described in this subsection, the 12U COTS structure from ISISPACE, shown in Figure 10.21, is selected.

10.2.3. TRIAD Containerised Deployer

In order to deploy each TRIAD from their respective kick-stage after it has ejected the spacecraft from Earth's sphere of influence, a deployment mechanism has to be devised. Such a mechanism has to be able to transfer the large acceleration and vibrational loads stemming from launch and ejection from Earth's sphere of influence, while able to reliably let go of the TRIAD when instructed to do so. Two main approaches are considered: A containerised deployer or an open deployment mechanism. In what follows, the difference between these approaches and the final decision are discussed in more detail.

Containerised Versus Open Deployment Mechanisms

The key difference between a containerised and open deployer lies in how they interface to the payload they are responsible for deploying. Containerised deployers, as the name suggests, are essentially boxes into which the flight hardware is placed and stored during launch and ascent. When the time comes, one side of the deployer opens up and the spacecraft within is launched outwards through the use of spring-loaded pusher plates installed on the opposite end. Open deployers instead usually interface at the bottom of the flight hardware through the use of a clamp band, or any other release mechanism.

Although not scalable to large spacecraft, containerised deployers are preferable from a structural point of view. By enclosing the entirety of their payload, they are able to interface with it from all corners, and hence transfer the large acceleration loads much more effectively. This greatly reduces the performance requirements of the spacecraft bus, as not required to carry the loads itself. Specifically, deployers are very common when it comes to spacecrafts within the CubeSat standard, as already premade deployers can be purchased from manufacturers with not compatibility issues.

For DASH, some extra considerations must be taken into account when choosing a deployer type. Being based on the CubeSat standard, it might seem trivial to find the correct deployer, but this is not the case, due to the nature of the general mission configuration. As individual CubeSats are assembled into TRIADs, normal COTS deployers are not an option; a custom version has to be made just for DASH. Although potentially expensive, this choice has been deemed superior to using open deployment mechanisms for one key reason. Using a containerised deployer approach allows DASH to leverage all the aforementioned structural benefits, which allow to greatly reduce the loads and forces to be sustained by the mechanisms connecting the SHEPHERD and DOTs into a TRIAD. Although deemed technically feasible, these mechanisms are still underdeveloped, expecting them to carry the large loads and vibrations directly and not supported by a containerised deployer would be unrealistic, or at the very least risky from a technology readiness point of view. A containerised deployer approach is hence chosen for the DASH mission.

ISISPACE Custom Containerised Deployer

After establishing the need for a custom deployer, the DASH team directly contacted ISISPACE, a European spacecraft components and deployers manufacturer, to assess the feasibility of the deployer required by the DASH mission. Through two direct meetings with ISISPACE employees working on the development and production of CubeSat containerised deployers, the team was able to positively assess the feasibility of meeting DASH's performance requirements. Based on the exact final dimensions of a TRIAD, see Figure 10.22, ISISPACE confirmed the feasibility of leveraging their expertise and heritage to develop a custom deployer to hold and deploy a TRIAD within the DASH mission architecture.

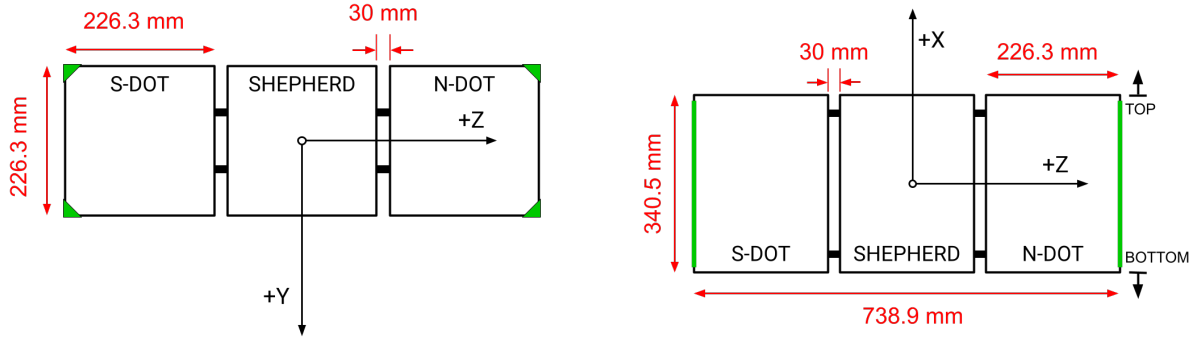

(a) Top view **(b)** Side view

Figure 10.22: TRIAD dimensions in red, deployer rail positioning in green

The deployer drafted and discussed in collaboration with ISISPACE would interface with the triad at each of its four corners with standard deployment rails (see the green lines in Figure 10.22), and deploy the TRIAD upwards in the positive X-axis direction (see Section 3.2.1 for an overview of TRIAD's coordinate system). Based on their experience with current deployers designs, some estimates were provided regarding the custom deployer tolerances and development costs. Firstly, it was decided to interface with only the four outermost edges. As ISISPACE explained, attempting to interface to the SHEPHERD edges would not actually serve to distribute the loads due to potential tolerance issues. This means that SHEPHERD will only be supported through the separation mechanism of the DOTs, along with four load-introducing pillars on the bottom. The pusher plates that eject the TRIAD are only connected tot the DOTs.

Regarding space around the standard 12U busses: the DASH team was assured a gap of 10 mm to 20 mm is reasonable in addition to the bus dimensions. This means there are up to 2 cm in each direction in addition to the bus volume to mount externally deployable structures. Furthermore, given the geometry of a TRIAD and standard pusher-plates designs, ISISPACE estimated up to 40 mm of space in addition to the CubeSat bus below the central SHEPHERD spacecraft.

Regarding the research and development for this deployer, given the most up-to-date mission configuration and budgets, ISISPACE estimates about a 1-year development cycle and a total cost between 1 and 2 million 2022 EUR. This cost includes not only the research and development, but also the production and delivery of the three required deployers for the three TRIADs composing the DASH mission.

11 Thermal Control System

During the entire lifetime of the satellites, from launch and the long transfer to nominal operations, the system will be exposed to extremely harsh thermal environments, especially for the DASH which is a deep space mission. As the DASH mission will use an electric propulsion system that requires relatively high power output, the temperatures during transfer burns of the ion engine will rise significantly also. Conversely, when the engine is shut off at a large distance from the Sun, the spacecraft's temperature could drop drastically, causing risks for the correct functioning of critical components.

In order to assure that all the components and subsystems of the DASH mission survive all possible scenarios in the right operational temperature, a thermal control system (TCS) is required. The purpose is to keep the temperature distribution within reasonable bounds at all locations in the satellites. To decide on which components - either passive or active - are required to fulfil this purpose, a detailed thermal analysis is performed.

Section 11.1 introduces the modelling methodology, after which the initial results of that analysis are presented in Section 11.2. These insights are then used to make all design decisions for the components of the TCS in Section 11.3, including a final analysis of the effectiveness of the solution. Finally, the model verification and validation is discussed in Section 11.4, including important recommendations to increase the confidence in the design.

11.1. Multi-Node Thermal Model

During the preliminary design phase, an initial estimate of the thermal conditions was made based on a highly simplified single-node thermal analysis. This basically estimates the average temperature of the spacecraft by balancing the incoming radiation, outgoing radiation and internal dissipation and finding the equilibrium temperature. However, such approach does not give any insight into the internal temperature distribution. The latter is of course relevant, as the most extreme temperatures will be the driving factors in the design of a TCS. Certainly because of the centralised heat source at the location of the ion engine, the need for a multi-node analysis arises to increase the resolution of the thermal simulation.

A number of dedicated software packages that provide functionality for detailed thermal analysis. For instance, the ESATAN Thermal Modelling Suite (ESATAN-TMS) was developed specifically to allow straight-forward definition of thermal network quantities and material properties, as well as extensive possibilities for validation and model checking [66]. ESATAN has a possibility for lumped parameter models, which makes it significantly easier to get preliminary results than with alternatives like ANSYS [39], which work exclusively with detailed Finite-Element Methods (FEM). From these considerations, there is a strong preference to perform this first analysis with ESATAN-TMS. However, this was hindered by several licensing complications. Therefore, the present work uses a custom basic implementation of a thermal network, based on the same underlying principles. Although this simplified analysis is designed to expose the most important thermal characteristics, it is highly recommended to perform further validation using more refined meshes in existing software to increase confidence in the design.

11.1.1. Model Theory and Implementation

For the purpose of estimating the thermal distribution, the spacecraft is divided into discrete elements that are represented by a control volume for the heat flux. These elements are referred to as *nodes* and they are linked to other nodes and possibly the space environment through conduction and radiation characteristics. Due to the vacuum environment, any contribution of convection can be neglected.

The first source of heat originates from solar radiation. Provided that J is the solar flux density at the

location of the satellite and $J_{Sun,1AU} = 1368\,\mathrm{W\,m^{-2}}$, $A_{p,i}$ is the projected area of node i, perpendicular to the incoming solar radiation and α is the absorptivity of the node's material, the resulting heat flux in any of the nodes can be approximated as

$$\dot{Q}_{solar,i} = J_{Sun}\alpha A_{p,i} F_e; \qquad \text{where } J_{Sun} = J_{Sun,1AU}\left(\frac{R_{Sun,sat}}{R_{Sun,Earth}}\right)^2. \tag{11.1}$$

The view factor F_e is 1 when the node is in the Sun and 0 when it is shadowed completely by other nodes or the Earth. A very similar formula could be used for possible albedo effects, although these will only have any significant contribution while in orbit around Earth. In Equation 11.2, α_{albedo} is the albedo coefficient of the Earth, which is assumed to be 0.26. This is the fraction of the solar flux that is reflected back into space [15]. The angle ξ is between the Sun, the centre of the Earth and the spacecraft.

$$\dot{Q}_{albedo,i} = \alpha_{albedo} J_{Sun}\alpha A_{p,i} F_{p,i} \cos\xi. \tag{11.2}$$

While close to Earth, the infrared (IR) radiation of the planet also comes into play. This is essentially the same calculation as for the solar heat (Equation 11.1), except that the wavelength of the radiation is now in the infrared spectrum, so the emissivity ε_i is used instead of absorptivity. The value for Earths heat flux density is assumed to be $J_{Earth} = 236\,\mathrm{W\,m^{-2}}$ [10].

$$\dot{Q}_{p,i} = \varepsilon_i J_{Earth} A_{p,i} F_{p,i} \qquad \text{where } J_{Earth} = J_{Earth,R_E}\left(\frac{R_E}{R_{Earth,sat}}\right)^2. \tag{11.3}$$

The last two contributions are in principle also applicable to the target asteroid, but the albedo and infrared radiation of Didymos may be neglected, as its size is very small and the heat fluxes associated are orders of magnitude smaller compared to the other heat generating mechanisms.

All of the above is already considered when only analysing a single node. The multi-node approach, however, takes the interactions between nodes into account. The heat that flows from node j to node i over time is defined by Equation 11.4. There, $A_{ij,eff}$ and $L_{ij,eff}$ are the effective area and distance between the nodes, respectively and $k_{ij,eff}$ is the effective conductance of the linking material. Note that this value is negative if the temperature T_i is larger than T_j, in which case heat flows from i to j. Equation 11.5 then describes the heat flow between the nodes by radiation. Here, $\sigma = 5.67{\times}10^{-8}\,\mathrm{W\,m^{-2}\,K^{-1}}$ is the Stefan-Boltzmann constant, A_i is the area of the node and $F_{j\to i}$ is the view factor between the faces of the nodes. The calculation of this factor is illustrated in Figure 11.1 and detailed in Equation 11.6. For the purposes of the present analysis, the integral in this equation is approximated by evaluating the integrand only once for the entire area of the node. Increasing the number of nodes would then also refine this estimate. Note that Equation 11.5 can also be used to calculate the heat flowing into space. The other node then represents outer space and can be assumed to have a temperature of 0 K.

$$\dot{Q}_{cond,ji} = C_{ji}\left(T_j - T_i\right) = \frac{k_{ij,eff} A_{ij,eff}}{L_{ij,eff}}\left(T_j - T_i\right) \tag{11.4}$$

$$\dot{Q}_{rad,ji} = \sigma\varepsilon_i\varepsilon_j A_i F_{j\to i}\left(T_j^4 - T_i^4\right) \tag{11.5}$$

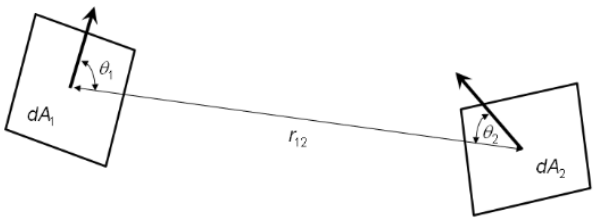

$$F_{j\to i} = \frac{1}{A_i}\iint_A \frac{\cos\theta_j \cdot \cos\theta_i}{\pi r_{ij}}\,dA_j\,dA_i \tag{11.6}$$

$$\approx \frac{\cos\theta_j \cdot \cos\theta_i}{\pi r_{ij}} A_i \tag{11.7}$$

Figure 11.1: View factor calculation between two surfaces

Finally, nodes that represent heat-generating components will also introduce a heat flux $\dot{Q}_{gen,i}$. Combining all of these effects together results in the complete heat balance equation for each of the nodes. Provided that the initial temperature state is known, this differential equation can be propagated in time to find the thermal behaviour [14]. Alternatively, it could be used to find the steady-state solution in a constant thermal environment. The latter would start from an initial guess.

$$C_i \frac{dT_i}{dt} = \dot{Q}_{sol,i} + \dot{Q}_{alb,i} + \dot{Q}_{planet,i} + \dot{Q}_{gen,i} + \sum_{j=1}^{n} C_{ji} \left(T_j - T_i\right) + \sum_{j=1}^{n} \sigma A_i \varepsilon_i \varepsilon_j F_{ij} (T_j^4 - T_i^4) - \varepsilon_i A_i \sigma T_i^4 \quad (11.8)$$

These individual equations can of course be assembled into a system of ordinary differential equations to allow for a more structured integration method [2, 61]. In Equation 11.9, the temperature vector $\vec{T}$ contains the temperature state of all the nodes at a specific time and $[C]$ represents the diagonal matrix of heat capacities. Furthermore, the links between all nodes are lumped in the conductance matrix $[K]$ and the radiation matrix $[R]$. The elements on the diagonal are negative and represent outgoing radiation, whereas all others are positive to accumulate all incoming radiation. Finally, the vector $\dot{\vec{Q}}_{ext}$ contains all external heat influx, including any generated heat at the nodes.

$$\frac{d}{dt}\vec{T} = [C]^{-1} \left([K]\,\vec{T} + [R]\,\vec{T}^4 + \dot{\vec{Q}}_{ext} \right) \quad (11.9)$$

A simple but versatile solver is implemented in Python 3.8 [70], that allows specifying any number of *nodes* and *connections*, after which the above system of equations is integrated using a fourth-order Runge-Kutta implementation [8]. The implementation assumes that the heat capacities, conductances and radiation properties between the nodes remain unchanged. The external heat fluxes (solar, albedo, planet IR and generated heat) can either be constant for a steady-state solution or vary with time for transient temperature distributions.

11.2. Thermal Analysis for DASH

Now that a model is created to solve basic thermal networks, a critical step is to define the geometrical layout of the DASH mission in terms of a limited number of nodes. The solution of these problems is subject to the *rubbish in, rubbish out (RIRO)* principle: If the problem itself is ill-defined, a flawless solver will still produce useless results. An accurate representation of the geometry with valid assumptions is therefore essential to get to realistic insights. Please refer to Section 11.4 for more details on the validation methods.

In the present work, the SHEPHERD and both DOTS are each modelled by a set of seven interconnected nodes: one for each outer face and one that represents the internal temperature. Because the ion engine is expected to be a large heat source, an additional node for that is added in the SHEPHERD. The walls of each CubeSat are then connected through a conductive and radiative path. Furthermore, each of the solar panels is represented by a single node, that is connected to the SHEPHERD through a conductive link. The heat transfer between the CubeSats is modelled as a combination of conduction through the separation mechanism and radiation between the connecting walls of SHEPHERD and DOTs, respectively.

Any direct thermal interaction between the solar panels and DOTs is neglected, except for shadowing from the Sun or the Earth. Note that all the internal dissipation is grouped in the internal node of each satellite, except for the engine, which has a node of its own.

The entire layout for the thermal simulations is depicted by Figure 11.2. This image is not to scale and simply serves to visualise the nodes and their connections. It is important to mention that all these nodes are considered isothermal for the present analysis. This is of course a major assumption that reduces the relevance of the results. However, adding more nodes and connections would greatly add to the complexity and increase the likelihood of human error while creating the geometry. For increased mesh density, it is recommended to use more advanced simulation software.

Table 11.1 lists all the mentioned nodes and their respective properties. A list could also be made to detail all the links and their conductive and radiative properties. However, this would be a rather lengthy list with a lot of repetitive information. Notice that the emissivities and absorptivities are not given in Table 11.1. This is because they heavily depend on the thermal design, introduced in Section 11.3.

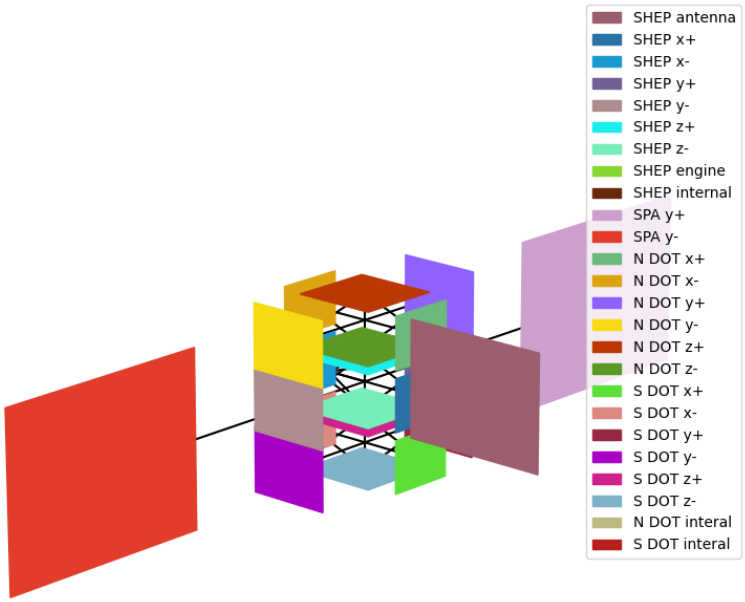

Figure 11.2: Thermal nodes and connection layout. The areas are not to scale.

Table 11.1: List of nodes for thermal analysis

Node Nr.	Node ID	Loc. Coords [U]	Mass [kg]	A_i [m^2]	Heat [W]	α	ε
		Rotating Solar Panels					
1	SPA $y+$	(0, 11.3, 0)	1.24	0.44	0	*	*
2	SPA $y-$	(0, -11.3, 0)	1.24	0.44	0	*	*
		Shepherd					
3	SHEP $x+$	(1.5, 0, 0)	0.8	0.04	0	*	*
4	SHEP $x-$	(-1.5, 0, 0)	0.8	0.04	0	*	*
5	SHEP $y+$	(0, 1, 0)	1.2	0.06	0	*	*
6	SHEP $y-$	(0, -1, 0)	1.2	0.06	0	*	*
7	SHEP $z+$	(0, 0, 1)	1.2	0.06	0	*	*
8	SHEP $z-$	(0, 0, -1)	1.2	0.06	0	*	*
		Internal					
9	SHEP engine	(-1.3, 0, 0)	0.66	0	50	-	-
10	SHEP internal	(0, 0, 0)	11	0	5	-	-
11	NDOT internal	(0, 0, 2.3)	13	0	5	-	-
12	SDOT internal	(0, 0, -2.3)	13	0	5	-	-
		N-DOT					
13	NDOT $x+$	(1.5, 0, 2.3)	0.8	0.04	0	*	*
14	NDOT $x-$	(-1.5, 0, 2.3)	0.8	0.04	0	*	*
15	NDOT $y+$	(0, 1, 2.3)	1.2	0.06	0	*	*
16	NDOT $y-$	(0, -1, 2.3)	1.2	0.06	0	*	*
17	NDOT $z+$	(0, 0, 3.3)	1.2	0.06	0	*	*
18	NDOT $z-$	(0, 0, 1.3)	1.2	0.06	0	*	*
		S-DOT					
19-24	SDOT [..]	Identical to N-DOT nodes (mirrored over local xy plane)					

To model the worst case scenarios that the DASH mission will have to endure, a hot and cold case are identified. The hot case occurs just after deployment from the kick stage, when the TRIAD has

opened its solar panels and initiated full thrust towards Dydimos. At this point, the satellite group is at its closest to both Earth and the Sun, taking in the maximum amount of solar energy and IR radiation. Additionally, this is the only time when the engine can operate at full power, as the power available will decrease as the TRIAD moves further from the Sun.

Conversely, the cold case happens at the very end of the payload operations phase. During operations at Didymos in early 2027, the asteroid will be moving away from the Sun, such that the end-of-life distance (2.20 au from the Sun) is also the maximum distance. At this point, the SHEPHERD and DOTs do have a peak internal dissipation around 30 W, which prevent freezing of the internal layout.

Figure 11.3 shows the original steady-state temperature simulation, using aluminium for all the walls and connections ($\alpha = 0.25$, $\varepsilon = 0.15$, k =239 W m^{-1} K^{-1}). Note that the figure suggests that a transient analysis was performed; however, it is simply a steady-state simulation starting from an initial guess of 300 K. As the thermal model was initially designed to do transient analysis based on the entire trajectory, the same model was used for these steady-state estimates.

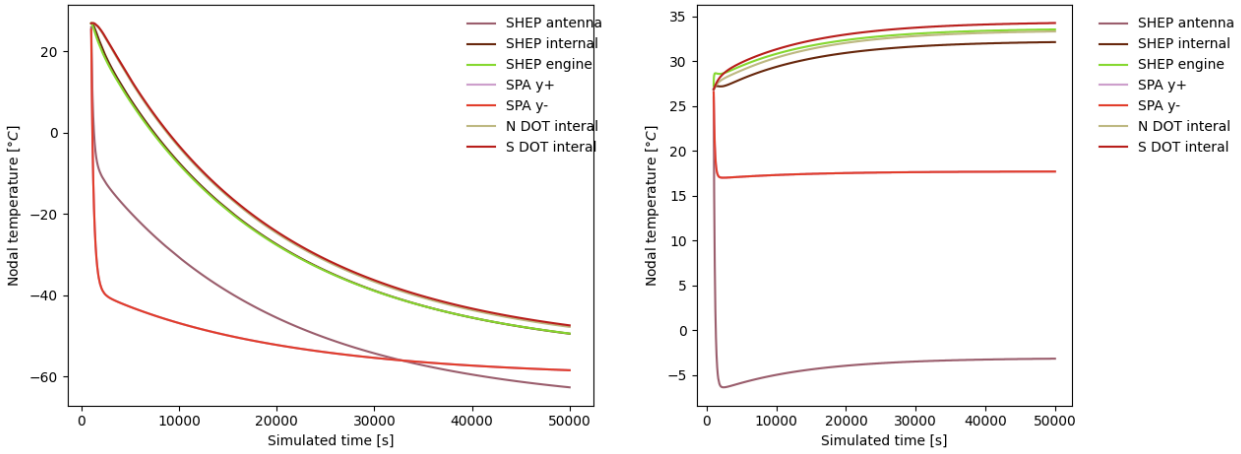

(a) Cold Case

(b) Hot Case

Figure 11.3: Thermal steady-state simulation before thermal design.

This first estimate already assumes close conductive links between the engine and the side walls, as well as an engine efficiency of 60 %, such that the hot case is actually much less constraining than the cold case. Without special coatings, taping or MLI, the spacecraft would be expected to survive the hot case. However, at the end of payload operations, most systems would break as a result of the cold environment. The solutions for these problems are presented hereafter.

11.3. Thermal Control Design

Now that the thermal analysis has been made, the actual design of the TCS can be presented. First of all, the subsystem operating temperatures for all DASH subsystems are listed in in Table 11.2. It shows the temperatures for operating and non-operating situations. The thermal control components must ensure that all of the local temperatures are maintained within the narrowest limit of the temperature ranges shown.

Introduction of the options

There are several categories that exist for thermal control components. One of them is either utilising passive or active components. The main difference among the two types is that passive does not consume power when operated, whereas active is the opposite. Typical types of passive components with explanation about each of them are shown below in a list [62].

1. **Painting, surface coating:** Properties of the surface can be modified by applying painting or surface coating to it. They typically function in incresing or decreasing the solar absorptivity or IR emistivity of a certain surface. They have a feature of being able to apply non-flat surfaces easily compared to taping.

Component	Operating Temperatures [°C]	Non-Operating Temperatures [°C]
ADCS	-30 to +85	
Sun Sensor	-30 to +85	
IMU	-40 to +85	-55 to +90
CDHS	-25 to +65	
ISL Antenna	-20 to +80	
High gain antenna	-55 to +125	
EPS	-40 to +70	-40 to +85
Solar panels	-40 to +125	-40 to +125
Structure	-40 to +80	-40 to +80
ISL transceiver	-30 to +85	-30 to +85
Earth link transceiver	-20 to +50	-30 to +60
Engine	-40 to +160	-60 to +160

Table 11.2: Operating temperature of components

2. **Taping:** Taping has similar functions as the before mentioned painting and surface coating. However, it is easy to apply and remove, is comparatively inexpensive, and has a longer usable lifetime compared to painting and coating. It can also be added later in the assembly process if it is necessary for design modification.
3. **Polyimide film tape and MLI tape:** The main function for these in CubeSat situations are that they can insulate wires and cables.
4. **Thermal Straps:** Thermal Straps functions in increasing the conductivity between a heat source and a sink. Metal is the typical material type used to manufacture them.
5. **Thermal Interface materials:** Interface materials are commonly used between heat dissipating electronics boxes and mounting surfaces to thermally sink the hot components to a colder surface and reduce the temperature of the electronics.
6. **Passive Thermal Louvers:** Eventhough louvers are typically active components, NASA GSFC has developed one acting passively that uses bimetallic springs to adjust the positions of the flaps. When the temperature of the overall S/C increases, the springs expand and the flaps and open and radiate heat out, whereas the opposite happens when the S/C temperature drops. This fact makes it possible for louvers to be applied to CubeSats, in which conventionally they were used for conventional satellites only due to its massive power consumption [53].
7. **Deployable radiators:** The deployable radiatiors are noramally stowed when not needed. Once it is demanding,the radiators are deployed and heat is radiated externally from the S/C.
8. **Phase Change materials:** The phase change material absorbs heat dissipated from the heat source and converts in a liquid state (initially a solid state). Once the source dissipated heat decreases, the material converts back into a solid state. In this way, the temperature range of the S/C is maintained in a certain limit.

Additionally, typical types of active components with explanation about each of them are shown below in a list.

1. **Kapton Heater:** These generate heat whenever current is applied. They are applied to batteries due to the narrow temperature range of them.
2. **Cryocoolers:** These are refrigeration systems which are typically used to cool instruments such as high precision IR sensors, imaging spectrometers, interferometers and midwave infrared (MWIR) sensors that require to function at extremely low temperature. The low temperature improves the dynamic range and extends the wavelength coverage of them.
3. **Active Thermal Architecture:** This is a project aiming to release a active thermal control technology for CubeSats. It consists of a first stage, with a mechanically pumped fluid loop which circulates heat through the system. For the second stage, a miniature tactical cryocooler exists which provides direct cooling to the payloads.

Another type of category is either using conduction or radiation in order to capture or dissipate heat in the S/C. In between the options introduced above, components such as thermal straps utilise conduction in order to execute thermal control. Apart from those, the rest of the options use radiation as their main method to control thermal environment of the spacecraft [6].

Final choice

Among the options introduced in the previous section, a number of specific components were chosen. From theory and from the previously introduced simulation framework, it is clear that regulating the equilibrium temperature of the satellite system comes down to balancing the incoming and outgoing radiation, along with the internally generated heat dissipation. Balancing radiation is done by tailoring the radiating surfaces such that their steady temperature is in the required range. According to Kirchoff's law, the solar absorptivity α and infrared emissivity ε are equal at every wavelength [26]. However, the input radiation is mostly in the visible light regime and outgoing radiation consists mainly of thermal infrared waves. Therefore, it is possible to engineer the materials of the radiator surfaces such that they either absorb or emit more. Using Equation 11.1 and Equation 11.5, it is clear that the balanced temperature of the radiator is proportional to the one over fourth power of the α/ε ratio:

$$T_R \propto \left(\frac{\alpha}{\varepsilon}\right)^{\frac{1}{4}}. \tag{11.10}$$

Choosing an applicable radiator material is one of the main ways to passively influence the thermal balance. Figure 11.3 gives an overview of these properties for conventional thermal control materials. Using this fact and figure, the decision was made on which components to choose for the radiator materials applied to certain surfaces.

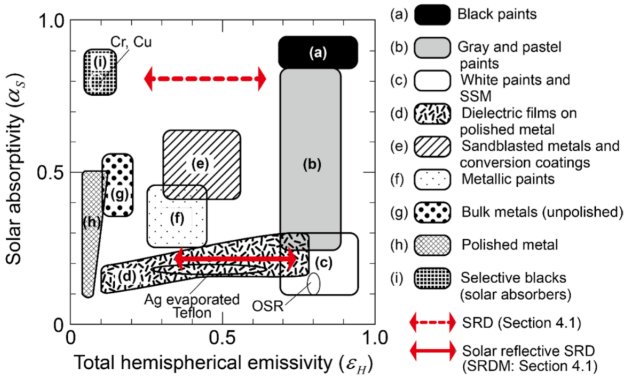

Figure 11.4: Total emissivity and absorptivity values for conventional passive thermal control materials and a smart radiation device (SRD) for spacecraft [26]

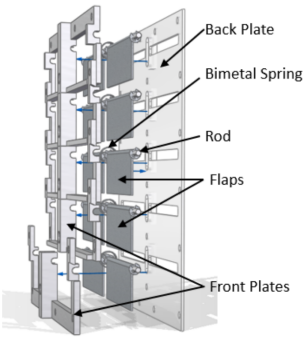

Figure 11.5: Exploded view of a thermal louver with a 1U form factor [53]

In Table 11.4 and Table 11.3, the chosen ones are shown. Conventionally, CubeSats use active electrical heater attached to the batteries and passive control systems on the rest of the parts [78]. However, in the situation of the DASH, the batteries were considered to be part of the EPS, which normally have batteries with attached heaters on them for thermal control. That is why in the two tables shown, the heaters for the batteries are not mentioned [27].

The thermal interface material is placed between the engines and the walls that are in contact with it have a short distance between them. The thermal straps are placed between the engine and side walls as well as between payload and walls, due to the payload being sensitive to temperature variant. The white coating and black coating will be applied on the back of the solar panels and on the internal electrical components, respectively. The taping will be applied on the exposed surfaces of both the SHEPHERD and DOTs. Finally, the passive thermal louvers are placed on all the surfaces separation is present, i.e. 2 surfaces for the SHEPHERD and 1 each for both DOTs.

Based on all the above adjustments, new estimates are made for the cold and hot case and the results are shown in Figure 11.6a and Figure 11.6b, respectively. Several observations can be made

Type	Component	Mass [kg]	Volume [U]	Cost [kEUR]	Absorptivity	Emissivity
Thermal interface material	Bergquist Gap Pad 3000S30	0.19	0.06	1.8	-	-
Thermal Straps	Aavid k-core straps	0.072	0.0014	2	-	-
White Coating	AZ technology AZ-2100-IECW	0.05	-	2	0.15	0.9
Black Coating	AZ technology AZ-1000-ECB	0.047	-	2	0.97	0.89
Taping	Sheldahl Silver Coated FEP Reinforced with Polyimide	0.07	-	5	0.75	0.09
Passive thermal louver	NASA GSFC	0.12	0.136	5	-	-

Table 11.3: Thermal Passive Components of the SHEPHERD

Type	Component	Mass [kg]	Volume [U]	Cost [kEUR]	Absorptivity	Emissivity
Thermal interface material	Bergquist Gap Pad 3000S30	0.19	0.06	1.8	-	-
White Coating	AZ technology AZ-2100-IECW	0.05	-	2	0.15	0.9
Black Coating	AZ technology AZ-1000-ECB	0.047	-	2	0.97	0.89
Taping	Sheldahl Silver Coated FEP Reinforced with Polyimide	0.07	-	5	0.75	0.09
Passive thermal louver	NASA GSFC	0.12	0.136	5	-	-

Table 11.4: Thermal Passive Components of the DOTs

regarding the final temperature distribution. For the hot case, all the components are well within their operational margins. And considering that most of those components are actually non-operational during this time, this critical case can surely be dealt with by the thermal design. The thermal straps provide a fast way for the generated heat to reach the outer walls and radiate into space, the same is true through the thermal interface material, which bridges the gap towards the sides of the CubeSats.

The Cold case, however, imposes some critical cases. The projected solar panel temperature at this time is around −50 °C. This is 10 degrees below the operational range and therefore critical. However, since this will only occur at the end of the science operations and the non-operating temperatures go down to −60 °C, the risks of reduced power can be accepted for the time being. It is highly recommended to further investigate if the solar panels could indeed extend their operational range without significant performance degradation or critical failure.

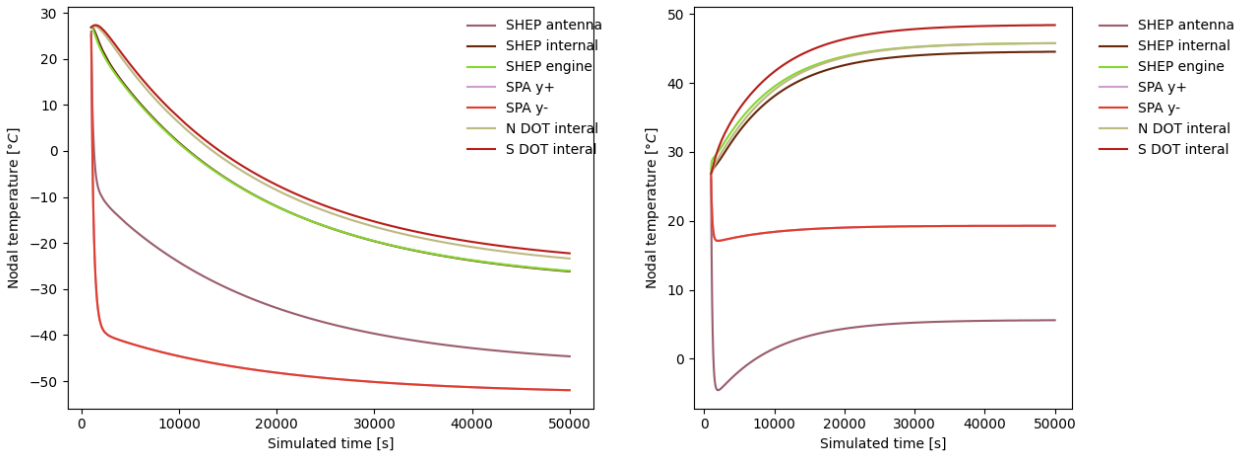

(a) Cold Case **(b)** Hot Case

Figure 11.6: Thermal steady-state simulation

One last observation is that the earth-link transceiver comes very close to its operational minimum as well. As shown in Table 11.2, it should not operate below −20 °C. The current estimates show that the SHEPHERD internal temperature could drop slightly below this limit. However, at this time, one could question the validity of assuming an isothermal environment within the satellite. It is perfectly possible that the temperature at this transceiver is higher than average within SHEPHERD. The addition of more nodes within the satellites would be required to get to a valid conclusion. If required, additional

insulation could be added locally around the transceiver or the conductive path could be reduced such that it could hold its own thermal energy better without active heating.

11.4. Model Verification, Validation and Recommendations

Several efforts were made to verify and validate the thermal model. First of all, unit tests were implemented to automatically test the partial functions that calculate the various heat sources at every time step. This was achieved by setting up a set of default inputs and expected outputs and checking whether these matched. Most unit tests were written during the development of the code, however, some were only made afterwards. This can be seen as a weakness, since it constrains the thought process while creating the tests. It is recommended to revise these unit tests for higher confidence in the test suite.

Furthermore, a test was performed on a higher level to ensure the correct implementation of conductive *connections* between *nodes*. The linear heat transfer in a circular rod was modelled using 2 nodes. A sketch of the situation is shown in Figure 11.7. The expected thermal balance was found for a range of thermal conductivities k, mass fractions (changing the mass with T_1 and T_2), distances d and effective areas A. These results provide confidence in the conduction modelling, but don't say anything about the radiative scenarios.

To ensure radiation is correctly calculated, two additional tests were created: one to model the interaction of a node with the environment, and another to model radiation between two non-touching nodes. For the former, only one node was created, explicitly setting the location of Earth and the Sun at a 90° angle with respect to the node. changing the orientation and area of the node, as well as its distance to the Sun and the Earth, allowed to verify all different aspects of the incoming radiation. Then moving the spacecraft to infinite distance from those two bodies allowed to isolate the influence of internally generated heat. For the second radiation test, two nodes were created in isolation of the environment, in a configuration as presented by Figure 11.1. Changing their relative orientation and distance as well as mass and temperature revealed the correct behaviour of the inter-nodal radiation modelling.

Even though rather extensive verification was performed on the modelling techniques themselves, this does not provide any assurance that the actual spacecraft model represents reality. To validate that this is indeed the case, either another more advance simulation tool or experimental results must be used. It is strongly recommended to implement the same model into a software system like ESATAN-TMS and use their automatic mesh generation and ray-tracing algorithms to validate the implementation from the present work.

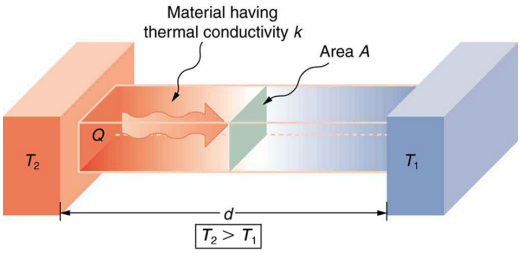

Figure 11.7: Linear transfer in a rod

12
Command and Data Handling Subsystem

The CDHS can be seen as the 'brain' of the S/C. All the data flows through this system is either relayed to the different subsystems, payload, or to the communication subsystem which will send signals to the ground station. In this section, the architecture of the CDHS will be further explained, and the components that will be used are listed.

12.1. CubeSat Distributed File System

For the data storage and processing of the payload satellites, we will make use of the CubeSat Distributed File System (CDFS). This system has already been thoroughly discussed in the Midterm Report [25], but will be briefly discussed here again. The CDFS will make use of two 'slaves' and one 'master'. In the DASH mission, the slaves are called the DOTs and the master is called the SHEPHERD. The slaves will gather and process the data, and will send it to the master, which will relay it back to the ground. The communication process between the CubeSats will be further explained in the telecommunications subsystem chapter.

12.2. CDHS Component Selection

For the CDHS, only COTS components will be used. Each CubeSat will be equipped with the same CDHS, apart from the data storage, which will be (space grade COTS) SD-cards. For the three SHEPHERD CubeSats, or also called, the 'master', these satellites will be equipped with 32 GB SD-cards, which will be produced by ISISPACE[1]. The 'slave' CubeSats will be equipped with 8 GB SD-cards. This is done, because the masters will need to process and store all the data sent by the slaves. Next, all the CubeSats will be using the onboard computer (OBC), including an FM daughterboard provided COTS by ISISPACE. Logically, the motherboards of the master CubeSats will have the master configuration and the slave CubeSats will have the slave configuration, as specified by ISISPACE[2]. The OBC will use an I2C bus. The mass for the OBC (including the daughterboard) will be 0.1 kg and the size will be 0.15U. Finally, for the operating system all CubeSats will use the FreeRTOS operating system.

12.3. Sensitivity analysis

For the sensitivity analysis of the CDHS, there are only a few design parameters. The most important parameter is the data storage capacity. Currently, the storage is set at 32 GB for the SHEPHERD CubeSat. This SD-card is the maximum ISISPACE can provide. If there were to needs to extend the data storage of the SHEPHERD, a COTS or custom SD-card from another manufacturer should be bought, and verified if it is compatible with the ISISPACE OBC. Furthermore, for the CubeSat, the mass and size are also design parameters. However, since the CDHS is already small compared to the other subsystems, it should not be a problem if the mass or size would increase with a certain margin.

12.4. Data Handling Block Diagram

As has been done before in the midterm report, the data flow through the CubeSats is shown in a data handling block diagram. In the following Figure 12.1, the data handling block diagram is presented.

[1] URL https://www.isispace.nl/product/on-board-computer/ [cited 7 June 2022]
[2] URL https://www.isispace.nl/wp-content/uploads/2016/02/ISIS-IOBC-OS-0001-OBC_Option_Sheet-03_01.pdf [cited 7 June 2022]

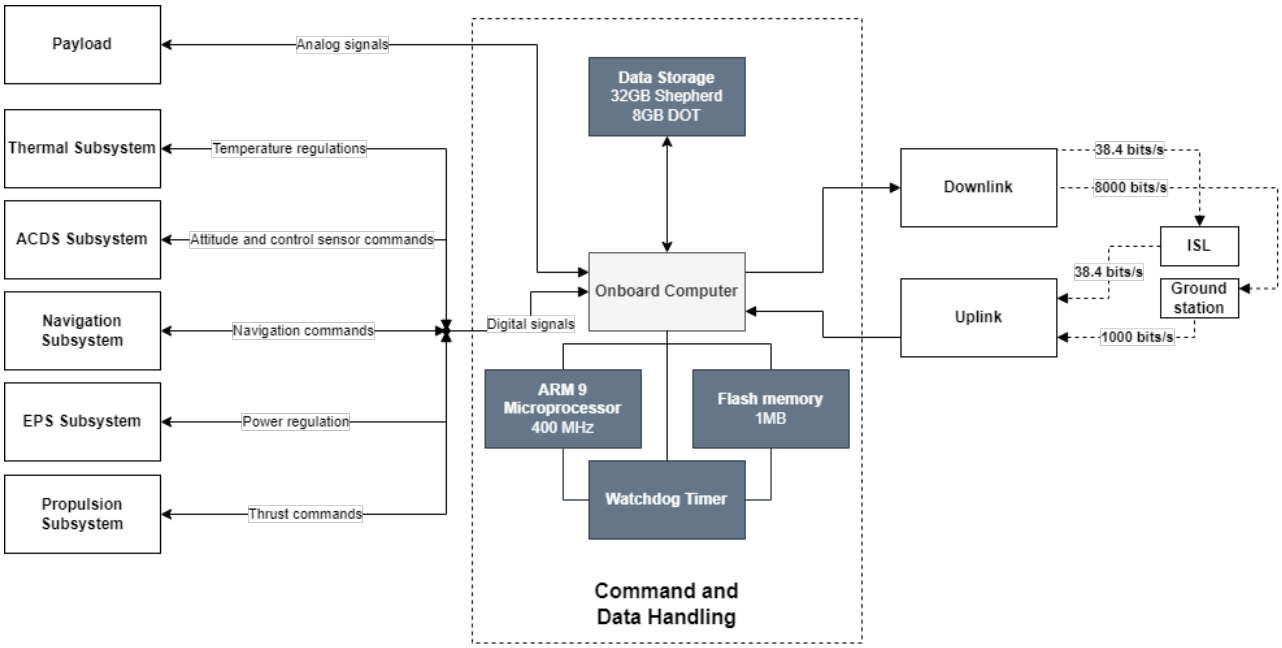

Figure 12.1: Data Handling Block Diagram

13 Telecommunication System

In this subsection the telecommunications architecture is outlined with the choice of components enabling a communication link with Earth as well as a communication link between the satellites. For the inter-satellite link, the configuration is chosen first in Section 13.1 to narrow down the options for that architecture segment. Then, based on the configuration, in Section 13.2, the components for the ISL segment are chosen. Finally, Section 13.3 deals with the Earth-Link components.

13.1. Inter-Satellite Link Configuration

Numerous components were identified to be feasible for the ISL. There are various transceivers with various antennas for different frequency bands. For DASH, X-Band, S-Band and UHF are considered. X-Band is eliminated to avoid interference with the Earth-Link segment; therefore, two configurations are possible. Firstly, there is the S-Band usage with a patch antenna on each face of the CubeSat. For this, three full-duplex transceivers are used on average, which accommodate two of the antennas. Secondly, there is the UHF usage with a system of antennas on one or two of the faces which is enough to provide omnidirectional coverage, this is assumed to use two transceivers at most. To determine a definite component choice, a trade-off is performed. This is necessary to narrow down the feasible combinations given that the ISL link budget is not very constraining. For this purpose, several criteria along with their weights (from 1 to 5) are defined as shown in Table 13.1. It should be noted that only the transceivers' volume is considered, as these occupy space within the CubeSat.

Table 13.1: ISL configuration trade-off criteria

Criterion	Volume	Mass	Cost	Power Used	Risk
Score	5	3	3	5	4

Most weight is given to volume and power used. This is done to ensure other subsystems can be incorporated into the CubeSats without many constraints, especially when the Earth-link segment in the SHEPHERD will already likely occupy a significant part of the budget. Next, risk is given a high importance as the ISL is vital for the CubeSats to perform their mission; if the ISL fails for a CubeSat, it is not capable of performing required operations. As for the cost and mass, these are less driving, as the costs are largely dominated by the Earth-link segment which means that the total telecommunication system costs will not change that much relatively but still possibly enough to constrain the choice of other subsystem or payload components. Then, for the mass, it is not likely to constrain other subsystems or the payload, however, reducing it does contribute to the efficacy of propulsion. It is worth noting that the performance of the configurations was also considered as a criterion, however, both configurations can achieve the required performance, therefore, this is not considered as a factor in the trade-off.

Based on the previously defined criteria, the trade-off is performed. For each criteria, the best configuration is identified and then it receives points equal to the weight of the respective criterion. The overall winner is considered to be the one that has the most amount of points. The trade off can be seen in Table 13.2.

Table 13.2: ISL configuration trade-off, the costs are given in the euro value in 2021

	Volume	**Mass**	**Cost**	**Power Used**	**Risk**	**Result**
S-Band system	0.918 U	1.17 kg	41 705.63 EUR	37.3 W	redundancy and no deployment	4
UHF system	0.168 U	0.181 kg	13 256.94 EUR	4.37 W	redundancy and needs deployment	16

Concerning the values in Table 13.2, these are based on average values of researched components. From these, the characteristics for the configurations are computed. As for the risk criterion, the failure of one of the antennas is more significant for the S-Band, as failure of one point means that the respective direction becomes unusable. The UHF antenna system, on the other hand, still provides omnidirectional coverage. Additionally, the UHF system also introduces the deployment risk, which can lead to loss in performance or in the worst case, although unlikely, can instantly lead to the failure of a CubeSat. This, all in all, makes the risks with the UHF system more significant that for the S-Band system.

13.2. Inter-Satellite Link Components

First and foremost, for the Inter-Satellite Link it is crucial for the CubeSats to be able to transmit and receive data and also for navigation purposes. This means that with the UHF configuration needs to be able to guarantee omnidirectional transmitting as well as receiving capabilities. In terms of components, this can be achieved through the use of two half-duplex transceivers or a single full-duplex transceiver. At the same time, two antenna systems are necessary, one for receiving and one for transmitting.

13.2.1. Transceiver Choice

At this stage, several transceivers are considered, these can be seen in Table 13.3 along with their characteristics scaled for the ISL configuration. This implies that the transmitting and receiving power are added up, for instance, when two half-duplex transceivers are used.

Table 13.3: Transceivers considered for ISL

Transceiver	Manufacturer	Type	Tot. Volume	Tot. Power	Tot. Mass
UHF TRANSCEIVER II[1]	EnduroSat	Half-duplex	0.392 U	2.6 W	0.188 kg
Pulsar UTRX[2]	AA Clyde Space	Haf-duplex	0.285 U	5.1 W	0.2 kg
UHF Radio SAT2RF1-1D[3]	NanoAvionics	Half-duplex	0.0242 U	10.4 W	0.015 kg
NANOcomm-2[4]	Skylabs	Full-duplex	0.104 U	8 W	0.12 kg
NanoCom AX100[5]	GOMSpace	Half-duplex	0.0338 U	3.3 W	0.049 kg

For the transceiver choice, three criteria are considered based on the available information, these are the total volume, the maximum total power consumed, and, the total mass occupied. The objective is to have low values in these characteristics as much as possible. Several options stand out: NanoCom AX100, while not the best with regard to any criterion, has the second lowest value for each. UHF TRANSCEIVER II performs the best in power, but performs the worst in terms of volume and second worst in terms of mass. UHF Radio SAT2RF1-1D does the best in total volume and total mass but performs the worst in terms of power. Intuitively, NanoCom AX100 is considered the best option to go with overall given its consistent performance while the criteria are considered to be similarly important, especially power and volume with mass being considered less important similarly to the configuration trade-off. Essentially being second best in all criteria is considered to outperform the winning performance of the other subsystems in other criteria. Ultimately, the optimal choice does depend on the relative importance of the criteria. To evaluate this, each option is given a hierarchical score from 1 to 5 where the best gets 5 points and the worst gets 1 point. Then, the criteria are given a weight of 1 to 5 in all possible combinations. This resulted in NanoCom AX100 winning in 65.6 % of the possible combinations. The next closest option is UHF Radio SAT2RF1-1D with 33.6 %, which is almost twice as small in the NanoCom AX100case. This shows that NanoCom AX100 still wins in

[1]URL https://satsearch.co/products/endurosat-uhf-transceiver-ii [cited 1 June 2022]
[2]URL https://www.aac-clyde.space/wp-content/uploads/2021/10/AAC_DataSheet_Pulsar_UTRX.pdf [cited 1 June 2022]
[3]URL https://satsearch.co/products/nanoavionics-uhf-radio-sat2rf1-1d [cited 1 June 2022]
[4]URL https://www.skylabs.si/products/nanocomm-2 [cited 1 June 2022]
[5]URL https://gomspace.com/shop/subsystems/communication-systems/nanocom-ax100.aspx [cited 1 June 2022]

various cases where the criteria is not that balanced. Based on this, NanoCom AX100 is taken as the transceiver choice.

13.2.2. Antenna Choice

For the antenna choice it is looked at which antenna system will take least space and mass given that the space available in the SHEPHERD unit is limited. The nominal power usage is neglected given that it is small, instead, the peak power is considered since it is orders of magnitude larger. Another consideration is the compatibility with the DASH CubeSats, being the DOTs and the SHEPHERD. The considered options can be seen in Table 13.4.

Table 13.4: Antennae considered for ISL

Antenna	Manufacturer	Tot. Volume	Tot. Mass	Peak Power	Compatible Form
UHF ANTENNA III[1]	EnduroSat	0.235 U	0.17 kg	1.25 W	1 x 1
Deployable Antenna System for 6U/12U CubeSats[2]	ISISPACE	0.127 U	0.23 kg	2.3 W	1 x 1 / 2 x 2
Antenna System[3]	C3S Electronics Development	0.36 U	0.4 kg	5 W	1 x 1
UHF Antenna[4] System 2X2U	NanoAvionics	1.38 U	0.12 kg	8.3 W	2 x 2
Ant-6f UHF[5]	GOMSpace	0.489 U	0.18 kg	2.5 W	1 x 2

First and foremost, based on the compatible CubeSat face form that is required, namely 2 x 2 (20 x 20 cm^2), two viable options can be observed, these are the ISISPACE Deployable Antenna System for 6U/12U CubeSats and the NanoAvionics UHF Antenna System 2X2U. These are considered to be viable given that these are compatible with the 12U CubeSat dimensions. Between these two options, it is immediately apparent that the ISISPACE option is significantly smaller in volume than the NanoAvionics option but it is almost twice as large in mass. Furthermore, the ISISPACE option also has a significantly lower peak power. Given that the CubeSats are more power and volume constrained rather than mass constrained, the ISISPACE option is the winner. This is the case as its relative performance in both volume and power is better than the relative of the NanoAvionics option in mass.

13.2.3. ISL Link Budget

The specific link budget for the chosen components can be seen in Table 13.5, this is based on the link budget performed in [25], as can be seen, the link budget closes with a wide margin as alluded to earlier. In terms of coding, convolutional coding is chosen in order to maximise the performance of the ISL in terms of coding gain based on the capabilities of the NanoCom AX100 transceiver.

Table 13.5: ISL Link Budget with the chosen components

ISL Link Budget	
Parameter	**Value**
P_{tr}	1.0 W
G_t	0 dB
G_r	0 dB
d_{max}	60 km
f	440 MHz
L_c	3.0 dB
L_p	0 dB
T_s	29.6 K
k_b	1.38×10^{-23} J K^{-1}
R	38.4 kbit s^{-1}
SNR_{req}	6.4 dB
Link Margin	37.37 dB

For this link budget, a cable/circuitry loss, L_c, of 3.0 dB is

[1]URL https://satsearch.co/products/endurosat-uhf-antenna [cited 1 June 2022]
[2]URL https://www.cubesatshop.com/product/isis-deployable-antenna-system-for-6u-12u-cubesats/ [cited 1 June 2022]
[3]URL https://catalog.orbitaltransports.com/content/brands/c3s/C3S_ANTENNA_datasheet.pdf [cited 1 June 2022]
[4]URL https://satsearch.co/products/nanoavionics-uhf-antenna-system-2x2u [cited 1 June 2022]
[5]URL https://gomspace.com/UserFiles/Subsystems/datasheet/gs-ds-nanocom-ant6f-uhf-21.pdf [cited 1 June 2022]

used in order to be conservative about the system losses. As for the system noise temperature, it is once again assumed from [3]. However, in order to implement a more accurate calculation. An estimation of the actual value for the DOTs and the SHEPHERD should be performed. Although the link is likely still gonna have a wide margin, a more accurate estimate should be made. This should then be verified and validated.

13.2.4. ISL Multiple Access

One important aspect of the ISL is that all CubeSats operate at the same frequency for communication, this means that without defining a proper communication protocol, the signals will interfere and will therefore cause the loss of data. Two types of multiple access protocols can employed to tackle loss of data packets due to signal collision, as defined in [56]. These are contention based protocols and collision-free protocols. The first type revolves the use of a collision resolution protocol when collision between the signals occurs while the second type revolves around avoiding collision altogether. For DASH, a contention protocol, Carrier-sense multiple access with collision avoidance, can be employed with the NanoCom AX100 transceiver for sure, however, this does not allow for simultaneous communication between CubeSats. As for collision-protocols, time division multiple access is discarded given that simultaneous communication is required. Then, frequency division multiple access is considered, however, because the number of CubeSats is greater than two, this will not resolve collision. This leaves code division multiple access, which does not limit the amount of users and allows the a user to join at any time as stated in [35] which allows for the scalability of the mission. It has to be noted that at this stage the implementation of this technique is something to be more thoroughly researched.

13.3. Earth-Link

When it comes to establishing a link with the ground, that is far more challenging than ISL. This is the case given that traditional components, which are used for missions in Earth orbit, do generally simply not offer the necessary performance. Therefore, the list of possible components ultimately considered is limited. From this list it is crucial to have a combination of a radio and an antenna that together provide a signal potent enough to have a closing link budget while also fitting within the SHEPHERD's design. Within the DASH mission, there are two segments requiring that telecommunication system to establish a link with the ground, these are the transfer phase and the payload operations phase. During both phases, the distance to Earth varies, as such, in order to maintain a feasible link the data rates will have to the lower throughout certain periods in order to maintain a closing link. This means that depending on the combination of transceiver and antenna, the achievable data rates can mean that the transmission of data will still have to be performed for a period of time after payload operations activities have been performed. Although it would be preferable to transmit all payload data over the six month period, the performance achieved might be at the cost of a lot of volume which is an aspect that is very constrained for the SHEPHERD. In order to choose a component, transfer is considered as the data transmission, consisting of navigation and housekeeping data, has to be performed strictly within the phase while transmission for payload data this is more flexible.

For the radio, the considered options are designed for deep space operation and are also the only options found offering sufficient performance. These can be seen in Table 13.6.

Table 13.6: Considered transponders

Transponder	Developer	Tx Power	Volume	Mass	Tot. Power
Iris V2 Transponder[1] [2]	JPL	5 W	0.5 U	1.1 kg	25.9 W
X-BAND Transponder[3]	IMT	15 W	1.5 U	1.2 kg	94.4 W

[1] URL https://www.nasa.gov/sites/default/files/atoms/files/brochure_irisv2_201507.pdf [cited 6 June 2022]
[2] URL https://satcatalog.s3.amazonaws.com/components/1076/SatCatalog_-_Space_Dynamics_Laboratory_-_IRIS_v2.1_-_Datasheet.pdf?lastmod=20220217200355 [cited 6 June 2022]
[3] URL https://www.imtsrl.it/products/x-band-transponde [cited 6 June 2022]

As for the antennae, these can be seen in Table 13.7

Table 13.7: Considered antennae

Antenna	Developer	Gain	Stow. Volume	Aperture	Mass
MarCO HGA [30]	JPL/Space Dynamics Laboratory	29.2 dB	0.8 U	60 cm x 34 cm	1 kg
KaTENna[4] [9]	JPL/TENDEG	36.95 dB	3 U	diam. 1 m	2.5 kg
LaDeR [1]	JPL	39.6 dB	2.8 U	1.5 m x 1.5 m	1.75 kg

From these options, there are six possible combinations, these are to be compared in terms of mass and volume along with their link budget performance. For the link budget only downlink is considered given that uplink is not a factor due to the power being provided by the ground station being sufficient. As for the power consumption, this is not considered a factor given that the CubeSat equipped with the Earth-Link segment, the SHEPHERD, is assumed to be able to fit the power required into the budget due to the large power it has to provide for propulsion during transfer. The link budget is set up with similar parameters as in [25], the maximum distance in transfer is taken as 3.4 AU, and, the downlink and uplink data rate is taken as 1000 bit s^{-1} based on the Mars Cube One mission[1]. The characteristics of the component combinations can be seen in Table 13.8.

Table 13.8: Characteristics of the Earth-Link component combinations, the link margin is calculated for the transfer phase

Transponder	Antenna	Tot. Stow. Volume	Tot. Mass	Link Margin
Iris V2 Transponder	MarCO HGA	1.1 U	2.1 kg	1.98 dB
Iris V2 Transponder	KaTENna	3.5 U	3.6 kg	9.73 dB
Iris V2 Transponder	LaDeR	3.3 U	2.85 kg	12.38 dB
X-Band Transponder	MarCO HGA	2.1 U	2.2 kg	6.75 dB
X-Band Transponder	KaTENna	4.5 U	4.7 kg	14.40 dB
X-Band Transponder	LaDeR	4.3 U	2.95 kg	17.15 dB

From these options, the MArCO HGA in combination with the X-BAND Transponder is the one that is chosen. As can be seen, out of the combinations with a closing margin, it performs the worst, however, that does comes with a lower stowing volume and mass. Without considering power, as mnentioned earlier, the combination of the X-BAND Transponder along with the MArCO HGA is the clear winner. It is also worth noting that in the case of requiring a higher data rate during transfer, this option allows for a data rate of 2000 bit s^{-1} with a link margin of 3.74 dB.

As far as transmitting data during payload operations is concerned, given that DASH is required to transmit 130 Gbit of payload data, as stated in DASH-GOM.02-MI.15. To do this most effectively, the capability of the DSN to receive signals from multiple transmitters is used in order transmit data at a higher rate. Given that this works for two transmitters[2], the effective data volume that was to be transmitted per SHEPHERD is 65 Gbit. In order to determine the capacity of the communication system, the distance across payload operations (ranging from 1.6 to 3.14 AU) was used with a resolution in days. With this, assuming an availability of 12 h d^{-1}, the total transmitted data volume was calculated across the payload operation phase for each day by optimising the data rate to still maintain a link with the ground, for the calculation, the data rate associated with each day is rounded down to the nearest hundred to diminish overestimation. From this, the transmitted data volume was calculated to be 34 Gbit, which is below the required 65 Gbit. Furthermore, the transmitted data volume should also include other data associated with the CubeSats, being telemetry and navigation although this

[4]URL https://www.tendeg.com/_files/ugd/c5273f_0081c8a108f5424683ac6fd36d0025fe.pdf [cited 6 June 2022]
[1]URL https://directory.eoportal.org/web/eoportal/satellite-missions/m/marco [cited 5 June 2022]
[2]URL https://deepspace.jpl.nasa.gov/files/820-100-F1.pdf [cited 13 June 2022]

is assumed to be a small fraction of the data. Therefore it can be concluded that complying with the 130 Gbit requirement is unfeasible. Given that the 130 Gbit was based on the estimated capability of the HERA mission, this is likely unfeasible for DASH given that HERA has superior capabilities compared to CubeSats allowing for more data transmission. Therefore, it is recommended in order to ensure that all data can be transmitted, that the SHEPHERD class CubeSat is used for an additional six months after payload operations to transmit the remaining data. This leads to a calculated data volume of 71 Gbit of transferred data for this scenario. It is worth noting that assuming an availability of 11 hours would lead to a data volume of 68 Gbit, given that this only includes payload data, 12 hours is preferred for the mission feasibility. A recommendation would be to cluster the transmission time as much as possible during the periods at which this distance to the Earth is the closest to make use of higher data rates and not transmitting as much when the Earth is further away as lower data rates are possible only.

It has to be noted that for the implementation of the MarCO HGA, the deployment mechanism has to be a bit different than in the MArCO mission. This is the case as the antenna is stowed on a 30 x 20 cm^2 side but deployed on an adjacent 20 x 20 cm^2 side. At the same time, the feed has to be deployed separately, this needs its own mechanism. Similar, to the antenna, this is assumed to be done through a burn-wire mechanism as stated in [30].

In Table 13.9 the link budget for the transfer phase can be seen, this particular phase is chosen given that the

In order to gauge whether the link budget gives a reasonable estimate of the communication system performance, the link budget from MarCO is used as seen in [38]. By adjusting the transmitting power, the distance and the gains to match MarCO a downlink margin of 2.7 dB and an uplink margin of 27.48 dB are obtained. As far as downlink is concerned, the value obtained is close to the 2.4 dB reported in [38]. As for the uplink result, this one too large compared to the 7.5 dB for the MGA case, this is likely attributed to not considering all the losses associated with uplink with the DSN. In the MGA the result is closer with a value of 23.3 dB compared to the reported 14.7 dB. As for downlink, the value obtained is 5.8 dB which is larger than the reported 4.3 dB. This means that the link budget is slightly overestimating downlink performance and significantly overestimating uplink performance. Given that the high gain antenna is to be used for uplink as well in DASH, a margin is obtained to still guarantee uplink performance. As for downlink, given that the deviation in accuracy is not that large, the performance of the mission is assumed to be impacted marginally, it might be that the data rates need to be slightly adjusted but the downlink for DASH should still be viable. In further design stages, the losses should be modelled to have a calculations representing the circumstances of the mission more accurately, this should then also be verified and validated.

Table 13.9: Link Budget for the Earth-Link with chosen components at 3.4 AU

Link Budget for Earth-Link		
Parameter	**Downlink Value**	**Uplink Value**
P_{tr}	15 W	20 kW[52]
G_t	29.2 dB	73.23 dB[52]
G_r	74.28 dB[52]	29.2 dB
d_{max}	3.4 AU	3.4
f	8.4 GHz	7.145 GHz
L_c	3.0 dB	3.0 dB
L_p	3.0 dB	3.0 dB
L_a	0.034 dB	0.034 dB
T_s	29.6 K[3]	460 K[3]
k_b	1.38×10^{-23} J K^{-1}	1.38×10^{-23} J K^{-1}
R	1 kbit s^{-1}	1 kbit s^{-1}
SNR_{req}	1.1 dB	9.6 dB
Link Margin	6.49 dB	29.59 dB

13.4. Sensitivity Analysis

As far as the sensitivity analysis is concerned, for the ISL segment, it can be looked at whether the usage of an S-Band configuration could have still yielded a component choice with less volume, mass or power than the actual component choice given that the configuration trade-off has been performed

based on an average. This, however, does not seem to be the case based on the volumes occupied within the CubeSat and total masses of the considered COTS S-Band components. From the list seen in Table 13.10 the volumes occupied by the transceivers are larger than the chosen option, same goes for the masses. As for the antennas, although volume is not that important given that they are placed outside, the total mass for the chosen ones is lower than the S-Band one. For this, the component data is based on the datasheets or website information[3] [4] [5] [6] [7] [8] [9] [10] [11] [12]

Table 13.10: S-Band configuration components

Component	**Tot. Volume [**U**]**	**Tot. Mass [**kg**]**
Transceivers		
SPACECOM XLINK-S Transceiver	0.6	0.6
Rakon's NewSpace S-band Transceiver	1.6245	0.9
NANOlink-boost-2 – S-Band TM/TC CCSDS Communication Subsystem	0.544635	0.744
NANOlink-boost-dp-2 – S-Band TM/TC CCSDS Communication Subsystem	0.82992	1.215
GOMSPACE NanoCom SR2000	0.77780388	0.93
SPACECOM SLINK-S Transceiver	1.736475	1.26
Antennas		
ISISPACE S-band Patch Antenna	0.265401747	0.3
S-Band Patch Antenna RHCP for HISPICO	0.048	0.372
S-BAND ANTENNA ISM	0.633864	0.384
SSA03 – Compact High Gain S-Band Patch Antenna	0.032805	0.0585
ANYWAVES - Compact-S-Band TT&C-Antenna	0.294973211	0.462

When it comes to the Earth-Link components, given that the SHEPHERD is volume constrained, the loss in performance in terms of antenna choice has to be accepted to even being able to carry a high gain antenna in the first place. Although higher data rates would be possible with LaDeR or KaTENna, making the necessary transmission time shorter, these antennas would not fit inside the SHEPHERD based on its current layout.

13.5. Budgets

An important part of the telecommunication subsystem with regard to the mission is the associated mass, volume and cost budget of the components. This is done by requesting the information for the parts or estimating the budget parameters with similar components. Not all the costs were available, this meant that in some cases these had to be estimated based on similar components. The results for a TRIAD are presented in Table 13.11.

[3] URL https://www.isispace.nl/product/s-band-patch-antenna/ [cited 15 June 2022]
[4] URL https://www.cubesatshop.com/product/s-band-patch-antenna-rhcp-hispico/ [cited 15 June 2022]
[5] URL https://www.endurosat.com/cubesat-store/cubesat-antennas/s-band-patch-antenna/ [cited 15 June 2022]
[6] URL https://satsearch.co/products/exa-ssa03-compact-high-gain-s-band-patch-antenna [cited 15 June 2022]
[7] URL https://satsearch.co/products/anywaves-compact-s-band-ttc-antenna [cited 15 June 2022]
[8] URL https://www.iq-spacecom.com/images/downloads/XLink-S_Datasheet_032022.pdf [cited 15 June 2022]
[9] URL https://satsearch.co/products/skylabs-nanolink-boost-2-s-band-tm-tc-ccsds-communication-subsystem [cited 15 June 2022]
[10] URL https://satsearch.co/products/skylabs-nanolink-boost-dp-2-s-band-tm-tc-ccsds-communication-subsystem [cited 15 June 2022]
[11] URL https://gomspace.com/shop/subsystems/payloads/software-defined-radio.aspx [cited 15 June 2022]
[12] URL https://www.iq-spacecom.com/products/slink [cited 15 June 2022]

Table 13.11: Telecommunication budgets

Component	Volume [U]	Mass [kg]	Nom. Power [W]	Peak Power [W]	Qty.	Cost [EUR]
			SHEPHERD			
X-Band Transponder	1.16	1.2	81.6	94.4	1	650k
MarCO HGA	0.833	0.931			1	200k
HGA Feed	0.0182	0.057			1	
NanoCom AX100	0.0169	0.0245	2.82	3.43	2	6k
Deployable Antenna System	0.0634	0.115	0.030	2.3	2	8k
SHEPHERD Total:	2.1718	2.467	87.3	105.86	1	878k
			DOT			
NanoCom AX100	0.0169	0.0245	2.82	3.43	2	6k
Deployable Antenna System	0.0634	0.115	0.030	2.3	2	8k
DOT Total:	0.1606	0.2797	5.7	11.46	2	56k
TRIAD Total:	2.493	3.0264	93	117.32	2	934k

13.6. Communication Flow Diagram

In Figure 13.1, the communication flow diagram can be observed, here the communication link between the different components can be observed, furthermore, the communication link between the ground station and the CubeSats is also present as well as the inter-satellite link. It has to be noted that at this stage, the data rates within the CubeSat components are not known. Therefore, it is imperative that in the next stage this is done in other to enable a more accurate analysis with respect to telecommunication.

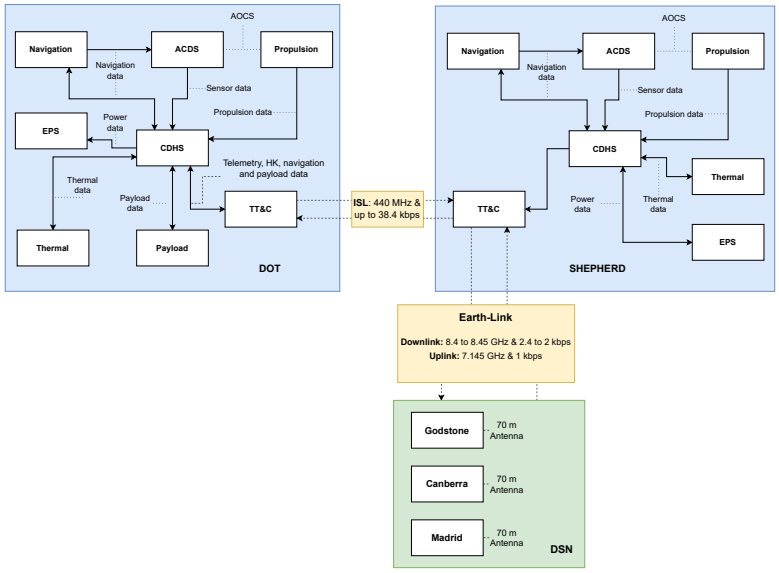

Figure 13.1: Communication flow diagram

14

Attitude Determination and Control System

After the preliminary sizing that was done previously [25], it is decided that the ADCS will be composed of COTS components. In this chapter, it is considered for each ADCS component, what requirements drive their design and minimum performance and then an COTS component is selected based on meeting this performance requirement and the optimisation of mass, volume, power and cost. If the cost was unavailable even after contacting the manufacturer, this is listed in the data as not available. As volume and power are constraining, these are considered to be more important for the selection of the component. Components with exceedingly high values for these properties, such that their use in the design would be unrealistic, were excluded from consideration. The options considered are taken from NASA's small S/C state-of-the-art report [77], CubeSatShop [1], SatCatalog [2], SatSearch [3] and SmallSatCatalog [4]. This chapter starts with a summary of the control characteristics of the S/C. Afterwards, the COTS components selection is done. The chapter is concluded with an analysis of the sensitivity of the selection with respect to the driving requirements.

14.1. Control Characteristics

As presented previously [25], the ADCS sensors consist of two star trackers, six sun sensors and an Inertial Measurement Unit (IMU). These provide accurate attitude determination to the S/C and are driven by the accuracy requirements of the operations being performed. The primary actuators are reaction wheels, configured in a pyramid. These allow the S/C to control its attitude, slew and counteract disturbance torques. Finally, the thruster system allows for momentum dumping and orbital manoeuvring.

The disturbance torques that the S/C will experience are the solar radiation pressure torque and the gravity gradient torque. The gravity gradient torque is negligible compared to the solar radiation pressure torque, which is in the order of 3×10^{-8} N m.

14.2. Star Trackers

The star trackers are used for high accuracy attitude determination, for which the driving requirement is found during the transfer to Didymos. In this phase, the attitude must be controlled with an accuracy of at least 15 arcsec to enable line of sight measurements for navigation [19].

Based on this requirement, three star trackers are considered, which are listed in Table 14.1.

Table 14.1: COTS star trackers

Name	Accuracy [arcsec]	Mass [kg]	Power [W]	Volume [U]	Cost [k EUR]
arcsec Sagitta	10	0.26	1.2	0.214	45
Sodern Auriga-CP	11	0.21	1.1	0.347	50
Terma T1	9	0.92	0.75	0.4	N.A.

The arcsec Sagitta is selected for its low mass, volume and cost. Its high power is accepted because it's only marginally higher than that of the Sodern Auriga-CP and because the low power of the Terma T1 does not weigh up against its high mass and volume.

[1] URL https://www.cubesatshop.com/ [cited 2 June 2022]
[2] URL https://www.satcatalog.com/ [cited 2 June 2022]
[3] URL https://satsearch.co/ [cited 2 June 2022]
[4] URL https://catalog.orbitaltransports.com/ [cited 2 June 2022]

14.3. Sun Sensors

The sun sensors provide low accuracy attitude determination when the star trackers are blinded or not active, such as when the CubeSats have just been deployed, and the direction of the sun must be determined, so the solar panels can charge the batteries. As the solar panels were sized for a maximum angle of incidence of 0.5 ° [25], the sun sensors need to provide 0.5 ° of accuracy.

The sun sensors that are considered, based on compliance with this requirement, are listed in Table 14.2.

Table 14.2: COTS Sun sensors

Name	Accuracy [deg]	Mass [kg]	Power [W]	Volume [U]	Cost [k EUR]
Lens R&D BiSon64-ET	0.5	0.023	0	0.022	9
Solar MEMS Technologies nanoSSOC-A60	0.3	0.025	0.01	0.0022	2.5
NewSpace Systems NCSS-SA05	0.5	0.005	0.05	0.0022	11
GomSpace NanoSense FSS	0.5	0.003	0.026	0.0013	N.A.

The Solar MEMS Technologies nanoSSOC-A60 has an exceedingly low cost. This is very attractive for a mission whose objective is to make space exploration financially viable. It also has a low power and a reasonably low volume. Its drawback is in its large weight. The NCSS-SA05 and NanoSense FSS have lower masses, but also higher prices (when estimating the NanoSense's cost to be in line with the BiSon64-ET and the NCSS-SA05) and higher power requirements. Therefore, as mass is not a constraining factor, the nanoSSOC-A60 is selected.

14.4. Inertial Measurement Unit

IMUs provide data on the accelerations and rotation rates of the S/C. The driving requirement for the IMU comes from the line of sight measurements for navigation. As the measurement rate is chosen to be in the order of tens of seconds in literature [19], it is assumed that the measurements are done once every 30 s. Therefore, the IMU must not have a bias of more than 0.5 arcsec/s.

The IMUs that are available, after filtering for this requirement, are listed in Table 14.3.

Table 14.3: COTS Inertial Measurement Units

Name	Accuracy [arcsec/s]	Mass [kg]	Power [W]	Volume [U]	Cost [k EUR]
Inertial Labs IMU-NAV-100 Tactical A	0.5	0.155	0.8	0.138	7
MEMSENSE MS-IMU3050	0.3	0.079	2.5	0.047	4.6
NovAtel OEM-IMU-STIM300	0.5	0.055	1.5	0.039	N.A.

The IMU-NAV-100 Tactical A has the highest mass and volume, and the MS-IMU3050 has very stringent power requirements. As the OEM-IMU-STIM300 has the lowest mass and volume and takes the middle road in terms of power, it provides the best balance of properties, even when prioritising volume and power and taking into account that the cost is not known. Therefore, the OEM-IMU-STIM300 is selected, the cost of which is estimated to be 5 kEUR to 8 kEUR based on its performance and the prices of the other two IMUs.

14.5. Reaction Wheels

The reaction wheels provide slew rates to the S/C and counteract disturbance torques. They must be able to store 13 mN m s of momentum and produce at least 1.7 mN m of torque [25].

The reaction wheels that are considered, based on these requirements, are listed in Table 14.4.

Table 14.4: COTS Reaction Wheels

Name	Torque [mNm]	Momentum Capacity [mNms]	Mass [kg]	Power [W]	Volume [U]	Cost [k EUR]
BlueCanyon RWP015	4	15	0.13	1	0.034	N.A.
CubeSpace CubeWheel Large	2.3	31	0.225	4.5	0.1	7.4
Hyperion Technologies RW400	12	50	0.375	1.9	0.068	30
Sinclair Interplanetary RW-0.03	2	40	0.185	1.8	0.1	23
GomSpace NanoTorque GSW-600	2	19	0.18	2.5	0.052	N.A.

The BlueCanyon RWP015 performance is closest to the design requirements and therefore has the lowest mass, volume and power. This makes it the obvious choice, and it is selected despite its price being unknown. Should the price be unfeasibly high, the GomSpace NanoTorque GSW-600 is a good alternative considering its low volume and relatively low weight. The remaining reaction wheels are too big and heavy to be easily incorporated in such a small CubeSat. The cost of the RWP015 is estimated to be 15 kEUR to 25 kEUR, based on the other available costs and its high performance.

14.6. Cold Gas Thruster System

The cold gas thruster system performs orbital adjustments and reaction wheel desaturation. It therefore needs to be able to provide thrust in the order of millinewtons to not overshoot when it does orbital adjustment, and it needs to be able to provide enough ΔV to last the entire mission. There are not many COTS complete cold gas RCS thruster systems available. However, a COTS cold gas thruster system, the Aurora Propulsion Technologies ARM-AO, was found. It is able to provide thrust in the range of 0.6 mN to 4 mN. If made to have a capacity of 20 m s^{-1}, as needed for the DOTs, it has a volume of 1 U, a total mass of 1.2 kg and use a peak power of 10 W. The cost of one such module is between 80 kEUR and 120 kEUR.

14.7. Budgets

Now that all the COTS components have been selected, the budgets for the ADCS system can be set up. These are shown in Table 14.5, and correspond to a single CubeSat. The power shown is the peak power, corresponding to the momentum dumping. During this operation, both the thrusters and the reaction wheels are active. The cost is given in a range due to the uncertainty of the prices which have had to be estimated. The lower bound corresponds to the sum of all the lowest estimates and the upper bound corresponds to the sum of all the highest estimates. Both numbers include a 10% safety margin.

Table 14.5: Preliminary sizing of the ADCS for a single CubeSat

Mass	Power	Cost	Volume
2.45 kg	15.5 W	275-365 k EUR	1.85 U

14.8. Sensitivity Analysis

The sensitivity analysis for the selection of COTS ADCS components is done by considering the uncertainty of the requirements which drive the selection. If there are viable and more optimal components available that fall short of the necessary performance, then if the requirement has been overestimated and is too stringent, the selected component is not the optimal one for the design.

For the star trackers, there are no available components that do not meet the pointing accuracy requirement by a small amount. All of them have a significantly lower accuracy than 15 arcsec. Therefore, there is high confidence that this component is the optimal one.

With regard to the sun sensors, there is the Bradford Engineering CSS-01/02, which has an accuracy of 1.5°, but weighs almost ten times more than the currently selected sun sensor. Also, there is the Space Micro MSS-01, with an accuracy of 1°, and a slightly higher mass. Its cost, however, is on the high end at more than 11.3 kEUR. The nanoSSOC-A60's very low price and its small size makes it very likely that it would be the optimal component even at less stringent requirements.

There are several IMUs available with bias stabilities of around $1\,°\,h^{-1}$ that have drastically reduced power requirements and sizes, such as the Epson M-G370 and the NovAtel OEM-IMU-EG370N. There is therefore unfortunately not a high confidence that the OEM-IMU-STIM300 is the most optimal component, should the requirement have been overestimated.

There are already reaction wheels considered that meet the requirements by a wide margin. These wheels all have exceedingly high masses or power requirements. It is therefore very likely that the BlueCanyon RWP015 is the most optimal component.

Due to the low amount of commercially available complete cold gas RCS thruster systems, there is a low chance that the Aurora ARM-AO is not the optimal COTS component for orbital manoeuvres and momentum dumping.

15
Navigation System

As stated in previous design work, the navigation subsystem has 5 main functions to fulfil within the DASH mission: computing the position and velocity within a certain accuracy, provide relative positioning between the DOTS and SHEPHERD, give commands to the thrusters through an incorporated thruster model, and it must do everything autonomously. Therefore, throughout this chapter, these functionalities will be further specified in terms of the physical and software architecture, and their quantitative performance to further define the subsystem. Primarily, in order to roughly determine the required navigational accuracy, example approach and close proximity orbits for the science operations are established. Then follows a short overview of the navigational methods, sensor distribution within the TRIAD, state estimation protocols and requirement definition analysis. Furthermore, the guidance and control algorithms to be used are specified followed by an uncertainty analysis and its implications on the control output. Finally, a simulation is designed and run to find the necessary Delta-V to maintain a certain orbit considering the disturbances.

15.1. Operational Orbits

The operational orbits depend heavily on the type of science to be performed, as the orbits for DOTS operating very close to the surface would differ from those of other orbiters. Disregarding the intricacies of the different orbits to be catered to, a general approach orbit can be determined as well as the orbits in close proximity. However, first it is important to address the navigational accuracy required for the interplanetary transfer performed by the ion engines onboard the SHEPHERD. It is fitting to look at the M-ARGO mission for guidance, as the interplanetary phase of the mission is almost identical to that of the TRIADs. As a result, given the analysis performed on the interplanetary navigational methods of the M-ARGO CubeSat, under optimal conditions, the navigational accuracy is represented by a 3-sigma error of 1000 km and 0.1 m s^{-1}, which is considered to be sufficient for the interplanetary phase as the transfer manoeuvres must be recalculated anyways during the course of the transfer. As a result, the trajectory will be corrected for these offsets in the spacecraft state in discrete intervals after the thrusting arcs.

15.1.1. Approach

The approach phase starts when the interplanetary transfer phase ends, which means that it begins when Didymos is already occupying the size of 1 pixel in the navigational camera, which allows for LOS measurements to its centroid. Thus, it marks the end of beacon LOS measurements and the start of centroid determination, but these methods will be explained in more detail in Section 15.2. Therefore, as the TRIAD (or TRIADs) is now approaching the system, it needs to insert itself into the orbit that it desires, but it should be taken into account that the order of magnitude of the accelerations imposed on the TRIAD are quite small (see Table 15.1). As a result the manoeuvres that are performed are quite different to that of traditional orbital manoeuvres.

Table 15.1: Expected magnitude of perturbations for the Didymos system.

Acceleration	***Magnitude [m/s^2]***
Didymos	10^{-5}
Dimorphos (2nd body)	10^{-8}
Solar Radiation Pressure	10^{-7}
C_{20} and C_{22} Perturbations [71] [50]	10^{-14}
Total	10^{-5}

For starters, there are certain assumptions which can be made in the approach phase following the steps of Vertisano et al. [71] where an initial approach distance of roughly 1120 km from the asteroid

is assumed. This assumption is valid considering that the navigational camera's resolution (GSD: 0.08 m at 800 m; see chapter 16) is capable of having Didymos occupy 1 pixel when at 15 600 km, so LOS measurements can be performed at this distance. Additionally, the TRIAD is approaching at 2 m s^{-1} initially and the end goal is to hover for about 25 days at a distance of 10 km from the surface of Didymos to produce sufficiently accurate renders of the surface morphology so as to be able to perform feature tracking based navigation. It is estimated that 0.35 m per pixel of resolution is sufficient to generate the relevant renders and shape models, which is assumed from the OSIRIS-Rex mission definition [44]. Thus, the selected camera is proficient enough to be able to satisfy this criteria at 10 km.

Furthermore, a fixed amount of manoeuvres can be considered for this approach phase, each with differing performances. Regardless, the control input is defined by attempting to reach a point between the final hovering distance and the initial starting point as is shown in Figure 15.1. This can also be described mathematically as shown in Equation 15.1 where N depicts the amount of burns desired [63]. Furthermore, the control sequence to do so can be done by implementing a guidance algorithm, solving a Lambert problem for an initial estimate assuming a certain flight-time. In future design work, the amount of burns can also be optimised to minimise the fuel consumed, which ties quite nicely with the guidance algorithms considered for the DASH mission, as will be elaborated on in Section 15.3.

$$x_{i+1} = x_i + \left(x_{\text{goal}} - x_i\right)/(N-i+1) \quad (i = 1, 2, \cdots, N \tag{15.1}$$

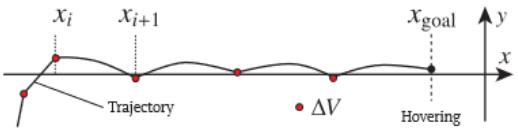

Figure 15.1: Burn procedure for a fixed amount of manoeuvres [63]

By following this sequence of manoeuvres, and assuming 5 are performed (N=5) and that the flight-time is 5 days per manoeuvre and 2 days per hovering manoeuvre, then one obtains the trajectory shown in Figure 15.2. This trajectory assumes an initial error in the knowledge of the gravitational parameter of Didymos, which is shown in the initial overshoot. It is safe to assume that this will likely be the procedure for the DASH mission, even though proper estimation of the Delta-V is required and optimisation must be performed to cater to the mission goals. On a final note, the TRIAD would still be interfaced and the propulsion module of the SHEPHERD would perform the manoeuvres as the DOTS propulsion system would not be capable of doing so.

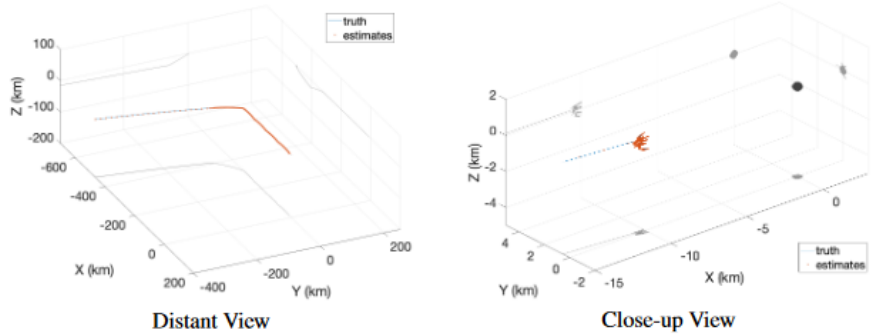

Figure 15.2: Example Approach Trajectory [63]

15.1.2. Close-Proximity

After having performed the hovering to estimate the gravitational parameter and also perform the preparations for feature tracking, more accurate control sequences can be established to minimise the necessity for corrections. Like previously, more accurate trajectories must be generated once

more high-level planning is generated to cater to the science goals, but for an initial estimate, one can consider the example trajectory generated by Takahashi and Scheeres, shown in Figure 15.3. This consists of an initial gradual descent for better estimations of the gravitational parameter, followed by transitions between multiple hovering locations and ending in an insertion to a terminator orbit, which seems appropriate for the DOTS' operational profile. By implementing a Monte Carlo analysis with 1000 runs, it is possible to say that the Delta-V used during this trajectory ranges from 2.70 to 2.82 $m\,s^{-1}$ with a mean of 2.759 $m\,s^{-1}$[63]. This shows that the constraints implied on the propulsive elements are relatively relaxed, even when considering that the results produced are based on an asteroid that is roughly 6 times less massive than Didymos, which would raise the required Delta-V. Nevertheless, considering the amount of propellant stored within the DOTs (providing roughly 20 $m\,s^{-1}$) and the SHEPHERD (to be provided by the high efficiency engine), there should be no issues with the propellant mass required to follow a similar trajectory for the Didymos system.

Additionally, this would comprise a total operational phase of 160 days, which is quite close to the current assumed operational time of 180 days, but it should be noted that while one of the DOTS or the SHEPHERD follow this trajectory, the rest could follow their own optimised trajectory depending on the payloads within the CubeSat or their ultimate goal. For example, the DOT that will be exploring Dimorphos will have a substantially different orbit than the proposed one, and the DOT that will take radar measurements as well (see chapter 16). Nevertheless, the modifications needed to do so are quite small, so it is assumed that the Delta-V requirements will remain in the same order of magnitude. In future work, the individual trajectories per DOT and SHEPHERD will be defined accurately within a mission timeline.

It is also important to consider other types of trajectories, such as those that HERA takes, which are essentially composed by initial hyperbolic arcs to characterise the binary asteroid system and relay the information to the ground-station where, using the data gathered, more precise orbit determination can be performed and the autonomous navigation performance can be evaluated. After this, using an initial condition and a final desired state, the autonomous navigation could essentially compute the required trajectory and manoeuvres with more accuracy and they can also be validated in the ground-station [22]. This component is left as future studies given the time constraints of the study performed.

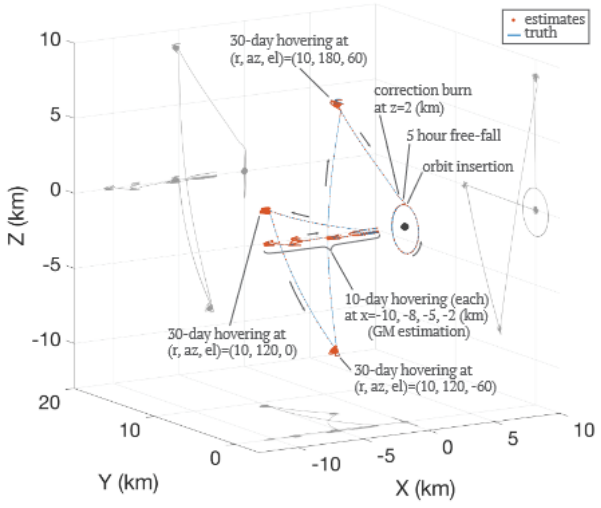

Figure 15.3: Example Close Operations Trajectory [63]

15.2. Navigation

Navigation comprises the estimation of the spacecraft state within a given reference frame. There are 3 reference frames which concern the DASH mission: ECLIPJ2000 (non-accelerating, Sun-centered), ECI (Earth Centered INertial, and the AHF (Asteroid Hill Frame). Within each of the mission phases, the coordinates of the TRIADs, SHEPHERDs and DOTS are expressed relative to either the Earth,

Sun or Didymos, chronologically in order. In order to specify the methods required, it is important to first determine what is the required navigational accuracy with respect to the position and velocity estimates (as these make up the spacecraft state). Thus, considering the orbits specified previously and the close operation of several CubeSats, there needs to be a high relative accuracy compared to that of ground-based navigation, which causes errors in position of roughly 3 km [54].

Consequently, autonomous or semi-autonomous methods must be incorporated in the system to achieve higher accuracy for close fly-by operations, which is required for the mission goals. Considering that HERA has the same goals, then it is pertinent to assume that the navigational accuracy achieved by the HERA mission, or more precisely heritage provided Asteroid Impact Mission (AIM) preliminary analysis from which the HERA mission is based on [1]. The maximum errors observed in this analysis are 128.70 m and 37.76 mm s^{-1} in position and velocity, respectively, from which the feasibility of the mission was confirmed for close fly-by operations (distance of 200 m from the surface)[54]. However, it should be taken into account that this navigational accuracy is based solely on LOS measurements to the asteroid using a centroiding and feature tracking, without altimetry data, which will be available for the DASH mission, which means that higher accuracy will be achieved, as will be shown throughout this section.

15.2.1. Methods

The navigational methods to be used for the transfer phase are comprised by *beacon LOS measurements* with *ground-station radiometry* left as a redundancy and to be able to ensure that the navigational system is working correctly. Furthermore, once the approach phase begins, *centroiding* using LOS measurments from the navigational cameras will be used to get in proximity of the asteroid until the 10 km mark is reached. Then, once shape model generation has finalised during hovering, the TRIAD may separate and *feature tracking* supported by *LIDAR measurements* become the preferred method for absolute positioning in the AHF, while *inter-satellite radiometry* using the ISL transponder enable relative positioning between the DOTS and SHEPHERDs. Additionally, the measurement models will be briefly described.

Beacon LOS

The method revolves around attempting to triangulate a spacecraft's position by taking LOS measurements to 2 planets or bodies with known ephemeris (and thus position) as shown in Figure 15.4. By doing so, a least-squares problem can be formulated as shown in Equation 15.2 and the distance to the bodies can be computed and the position is found. The representative error of this method applied to the M-ARGO mission is around 10 000 km and 0.005 km s^{-1} for the first 100 days and then improves from 200 days onward (when observation conditions improve) to yield 1000 km and 0.0001 km s^{-1} in position and velocity respectively [19].

Furthermore, the LOS measurement to the object is determined by projecting the image to the camera imaging plane and then The error in position can be modelled as a function of the angle between the planets and the as was shown in the works of Broschart et al. in Equation 10 [7]. On a final note, the assumptions made in this analysis are that M-ARGO determines its position **once every 7 days** using a measurement window of 15 minutes on each body taking one measurement per minute and a LOS accuracy of 15 arcseconds.

[1] URL https://directory.eoportal.org/web/eoportal/satellite-missions/content/-/article/hera [cited 10 June 2022]

$$\underbrace{\begin{bmatrix} 1 & -\hat{\boldsymbol{\rho}}_1^\top \hat{\boldsymbol{\rho}}_2 \\ -\hat{\boldsymbol{\rho}}_2^\top \hat{\boldsymbol{\rho}}_1 & 1 \end{bmatrix}}_{\boldsymbol{A}} \underbrace{\begin{bmatrix} \rho_1 \\ \rho_2 \end{bmatrix}}_{\boldsymbol{x}} = \underbrace{\begin{bmatrix} \hat{\boldsymbol{\rho}}_1^\top (\boldsymbol{r}_1 - \boldsymbol{r}_2) \\ \hat{\boldsymbol{\rho}}_2^\top (\boldsymbol{r}_2 - \boldsymbol{r}_1) \end{bmatrix}}_{\boldsymbol{b}} \tag{15.2}$$

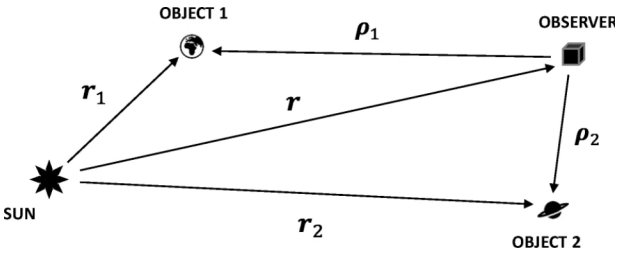

Figure 15.4: Beacon LOS method and variable definition [19]

In future work, optimal selection of the navigational beacons should be performed based on a final interplanetary trajectory. This optimisation depends on several variables such as the Sun-body angle, obstructions in the LOS and the observable magnitude of the beacon. An example optimisation for the M-ARGO mission is shown in Figure 15.5.

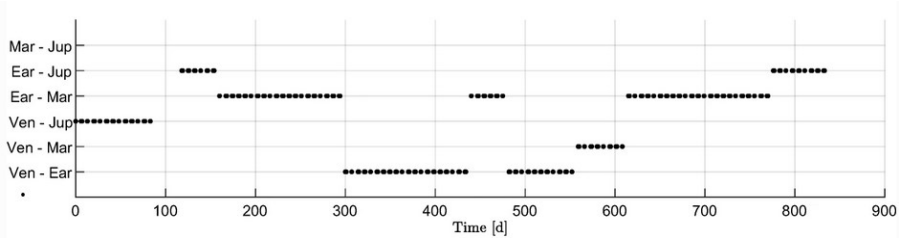

Figure 15.5: Optimal couples of beacons during the M-ARGO interplanetary transfer [19]

Ground-Station Radiometry

Ground-station measurements are performed primarily through Δ-DOR and Doppler Tracking methods and they each have representative errors in the order of 4 km [45] and 0.1 mm s^{-1} [32]in range and range rate measurements, respectively. Equation 15.3 shows how the ranging values are interpreted within the navigational state estimation with ρ and $\dot{\rho}$ representing the range and range rate, respectively, while ζ_g represents the measurement noise for each parameter[71].

$$z_g = [\rho \dot{\rho}]^T + \zeta_g \tag{15.3}$$

Centroiding

The concept behind centroiding is the same as that of LOS measurements, only that the attitude to the asteroid is computed while the range to the asteroid is not one of the byproducts of the algorithm. This is due to the scale-indetermination of LOS measurments, which means not being able to compute the distance to the body, as is depicted in Figure 15.6 However, the distance to the asteroid system can be computed by looking at both Didymos and Dimorphos and computing LOS measurements as before, which is a beneficial aspect of investigating a binary asteroid [46]. This can be done from a distance lower than 2000 km as at this moment, Dimorphos will occupy roughly one pixel in the camera's imaging plane, thus, the LOS measurement can be performed.

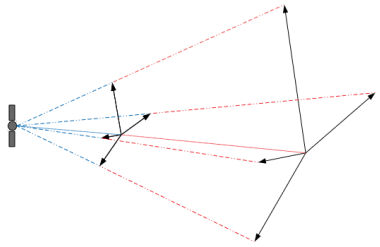

Figure 15.6: Line-Of-Sight method working principle [48]

Feature Tracking

The final optical technique relies on obtaining azimuth and elevation angles to the asteroid based on landmark detection through image processing and then producing a LOS measurements to the land-

mark. Before this can be done, shape models must be generated through an Early Characterisation Phase, which is done while hovering and approaching the asteroid system. There are several techniques within feature recognition and tracking: Keypoint Detection and Matching and Crater Detection and Matching, both followed by outlier rejection [13]. The complexity of feature tracking algorithm design and implementation escapes the purpose of the preliminary design work, so it is left for future work.

As for the current stage, it can be said from a comparative analysis through simulation based on accuracy, robustness to lighting conditions, and performance in multi-agent stereo-vision for 3D mapping, that Scale-Invariant Feature Transform (SIFT) among the keypoint detection and matching algorithms is the best for accuracy for distributed systems. Meanwhile Speeded-Up Robust Features (SURF) is a close second, but also outperforms SIFT in terms of lighting invariance and 3D mapping through stereo-vision. Nevertheless, the paper by Dennison and D'Amico recommends using SIFT.[13]

LIDAR

The range to the asteroid can be determined through a measurement from the LIDAR instrument. This aids in maintaining a safe distance to the surface and also supports close fly-by operations if any payloads require so due to performance requirements. As expected, the LIDAR instrument also introduces errors through mesurement noise and the characteristic error of the sensor which in the case of DLEM 20, it has a measurement error of 3 m (3σ).

Inter-Satellite Radiometry

The ISL consists of two way ranging between the CubeSats such that no clock synchronisation is required. The measurements are much like the how the ground station radiometry operates, with range and range rate (Doppler) measurements using the ISL transponder available on every DOT and SHEPHERD. Furthermore, the measurements allow for collision prediction and avoidance planning by maintaining a fixed relative distance at which the CubeSats are allowed to be.

There are several aspects of the orbits that determine the accuracy of the measurements performed. One of these is the proximity of the orbits of the CubeSats: the closer they are the higher the navigation uncertainty. Also, it should be noted, that a full state estimation is not possible, so this must be coupled with other navigational methods to achieve full state determination. However, using an architecture such as LiAISON allows for absolute estimation when at least one of the CubeSat orbits had a unique size, shape and orientation, which is also substantially aided by asymmetrical acceleration fields, which is perfect due to the highly asymmetric gravity field of Didymos. Meanwhile, if they are coplanar, for example, observability issues arise and the achievable accuracy decreases [69]. A study by Qin et al. shows that non-coplanar orbits do increase the overall navigation accuracy and provide a fuller state estimation, so this should be considered for the future planning of the operational orbits [55]. Additionally, the expected 1σ accuracy of such links with range and range rate measurements is 2 m and 0.1 mm s^{-1}, but combined with optical navigation, it has been shown that a distributed architecture at the 433 Eros asteroid sub-meter precision can be achieved [28] [69]. It should also be noted that only direct measurements (inter-satellite ranging) are being used to compute the relative position, as indirect methods would not be making use of the ranging possibilities using the ISL transponder.

As for the direct measurements, they are transponder based, which means that the transponder needs to have reception and transmission occur almost at the same time on different frequencies, which substantially reduces transmission power and allows the estimation of frequency-dependent effects such as plasma effects. There are also other effects that will have consequences on the measurements such as propagation delay and the repetitiveness of the generated signals which cause ambiguity, but both can be compensated for with a-priori estimates of the spacecraft states. [69]

Furthermore, for the ranging measurements, a time-derived approach is taken, as the ISL data rate is limited to 38.4 kbps, which restricts the usage of telemetry-based methods, and due to its performance at the prescribed data-rate as can be seen in Figure 15.7. Time-derived refers to the estimation of range based on the transfer time, but also applying correction factors due to internal delays and the aforementioned effects. Also, special consideration must be taken to the drift in the spacecraft's

clocks, which can be improved by calibration and the usage of a ”coordinated-time” timestamp. Meanwhile there is only one option for range rate measurements, but it has very small systematic errors and high accuracy can be achieved with larger integration times (there are simple relations to calculate the error for both measurements which can be found in [69]).

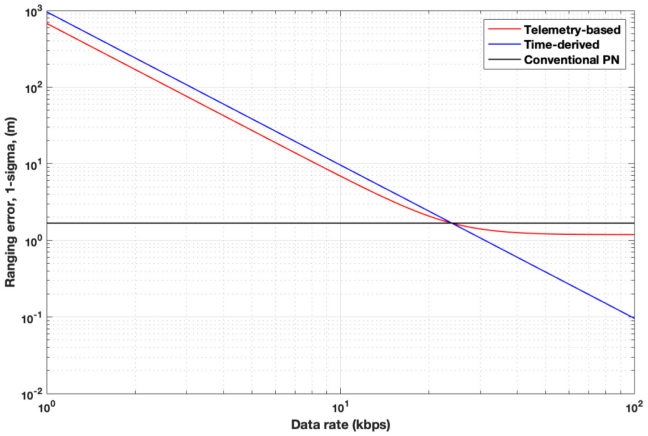

Figure 15.7: Ranging error vs data rate for different methods [69]

15.2.2. State Estimation

Now that all the methods, including their types of measurements, and accuracies have been detailed and analysed, it is important to describe how the data coming from all the sensors is combined to provide the best possible estimate of the spacecraft state in a short amount of time. This estimation is generally done through a navigation algorithm, such as a Kalman Filters, which reconstructs the trajectory of the spacecraft by combining the measurement data either simultaneously or updating them as they are performed [48].

The comparison between the navigation algorithms is done by trading-off the robustness, numerical precision, computational cost and direct availability of the estimates. Thus, based on these performances, the navigational filter is selected: Unscented Kalman Filter (UKF). This can also be visualized through Figure 15.8, where the UKF has good performance in both the controlled position and velocity. The literature seems to agree that this filter has the highest performance for collaborative spacecraft in terms of the robustness, its ability to handle non-linearities accurately at low computational cost, and medium to low relative computational cost [48, 71]. As a result, the selection of the UKF is expected to be final, unless another type of navigational algorithm exceeds its performance in the future. More information on the theoretical formulation of the filter can be found in the work of Vertisano et al. and Moreno Villa (see [48, 71]).

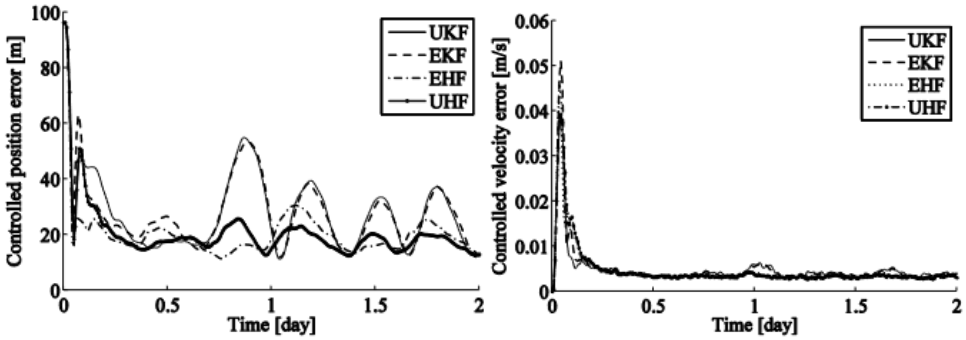

Figure 15.8: Comparison of controlled position (left) and velocity (right) average RMSE for various types of navigation algorithms [71]

15.2.3. Sensor Distribution

The distribution of sensors within the TRIADs is of paramount importance, as this will change the accuracy within the computed position and also the controlled position. The choice of distribution is mainly done through performing a Monte Carlo analysis on a simulated measurement model with enforced uncertainties with each spacecraft having different instruments and allowing it to run for a fixed amount of time to see how the error propagates. Due to the current stage of the design work it was not possible to perform such an analysis, but results and conclusions from similar analyses can be combined to reach to a good estimation of the sensor distribution for acceptable accuracy and robustness to failure. Furthermore, sharing information is quite vital for the system, as by doing so one can reduce the estimation and controlled error up to 50% in position and 60% in velocity [71]. Before discussing the results, it is important to note that the SHEPHERD is fitted with an additional OBC when compared to the DOTS due to the large amount of data that it will be handling for telemetry and navigation (in LiAISON there is a need for a chief spacecraft).

As will be described in chapter 16, all spacecraft are fitted with a navigational camera (some more proficient than others) and the ISL transponder, which means that all will be able to perform optical navigation and inter-satellite measurements, but the Sheperd will also have a LIDAR sensor (DLEM20). It is also important to consider that there will be 9 spacecraft in total to perform the measurements and share information with the rest of the system, which means that the achievable accuracy is quite high. Taking this into account, one could compare this architecture with the results from the work of Vertisano et al. where several configurations and sensor performances were evaluated [71]. More importantly, the analysis only considers 4 spacecraft all fitted with a camera, LIDAR and ISL transponder, so a conservative estimate of accuracy will be derived, and the control strategy is based on a Lyapunov control function to control the spacecraft towards the target location at each time step. It is fitting to look at the worst-case scenario implemented in the analysis and the best-case scenario to achieve an understanding of the possible accuracies, both are shown in Table 15.2. As can be seen, the worst case average RMSE is for case 5 within the study, which is 26.89 m and 3.90 mm s^{-1} in position and velocity, respectively, which adds perspective into what the representative errors for the DASH mission are.

Table 15.2: Instruments on each spacecraft in the analysis of Vertisano et al. [71]

Case	*S/C 1*	*S/C 2*	*S/C 3*	*S/C 4*	*Worst Case Average RMSE*	
Case 1 (best)	I	C,LR,I	C,LR,I	C,LR,I	S/C 3	Position: 12.57 m Velocity: 1.61 mm s^{-1}
Case 5 (worst)	I*	I*	C,LR*,I	C,LR*,I	S/C 3	Position: 26.89 m Velocity: 3.90 mm s^{-1}

I=ISL Transponder || LR=LIDAR || C=Camera || *= bad condition

Considering that the analysis uses sensors with lower performance than those selected, and that the DASH mission will have much more redundancy within its architecture due to the amount of satellites that are in the system and the amount of sensors within each spacecraft, the achieved accuracy in the best case scenario (no-failures) will be higher than that achieved by the analysis. Furthermore, this helps towards the necessary accuracy that will be required for DOTS operating very close to the surface of the asteroid (for radar purposes, for example).

15.3. Guidance and Control

Guidance laws allow the spacecraft to compute the necessary trajectory and corrections to arrive at a desired destination. However, there are certain issues that arise within the calculations of the trajectories such as spacecraft collision or collision with the surface or even the amount of time that it takes to compute all the trajectory. Naturally, a selection process must ensue as there are several guidance laws and control methods, as will be explored.

15.3.1. Methods

The guidance laws considered for the current design stage are: fixed (and variable)-time-of arrival, model predictive control, and differential algebra. Fixed-time-of arrival (FTOA) is a relatively simple linearised guidance law that has been used broadly for space trajectory computation due to its high TRL and maturity, but is now being superseded by other guidance laws which have lower fuel consumption, especially in low-thrust applications (as is the case for the DASH mission). Model predictive control (MPC) was developed using optimum guidance and control laws and aims to reach a way-point in a given amount of time, with the distribution of way-points helping the spacecraft stay close to the desired trajectory during the transfer. Furthermore, it also has a small computational load, but, aside from its complexity, also struggles with finding optimum solutions to large correction manoeuvres. Finally, differential algebra algorithms are based on n^{th} order solutions to a ODE system with boundary conditions, of which the Lambert solver forms part of (the simplest type), and it can accommodate all types of thrusting schemes. Nevertheless, it has very low maturity and the complexity of the algorithm increases once the spacecraft dynamics become more complex. [48]

As a result, looking at the benefits and detriments of each method, and also considering how well MPC complements convex optimisation, as shown by Morgan and Chung, which is a quick optimisation method that has been used in multivehicle trajectory design and has been proven to work for formation reconfiguration with collision free trajectories, so it is quite appropriate for the DASH mission considering its very low computation time, as will be shown. Additionally, the novelty behind MPC implementation with SCP is that it decentralises computations and communications which is required for swarm reconfiguration, so the algorithm is able to handle the positions of even thousands of spacecraft in real time. [49]. Consequently, the adopted guidance law is MPC using Sequential Convex Programming (SCP) to compute the necessary control inputs while minimising fuel consumption.

15.3.2. MPC-SCP Algorithm

The principal behind sequential convex programming is solving non-convex optimisation problems that are subject to certain constraints that are in ”convex form” using algorithms that are fast thanks to the properties of convexity [49]. The key concept here is being able to formulate all constraints and dynamics in their convex form, even if it is an approximation. Luckily, this is possible for the spacecraft dynamics, collision avoidance constraints, and the overall fuel minimisation constraint for the whole system, as proven by Morgan and Chung. More information on the mathematical formation of the navigational problem, the pseudocode, and algorithms used to solve these problems can be found in [49]. In the future, the implementation of convex problem solving into Python (using modules such as CVXPY 1.2) can be performed to get an accurate depiction of the algorithm working in real time at the asteroid location, as the study only simulates the algorithm with Earth being the main gravitational body.

To give an overview of the concept behind the MPC-SCP algorithm without going into excessive detail, Figure 15.9 is used. The SCP optimization gives the necessary control inputs to reach a certain desired final position in a given amount of time. In this figure it is shown how MPC is implemented within the SCP problem: the overall reconfiguration problem to be solved through SCP is broken up into multiple parts. At the beginning of each of these parts, the SCP problem is solved again to avoid what occurs when only solving it once: initial sensor or actuator error can cause a large deviation from the desired final position if the actuator commands are only evaluated once, as is shown on the right. However, if the problem is solved repeatedly, then the positions are updated mid-trajectory, which is representative of the way-points in the traditional MPC algorithms [49].

There are considerable advantages to adopting this model. For starters, as described before, there is considerable robustness to sensor and actuator inaccuracies by solving multiple SCP problems. Additionally, the fast computation speed allows for multiple iterations to be performed until a decision is made to increase accuracy and not propagate too many deviations between desired and actual trajectories forward, as they will be accounted for when computing future trajectories. Also, the method is effective for formations containing tens of spacecraft but scales badly with the number of collision constraints as this increases quadratically. Thus, it fits the DASH mission quite well. Finally, SCP is

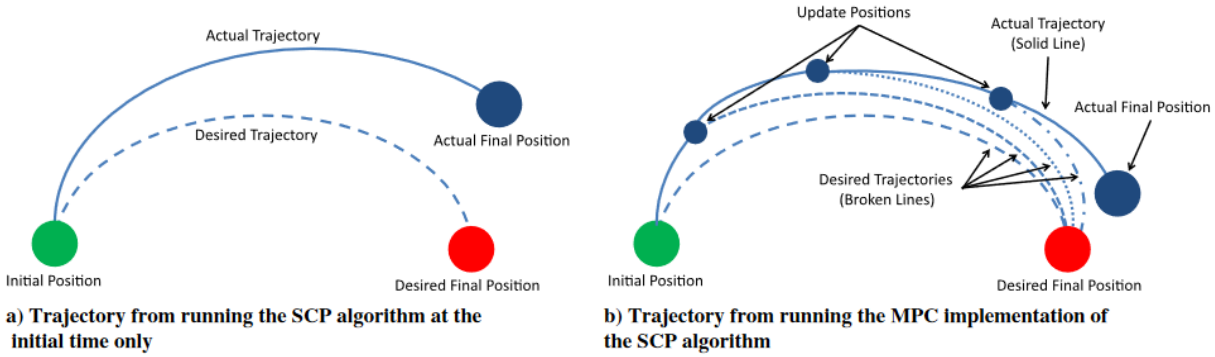

Figure 15.9: Trajectory comparisons between SCP and MPC-SCP optimization in a 2D representation of the convexification of the collision avoidance constraint [49]

better than solving the convex programming problem as it allows the spacecraft to take trajectories that would otherwise be restricted as convex programming takes an overly conservative guess of the prohibited zone. This is the area around the spacecraft where other spacecraft are not allowed to be in to avoid collision; considering the prior analysis, an estimate for the radial limit of this zone is 37.5 m (3-sigma error in best-case position estimate).

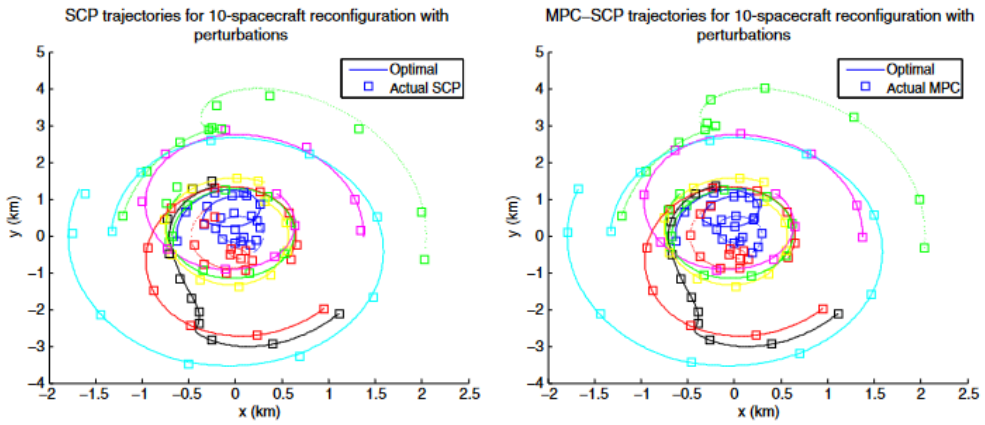

Figure 15.10: Comparison of SCP and MPC-SCP trajectories considering actuator and sensor errors [49]

The performance of the MPC-SCP algorithm is outstanding in terms of the controlled position error between the final desired position and the actual position, and it heavily outperforms using only an SCP algorithm. The results are shown in Table 15.3 while the trajectories are shown in Figure 15.10, where the performance of the decentralised MPC-SCP algorithm (when considering actuator and sensor errors) is very high in its final position deviation and also the average computation time of solving the SCP problem. Furthermore, the only reason why it uses more Delta-V is because it applies corrections during the transfer arc to the final position, so the increase in fuel consumption is the reason why the position error remains so low. It should be noted that the sensor errors used imply a position and velocity maximum errors of 1 m 7.5 mm s^{-1}, which imply high accuracy requirements based on the analysis made on the sensor distribution, but this is expected as the analysis is made on Earth-bound formation reconfiguration (GPS can be used). Additionally, the maximum control acceleration error is 0.1 mm/s^2 which, with a spacecraft mass of 20 kg, translates to a maximum allowable thruster error of 2 mN. As a result, the average terminal error position error is the controlled position error considering the previously mentioned navigational errors, which are considerably low, to this error one has to add the navigation algorithm's true error, which would already introduce large errors when identifying the optimum trajectory.

Table 15.3: Comparison of SCP and MPC-SCP guidance and control laws considering actuator and sensor errors [49]

Method	*Number of S/C*	*Performance Crtieria*		
		Average Delta-V [m/s]	**Average Terminal Error [m]**	**Computation Time [s]**
Only SCP	10	2.102	163.6	37.36
	100	1.916	166.6	413.29
MPC-SCP	10	2.995	1.067	3.79
	100	2.894	1.013	10.32

Consequently, a larger terminal error is expected to be enforced in future analysis to determine the true controlled position error. Furthermore, the sensitivity of the control input to the errors in the state determination from the navigation filter should be explored in more detail, but some information can be obtained from looking at the controlled position error of the analysis from Vertisano et al. For starters, it is understood that using the Lyapunov control function exerts a thrust that is proportional to the position error, simply by how the control function is defined (see Equation 15.4), which, looking at the results, maximises at being 17.2% larger than the position error [71]. Meanwhile, the increase in the accuracy when no errors in sensors and actuators are considered for the MPC-SCP method is reducing the error by 1.0623 m, so that can be considered as the representative error of the method with respect to a maximum error in position, velocity, and control inputs. Nevertheless, the analysis must be replicated in future work at the asteroid location with the appropriate errors representative of the sensor accuracies, navigation filter performance and thruster accuracy, to determine the controlled position error for this type of guidance and control law, but this type of approach looks very promising to implement on a distributed system. On a final note, the component choices for the system are shown in chapter 16, as these payloads are some of the main instruments needed to fulfil the science goals.

$$\mathbf{u} = -\left(\mathbf{a}_{\text{Sun}}\left(\delta\mathbf{r}\right) - \frac{\mu_A}{\delta r^3}\delta\mathbf{r}\right) - \kappa\left(\delta\mathbf{r} - \delta\mathbf{r}_{\text{ref}}\right) - c_d\delta\dot{\mathbf{r}} \tag{15.4}$$

15.4. Delta-V Simulation

The purpose of this simulation is to calculate the ΔV needed for the autonomous station keeping and the counteracting of the orbit perturbations of the satellites for a fixed amount of time. The control of the spacecraft is done using the Lyapunov control function to remain in the specified position. It is run for a self-stabilising terminator orbit and for a simple leader-follower satellite configuration. No positional uncertainty is included in the simulation, but it is recommended for future development that this uncertainty is included and a Monte Carlo analysis is done. The program was verified by propagating standard circular orbits and witnessing no deviation from what was expected given the resultant force acting on the spacecraft.

15.4.1. Simulation Assumptions

A number of assumptions have been made to facilitate the simulation, they are as follows:

- The geometries of Didymos and Dimorphos are assumed to correspond to the physical models developed by S.P. Naidu et al. [51] The bodies are then modelled as ellipsoids, as shown in Figure 15.11.
- The asteroid Hill frame coordinate system has its x-axis
- The gravity perturbations are modelled using second degree gravity field. This means that the perturbations can be modelled using only the C20 and C22 gravity field coefficients. These coefficients are functions of the axis ratios of the ellipsoids used to model the asteroids, but only perturbations from Didymos are deemed relevant given that its mass is larger than Dimorphos' by two orders of magnitude.
- A constant frontal area to the Sun is assumed
- In order to simplify the orbit propagation, all bodies are modelled as point masses. Therefore, the gravity between the bodies only acts in the direction of the centre of mass. The complete gravity is therefore modelled as gravity from a point mass and the perturbations from a second

degree gravity field.

- To calculate the effects of the solar radiation pressure, the sunlit area has been assumed to be constant. This prevents the need to track the orientation of the spacecraft and allows modelling it as a point mass. In order to be conservative, the constant value is set to be the maximum possible sunlit area.
- The simulation uses a system with Didymos as the main body. This is justified if the effects of the gravity of the sun can be neglected when considering a reference frame centred around Didymos. At 1.6 AU from the sun, a distance variation of 20 km from Didymos, well outside the range of the orbital manoeuvres considered, constitutes a difference in gravitational acceleration of 0.000013%, approximately $3\times10^{-10}\,\mathrm{m\,s^{-2}}$. Therefore, all bodies in the system can be safely assumed to experience the same acceleration due to the sun, and so this won't make a difference for their movement relative to each other.
- Consistent with previous findings [25], the propellant mass available to the thruster on board the spacecraft is set to be 1.84 kg.
- No ephemeris is available for Dimorphos. Therefore, its position in its orbit at the start of the simulation is randomised.
- The position and control error are modelled as a random sample from a Gaussian distribution using a standard deviation of 5 m and $20\,\mu\mathrm{m\,s^{-2}}$ (20% of maximum thrust).
- The steady dissipation coefficient, c_d, and the elastic coefficient, κ, in Equation 15.4 are assumed to be $10^{-5}s^{-1}$ and $10^{-6}s^{-2}$, respectively. These values were iterated upon until a desirable trajectory was achieved.

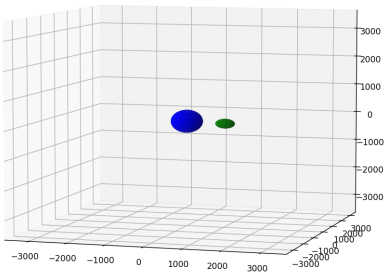

Figure 15.11: Physical models of Didymos and Dimorphos.

15.4.2. Results

The simulation was run 100 times with a time step of 10 s over a period of 27.778 hours, which does not cause significant errors in the acceleration computation given the slow movement of the spacecraft around Didymos due to the low mass. Additionally, it is assumed that the spacecraft is at an entry trajectory for close operations at the asteroid, initialising at $y = 3000$m and a velocity in the z direction, v_z, of $0.108\,\mathrm{m\,s^{-1}}$. The trajectories are shown in Figure 15.12, while the distribution of Delta-V's for each Monte Carlo run is shown in Figure 15.13. As can be seen, an average of $0.529\,216\,\mathrm{m\,s^{-1}}$ of velocity increments are necessary in order to be able to perform the orbital manoeuvre.

This result is highly inconsistent with the results from Takahashi and Sheeres, which is performed over a period of 160 days with an average use of $2.759\,\mathrm{m\,s^{-1}}$ of velocity increments [71]. This is due to the Lyapunov control function which has several deficiencies when compared to the optimisation approach taken in chapter 7, which could not be immediately implemented due to differences within the solvers. The main difference is that the approach taken Takahashi and Sheeres relies on Lambert problem solving to identify the required trajectory and then uses a guidance law to identify the necessary initial velocity to complete the transfer effectively, while the Delta-V is computed using the Lambert solver. This is a substantially different and optimised approach, whereas the Lyapunov function simply attempts to achieve the desired position under any means necessary, without considering the best burn approaches. As a result, a large reward to the mission analysis would come by from simply applying an optimised control approach.

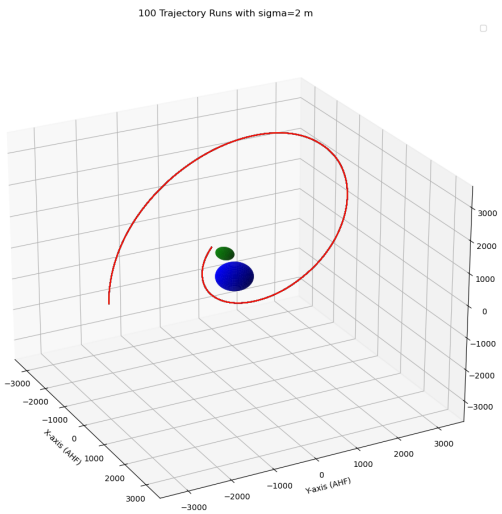

Figure 15.12: Trajectory for spacecraft using 100 Monte Carlo runs with a position dispersion of $\sigma = 2$m

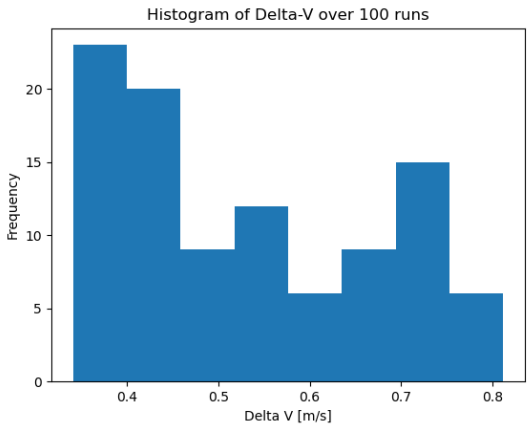

Figure 15.13: Delta-V histogram for the 100 Monte Carlo runs with a position dispersion of $\sigma = 2$m

Furthermore, the control function is also very sensitive to the position and control errors, as increasing the standard deviation of the Gaussian distribution results in a substantially different trajectory and used Delta-V. This effect can be seen in Figure 15.14 for $\sigma = 3, 2, 1$m, respectively (from left to right). This also implies that it is not robust at all to the errors brought about by sensors and actuator deficiencies, considering that the case for $\sigma = 3$m is put into an orbit that does not even complete a revolution, indicating it has deviated substantially from the target orbit and is trying to correct itself by thrusting in the opposite direction, but this only makes it lose energy and cause the trajectory to become closer and closer to the surface of the asteroid. This effect can be seen when seeing how smaller standard deviations of position allow for the spacecraft to follow the reference orbit closer and also require a considerably lower average Delta-V, which is summarised in Table 15.4.

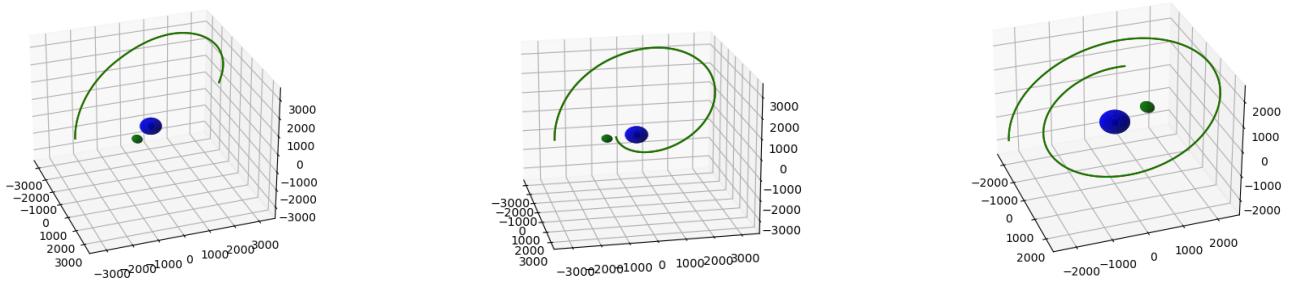

Figure 15.14: Trajectories for a position error with a Gaussian distribution with $\sigma = 3, 2, 1$m (from left to right); all axes are in meters

Table 15.4: Average Delta-Vs for the Monte Carlo analysis for different position uncertainties

	$\sigma = 1$*[m]*	$\sigma = 2$*[m]*	$\sigma = 3$*[m]*
Delta-V [m/s]	0.155970	0.529216	0.831964

In conclusion, given the lacking results of the simulation, there are no relevant outcomes from the simulation except being able to state that the Delta-V requirements are not stringent given that using an under-performing control algorithm, a low Delta-V requirement follows for low position errors, which are expected due to the prior analysis. However, by replacing the guidance law and implementing other system parameters such as the multi-spacecraft data fusion, or the communications delay, it can deliver high quality and a large quantity of results for different orbit types.

16 Payload

In this chapter, the payload distribution among the different CubeSats will be discussed. These payloads have as primary goal gathering scientific data, but some imagers are also used for navigation. Since the mission uses a grouped transfer concept, for each TRIAD will have two DOTs fully focused on payload, and one SHEPHERD with payload for navigation.

16.1. TRIAD One

The SHEPHERD CubeSat will have the same payload for each TRIAD, so it will only be discussed here. The SHEPHERD CubeSat has two payloads. Firstly, there is the DLEM20 [1]. This payload is a laser rangefinder, which uses LIDAR technology to navigate during operations. Next, there is Hyperion IM200[2], which is a small imager. This payload will be used for navigation during the scientific operations. For each TRIAD, the payload CubeSats will be divided in two 'DOTs'. Both of the DOTs will use the Simera Sense MultiScape100 CIS[3] payload. This payload is a visual camera, which will also be used for navigation. The usage of these payloads was further elaborated in chapter 15. On the S-DOT CubeSat, the GRASS[4] gravimeter is used. On the N-DOT will be the VISTA[5] volatile thermogravimetre. Below in Table 16.1, the exact payload division with the size, mass and power required is given.

Table 16.1: Payload Division TRIAD One

CubeSat	Payload	Size [U]	Mass [kg]	Power Required [W]	Cost [EUR]
SHEPHERD	DLEM20	0.04	0.033	1.8	4.780
	Hyperion IM200	0.06	0.06	0.7	-
S-DOT	MultiScape100 CIS	1.8	1.1	5.8	130.000
	GRASS	0.2	0.38	0.15	-
N-DOT	VISTA	0.1	0.09	2	-
	MultiScape100 CIS	1.8	1.1	5.8	130.000

For the next TRIADs, the payload on the SHEPHERD will no longer be specified, since it will have the same payload as in this TRIAD. But do keep in mind the other TRIADs will contain a SHEPHERD CubeSat as well.

16.2. TRIAD Two

For the second TRIAD, both DOTs will also make use of the MultiScape100 CIS, and the S-DOT will use the same GRASS payload as in TRIAD One. However, the N-DOT woll make use of the ASPECT hyperspectral imager [6]. Below, in Table 16.2, the division can be seen.

[1] URL https://pdf.directindustry.com/pdf/jenoptik-i-defense-civil-systems/dlem-20-dlem-30-dlem-45/65823-978842-_3.html [cited 1 June 2022]

[2] URL https://www.aac-clyde.space/what-we-do/space-products-components/payloads/im200#expandable-form-panel- [cited 12 June 2022]

[3] URL https://simera-sense.com/products/multiscape100-cis/ [cited 1 June 2022]

[4] URL https://www.heramission.space/hera-mission-juventas-cubesat [cited 31 May 2022]

[5] URL https://www.heramission.space/hera-mission-milani-cubesat [cited 13 June 2022]

[6] URL https://www.esa.int/ESA_Multimedia/Images/2021/06/ASPECT_hyperspectral_imager [cited 10 June 2022]

Table 16.2: Payload Division TRIAD Two

CubeSat	Payload	Size [U]	Mass [kg]	Power Required [W]	Cost [EUR]
S-DOT	MultiScape100 CIS	1.8	1.1	5.8	130.000
	GRASS	0.2	0.38	0.15	-
N-DOT	ASPECT	2.5	1.25	7	-
	MultiScape100 CIS	1.8	1.1	5.8	130.000

16.3. TRIAD Three

In the third TRIAD, the S-DOT and N-DOT will have the same payload. They will both use the MultiScape100 CIS for navigation, and furthermore also the Thoth Argus 1000[7] thermal infrared spectrometer. The DOTs have the same payloads to add redundancy, and furthermore because the two CubeSats will fly different orbits, and will thus be able to analyse the composition of the asteroid two times faster. In Table 16.3 below, the exact payload division with the size, mass and power required is given.

Table 16.3: Payload Division TRIAD Three

CubeSat	Payload	Size [U]	Mass [kg]	Power Required [W]	Cost [EUR]
S-DOT	MultiScape100 CIS	1.8	1.1	5.8	130.000
	Thoth Argus 1000	2	0.23	2.52	-
N-DOT	Thoth Argus 1000	2	0.23	2.52	-
	MultiScape100 CIS	1.8	1.1	5.8	130.000

16.4. Additional Payload Considerations

In chapter 17, it is shown that there is still space left over in the DOT CubeSats after the payload above has been added. Thus, there are additional payload considerations which can be made as a result of, for example, future scientific CubeSat technology or if the distributed network is used for a different mission objective. For this, a synthetic aperture radar (SAR) is a good example. There are already CubeSat sized SAR's, but these either require landing, or do not have flight heritage, and thus have a low TRL. Currently, existing SAR's that have flown in for example UAV's, are too big for CubeSats, but in the future this will certainly be improved and should be looked at again.

[7] URL https://satsearch.co/products/thoth-technology-argus-1000-spectrometer [cited 13 June 2022]

17 Subsystems Integration

In this chapter the internal configuration of the CubeSats will be presented. First the SHEPHERD configuration will be introduced followed by the DOTs. Once the configuration is set, a centre of gravity estimation is performed for each CubeSat and a detailed mass budget per component is conferred.

17.1. Internal Configuration

The internal configuration of the CubeSats will be shown in this section. A set of renders and a technical drawing is included for each.

17.1.1. SHEPHERD

Renders of the internal view are shown in Figure 17.1 and Figure 17.2. Moreover, Figure 17.3 shows a separated configuration render where both the SHEPHERD solar panels and antennas are deployed. Below, Figure 17.4 shows a technical drawing illustrating all components present and where they go internally. A component breakdown is shown in the bill of material, where each component can be identified by their respective number on the inside and exploded view.

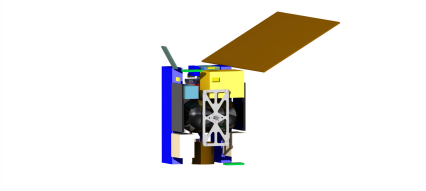

Figure 17.1: Internal view of components, front view

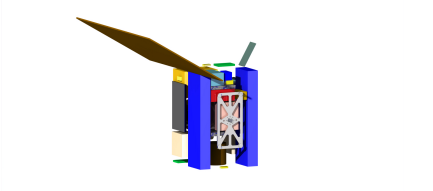

Figure 17.2: Internal view of components, rear view

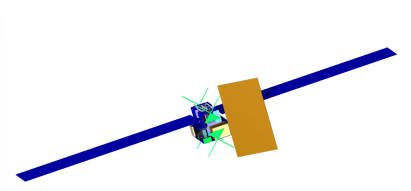

Figure 17.3: Separated Configuration

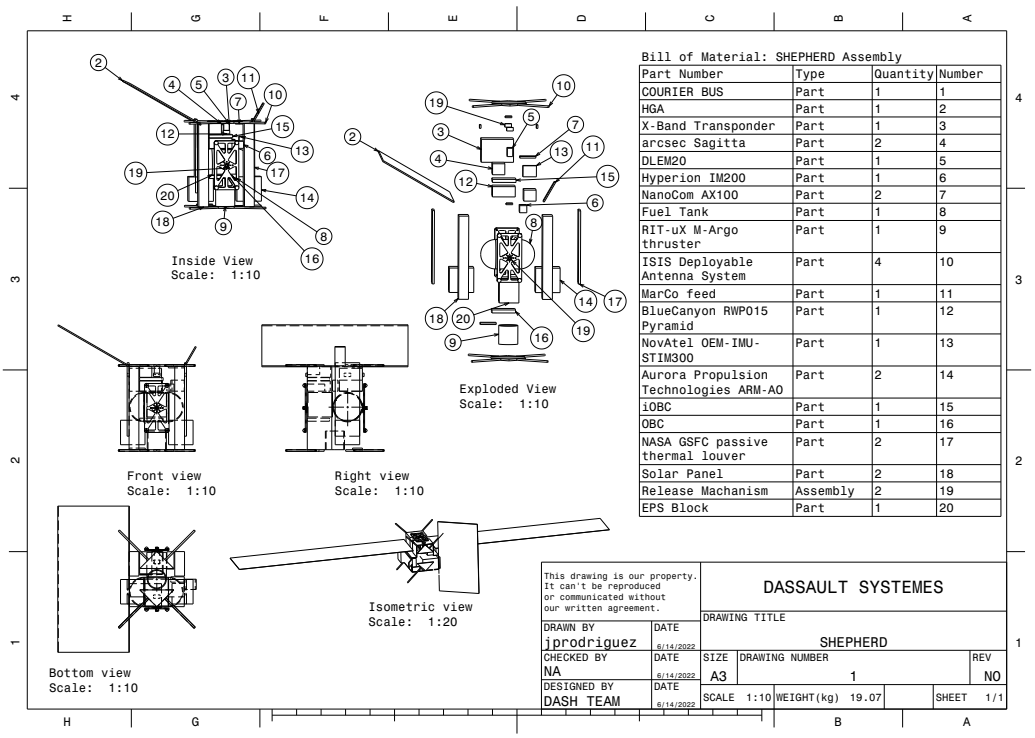

Figure 17.4: SHEPHERD assembly drawing

17.1.2. DOTs

Similarly, renders of the internal view of the DOT are shown in Figure 17.5 and Figure 17.6. Moreover, Figure 17.7 shows a separated configuration render where both the DOT solar panels and antennas are deployed. Below, Figure 17.8 shows a technical drawing illustrating all components present and where they go internally. A component breakdown is shown in the bill of material, where each component can be identified by their respective number on the rear, inside, and exploded view.

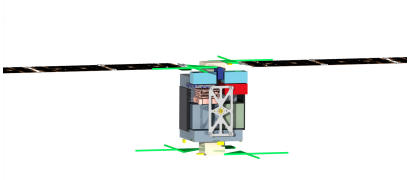

Figure 17.5: Internal view of components, front view

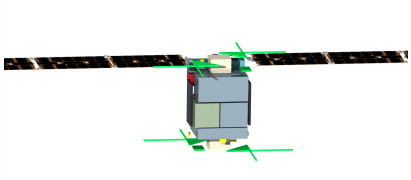

Figure 17.6: Internal view of components, rear view

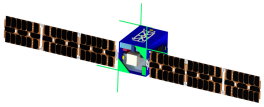

Figure 17.7: Separated Configuration

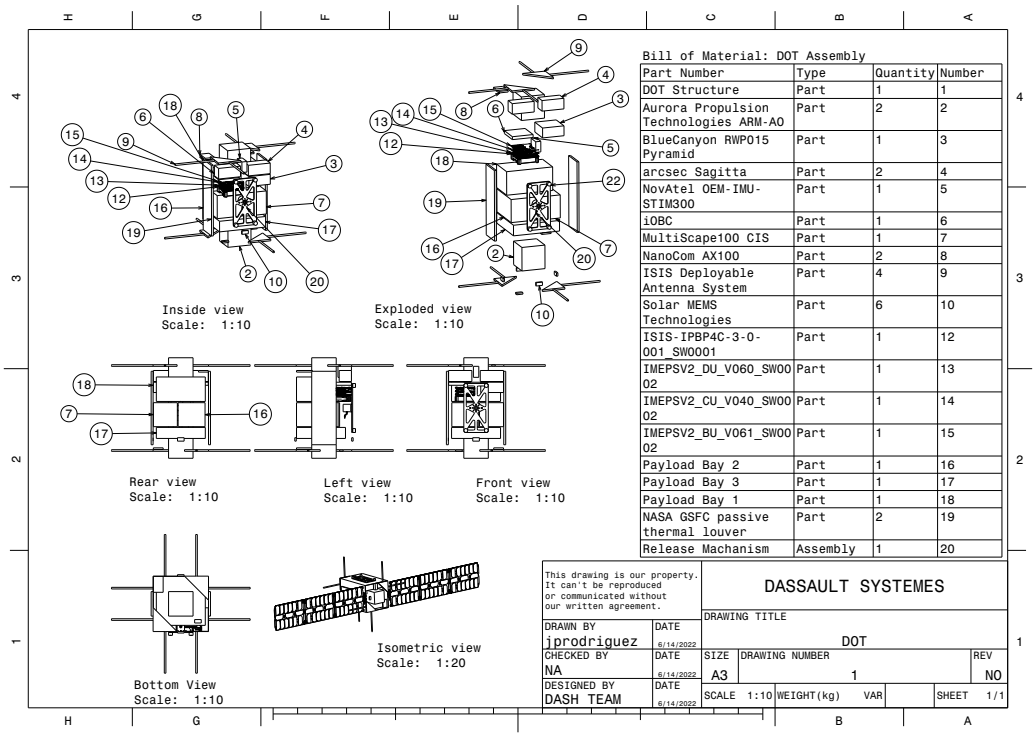

Figure 17.8: DOT assembly drawing

17.1.3. TRIAD

Two TRIAD renders are presented, Figure 17.9 and Figure 17.10, illustrating the transfer and separation configuration, respectively. These configurations are also shown in the technical drawing, where each CubeSats is identified by balloons. Moreover, the separation and overall dimensions for the transfer configuration is provided. This is important in the case of a custom containerised deployer since both the manufacturing and the DASH team would need to abide strictly by these dimension for a successful design.

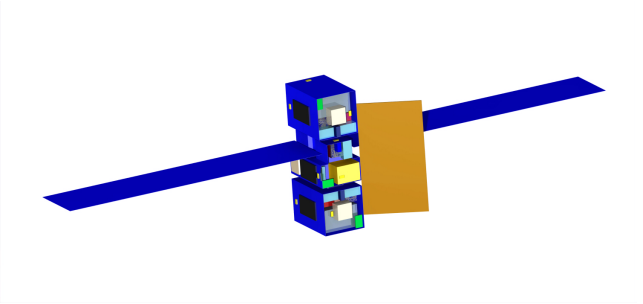

Figure 17.9: Transfer configuration render

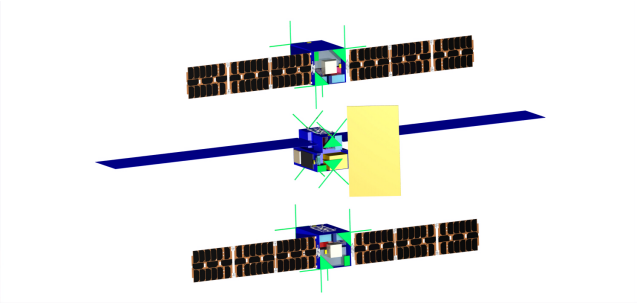

Figure 17.10: Separation configuration render

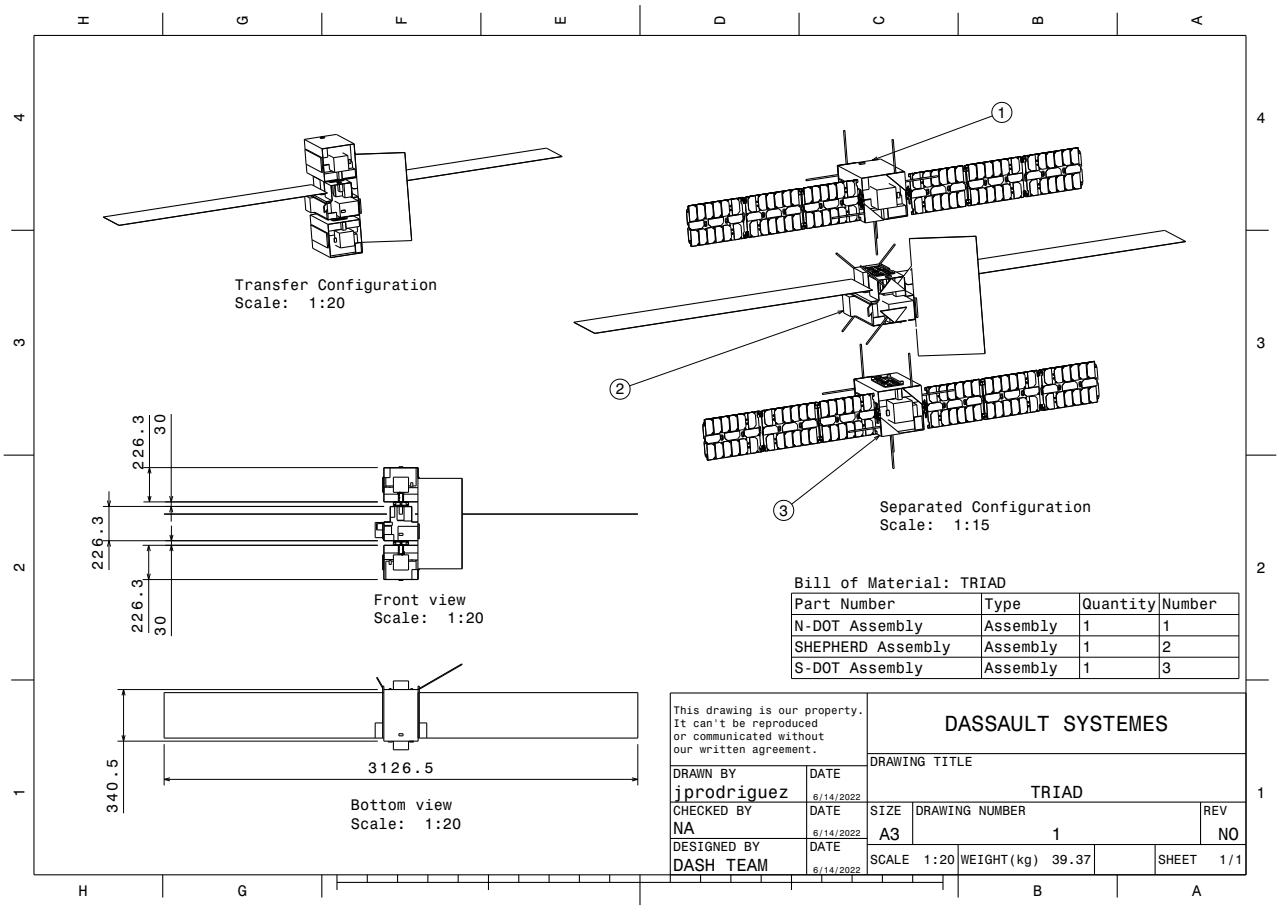

Figure 17.11: TRIAD assembly drawing

17.2. Centre of Gravity Estimation

In this section, the centre of gravity for each CubeSat will be presented. This estimate is based on each subsystem component location on the bus and it's mass. The coordinate system for each CubeSat, alongside the global coordinate system, is shown below in Figure 17.12.

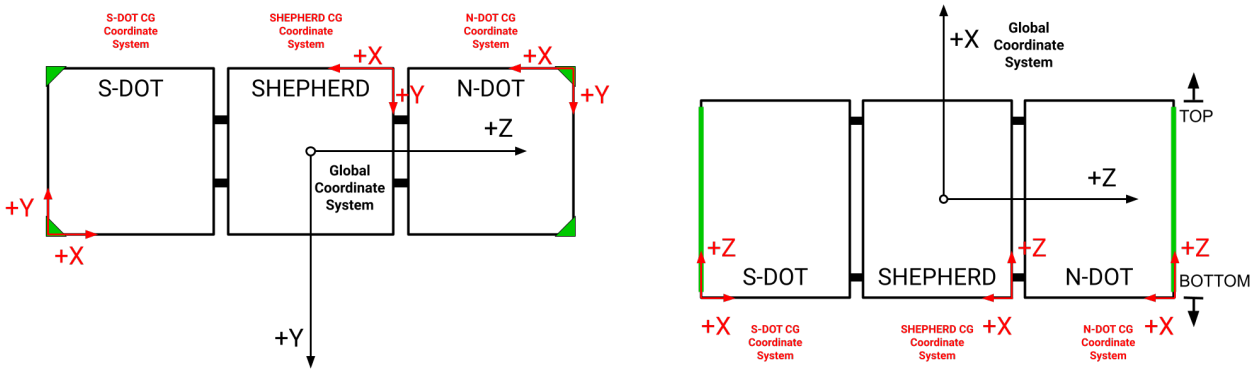

(a) Top view **(b)** Front view

Figure 17.12: CG coordinate system and Global coordinate system

It should be noted that, although not performed here, estimating the centre of gravity for the TRIAD configuration should be fairly straightforward. This could be done by transferring the centre of gravity position of each CubeSat to the global coordinate system and recomputing the new location for the three CubeSats in that coordinate frame. Awareness of the TRIAD centre of gravity is important to ensure thrust alignment during transfer and needs to be performed at later stages of the design.

17.2.1. SHEPHERD and DOTs

The centre of gravity location is shown below on Figure 17.13, Figure 17.14 and Figure 10.17 for the S-DOT, SHEPHERD and N-DOT, respectively. Each blue point represents a point mass for each component present in the bus. Later, these components, its location and mass is also shown in Table 17.1. The red star shows the cg location and the black crosses are the CubeSat bounding box. The location is computed assuming a lumped mass acting at the centroid of each component. Furthermore, a deployed configuration for the solar panel of the SHEPHERD is taken and a stowed one for the DOTs is assumed. This is done to estimate the centre of gravity location during transfer as this could later be used to estimate the final TRIAD centre of gravity location which would be useful for thrust alignment calculations and coming up with a correcting strategy. Furthermore, this is also the separation configuration for the DOTs so this centre of gravity calculation is useful for estimating the rotational separation velocity and coming up with a strategy to counter it once released.

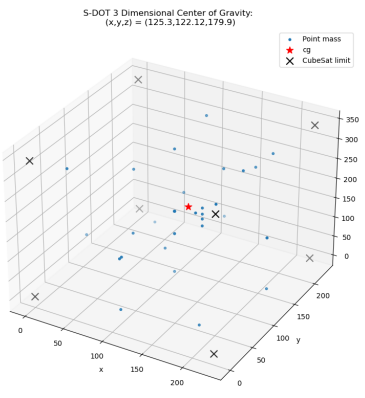

Figure 17.13: CG location for S-DOT

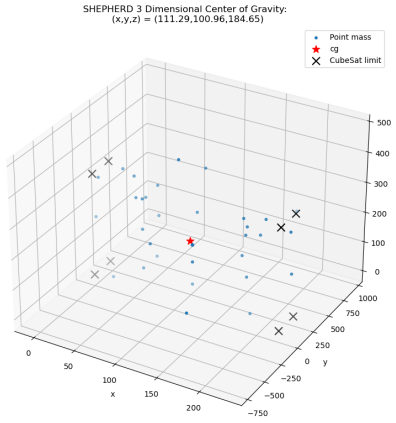

Figure 17.14: CG location for SHEPHERD

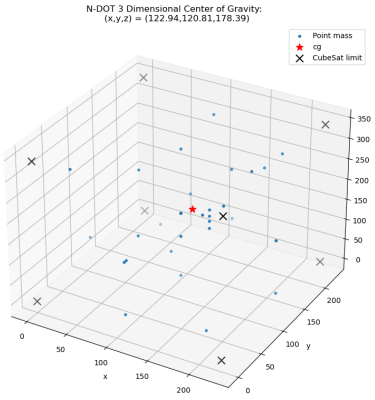

Figure 17.15: CG location for N-DOT

17.3. Mass Budget

In this section, per-component mass budget is presented. Components are presented in Table 17.1, identified by their unique ID, positing on each CubeSat, based on the coordinate system defined in Section 17.2, and their mass.

Table 17.1: Mass Budget per TRIAD

S-DOT		
EPS		
Component (ID)	**(x,y,z)**	**Mass**
left_solar	[113.15, 0, 170.25]	0.75
right_solar	[113.15, 226.3, 170.25]	0.75
battery_pack	[170.796, 72.429, 207.5]	0.252
battery_unit	[170.796, 72.429, 251.5]	0.0487
distribution_unit	[170.796, 72.429, 224.5]	0.0574
conditioning_unit	[170.796, 72.429, 236.5]	0.058
wiring	[113.15, 226.3, 170.25]	0.2
Telecommunication		
Component (ID)	**(x,y,z)**	**Mass**
NanoCom_AX100_1	[33.5, 21, 320.25]	0.0245
NanoCom_AX100_2	[33.5, 205.3, 4.25]	0.0245
ISIS_Deployable_Antenna_System_1	[113.15, 113.15, 113.15]	0.115
ISIS_Deployable_Antenna_System_2	[113.15, 113.15, 113.15]	0.115
Structures		
Component (ID)	**(x,y,z)**	**Mass**
COTS	[113.15, 113.15, 170.25]	1.7
Release_mechanism	[228.3, 113.15, 170.25]	0.357
ERM	[228.3, 113.15, 170.25]	0.075
ADCS		
Component (ID)	**(x,y,z)**	**Mass**
BlueCanyon_RWP015_Pyramid	[178.8, 178.8, 254.5]	0.74
arcsec_Sagitta_1	[200.3, 177.8, 301]	0.26
arcsec_Sagitta_2	[200.3, 48.5, 301]	0.26
Solar_MEMS_Technologies_nanoSSOC_A60_1	[113.15, 184.3, 343.5]	0.025
Solar_MEMS_Technologies_nanoSSOC_A60_2	[113.15, -3, 42]	0.025
Solar_MEMS_Technologies_nanoSSOC_A60_3	[-3, 113.15, 42]	0.025
Solar_MEMS_Technologies_nanoSSOC_A60_4	[229.3, 113.15, 42]	0.025
Solar_MEMS_Technologies_nanoSSOC_A60_5	[113.15, 229.3, 42]	0.025
Solar_MEMS_Technologies_nanoSSOC_A60_6	[184.3, 43.15, -3]	0.025
NovAtel_OEM_IMU_STIM300	[197.8, 113.3, 318]	0.055
Aurora_Propulsion_Technologies_ARM_AO_1	[113.15, 113.15, 325.5]	0.6
Aurora_Propulsion_Technologies_ARM_AO_2	[113.15, 113.15, 15]	0.6
Navigation		
Component (ID)	**(x,y,z)**	**Mass**
iOBC	[177.3, 46, 269.3]	0.1
MultiScape100_CIS	[89, 176.3, 143]	1.1
Thermal		
Component (ID)	**(x,y,z)**	**Mass**
White_coating	[113.15, 113.15, 170.25]	0.05
Acrylic_966_Adhesive	[113.15, 113.15, 170.25]	0.237
Silvered_FEP_tapes	[113.15, 113.15, 170.25]	0.07
Thermal_louver	[113.15, -4, 170.25]	0.12
CDHS		
Component (ID)	**(x,y,z)**	**Mass**
OBC	[113.15, 113.15, 170.25]	0
Payload		
Component (ID)	**(x,y,z)**	**Mass**
lumped_payload	[113.15, 113.15, 170.25]	0
payload_bay_1	[61, 113.15, 247]	0.33
payload_bay_2	[86, 69.15, 143]	0.33
payload_bay_3	[101, 113.15, 68.5]	0.33
Total		**9.86**

SHEPHERD		
EPS		
Component (ID)	**(x,y,z)**	**Mass**
Part_of_ExoTerra_Bus	[173, 112.4, 183.6]	1.69
left_solar	[175, -715.1, 170.25]	1.236
right_solar	[175, 941.4, 170.25]	1.236
Telecommunication		
Component (ID)	**(x,y,z)**	**Mass**
X_Band_Transponder	[48, 66.75, 285.6]	1.2
MarCO_HGA	[113.15, -83.75, 485.5592551]	0.931
NanoCom_AX100_1	[21, 33.5, 3.25]	0.0245
NanoCom_AX100_2	[21, 192.8, 337.25]	0.0245
ISIS_Deployable_Antenna_System_1	[113.15, 113.15, 113.15]	0.115
ISIS_Deployable_Antenna_System_2	[113.15, 113.15, 113.15]	0.115
HGA_deployment_mechanism	[113.15, 113.15, 170.25]	0.01
HGA_feed_deployment_mechanism	[113.15, 113.15, 170.25]	0.01
MarCO_feed	[113.15, 305.9743371, 386.5]	0.057
Structures		
Component (ID)	**(x,y,z)**	**Mass**
COTS	[113.15, 113.15, 170.25]	3.5
Release_mechanism_1	[231.3, 113.15, 170.25]	0.357
Release_mechanism_2	[-7, 113.15, 170.25]	0.357
ADCS		
Component (ID)	**(x,y,z)**	**Mass**
BlueCanyon_RWP015_Pyramid	[178.8, 89.4, 259.9]	0.74
arcsec_Sagitta_1	[177.8, 67.9, 318]	0.26
arcsec_Sagitta_2	[48.5, 200.3, 261.4]	0.26
Solar_MEMS_Technologies_nanoSSOC_A60_1	[-3, 113.15, 305.5]	0.025
Solar_MEMS_Technologies_nanoSSOC_A60_2	[61, 229.3, 305.5]	0.025
Solar_MEMS_Technologies_nanoSSOC_A60_3	[62, -3, 305.5]	0.025
Solar_MEMS_Technologies_nanoSSOC_A60_4	[229.3, 113.15, 305.5]	0.025
Solar_MEMS_Technologies_nanoSSOC_A60_5	[42, 113.15, 343.5]	0.025
Solar_MEMS_Technologies_nanoSSOC_A60_6	[183.3, 113.15, -3]	0.025
NovAtel_OEM_IMU_STIM300	[112, 197.8, 261.4]	0.055
Aurora_Propulsion_Technologies_ARM_AO_1	[61, 211.3, 70.25]	0.6
Aurora_Propulsion_Technologies_ARM_AO_2	[61, 15, 70.25]	0.6
Navigation		
Component (ID)	**(x,y,z)**	**Mass**
DLEM20	[200.3, 113.9, 323.5]	0.033
iOBC	[180.3, 90.9, 288.1]	0.1
Hyperion_IM200	[189.95, 168.9, 253.4]	0.059
Thermal		
Component (ID)	**(x,y,z)**	**Mass**
Thermal_interface_material	[113.15, 113.15, 170.25]	0.359
Pyrovo_Pyrolytic_Graphite_Film_PGF_thermal_straps	[113.15, 113.15, 170.25]	0
White_coating	[113.15, 113.15, 170.25]	0.05
Sheldahl_metallized_tape_coatings_second_surface_silvered_FEP_tapes_1	[113.15, 113.15, 170.25]	0.07
Sheldahl_metallized_tape_coatings_second_surface_silvered_FEP_tapes_2	[113.15, 113.15, 170.25]	0.07
NASA_GSFC_passive_thermal_louver_1	[62, -4, 205.125]	0.12
NASA_GSFC_passive_thermal_louver_2	[62, 230.3, 205.125]	0.12
CDHS		
Component (ID)	**(x,y,z)**	**Mass**
OBC	[180.3, 90.9, 122.4]	0.1
Payload		
Component (ID)	**(x,y,z)**	**Mass**
lumped_payload	[113.15, 113.15, 170.25]	0
Propulsion		
Component (ID)	**(x,y,z)**	**Mass**
RIT_uX_M_Argo_thruster	[113.15, 113.15, 38]	0.66
Fuel_Tanks	[61, 113.15, 132.25]	1.85
Fuel	[61, 113.15, 132.25]	1.947
Total		**19.07**

N-DOT		
EPS		
Component (ID)	**(x,y,z)**	**Mass**
left_solar	[113.15, 0, 170.25]	0.75
right_solar	[113.15, 226.3, 170.25]	0.75
battery_pack	[170.796, 72.429, 207.5]	0.252
battery_unit	[170.796, 72.429, 251.5]	0.0487
distribution_unit	[170.796, 72.429, 224.5]	0.0574
conditioning_unit	[170.796, 72.429, 236.5]	0.058
wiring	[113.15, 226.3, 170.25]	0.2
Telecommunication		
Component (ID)	**(x,y,z)**	**Mass**
NanoCom_AX100_1	[33.5, 21, 320.25]	0.0245
NanoCom_AX100_2	[33.5, 205.3, 4.25]	0.0245
ISIS_Deployable_Antenna_System_1	[113.15, 113.15, 113.15]	0.115
ISIS_Deployable_Antenna_System_2	[113.15, 113.15, 113.15]	0.115
Structures		
Component (ID)	**(x,y,z)**	**Mass**
COTS	[113.15, 113.15, 170.25]	1.7
Release_mechanism	[228.3, 113.15, 170.25]	0.357
ERM	[228.3, 113.15, 170.25]	0.075
ADCS		
Component (ID)	**(x,y,z)**	**Mass**
BlueCanyon_RWP015_Pyramid	[178.8, 178.8, 254.5]	0.74
arcsec_Sagitta_1	[200.3, 177.8, 301]	0.26
arcsec_Sagitta_2	[200.3, 48.5, 301]	0.26
Solar_MEMS_Technologies_nanoSSOC_A60_1	[113.15, 184.3, 343.5]	0.025
Solar_MEMS_Technologies_nanoSSOC_A60_2	[113.15, -3, 42]	0.025
Solar_MEMS_Technologies_nanoSSOC_A60_3	[-3, 113.15, 42]	0.025
Solar_MEMS_Technologies_nanoSSOC_A60_4	[229.3, 113.15, 42]	0.025
Solar_MEMS_Technologies_nanoSSOC_A60_5	[113.15, 229.3, 42]	0.025
Solar_MEMS_Technologies_nanoSSOC_A60_6	[184.3, 43.15, -3]	0.025
NovAtel_OEM_IMU_STIM300	[197.8, 113.3, 318]	0.055
Aurora_Propulsion_Technologies_ARM_AO_1	[113.15, 113.15, 325.5]	0.6
Aurora_Propulsion_Technologies_ARM_AO_2	[113.15, 113.15, 15]	0.6
Navigation		
Component (ID)	**(x,y,z)**	**Mass**
iOBC	[177.3, 46, 269.3]	0.1
MultiScape100_CIS	[89, 176.3, 143]	1.1
Thermal		
Component (ID)	**(x,y,z)**	**Mass**
White_coating	[113.15, 113.15, 170.25]	0.05
Acrylic_966_Adhesive	[113.15, 113.15, 170.25]	0.237
Silvered_FEP_tapes	[113.15, 113.15, 170.25]	0.07
Thermal_louver	[113.15, -4, 170.25]	0.12
CDHS		
Component (ID)	**(x,y,z)**	**Mass**
OBC	[113.15, 113.15, 170.25]	0
Payload		
Component (ID)	**(x,y,z)**	**Mass**
lumped_payload	[113.15, 113.15, 170.25]	0
payload_bay_1	[61, 113.15, 247]	0.52
payload_bay_2	[86, 69.15, 143]	0.52
payload_bay_3	[101, 113.15, 68.5]	0.52
Total		**10.44**

18
Performance Analysis

Following the design and definition of all relevant mission subsystems, the mission budgets are here summarised. Firstly, in Section 18.1, the mass, power, volume, and data budgets for both DOTs and SHEPHERDs are provided. Next a comprehensive cost analysis for the DASH mission is performed from the ground-up starting all the way down from individual component costs. For each, a minimum, maximum, and expect cost is estimated to define a triangular cost probability density function. These probability density functions are combined and used to estimate cost through a Monte Carlo analysis method.

18.1. Budget Breakdown

In order to have a complete overview of the spacecraft, a budget breakdown has to be performed. This breakdown will show how all the resources on the spacecraft are divided among the subsystems. Below, in table Table 18.1, an overview of these budgets in given the SHEPHERD and DOTs respectively. Since the (non-navigation) payload within each spacecraft is different for each CubeSat, the payload budgets regarding mass and size have been included as averages. Furthermore, respective component and subsystem cost estimates are treated separately in Section 18.2. It is important to note that these estimates were made using a bottom-up approach, when trajectory estimated the wet mass and dry mass using a top-down approach. As such, these values obtained using bottom up are seen as refined values.

Table 18.1: Budget Breakdown for SHEPHERD and DOTs. For the power budget, it is important to note that not all power consumption happens at the same time. Refer to the modes of operations and FFBD to know what is switched on simultaneously.

Category	Subcategory	SHEPHERD	DOT	Unit
Mass	Thruster Mass	0.66	-	kg
	Propellant (+Tank) Mass	3.797	-	kg
	Structures Mass	4.214	2.792	kg
	Thermal Mass	0.669	0.597	kg
	CDHS Mass	0.1	0.1	kg
	EPS Mass	4.162	2.2161	kg
	TT&C Mass	2.467	0.279	kg
	ADCS Mass	2.665	2.665	kg
	Navigation Mass	0.192	1.2	kg
	Payload Mass	-	1.28 [1]	kg
	Total Mass	18.926	11.1	kg
	Total Triad Mass	41.13		kg
	Allowable Mass	57.54		kg
	Design Margin	16.6 (29 %)		kg
Size	Thermal Size	3.8	0.06	U
	Thruster Size	0.363	-	U
	Propellant (+Tank) Size	3.2	-	U
	EPS Size	-	0.477	U
	CDHS Size	0.15	0.15	U
	TT&C Internal Size	1.329	0.0338	U
	ADCS Size	1.85	1.72	U
	Navigation Size	0.21	1.9	U
	Payload bay Size	-	5.883	U

[1] This is an average, the specific payload mass for each DOT is in chapter 16.

Table 18.1 continued from previous page

Category	Subcategory	SHEPHERD	DOT	Unit
	Total Size	10.9	10.22	U
	Allowable Size	12	12	U
	Design Margin	1.1 (9 %)	1.78 (15 %)	U
Power	Propulsion Power Required	-114	-	W
	EPS	-3.0	-2.96	W
	Thermal Power Required	0	0	W
	CDHS Power Required	-0.4	-0.4	W
	TT&C Power Required	-105.86	-5.703	W
	ADCS Power Required	-15.5	-15.5	W
	Navigation Power Required	-8.7	-6.2	W
	EOL Power Generated	129	30	W
	Design margin	15 (12 %)	2.2 (7 %)	W
Area	Solar Panel Area	0.88	0.412	m^2
Data Storage	SD Data Storage	32	8	GB
Data Volume	DASH Data Volume	130		Gbit
	DASH Allowable Data Volume	142		Gbit
	Design Margin	12 (12 %)		Gbit

The final budget that must be analysed is that of the cost. A bottom-up approach is chosen, where the costs are broken down into independent categories. For this, the methodology outlined in SMAD [36] is followed. First, a set of ground rules and assumptions are laid out to constrain the form, content and scope of the cost estimate and to enable approximating element costs for things that are still uncertain. The various elements are then decided, and the total cost is estimated.

18.2. Cost Budgets Estimation

The cost estimate will be composed of 5 main categories. First, the spacecraft cost refers to the entire cost of all the spacecraft components, including their integration into one system. Note that this also contains the payload cost, which is not considered a part of the recurring cost. The mission has a budget requirement of 100 MEUR for these recurring costs, but since the purpose is to be as modular as possible and allow the integration of various different payloads, the payload costs are considered outside the mission scope.

As estimating the total cost of the mission at this preliminary stage involves numerous estimations and assumptions, it is helpful to list a range of expected costs for all of the contributions, after which the total cost can be estimated by a very simple Monte Carlo simulation, taking into account all the distributions. Table 18.2. For the purpose of this first analysis, a triangular probability distribution is assumed for all the components. As depicted in Figure 18.1, this assumes that probability density increases linearly from an absolute minimum towards the estimate and then decreases linearly towards the absolute maximum. The minimum cost represents an ideal estimate that that might be slightly unrealistic, but could be possible. For instance, if a product currently has a low TRL but might be ready to fly on DASH in several years. The maximum cost represents the price in case all the projected risks occur; i.e. the worst case scenario. Finally, the estimate value represents the most likely cost. This can either be an estimate based on a cost estimating relationship (CER), or a price that was directly requested from the commercial company that provides the component or service.

The main cost contributions and their estimates are listed in Table 18.2. The checkmarks in the final column indicate whether or not a certain contribution is considered part of the recurring costs of the mission. Note that the cost breakdown of the spacecraft bus (#.1.1) has the summed values for all of the subsystems. For more details, refer to the subsystem design from chapter 8 to chapter 16. For some other parts, more preliminary cost estimates were used; the CERs presented here are taken from SMAD [36] and relate to unmanned small spacecraft. The relation to calculate the cost

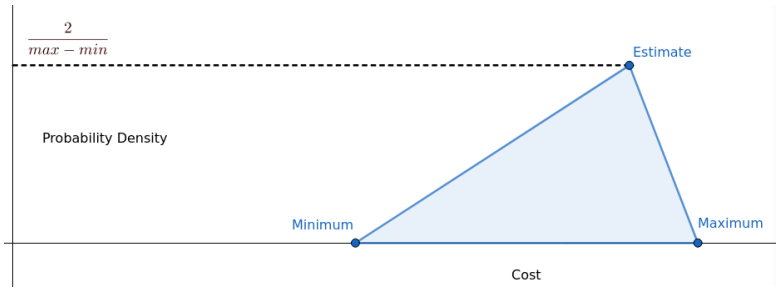

Figure 18.1: Triangular probability distribution for component costs (made using GeoGebra [31])

for assembly, integration and testing of the satellite is calculated separately for each of the CubeSats, after which the program level costs are based on the entire TRIAD of a SHEPHERD and two DOTs.

$$C_{\text{SC, AIT}} = 0.195 \times C_{\text{bus+payload}} \qquad \sigma = 34\% \tag{18.1}$$

$$C_{\text{program level}} = 0.320 \times \left(C_{\text{bus+payload}} + C_{\text{SC, AIT}}\right) \qquad \sigma = 40\% \tag{18.2}$$

$$C_{\text{flight support ops.}} = 560 \qquad \sigma = \text{not given} \tag{18.3}$$

$$C_{\text{AGE}} = 0.432 \times C_{\text{bus+payload}}^{0.907} \qquad \sigma = 37\% \tag{18.4}$$

The estimate value of the above costs is obtained by simply substituting the estimates for the relevant variables without any margin. The minimum and maximum are then found by doing the same and then respectively adding or subtracting 1 standard deviation (σ) from the result. In case the standard deviation is not given, a conservative estimate of 50 % is adopted.

One of the most constraining costs is the use of the DSN communication. Just like for most deep space missions, it is one of the scarce resources and accounts for a large portion of the costs. For the present work, the CER in Equation 18.5 is used. Here, $R_B = 1128$ EUR is the contact-dependent hourly rate, taking into account the necessary inflation. A_w is the aperture weighting, which is 4 for the 70 m antenna. Finally, N_c represents the number of contacts per week. For the current TT&C design, daily contact is assumed, meaning that N_c =7. Finally, everything is multiplied by the total contact time in hours to find the cost. A margin of 10 % is then used to obtain the minimum and maximum cost values.

$$C_{\text{DSN}} = R_B \left[A_w \left(0.9 + N_c/10\right)\right] T_h \tag{18.5}$$

Apart from the simple usage of the DSN facilities, a cost must also be foreseen for the people monitoring DASH's health. Although the mission is in principle autonomous, a human check is still necessary to increase the reliability and to allow interference from ground if something is not working as expected. During the transfer, health data is sent every 14 days, after which one person will be tasked to check the data for 2 hours. During science operations and the 6 months after that, data will be received daily and the equivalent of one working day per week is assumed to monitor the behaviour of the satellite herd. Assuming an hourly rate of 150 EUR, this leads to the following cost estimate for ground monitoring. A 50 % deviation is then used for the upper and lower bound of the estimate.

$$C_{\text{monitoring}} = 150 \times \left(\frac{\text{transfer days}}{14} \cdot 2 + 52 \cdot 8\right) \tag{18.6}$$

A final cost parameter that will have an enormous influence on the total mission cost is the cost of dedicated flight software. According to SMAD [36], a single line of code costs around 320 EUR (2021). Even though a lot of software can be reused from other missions, there is still a large expected effort to tailor to the specific needs of DASH. Certainly in terms of the navigation algorithms, the software cost is something that must not be overseen. However, estimating the total lines of code requires a much deeper study of the software requirements. Therefore, it is considered beyond the scope of the current cost estimate.

Table 18.2: Detailed cost breakdown. All costs are shown in 2021 equivalent euros.

Cost Element	Method	Element Cost [kEUR] Minimum	Estimate	Maximum	Recurring
SHEP.1.0 SHEPHERD Spacecraft					
SHEP.1.1 Spacecraft Bus					✓
SHEP.1.1.1 Structure + panels	chapter 10	250	500	1000	✓
SHEP.1.1.2 Thermal	chapter 11	10	19	34	✓
SHEP.1.1.3 ADCS	chapter 14	230	282	333	✓
SHEP.1.1.4 EPS	chapter 9	10	15	50	✓
SHEP.1.1.5 Propulsion	chapter 8	52	105	511	✓
SHEP.1.1.6 TT&C	chapter 13	322	878	1595	✓
SHEP.1.1.7 Navigation	chapter 15	10	18	34	✓
SHEP.1.1.8 CDHS	chapter 12	7	7	7	✓
SHEP.1.2 Payload	chapter 16	-	-	-	
SHEP.1.3 Spacecraft AIT	Equation 18.1	121	376	962	✓
DOT.1.0 DOT Spacecraft					
DOT.1.1 Spacecraft Bus					✓
DOT.1.1.1 Structure	chapter 10	18	19	28	✓
DOT.1.1.2 Thermal	chapter 11	5	12	21	✓
DOT.1.1.3 ADCS	chapter 14	230	282	333	✓
DOT.1.1.4 EPS + panels	chapter 9	57	88	103	✓
DOT.1.1.5 Propulsion	chapter 8	-	-	-	✓
DOT.1.1.6 TT&C	chapter 13	22	28	45	✓
DOT.1.1.7 Navigation	chapter 15	10	18	34	✓
DOT.1.1.8 CDHS	chapter 12	7	7	7	✓
DOT.1.2 Payload	chapter 16	-	-	-	
DOT.1.3 Spacecraft AIT	Equation 18.1	64	117	187	✓
2.0 Launch and Transfer					
2.1 Launch vehicle	Section 8.1	6500	7000	13000	✓
2.2 Kick Stage	Section 8.1	2450	3500	5000	✓
2.3 Deployer	Section 10.2.3	50	100	200	✓
2.4 Deployer D&D	Section 10.2.3	1000	1500	2000	
3.0 Ground C&C					
3.1 DSN Usage	Equation 18.5	28500	31600	35000	
3.2 Monitoring	Equation 18.6	41	82	122	✓
4.0 Program Level					
4.1 PM & SE	Equation 18.2	428	1224	2968	
4.2 Design Engineering					
4.3 System AIT					
4.4 Product Assurance					
5.0 Others					
5.1 Flight Support Ops	Equation 18.3	280	560	840	✓
5.2 AGE, GSE and PSE	Equation 18.4	293	712	1506	✓

Based on these estimates, it is still rather hard to see what can be expected in terms of total recurring costs. For this purpose, a basic Monte Carlo simulation is created that randomly picks a value for each of the cost components considering the probability distribution as shown in Figure 18.1. Running this for many times and visualising the results, as done in Figure 18.2, gives a clear idea on the spread of the cost estimate. This figure is made for the SHEPHERD, a single DOT, the additional costs and finally for an entire TRIAD. The 95th percentile cost is then chosen as the final estimate. This indicates that there is a 95 % chance that the actual cost is lower.

The results can be summarised in the final recurring cost budget for each of the TRIADS and DASH as a whole. With the 95th percentile estimate of 66.9 MEUR, DASH remains well below the total cost budget. Once more, it must be stressed that this estimate does not include payloads (these can be tailored to the specific mission at hand), nor does it take into account any design and development. Furthermore, the significant cost of using the DSN during this extended period of time is disregarded

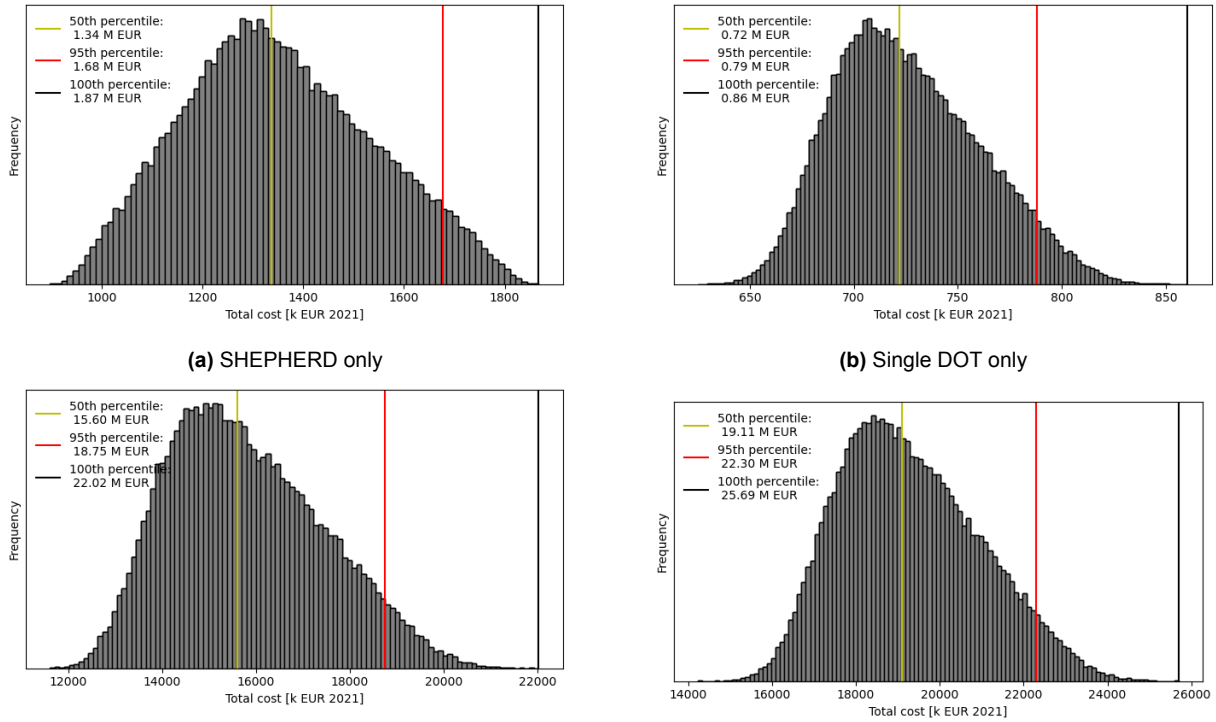

(a) SHEPHERD only

(b) Single DOT only

(c) Additional costs (everything with checkmarks in Table 18.2, except #.1.1)

(d) Entire TRIAD recurring cost

Figure 18.2: Monte Carlo analysis for the recurring cost of one TRIAD, based on the estimates of Table 18.2. Each of the graphs represents the results of 100 000 simulations.

within this estimate. The additional estimated 31.6 MEUR would bring the total cost to just below the maximum budget of 100 MEUR, although it is expected that the DSN costs could be negotiated, taking into account that dash is an institutional mission.

Element	**50th percentile** [MEUR]	**95th percentile** [MEUR]	**100th percentile** [MEUR]
SHEPHERD	1.34	1.68	1.87
DOT	0.72	0.79	0.86
Other costs	15.6	18.8	22.02
TRIAD (Min. viable mission)	19.1	23.3	25.7
DASH (No DSN)	57.3	66.9	77.1
DASH (Incl. DSN)	88.9	98.5	108.7

Table 18.3: Cost summary in 2021 equivalent euros

18.2.1. Cost Estimate Recommendations

Clearly, estimating costs at this stage of the design comes with many limitations. Therefore, a list of the main recommendations is made for a future iteration of this estimate.

- Integrate the development logic in the estimate for project level costs. This will allow for a more accurate breakdown of the non-recurring and recurring costs during all the phases of the rest of the potential project.
- A detailed estimate of the software costs can be made by setting very clear requirements on the software that still needs to be made or adapted and the reliability that is required. It is advised to take direct contact with people who could develop this software.
- More informed estimates on some of the bottom-up estimates are necessary. Within the subsystem level, many assumptions on cost ranges currently still have a large impact on the distribution of the cost prediction.

19
Verification and Validation

In this chapters the V&V procedures regarding the DASH mission are examined. For this, Section 19.1 discusses the general V&V process that is employed. Then, Section 19.2 explains the methods used for verification and validation. Lastly, Section 19.3, displays the mission requirements, system requirements and subsystem requirements, along with the system's compliance to them or how they are to be verified.

19.1. Verification and Validation Process

Verification and Validation is a process consisting of multiple stages, for the DASH mission, the stages outlined in [41] are used. These can be seen below:

1. **Requirement Validation:** Assess whether proper requirements are formulated
2. **Model Validation:** Assess the correctness of the models supporting design and verification.
3. **Product Verification:** Assess whether the designed system complies with the requirements.
4. **Product Validation:** Assess whether the designed system meets the needs of the stakeholders.
5. **Flight Certification:** Determine whether the fully integrated system is ready for flight.

It has to be noted that throughout this process, Software Verification and Validation has to be performed when necessary. In subsystem design, this is performed when applicable. This process is based on the strategy outlined in the Midterm Report [25].

At the current stage, the requirements are validated, this means that the models are to be validated in the segments where this is applicable. This is done in accordance with the techniques from [41] listed below.

1. **Face validity:** Results from the model or similar models are inspected by experts for a sanity check.
2. **Peer review:** Independent review of the internal theory behind the model.
3. **Functional decomposition and test:** Test the results of fractions of the model to input data and see if the results are as predicted.
4. **Comparison or empirical validation:** Compare performance of model to a similar model or a physical model.

Furthermore, product verification is started with, this is done through the use of a compliance matrix with all the requirements. In it, the requirements are outlined along with the design compliance to them. Given that in the current stage the system is not built yet in any form, numerous requirements are not verifiable and their compliance status is left as <TBD>. In the product validation stage, the product is assessed and its functional capabilities are compared to the stakeholder needs. This is to be done through the use of a validation matrix which essentially outlines for each need what tests are necessary to know if this need is fulfilled. Furthermore, through an Incompressible Test List (ITL), the minimum amount of tests to be performed is defined. Lastly, in the flight certification stage, the completion of the system integration activities, the completion of product verification and the completion of product validation is confirmed. Furthermore, the final reviews are conducted, these are Design Certification Review (DCR), Functional Configuration Audit, Physical Configuration Audit (PCA) and System Acceptance Review (SAR).

19.2. Verification and Validation Methods

For both product verification and validation, essentially a certain condition has to be met. The distinction is that verification is a technical assessment that revolves around the product complying with the requirements while validation is non-technical and revolves around the product meeting the needs of the stakeholders. For both, there are various ways to check compliance. For verification these are explained in Section 19.2.1 and for validation this is done in Section 19.2.2.

19.2.1. Verification

For product verification, three methods considered, these are defined in [41]. These methods are explained below:

- **Inspection:** Inspect whether the product or its documentation meets the requirement specification.
- **Analysis:** Method used when mathematical or other analysis techniques must be used in order to verify the requirement.
- **Testing:** Method used when the requirement contains a representative condition to fulfil in order to be verified.

Whenever possible, testing is employed, however, often the circumstances required are impossible to recreate. Therefore, analysis has to be employed instead in these cases. This does mean that the models and software used in analysis have to be verified and validated.

19.2.2. Validation

As far as product validation is concerned, this is to be done through the techniques mentioned in [41], these are outlined below:

- **End-to-End Information System Testing:** Demonstrate compatibility of the project information systems.
- **Mission scenario tests:** Demonstrate that the flight hardware and software execute the mission under flight-like conditions without the exact flight timeline.
- **Operational readiness tests:** Demonstrate under a real timeline that all the ground segment elements can execute the mission together.
- **Stress testing and simulation:** Assess the robustness of the system to performance variations and fault conditions.
- **Analysis:** Anything not validated through the techniques covered previously is assumed to be validated through analysis.

19.3. Requirement Compliance

In order to demonstrate the compliance with the requirements, these are displayed in a compliance matrix as explained earlier. Here it is explained how these requirements are verified or how they are to be verified. Furthermore, compliance status of the design at this stage with respect to the requirements is shown. In case no form of compliance has been checked for a requirements, it is marked as <TBD> given that the compliance has to be verified at a later stage. This is done for the mission requirements in Section A.1, system requirements in Section A.2 and the subsystem requirements in Section A.3.

20 Design Phase and Development Logic

Now that the main design features have been outlined together with the costs to confirm the mission feasibility, the mission horizon is now extended forward and future developments must be identified and planned. This is primarily done through design and development logic definition, which essentially shows the flow of procedures from the outcomes of this preliminary study, to launch and operations. Furthermore, it is also important to outline the opportunities for improvement within the mission with new technologies and advancements that are still not viable at this time. Thus, this chapter concentrates on the logistics and opportunities of the future.

20.1. Development Logic

Within the traditional engineering mindset, there are several methodologies and practices adopted by the space industry to manage and plan the design and development process of the mission. This comprises the design, manufacture, integration and testing of the mission elements in all levels: component, module, subsystem and system. This can also be categorised into the ESA mission phases, to add more structure to the chronology, which are shown in Table 20.1[1].

Table 20.1: ESA's mission phases with their expected starting dates

Phase Identifier	*Description*	*Start Date*
Phase 0	Mission Analysis and Identification	April 2022
Phase A	Feasibility Studies	April 2022
Phase B	Preliminary Definition	May 2022
Phase C	Detailed Definition	May 2023
Phase D	Qualification and Production	February 2024
Phase E	Utilisation	September 2024
Phase F	Disposal	July 2027

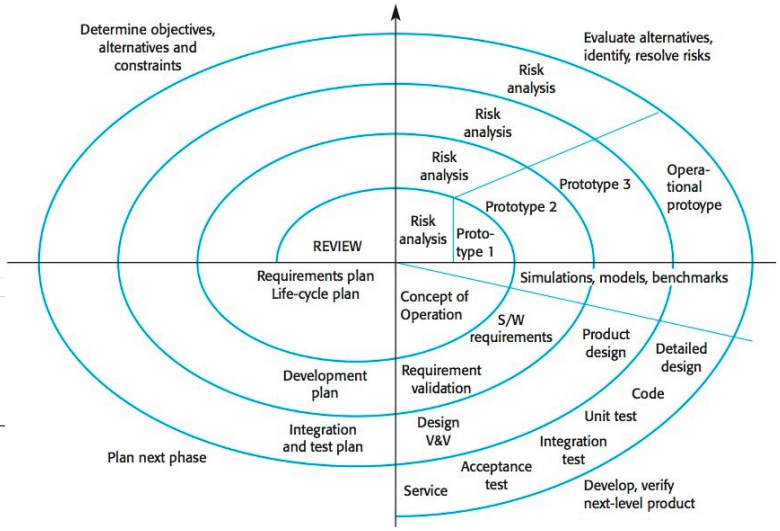

Figure 20.1: Spiral model for systems engineering

Given the (partially) repetitive nature of the design and construction of the CubeSats, due to only the payloads being the main differentiator, a different approach is considered when compared to the traditional "waterfall" method. The approach that concerns the DASH mission is a concurrent engineering variant of the spiral model for systems engineering, which is shown in Figure 20.1[2], and it attempts to maximise the efficiency in the production process of the 9 CubeSats and integrate them into the 3 TRIADs. The process to be followed is shown in a schematic format in Figure 20.2, and it exemplifies a "learn-on-the-go" strategy.

Following the outcomes of this preliminary design report, further iterations must be performed on a system and subsystem level to optimise the design, and once this is done, then the CubeSat engineering models are generated following the update of the requirements and subsystem designs and their documentation. Following that, the relevant planning of tests and testing of components, modules and subsystems, in order of increasing complexity, is performed and reported, which allows the

[1] URL https://www.esa.int/Science_Exploration/Space_Science/How_a_mission_is_chosen [cited 14 June 2022]

[2] URL https://medium.com/@chandu_22532/spiral-model-spiral-model-in-software-engineering-64e0ddee5269 [cited 14 June 2022]

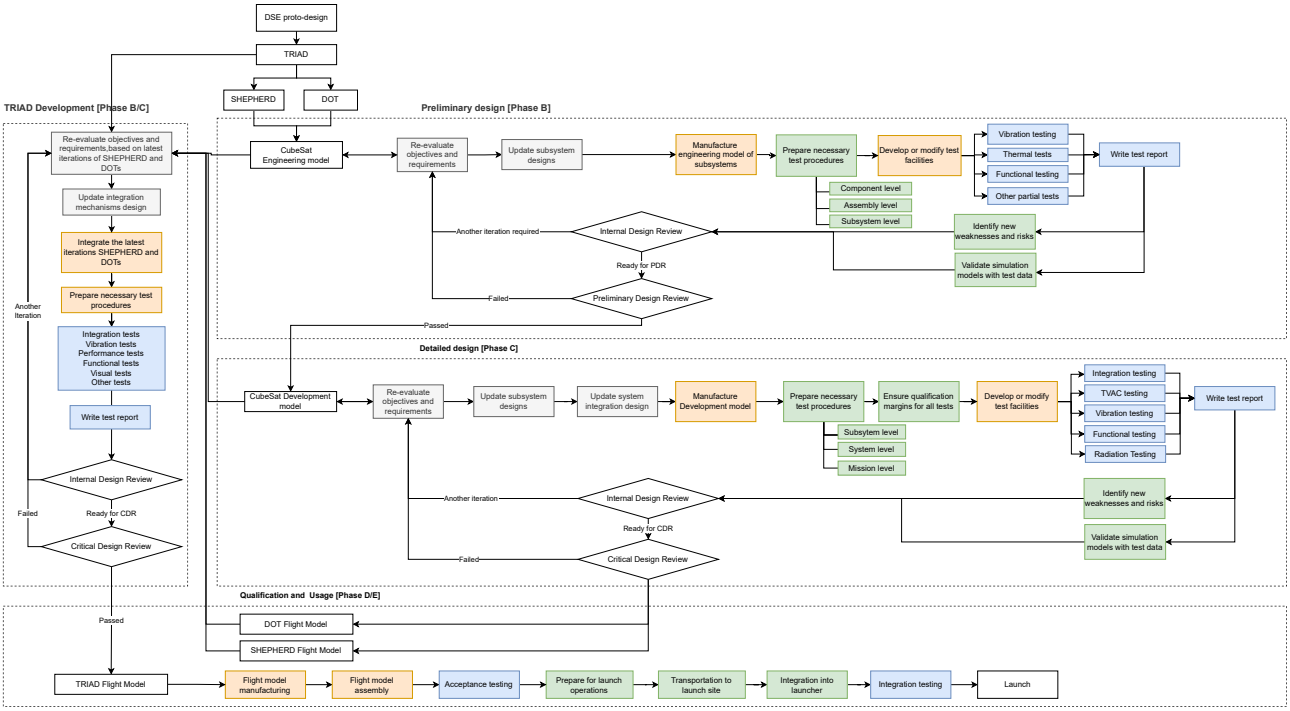

Figure 20.2: Development and testing iteration logic.

identification of several issues quite early on in the design stage, and as the main components are the same on the DOTS and SHEPHERDS, it helps in reiterations of the design for all CubeSats. Furthermore, the results are also used to validate simulation models with test data to increase the accuracy of iterations. This is finalised in a Preliminary Design Review, which marks the end of phase B, but not the end of design iterations. Additionally, if the model fails the initial or preliminary design review, then a new iteration is performed, but the engineering model is updated to the latest version, and can be used in TRIAD development for initial testing and to learn more about the system. Nevertheless, iteration is required until satisfactory results are achieved.

Now, detailed design can begin as the information acquired from phase B testing is incorporated into the design and a new iteration of the design and interfaces definition follows after updating the relevant requirements. This allows for integration of subsystems, leading to the manufacture of a development model which can be tested in numerous ways that aid in understanding the stand-alone CubeSat performance with functional tests, and integration tests, among others. As with the phase B testing, this allows the identification of risks that had not been considered previously which have to undergo mitigation strategies, leading to the improvement of the design while also validating simulation data. Phase C is finalised for the CubeSats when the critical design review is completed and passed, but like before if it does not pass it can still be used in TRIAD development. If the design is proficient, then a flight model for the CubeSat is manufactured, applying all the lessons learnt.

At this point, it should be noted that given the concurrent designing approach, different teams specialise in different CubeSats, so can have a manufacturing team for the DOTs, another for the SHEPHERDs . This in turn means that the DOTs and SHEPHERDs could be in different design phases due to issues within testing or because new insight was gained that implied a redesign of a system. Consequently, the lines between different phases become a blurred, especially for the TRIAD Development section, which uses both CubeSats, so the phase of the TRIAD development is only as advanced as the least advanced CubeSat (either the DOT or the SHEPHERD). Nevertheless, the TRIAD development consists of re-evaluating the requirements based on the iterations of the CubeSats and, if needed, redesigning the integration mechanisms (i.e. separation mechanism, wiring, etc.) and then testing the integrated model. This is ended as well with a critical design review.

Finally, once all flight models are generated, then they can be manufactured, assembled, rated with acceptance testing and then prepared for launch. Once launched, the utilisation phase ensues where

TRIADS transfer to Didymos and then perform the science operations. The mission itself ends when Didymos and Dimorphos have been characterised, and the end-of-life operations ensue by disposing of all CubeSats in a passively safe disposal orbit.

20.2. Project Gantt Chart

All the processes introduced previously must be completed within the launch time-frame of the mission, which is September 2024 for an optimum launch window. As a result, high-level planning must be performed and adhered to in order to not have to redesign the mission, or wait for the next launch window (2026). This is shown in the Mission Gantt chart in Figure 20.3.

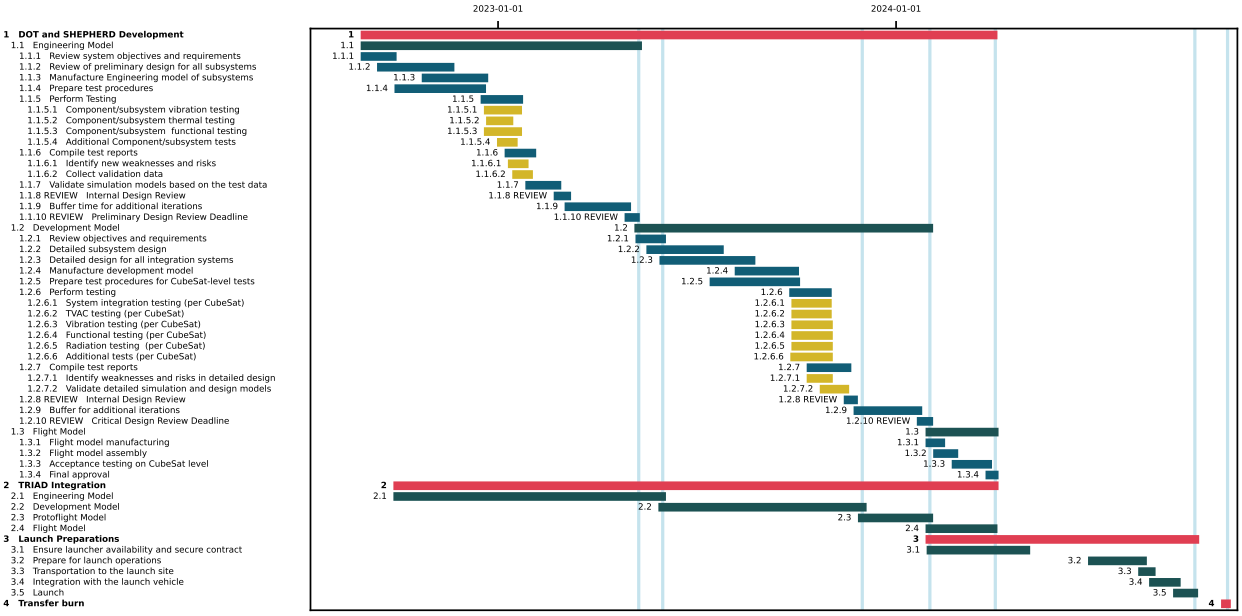

Figure 20.3: Gantt chart for futre development of the DASH mission

20.3. Near-Future Upgrade Possibilities

There are a number of technologies in development which could potentially benefit our mission, should they become available in the near future.

Rocket Lab is developing its neutron launcher, a commercially viable methane based launcher with the capacity to bring 1500 kg of payload as far into deep space as Mars or Venus. Additionally, there is SpaceX' Starship launcher, which has the ability to carry north of 100 metric tonnes into LEO. Launchers such as these will provide more options and potentially better performance to the mission.

The DSN is looking into several improvements, including opportunistic MSPA, telemetry ranging, shared uplink and dual exciters. These improvements will allow for a better, less constraining TT&C system.

Several organisations are doing research into miniaturised sample return. These technologies, in combination with additional development and added propellant, would allow the DASH mission to incorporate sample return, and have much more return on investment.

21

Conclusion and Recommendations

In this chapter the conclusions drawn throughout this report are described, in addition to that, recommendations for future work to be performed to advance the DASH mission are given with respect to the various technical segments.

21.1. Conclusion

The DASH team has finalised the final design of the mission at this stage. It has been designed across its segments to demonstrate the feasibility of a CubeSat distributed system. The potential that comes along with a distributed space network is huge given the lower cost and similar performance to its counterparts. Furthermore, there is a lot to gain from the DASH mission as there is a multitude of applications subdivided into commercial and scientific ones. As for the asteroids, these have a massive future potential with applications such a mining operations to the usage of asteroids as hubs.

With regard to the mission architecture, the DASH mission element names were defined, these being TRIAD, SHEPHERD, DOT, S-DOT, N-DOT. For the elements, their operation modes were also defined. Next, a functional analysis was performed, yielding a functional flow diagram and a functional breakdown structure, this incorporated the newly defined operations. When it comes to sustainability, the UN development goals were examined along with sustainable space exploration, with these in mind, DASH's approach with respect to sustainability was formulated. This revolves around improving the accessibility of space exploration to the public and performing research for the mining of asteroids and the deflection of asteroids for Earth protection. This is done while minimising space debris and applying lean manufacturing. With the mission concept of operations defined, a technical risk assessment was performed, here the risks were assessed and mitigation strategies and the contingency plan if necessary were formulated. These could be improved through a more detailed investigation. To start off, a optimal trajectory was found for the selected ion engines which lead into finding the smallest initial wet mass of the TRIAD, with an arrival date at 12 April 2027, a fuel mass of 1.77 kg, a panel mass of 2.96 kg and a TRIAD wet mass of 57.74 kg was computed.

With the support of the trajectory calculations made, the applicable kick stage and launcher was chosen. After, the electric propulsion module for the SHEPHERD was chosen to be the RIT-μX and the Aurora Propulsion Technologies ARM-AO system cold gas thruster was chosen. Once these were chosen, the available power for input to the subsystems of the S/C and storage volume available had to be decided in order to allocate each subsystem a certain amount of power that can be applied and to place each subsystem in the DOTs and SHEPHERD. Based on the EPS and solar panel chosen, it was found that the DOTs can maximum generated power of 90 W and 326 W for the SHEPHERD. On top of this, the structure was decided to be the Exoterra 12U bus. Now that ion and cold gas thrusters were chosen to be used in the SHEPHERD and DOTs, the largest consideration related was the thermal maintenance ability of the S/C due to the heat generated by them, with additionally taking into account the thermal environment of near Earth and deep space. By choosing the sufficient thermal control components, and placing them in the S/C in the right locations, the equilibrium temperature was able to be maintained which match the requirements for every subsystem.

Before designing the subsystems which rely on data transmitted and received, the CDHS was decided and after all the telecommunication system was decided. For the inter-satellite link utilised, which is the method utilised to achieve the main mission goal, the IMT X-Band Transponder and the MARCO HGA was chosen. Afterwards, the ADCS was chosen to locate and alter the trajectory of the S/C once there were unintended torque applied to it. Once the S/C has reached Didymos, the DOTs will be inserted into a self stabilising terminator orbit, a manoeuvre which will take about 2.76 m s^{-1} of ΔV. Certain methods were chosen for the navigation and all the S/C in a TRIAD are equipped with a navigational camera and an ISL transponder, with the SHEPHERD will additionally having a LIDAR

sensor. An MPC-SCP algorithm was used for the guidance and control of the spacecraft. Finally, the payload provided was distributed among the SHEPHERD and DOTs in the right manner.

Once all the subsystems have been designed and components decided, budget breakdown for mass, size, power required, area, bit rate, cost, and data storage was done for both SHEPHERD and DOTs, which are all important aspects of the mission. For the total cost, the result was calculated to be 83.1 MEUR for 95th percentile. Lastly, to sum up the mission the verification and validation methods suggested and the design phase ad development logic was purposed. With these procedures, the final detail design of the S/C has been achieved. The next section will introduce some recommendations for futuristic potential of the DASH mission.

Recommendations for Subsystems

For each of the mission subsystems, recommendations are provided for segments which could be further developed following the analysis included in this report.

Astrodynamics

- Optimise optimisation code (make it faster) to run many more times to create a more clear view of trajectory possibilities.
- Create trajectory simulation code involving more complex effects such as solar radiation pressure, non spherical earth/mars assumption, non instantaneous gravity assists, etc.
- Determine exact trajectory from launcher separation to Didymos transfer using tools such as GMAT.
- Determine sensitivity of trajectory to issues such as thrusting delays.

Propulsion

- Investigate exact engine specifications since the engine from M-ARGO is a modified (scaled up w.r.t. thrust) version of an Ariane Space engine.
- Investigate possibility of pulsing the engine at max thrust instead of throttling in order to maintain it always at the highest required Isp.
- Investigate degradation effective over time and exact operational lifetime for the chosen engine to see how far DASH can extend the mission.
- Investigate additional propulsion requirements in case a sample return/landing is implemented i.e. add propellant mass and volume for sample return on SHEPHERD, and add propellant mass to land a DOT/SHEPHERD.

EPS

- Determining exact wiring connections, wire length and from that wire weight.
- Look into possibilities for smaller batteries.
- Determine if increasing EPS power capabilities (by increasing panel size) could greatly increase payload capabilities (what is the limiting factor for payload).

Structures

- More detailed analysis better modelling assembly connection by modelling bolts instead of contact constraints.
- Performing structural analysis again once mass budget is more well known/updated.
- Perform random vibration analysis depending on LV
- Release mechanism position might need reconsideration depending on the cg of the DOTs.

Thermal Control

- Use ESATAN-TMS, ANSYS or comparable industry-standard software to validate the thermal implementation.
- After the testing phase, use the test data to validate the Python model.
- Do not use isothermal assumption within the CubeSats.

- Extend the Python model to include meshing of flat surfaces (automatic node generation), possibly ray tracing might be a nice feature for transient analysis.
- Consider adding active heaters in the DOTs, instead of relying purely on the thermal properties of the walls.
- Connected to the previous point, review the use of thermal louvers (possibly unnecessary if heaters are considered + their TRL is very low for CubeSat missions).

CDHS

- Future calculations on the actual computational load are required, which may lead to the need of only one OBC per CubeSat

Telecommunication

- The multiple access protocols for the inter-satellite link are investigated thoroughly such that these can be implemented, as this will form a crucial block enabling this communication link.
- The link budget should be refined, the losses should be modelled such that the mission is truly modelled.
- The model for the parameters should undergo verification and validation.
- Monitor developments in high gain antennas for CubeSats as these are still rare, if a better performing option is found that does not impact the space distribution between the components, then that option would benefit DASH a lot.
- extend the mission time for the SHEPHERDs in order to be able to transfer all 130 Gbit of data.
- Cluster the transmission times during the mission periods where the distance to Earth is smaller in order to make use of the higher available data rate.

Navigation

- It is of imperative importance that the control function is replaced by a more proficient and optimised approach.
- Incorporate the MPC-SCP guidance law into the Python simulation to get an accurate estimate of the Delta-V used in the DASH mission.
- Perform the optimal beacon selection for the interplanetary navigation.
- Add the possible use of infrared cameras for navigation when there is no sunlight or to get better centroid estimations when there are limbs.
- Implement measurement models and data fusion between the spacecraft into the Python simulation to characterise filter accuracy and implications on the control of orbits.
- Define the optimum orbits for each DOT and SHEPHERD depending on their payloads.

Bibliography

[1] Arya, M., Saudert, J., Hodges, R. E., & Pellegrino, S. (2019). Large-area deployable reflectarray antenna for cubesats. *AIAA Scitech 2019 Forum*. https://doi.org/10.2514/6.2019-2257

[2] Atar, C., & Aktas, M. (2022). Advances in Thermal Modeling and Analysis of Satellites. *Journal of Science*, *35*. https://doi.org/10.35378 /gujs.840191

[3] Babuscia, A., Cheung, K.-M., Scowen, P., & Crowell, J. (2017). Telecommunication System Design for Interplanetary CubeSat Missions: LunaH-Map. *2017 IEEE Aerospace Conference*.

[4] Battegazore, A., Munoz, J., Dixit, S., Doozandeh, T., Kramer, T., Lee, K., Lems, J., Pastinante, A., Rodriguez, J., & van Hulle, S. (2022). DASH A distributed space network for asteroid exploration Group 23 Baseline Report. Tech. rep., TU Delft, Delft.

[5] Battegazzore, A., Sebastian, J., Muñoz, C., Dixit, S., Doozandeh, T., Kramer, T., Lee, K., Lems, J., Pastinante, A., Rodríguez, J., & Van Hulle, S. (2022). A distributed space network for asteroid exploration Group 23. Tech. rep., TU Delft.

[6] Bauer, J., Carter, M., Kelley, K., Mello, E., Neu, S., Orphanos, A., Shaffer, T., Withrow, A., & Blandino, J. (2012). Mechanical, Power, and Thermal Subsystem Design for a CubeSat Mission. Tech. rep., WORCESTER POLYTECHNIC INSTITUTE.
URL https://web.wpi.edu/Pubs/E-project/Available/E-project-031212-121649/unrestricted/Mechanical,_Power,_and_Thermal_Subsystem_Design_for_a_CubeSat.pdf

[7] Broschart, S. B., Bradley, N., & Bhaskaran, S. (2019). Kinematic Approximation of Position Accuracy Achieved Using Optical Observations of Distant Asteroids. *Journal of Spacecraft and Rockets*. https://doi.org/10.2514/1.A34354

[8] Butcher, J. C. (1976). On the implementation of implicit Runge-Kutta methods. *BIT Numerical Mathematics 1976 16:3*, *16*(3), 237–240. https://doi.org/10.1007/BF01932265

[9] Chahat, N., Sauder, J., Mitchell, M., Beidleman, N., & Freebury, G. (2019). One-Meter Deployable Mesh Reflector for Deep Space Network Telecommunication at X- and Ka-band | IEEE Conference Publication | IEEE Xplore. In *2019 13th European Conference on Antennas and Propagation (EuCAP)*, (pp. 1–4).

[10] Chandrashekar, S., & Karlsson, T. (2017). Thermal Analysis and Control of MIST CubeSat. *Degree Project in Space Technology*.

[11] Chang, K. (1989). Force Limit Specification vs Design Limit Loads. *Jet Propulsion Laboratory*.

[12] Collard, T. A., Sheehan, J. P., & Gallimore, A. D. (2015). Pressurized Xenon Propellant Management System for the CubeSat Ambipolar Thruster. In *Joint Conference of 30th International Symposium on Space Technology and Science, 34th International Electric Propulsion Conference and 6th Nano-satellite Symposium*.

[13] Dennison, K., & D'amico, S. (2021). AAS 21-336 COMPARING OPTICAL TRACKING TECHNIQUES IN DISTRIBUTED ASTEROID ORBITER MISSIONS USING RAY-TRACING. *AAS 21*.

[14] Dinh, D. (2012). *Thermal Modeling of Nanosat*. Ph.D. thesis, San Jose State University.
URL https://scholarworks.sjsu.edu/cgi/viewcontent.cgi?article=7740&context=etd_theses

[15] Dornelles, G. L., Franco, B. M., Riva, L. F. O., Garcia, J. H., Guarnieri, D. L., Paiva, K. V., & Hughes, G. B. (2018). Thermal control analysis on a 6U CubeSat equipped with a high-power laser. In *CubeSats and NanoSats for Remote Sensing II*, (p. 29). SPIE-Intl Soc Optical Eng. https://doi.org/10.1117/12.2320750

[16] ECSS (2002). Space engineering Testing. Tech. rep., ECSS.

[17] ExoTerra (2022). *Courier 12U SEP Satellite Bus*. ExoTerra. Provided by ExoTerra through personal communication.

[18] ExoTerra (2022). Halo hall-effect thruster. Tech. rep., ExoTerra.

[19] Franzese, V., Topputo, F., Ankersen, F., & Walker, R. (2021). Deep-Space Optical Navigation for M-ARGO Mission. *Journal of the Astronautical Sciences*, *68*(4), 1034–1055. https://doi.org/10.1007/S40295-021-00286-9/FIGURES/9

[20] French, R., Mosleh, E., Mandy, C., Hunter, R., Currie, J., Sinclair, D., & Beck, P. (2021). Bringing Deep Space Missions within Reach for Small Spacecraft. *Rocket Lab*.

[21] Gharaibeh, M. A., & Obeidat, A. M. (2018). Vibrations analysis of rectangular plates with clamped corners. *Open Engineering*, *8*(1), 275–283. https://doi.org/10.1515/eng-2018-0030

[22] Gil-Fernandez, J., & Ortega-Hernando, G. (2018). Autonomous vision-based navigation for proximity operations around binary asteroids. *CEAS Space Journal 2018 10:2*, *10*(2), 287–294. https://doi.org/10.1007/S12567-018-0197-5

[23] Gilette, O., & Varga, R. (1970). NASA SPACE VEHICLE DESIGN CRITERIA ACCEPTANCE TESTING NATIONAL A E R O N A U T I C S A N D SPACE A D M I N STRATION. Tech. rep., NASA.

[24] Grimm, C. D., Lange, C., Lange, □. M., Mierheim, O., Witte, L., Sasaki, K., Chand, S., Ksenik, E., Grundmann, J.-T., Ho, T.-M., Biele, J., David Hercik, □., Auster, U., Lorda, □. L., Torres, A., & Garmier, R. (2020). The MASCOT separation mechanism A reliable, low-mass deployment system for nano-spacecraft. *CEAS Space Journal*, *12*, 343–365. https://doi.org/10.1007/s12567-020-00302-y

[25] Group #23 (2022). DASH Mission: Midterm Report. Tech. rep., Delft University of Technology.

[26] Hengeveld, D., Moulton, J., Lockyer, S., Taft, B., & Kwas, A. (2019). Enabling High-Power SmallSats with Advanced Thermal Management. *Small Satellite Conference*.

[27] Hengeveld, D., Wilson, M., & Moulton, J. (2018). Thermal Design Considerations for Future High-Power Small Satellites. In *8th International Conference on Environmental Systems*. Albuquerque, New Mexico.

[28] Hesar, S., & Mcmahon, J. W. (2015). Small Body Gravity Field Estimation Using LiAISON Supplemented Optical Navigation Solar gravity driven transfers around planetary bodies View project Efficient On-board Lambert's Solution View project. In *AAS CN&C Conference*.

[29] Hiller, R. (2017). Design of a CubeSat Separation Mechanism. Tech. rep., Western Michigan University.
URL https://scholarworks.wmich.edu/honors_theses/2794

[30] Hodges, R. E., Chahat, N., Hoppe, D. J., & Vacchione, J. D. (2017). A Deployable High-Gain Antenna Bound for Mars: Developing a new folded-panel reflectarray for the first CubeSat mission to Mars. *IEEE Antennas and Propagation Magazine*, *59*(2), 39–49. https://doi.org/10.1109/MAP.2017.2655561

[31] Hohenwarter, M., Borcherds, M., Ancsin, G., Bencze, B., Blossier, M., Delobelle, A., Denizet, C., Éliás, J., Fekete, A., Gál, L., Konečný, Z., Kovács, Z., Lizelfelner, S., Parisse, B., & Sturr, G. (2013). GeoGebra 4.4. http://www.geogebra.org.

[32] Iess, L., Benedetto, M. D., Marabucci, M., & Racioppa, P. (2012). IMPROVED DOPPLER TRACKING SYSTEMS FOR DEEP SPACE NAVIGATION. In *International Symposium on Space Flight Dynamics*.

[33] ISO (2019). ISO 24113:2019 – Space systems — Space debris mitigation requirements. *Space systems — Space debris mitigation*.

[34] ISRO, & Patrick Blau (2017). GSLV Mk. III User's Manual. Tech. rep., ISRO.

[35] Jamalipour, A., Wada, T., & Yamazato, T. (2005). A tutorial on multiple access technologies for beyond 3G mobile networks. *IEEE Communications Magazine*, *43*(2), 110–117. https://doi.org/10.1109/MCOM.2005.1391509

[36] J.R. Wertz, W. L. (1999). *Space Mission Analysis and Design*. Dordrecht, The Netherlands: Kluwer Academic Publishers, third edition ed.

[37] Klein, J. H., & Cork, R. B. (1998). An approach to technical risk assessment. *International Journal of Project Management*, *16*(6), 345–351. https://doi.org/10.1016/S0263-7863(98)00006-4

[38] Kobayashi, M. M., Shihabi, M., & Taylor, J. (2021). Mars Cube One Telecommunications Subsystem Design. Tech. rep., Jet Propulsion Laboratory, Pasadena.
URL http://descanso.jpl.nasa.gov.s3-website-us-west-2.amazonaws.com/DPSummary/DESCANSO18_MarCO.pdf

[39] Kohnke, P. C. (1982). ANSYS. *Finite Element Systems*, (pp. 19–25). https://doi.org/10.1007/978-3-662-07229-5_2

[40] Lagier, R. (2021). ARIANE 6 USER'S MANUAL . Tech. rep., Arianespace.
URL www.arianespace.com

[41] Larson, W. J. (2009). *Applied space systems engineering*. McGraw-Hill Learning Solutions.

[42] Le Floc'h, C., Aufaure, J., Salome, R., & Tschofen, J. (2000). New high pressure tank for xenon storage. In *Spacecraft Propulsion*, vol. 465, (p. 543).

[43] Lissi, F., Escorial, D., Martino, P., & Carnelli, I. (2021). Main challenges of Cubesat piggyback on an Interplanetary Mission: The HERA Cubesats, a technology demonstration case. Tech. rep., European Space Agency, Noordwijk.

[44] Lorenz, D. A., Olds, R., May, A., Mario, C., Perry, M. E., Palmer, E. E., & Daly, M. (2017). Lessons Learned from OSIRIS-REx Autonomous Navigation Using Natural Feature Tracking. In *IEEE Aerospace Conference*.

[45] Madde, R., & Morley, T. (2006). Delta-DOR: A New Technique for ESA's Deep Space Navigation. *ESA Bulletin 128*.

[46] Modenini, D., Zannoni, M., Manghi, R. L., & Tortora, P. (2017). AN ANALYTICAL APPROACH TO AUTONOMOUS OPTICAL NAVIGATION FOR A CUBESAT MISSION TO A BINARY ASTEROID SYSTEM. *4thIAA Conference on University Satellite Missions and CubeSat Workshop*.

[47] Momentus (2020). Vigoride User's Manual. Tech. rep., Momentus.

[48] Moreno Villa, V. (2018). Spacecraft Navigation Around Small Bodies in Early-characterisation Phases. *Delft University of Technology*.

[49] Morgan, D., Chung, S.-J., & Hadaegh, F. Y. (2012). Model Predictive Control of Swarms of Spacecraft Using Sequential Convex Programming. *‡ Senior Research Scientist and Technical Fellow; fred.y.hadaegh@jpl.nasa .gov. Fellow AIAA. 1725 JOURNAL OF GUIDANCE, CONTROL, AND DYNAMICS*, *37*(6), 13–16. https://doi.org/10.2514/1.G000218

[50] Naidu, S. P., Benner, L. A., Brozovic, M., Nolan, M. C., Ostro, S. J., Margot, J. L., Giorgini, J. D., Hirabayashi, T., Scheeres, D. J., Pravec, P., Scheirich, P., Magri, C., & Jao, J. S. (2020). Radar observations and a physical model of binary near-Earth asteroid 65803 Didymos, target of the DART mission. *Icarus*, *348*, 113777. https://doi.org/10.1016/J.ICARUS.2020.113777

[51] Naidu, S. P., Benner, L. A., Brozovic, M., Nolan, M. C., Ostro, S. J., Margot, J. L., Giorgini, J. D., Hirabayashi, T., Scheeres, D. J., Pravec, P., Scheirich, P., Magri, C., & Jao, J. S. (2020). Radar observations and a physical model of binary near-Earth asteroid 65803 Didymos, target of the DART mission. *Icarus*, *348*, 113777. https://doi.org/10.1016/j.icarus.2020.113777

[52] NASA (2000). *DSN Telecommunications Link Design Handbook*. Pasadena: California Institute of Technology.
URL http://deepspace.jpl.nasa.gov/dsndocs/810-005

[53] NASA (2015). CubeSat Form Factor Thermal Control Louvers Passive thermal cooling for CubeSats. *National Aeronautics and Space Administration*.

[54] Pellacani, A., Cabral, F., Alcalde, A., Kicman, P., Lisowski, J., Gerth, I., & Burmann, B. (2018). Semi-autonomous attitude guidance using relative navigation based on line of sight measurements – Aim scenario. *Acta Astronautica*, *152*, 496–508. https://doi.org/10.1016/J.ACTAASTRO.2018.08.051

[55] Qin, T., Qiao, D., & Macdonald, M. (2019). Relative orbit determination using only inter-satellite range measurements. *Journal of Guidance, Control, and Dynamics*, *42*(3), 703–710. https://doi.org/10.2514/1.G003819/ASSET/IMAGES/LARGE/FIGURE3.JPEG

[56] Radhakrishnan, R., Edmonson, W. W., Afghah, F., Rodriguez-Osorio, R. M., Pinto, F., & Burleigh, S. C. (2016). Survey of Inter-Satellite Communication for Small Satellite Systems: Physical Layer to Network Layer View. *IEEE Communications Surveys and Tutorials*, *18*(4), 2442–2473. https://doi.org/10.1109/COMST.2016.2564990

[57] Raja Reddy, M. (2003). Space solar cells-tradeoff analysis. *Solar Energy Materials and Solar Cells*, *77*(2), 175–208. https://doi.org/10.1016/S0927-0248(02)00320-3

[58] Ramakrishnan, S., & Narayana Moorthy, N. (2005). Polar Satellite Launch Vehicle User's Manual. Tech. rep., ISRO.
[59] Sippel, M., Stappert, S., Callsen, S., Dietlein, I., Bergmann, K., Gülhan, A., Marquardt, P., Lassmann, J., Hagemann, G., Froebel, L., Wolf, M., & Plebuch, A. (2021). A viable and sustainable European path into space-for cargo and astronauts. In *72nd International Astronautical Congress*.
[60] SpaceX (2021). Falcon 9 Payload User's Manual. Tech. rep., SpaceX.
[61] SUNDU, H., & DÖNER, N. (2020). Detailed Thermal Design and Control of an Observation Satellite in Low Earth Orbit. *European Mechanical Science*, *4*(4), 171–178. https://doi.org/10.26701/EMS.730201
[62] Tachikawa, S., Nagano, H., Ohnishi, A., & Nagasaka, Y. (2022). Advanced Passive Thermal Control Materials and Devices for Spacecraft: A Review. *International Journal of Thermophysics*, *43*(6), 1–37. https://doi.org/10.1007/S10765-022-03010-3/FIGURES/21
[63] Takahashi, S., Scheeres, D. J., & Scheeres, D. J. (2020). Autonomous Navigation and Exploration of a Small Near-Earth Asteroid (AAS 20-514). In *AAS/AIAA Astrodynamics Specialist Conference*.
[64] Tam, W., Debreceni, M., Hersh, M., & Nye, C. (1999). Low cost derivative tanks for spacecraft and launch vehicles. In *35th Joint Propulsion Conference and Exhibit*, (p. 2831).
[65] Tam, W. H., Jackson, A. C., Nishida, E., Kasai, Y., Tsujihata, A., & Kajiwara, K. (2000). Design and manufacture of the ETS VIII Xenon tank. In *36th AIAA/ASME/SAE/ASEE Joint Propulsion Conference and Exhibit*. American Institute of Aeronautics and Astronautics Inc. https://doi.org/10.2514/6.2000-3677
[66] te Nijenhuis, A. K., Brouwer, H. S. B., Jonsson, M., van Benthem, R. C., Bloem, E. A., & Vollmuller, B.-J. (2020). Thermal Modelling of CubeSats in ESATAN-TMS: A Modular Approach. In *46th International Conference on Environmental Systems, Conference Proceedings, ICES-2016-196*, (pp. 1–12).
[67] Topputo, F., Wang, Y., Giordano, C., Franzese, V., Goldberg, H., Perez-Lissi, F., & Walker, R. (2021). Envelop of reachable asteroids by M-ARGO CubeSat. *Advances in Space Research*, *67*(12), 4193–4221. https://doi.org/10.1016/j.asr.2021.02.031
[68] Tsai, P. H., Berleant, D., Segall, R. S., Aboudja, H., Batthula, V. J. R., & Howell, M. (2022). Spacecraft for Deep Space Exploration: Combining Time and Budget to Model the Trend in Lifespan. In *Lecture Notes in Networks and Systems*, vol. 360 LNNS. https://doi.org/10.1007/978-3-030-89912-7_25
[69] Turan, E., Speretta, S., & Gill, E. (2022). Autonomous navigation for deep space small satellites: Scientific and technological advances. *Acta Astronautica*, *193*, 56–74. https://doi.org/10.1016/J.ACTAASTRO.2021.12.030
[70] Van Rossum, G., & Drake, F. L. (2009). *Python 3 Reference Manual*. Scotts Valley, CA: CreateSpace.
[71] Vetrisano, M., & Vasile, M. (2016). Autonomous navigation of a spacecraft formation in the proximity of an asteroid. *Advances in Space Research*, *57*(8), 1783–1804. https://doi.org/10.1016/j.asr.2015.07.024
[72] Walker, R. (2016). Estec System Margin Policy for ESA IOD CubeSat Projects. Tech. rep., ESA.
URL www.esa.int
[73] Walker, R., Binns, D., Bramanti, C., Casasco, M., Concari, P., Izzo, D., Feili, D., Fernandez, P., Fernandez, J. G., Hager, P., Koschny, D., Pesquita, V., Wallace, N., Carnelli, I., Khan, M., Scoubeau, M., & Taubert, D. (2018). Deep-space CubeSats: thinking inside the box. *Astronomy & Geophysics*, *59*(5), 24–5. https://doi.org/10.1093/astrogeo/aty232
[74] Walker, R., & Bramanti, K. C. (2018). Miniaturised asteroid remote geophysical observer (m-argo): A stand-alone deep space cubesat system for low-cost science and exploration missions. In *Interplanetary Probe Workshop*. Boulder, Colorado USA.
[75] Wertz, J. R., Everett, D. F., & Puschell, J. J. (2011). *Space mission engineering : the new SMAD*. Hawthorne: Microcosm.
[76] Yilmaz, F., Haktanir, O. O., & Uygur, A. B. (2015). Quasi-static structural test of satellites. *RAST 2015 - Proceedings of 7th International Conference on Recent Advances in Space Technologies*, (pp. 421–424). https://doi.org/10.1109/RAST.2015.7208381
[77] Yost, B. (2021). Small Spacecraft Technology State of the Art report. Tech. rep., Ames Research Center, Moffet Field.
URL http://www.sti.nasa.gov
[78] Young, J. (2021). Advanced Concepts for Small Satellite Thermal Control. *Small Satellite Conference*.
[79] Yu, Y., Michel, P., Schwartz, S. R., Naidu, S. P., & Benner, L. A. M. (2016). Ejecta Cloud from a Kinetic Impact on the Secondary of a Binary Asteroid: I. Mechanical Environment and Dynamic Model. Tech. rep., AIDA.

A Requirements

A.1. Mission Requirements

For the mission or user requirements, it is looked at whether the mission is designed in accordance with this. This is essentially qualitatively looking into the mission design and verifying whether it is designed to comply with these requirements. Below in Table A.1, the mission requirements are given, including their method of verification. Whenever the compliance is indicated as <TBD>, this indicates that the verification on this requirement is beyond the scope of the present work.

Table A.1: Mission requirements compliance matrix

	ID	Requirement	Verification method	Compliance
	DASH-SCI.05-MI.01	The mission shall perform surface relative feature tracking.	Inspection	<TBD>
	DASH-SCI.07-MI.02	The mission shall adhere to the COSPAR planetary protection policy.	Inspection	Yes
🔑	DASH-GSP.01-MI.03	The mission shall be able to interface with the DSN ground stations.	Test	<TBD>
	DASH-GSP.02-MI.04	The mission shall be compatible with the provided communication facilities.	Test	<TBD>
	DASH-GSP.02-MI.05	The mission shall use the DSN for communications.	Analysis	Yes
	DASH-REG.01-MI.06	The mission shall comply with ITU-R SA.1014-3 regulations for deep space communication.	Inspection	Yes
🔑	DASH-SPA.01-MI.07	The mission shall consist of at least 3 separate spacecraft.	Analysis	Yes
	DASH-SPA.02-MI.08	The mission shall comply with Space debris mitigation requirements ISO 24113:2019.	Inspection	Yes
	DASH-SPA.03-MI.09	The mission shall collect scientific data characterising the DART mission impact.	Analysis	Yes
	DASH-GOM.01-MI.11	The total recurring cost of the mission, excluding payload and including launch and operations, shall not exceed 100 million EUR (2021).	Inspection	<TBD>
🔑	DASH-GOM.02-MI.13	The mission shall perform payload operations at the asteroid.	Analysis	Yes
	DASH-GOM.02-MI.38	The target asteroid shall be 65803 Didymos	Yes	
	DASH-GOM.02-MI.14	The payload operations shall be performed for at least 6 months.	Analysis	Yes
	DASH-GOM.02-MI.15	The mission shall downlink to Earth at least 130 Gbit of payload data.	Analysis	Yes
	DASH-GOM.02-MI.16	The mission shall accommodate at least 9 individual payloads.	Inspection	Yes
🔑	DASH-GOM.02-MI.17	The payload operations shall be performed at a distance of less than 30km from the asteroid.	Analysis	Yes
	DASH-GOM.02-MI.18	The mission shall achieve the performance objectives with at least 70% probability of success.	Analysis	<TBD>
🔑	DASH-GOM.02-MI.20	The mission shall adhere to the ISO 17770:2017 CubeSat standard.	Inspection	<TBD>
🔑	DASH-GOM.02-MI.21	The mission shall begin payload operations no later than December 2026.	Analysis	No

Table A.1 continued from previous page

	ID	Requirement	Verification method	Compliance
	DASH-GOM.02-MI.23	The mission shall collect continuous telemetry data during transfer and nominal operations.	Test	<TBD>
	DASH-GOM.02-MI.28	The mission shall withstand the LEO environment before transit, without critical failures.	Analysis	<TBD>
	DASH-GOM.02-MI.29	The mission shall withstand the deep space environment for the mission duration without critical failures.	Analysis	<TBD>
🔑	DASH-GOM.02-MI.30	The mission shall autonomously navigate in deep space.	Analysis	Yes
	DASH-GOM.02-MI.37	The mission shall perform autonomous attitude determination and control.	Analysis	Yes
	DASH-GOM.02-MI.31	The mission shall autonomously handle data.	Test	Yes
	DASH-GOV.04-MI.32	The mission shall comply with all national and United Nations Space Law Treaties and Principles.	Inspection	Yes
	DASH-RSM.01-MI.33	The mission shall not damage the parent/peer mission when launched in the same vehicle.	Analysis	Yes
	DASH-LVP.01-MI.34	The mission shall withstand the launch loads as specified in the launch vehicle catalogue without critical failure.	Analysis	<TBD>
	DASH-LVP.01-MI.35	The spacecraft shall withstand mechanical loads during transport to the launch site without critical failure.	Analysis	<TBD>

A.2. System Requirements

Originating from the mission requirements, the system requirements are generated. These are usually more technically detailed requirements, which have great influence on the detailed design of the different subsystems. The compliance matrix for these can be found in Table A.2.

Table A.2: System level requirements derived directly from the mission level requirements

	ID	Requirement	Verification method	Compliance
🔑	DASH-SCI.05-MI.01-SYS.01	The spacecraft shall perform short-range navigation up to 1000 km from the asteroid.	Analysis	<TBD>
🔑	DASH-SCI.05-MI.01-SYS.02	The spacecraft shall perform far-range navigation when further than 1000 km from the target	Analysis	<TBD>
	DASH-GSP.02-MI.04-SYS.03	The spacecraft shall apply CCSDS recommendations to all telemetry and command between the ground and flight systems.	Test	<TBD>
	DASH-REG.01-MI.06-SYS.04	The mission shall communicate only with the X-Band.	Test	Yes
	DASH-SPA.02-MI.08-SYS.05	The spacecraft shall be disposed of in accordance with the space debris mitigation regulations in the event of partial mission failure in LEO.	Inspection	<TBD>
	DASH-GOM.02-MI.15-SYS.09	The spacecraft shall be able to support the acquisition of payload data at a rate of at least 200 bits/s.	Test	<TBD>
	DASH-GOM.02-MI.16-SYS.10	The mission shall accommodate payloads with maximum individual mass of 5.5 kg.	Inspection	Yes
	DASH-GOM.02-MI.16-SYS.12	The mission shall accommodate the individual payloads with a total form factor of at least 2U.	Inspection	Yes
	DASH-GOM.02-MI.16-SYS.14	The spacecraft shall be mechanically compatible with the payload.	Inspection	<TBD>
	DASH-GOM.02-MI.16-SYS.15	The spacecraft shall be electronically compatible with the payload.	Inspection	<TBD>
	DASH-GOM.02-MI.17-SYS.17	The CubeSats shall communicate from of up to 60 km.	Test	Yes

Table A.2 continued from previous page

	ID	Requirement	Verification method	Compliance
	DASH-GOM.02-MI.15-SYS.18	The mission shall downlink up to 130 Gb of data	Analysis	<TBD>
	DASH-GOM.02-MI.18-SYS.19	The spacecraft shall withstand the launch loads without single point failure.	Analysis	<TBD>
	DASH-GOM.02-MI.16-SYS.20	The TRIAD shall have a maximum wet mass of 85 kg kg	Inspection	<TBD>
	DASH-GOM.02-MI.16-SYS.21	The TRIAD shall have a maximum dry mass of 75 kg	Inspection	<TBD>
🔑	DASH-GOM.02-MI.20-SYS.23	The individual CubeSats volume shall not exceed the 16 U form factor.	Inspection	Yes
	DASH-GOM.02-MI.23-SYS.25	The spacecraft shall route telemetry data to the launch vehicle during ascent	Test	<TBD>
	DASH-GOM.02-MI.23-SYS.26	The spacecraft shall route telemetry data to the ground station after separating from the launch vehicle	Test	<TBD>
	DASH-GOM.02-MI.29-SYS.35	The spacecraft shall not exceed a maximum temperature rate of change of 1.5° per second	Analysis	<TBD>
	DASH-GOM.02-MI.29-SYS.36	The spacecraft shall ensure a minimum operational internal temperature of −20 °C	Test	<TBD>
	DASH-GOM.02-MI.29-SYS.37	The spacecraft shall ensure a maximum operational internal temperature of 50 °C	Test	<TBD>
	DASH-GOM.02-MI.37-SYS.38	The spacecraft shall maintain the desired attitude with an accuracy of 15 arcseconds	Analysis	Yes
	DASH-GOM.02-MI.37-SYS.39	The spacecraft shall align to the required thrust vector with an accuracy of 15 arcseconds	Analysis	Yes
	DASH-GOM.02-MI.38-SYS.43	The TRIAD shall provide a total Delta-V of at least 1200 $m\,s^{-1}$ m/s during the transfer phase.	Analysis	<TBD>
	DASH-GOM.02-MI.38-SYS.45	Each CubeSat shall be able to provide 20 $m\,s^{-1}$ of total velocity increment during the operational phase to perform the scientific exploration	Analysis	<TBD>
	DASH-GOM.02-MI.38-SYS.46	The spacecraft shall allocate 0.25 m/s of Delta-V margin at end of life	Analysis	<TBD>
	DASH-GOM.02-MI.28-SYS.48	The spacecraft shall be able to withstand a maximum thermal gradient of 10 °C m^{-1} at low earth orbit	Analysis	<TBD>
	DASH-GOM.02-MI.29-SYS.50	The spacecraft shall withstand thermal loads in a deep space environment without system failures.	Test & Analysis	<TBD>
	DASH-GOM.02-MI.29-SYS.51	The spacecraft shall be able to withstand a maximal thermal gradient of 10 °C m^{-1} in deep space	Analysis	<TBD>
🔑	DASH-GOM.02-MI.30-SYS.52	The spacecraft shall perform its navigation using at least semiautonomous technology	Analysis	<TBD>
	DASH-GOM.02-MI.30-SYS.53	The spacecraft shall start to track Didymos from a distance of 18600 km from the centre of gravity.	Analysis	<TBD>
🔑	DASH-GOM.02-MI.30-SYS.54	The spacecraft shall autonomously determine its approach trajectory	Analysis	<TBD>
	DASH-GOM.02-MI.30-SYS.55	The spacecraft shall avoid direct non-mission-planned contact with the target asteroid	Analysis	<TBD>
	DASH-GOM.02-MI.37-SYS.56	The spacecraft shall determine its attitude with a precision of 20 arcseconds in LEO.	Analysis	Yes
	DASH-GOM.02-MI.37-SYS.57	The spacecraft shall determine its attitude with a precision of 20 arcseconds in deep space.	Analysis	<TBD>
	DASH-GOM.02-MI.37-SYS.58	The spacecraft shall determine its attitude with a precision of 20 arcseconds at the target asteroid.	Analysis	<TBD>
🔑	DASH-GOM.02-MI.30-SYS.60	The spacecraft shall determine its trajectory in deep space with 1000 km accuracy 14 days into the future.	Analysis	<TBD>
🔑	DASH-GOM.02-MI.30-SYS.61	The spacecraft shall determine its trajectory with respect to the Didymos asteroid with 10 m accuracy 5 hours into the future.	Analysis	<TBD>

Table A.2 continued from previous page

ID	Requirement	Verification method	Compliance
DASH-GOM.02-MI.30-SYS.62	The spacecraft shall manoeuvre out of formation if the flight system enters safe mode as to not interfere with other operational CubeSats.	Analysis	<TBD>
DASH-GOM.02-MI.31-SYS.65	The spacecraft distributed network shall be able to store a minimum of 8 GB of data at any point in time	Test	Yes
DASH-LVP.01-MI.34-SYS.66	The spacecraft shall be mechanically compatible with the launch vehicle interface	Test	<TBD>
DASH-LVP.01-MI.34-SYS.67	The spacecraft shall be electronically compatible with the launch vehicle interface	Test	<TBD>
DASH-LVP.01-MI.34-SYS.68	The spacecraft shall withstand 7 g of axial acceleration	Test	<TBD>
DASH-LVP.01-MI.34-SYS.69	The spacecraft shall withstand 2.4 g of lateral acceleration	Test	<TBD>
DASH-LVP.01-MI.34-SYS.70	The spacecraft shall have a natural frequency greater than 25 Hz	Test	<TBD>
DASH-GOM.02-MI.30-SYS.72	The spacecraft shall determine its position in deep space with an accuracy of 1000 km with respect to the Sun.	Analysis	<TBD>
DASH-GOM.02-MI.30-SYS.73	The spacecraft shall determine its position at the asteroid with an accuracy of 10 meters with respect to Didymos.	Analysis	<TBD>
DASH-GOM.02-MI.23-SYS.74	The mission shall downlink during transfer at 1000 bit s^{-1}	Analysis	Yes
DASH-GOM.02-MI.30-SYS.75	Each CubeSat shall we able to communicate with with any other CubeSat	Analysis	<TBD>

A.3. Subsystem Requirements

Based on the system requirements, the subsystem requirements dictate the constraints that the subsystems have to adhere to. These requirements are more specific to their respective subsystem.

Table A.3: Subsystem requirements compliance matrix

	ID	Requirement	Verification method	Compliance
		TT&C		
🔑	DASH-GOM.02-MI.23-SYS.74-TLC.01	The SHEPHERD shall be able to form a closing link during transfer at a data rate of 1000 bit s^{-1}	Analysis	Yes
🔑	DASH-GOM.02-MI.16-SYS.18-TLC.02	Communication between CubeSats shall have a closing link at up to and including a distance of 60 km	Test	Yes
	DASH-GOM.02-MI.16-SYS.18-TLC.03	Each TRIAD shall be able to transmit 65 Gbit	Test	No
	DASH-GOM.02-MI.16-SYS.18-TLC.06	The Earth-link downlink transmission shall use Turbo encoding	Test	Yes
	DASH-GOM.02-MI.16-SYS.18-TLC.07	The Earth-link shall be able to transmit data at up to 12 12 kbit s^{-1}	Test	Yes
	DASH-GOM.02-MI.16-SYS.17-TLC.08	The inter-satellite link shall support multiple access communication	Analysis	<TBD>
	DASH-GOM.02-MI.16-SYS.17-TLC.09	The Inter-Satellite Link antenna gain shall be at least 0 dB	Test	Yes
		CDHS		
🔑	DASH-GOM.02-MI.31-SYS.65-CDH.01	The CDH subsystem shall be able to store at minimum 8 GB of data	Inspection	Yes

Table A.3 continued from previous page

	ID	Requirement	Verification method	Compliance
🔑	DASH-GOM.02-MI.15-SYS.09-CDH.02	The CDH subsystem shall process the payload data at a speed of at least 40 bit s^{-1}	Inspection	<TBD>
	DASH-GOM.02-MI.23-SYS.25-CDH.03	The CDH subsystem shall route telemetry data to the launch vehicle during ascent.	Test	<TBD>
	DASH-GOM.02-MI.31-SYS.74-CDH.04	The CDH subsystem shall check each bit of data for possible bit flips by means of a watchdog timer.	Test	Yes
	DASH-GOM.02-MI.31-SYS.74-CDH.05	The CDH subsystem shall be able to be restarted by means of a watchdog timer.	Test	Yes
	DASH-GOM.02-MI.16-SYS.33-CDH.06	The CDH subsystem shall require a maximum power of 0.8 W.	Test	Yes
	DASH-GOM.01-MI.11-SYS.06-CDH.07	The cost of the CDH subsystem for each CubeSat shall not be more than 10000 EUR.	Inspection	Yes
	DASH-GOM.02-MI.31-SYS.65-CDH.08	The CDH subsytem shall use the Cubesat Distributed File System for data storage.	Inpection	Yes
	DASH-GOM.02-MI.15-SYS.09-CDH.09	The CDH subsystem shall have a clockrate of at least 400 MHz	Test	Yes
		ADCS		
	DASH-GOM.02-MI.20-SYS.23-ADC.04	The ADCS shall be smaller than 5 U	Inspection	<TBD>
	DASH-GOM.02-MI.23-SYS.38-ADC.06	The ADCS shall determine the spacecraft attitude during payload operations with an accuracy of 20 arcseconds	Analysis	Yes
	DASH-GOM.02-MI.23-SYS.38-ADC.07	The ADCS shall control the spacecraft attitude during payload operations with an accuracy of 20 arcseconds	Test	<TBD>
🔑	DASH-GOM.02-MI.23-SYS.38-ADC.08	The ADCS shall provide a stability of 20 arcseconds over 60 seconds during payload operations	Analysis	Yes
🔑	DASH-GOM.02-MI.23-SYS.39-ADC.09	The ADCS shall be able to achieve a slew rate of 180 degrees over 1200 seconds	Analysis	Yes
	DASH-GOM.02-MI.23-SYS.39-ADC.10	The ADCS shall determine the spacecraft attitude during manoeuvres with an accuracy of 15 arcseconds	Analysis	Yes
	DASH-GOM.02-MI.23-SYS.39-ADC.11	The ADCS shall control the spacecraft attitude during manoeuvres with an accuracy of 15 arcseconds	Test	<TBD>
	DASH-GOM.02-MI.23-SYS.39-ADC.12	The ADCS shall provide a stability of 20 arcseconds over 60 seconds during manoeuvres	Analysis	Yes
	DASH-GOM.02-MI.23-SYS.56-ADC.13	The ADCS shall determine the spacecraft attitude with a precision of 20 arcseconds in LEO	Analysis	Yes
	DASH-GOM.02-MI.23-SYS.57-ADC.14	The ADCS shall determine the spacecraft attitude with a precision of 20 arcseconds in deep space	Analysis	<TBD>
	DASH-GOM.02-MI.23-SYS.58-ADC.15	The ADCS shall determine the spacecraft attitude with a precision of 20 arcseconds at Didymos	Analysis	Yes
	DASH-GOM.02-MI.16-SYS.21-ADC.16	The ADCS shall be less than 6 kg	Test	Yes
		EPS		
	DASH-GOM.02-MI.38-SYS.44-EPS.03	The transfer stage solar arrays shall deploy with no interference to the payload CubeSats	Test	<TBD>
🔑	DASH-GOM.02-MI.16-SYS.13-EPS.04	An average power of 7 W of power for the scientific payloads shall be provided during the scientific phase	Analysis	Yes
🔑	DASH-GOM.02-MI.16-SYS.16-EPS.05	The EPS subsystem shall be able to provide a peak power of 9 W for 60 seconds to the scientific payload	Analysis	Yes
	DASH-GOM.02-MI.16-SYS.23-EPS.08	The undeployed solar array dimensions shall not exceed 226.3 mm by 340.5 mm	Test	<TBD>
	DASH-GOM.02-MI.16-SYS.23-EPS.09	The EPS subsystem shall not interfere with the mechanical deployer interface of the transfer vehicle	Test	<TBD>
🔑	DASH-GOM.02-MI.16-SYS.33-EPS.12	The DOT EPS subsystem shall provide an average power of 24.5 watts over the duration of the 6-month scientific phase	Analysis	Yes

Table A.3 continued from previous page

	ID	Requirement	Verification method	Compliance
🔑	DASH-GOM.02-MI.16-SYS.33-EPS.13	The SHEPHERD EPS subsystem shall provide an average power of 58.3 watts over the duration of the 6-month scientific phase	Analysis	Yes
🔑	DASH-GOM.02-MI.16-SYS.34-EPS.14	The DOT EPS subsystem shall be able to provide a peak power of 32.6 W for 300 seconds to the spacecraft bus	Analysis	Yes
🔑	DASH-GOM.02-MI.16-SYS.34-EPS.15	The SHEPHERD power system shall be able to provide average power of 130 W to the spacecraft	Analysis	Yes
🔑	DASH-GOM.02-MI.16-SYS.34-EPS.16	The SHEPHERD EPS subsystem shall be able to provide a peak power of 105 W for 50% of the time to the spacecraft during nominal operations	Analysis	Yes
		Navigation		
🔑	DASH-GOM.02-MI.30-SYS.59-NAV.01	The flight computer shall determine the spacecraft's trajectory in low earth orbit with 10 m accuracy 1.54 hours into the future with respect to Earth.	Analysis	<TBD>
🔑	DASH-GOM.02-MI.30-SYS.60-NAV.02	The flight computer shall determine the spacecraft's trajectory in deep space with 1000 km accuracy 7 days into the future with respect to the Sun.	Analysis	Yes
🔑	DASH-GOM.02-MI.30-SYS.61-NAV.03	The flight computer shall determine the spacecraft's trajectory with respect to the Didymos asteroid with 10 m accuracy 22 hours into the future.	Analysis	<TBD>
	DASH-GOM.02-MI.30-SYS.62-NAV.04	The navigation subsystem shall provide manoeuvres and a trajectory from the asteroid at a safe distance of 100 km from the target's surface if the flight system enters safe mode.	Analysis	<TBD>
	DASH-GOM.02-MI.30-SYS.52-NAV.08	The navigation subsystem shall perform its navigation using autonomous techniques when possible.	Analysis	Yes
	DASH-GOM.02-MI.30-SYS.52-NAV.09	The navigation subsystem shall be suplemented by ground-based tracking in the case autonomous techniques are not possible.	Analysis	Yes
	DASH-GOM.02-MI.30-SYS.53-NAV.10	The navigation sensors shall be able start to track Didymos from a distance of 1000 km from the centre of gravity.	Analysis	Yes
🔑	DASH-GOM.02-MI.30-SYS.54-NAV.11	The flight computer shall autonomously determine the spacecraft's approach trajectory in all mission phases.	Analysis	<TBD>
	DASH-GOM.02-MI.30-SYS.54-NAV.12	The flight computer shall receive and relay all sensor data to the CDHS in all mission phases.	Analysis	<TBD>
	DASH-GOM.02-MI.30-SYS.55-NAV.13	The flight computer shall provide autonomous trajectory correction procedures to avoid direct non-mission-planned contact with the target asteroid.	Analysis	<TBD>
	DASH-GOM.02-MI.30-SYS.55-NAV.14	The flight computer shall provide autonomous trajectory correction procedures to avoid direct collision with other CubeSats.	Analysis	<TBD>
	DASH-GOM.02-MI.30-SYS.62-NAV.15	The navigation subsystem shall enter in Contingency Management mode when a sensor fails.	Analysis	<TBD>
	DASH-SCI.05-MI.01-SYS.01-NAV.16	The navigation subsystem shall give preference to close-range navigation techniques at distances less than 1000 km from Didymos.	Analysis	<TBD>
	DASH-SCI.05-MI.01-SYS.02-NAV.17	The navigation subsystem shall give preference to far-range navigation techniques at distances larger than 1000 km from Didymos.	Analysis	<TBD>
		TCS		
	DASH-GOM.02-MI.28-SYS.48-TCS.01	The thermal control subsystem shall ensure that the S/C can withstand thermal gradient of 10 °C m^{-1} in LEO.	Analysis	<TBD>

Table A.3 continued from previous page

	ID	Requirement	Verification method	Compliance
	DASH-GOM.02-MI.29-SYS.35-TCS.02	The thermal control subsystem shall ensure that the S/C maximum temperature rate of change must not exceed 1 °C s^{-1}.	Analysis	<TBD>
🔧	DASH-GOM.02-MI.29-SYS.36-TCS.03	The thermal control subsystem shall maintain the S/C operational temperature to a minimum −20 °C .	Test	<TBD>
🔧	DASH-GOM.02-MI.29-SYS.37-TCS.04	The thermal control subsystem shall maintain the S/C temperature to a maximum 50 °C .	Test	<TBD>
	DASH-GOM.02-MI.29-SYS.51-TCS.06	The thermal control subsystem shall ensure that the S/C can withstand thermal gradient of 10 °C m^{-1} in deep space.	Analysis	<TBD>
		Propulsion		
🔧	DASH-GOM.02-MI.16-SYS.20-PRO.01	The ion propellant mass aboard SHEPHERD shall not exceed 2.06 kg	Test	Yes
	DASH-GOM.02-MI.16-SYS.21-PRO.02	The propulsion system dry mass aboard SHEPHERD shall not exceed 3 kg	Test	Yes
🔧	DASH-GOM.02-MI.20-SYS.23-PRO.03	The ion propellant volume aboard SHEPHERD shall not exceed a volume of 2000 cm^3	Inspection	Yes
	DASH-GOM.02-MI.38-SYS.43-PRO.04	The chemical propellant mass aboard any individual CubeSat shall not exceed 1.5 kg	Test	Yes
	DASH-GOM.02-MI.38-SYS.43-PRO.05	The chemical propellant volume aboard any spacecraft shall not exceed 1500 cm^3	Inspection	Yes
	DASH-GOM.02-MI.38-SYS.43-PRO.06	The ion engine aboard SHEPHERD shall not exceed 0.79 kg	Test	Yes
	DASH-GOM.02-MI.38-SYS.43-PRO.07	The ion engine aboard SHEPHERD shall not exceed 1000 cm^3	Inspection	Yes
	DASH-GOM.02-MI.38-SYS.43-PRO.09	The moment due to ion thrust vector misalignment shall not exceed 7.5 µN m	Analysis	Yes
🔧	DASH-GOM.02-MI.38-SYS.43-PRO.11	The thrust produced by the ion propulsion unit shall be a maximum of 25 mN	Test	Yes
🔧	DASH-GOM.02-MI.38-SYS.43-PRO.15	The ion propulsion unit shall be contained fully in the SHEPHERD	Inspection	Yes
	DASH-GOM.02-MI.30-SYS.62-PRO.18	A total Delta-V of 1 m s^{-1} shall be provided for safe mode orbital transfers	Analysis	Yes
	DASH-GOM.02-MI.38-SYS.45-PRO.19	A Delta-V of 20 m s^{-1} shall be provided for scientific operations during 6 months at 30 km from the centre of gravity of Didymos	Analysis	Yes
		Structures		
🔧	DASH-LVP.01-MI.34-SYS.68-STR.01	The spacecraft structure shall withstand at least 7g of axial acceleration	Test	<TBD>
🔧	DASH-LVP.01-MI.34-SYS.69-STR.02	The spacecraft structure shall withstand at least ±2.4g of lateral acceleration	Test	<TBD>
🔧	DASH-LVP.01-MI.34-SYS.70-STR.03	The spacecraft shall have a natural frequency greater than 25 Hz	Test	<TBD>
	DASH-GOM.02-MI.16-SYS.20-STR.04	The CubeSat structure shall have a maximum mass of at most 30% of the total dry mass	Test	<TBD>
	DASH-LVP.01-MI.34-SYS.68-STR.05	The Spacecraft structure shall endure at least 139 dB of Overall Sound Pressure Level	Test	<TBD>
	DASH-GOM.02-MI.16-SYS.14-STR.09	The CubeSat shall withstand all launch loads as decribed by the payload user guide manual from the manufacturer without plastic deformation	Test	<TBD>
🔧	DASH-GOM.02-MI.16-SYS.14-STR.10	The structure shall be large enough to host at least one payload with a form factor of at least 2U.	Analysis	<TBD>
🔧	DASH-GOM.02-MI.16-SYS.14-STR.11	The structure shall be mechanically compatible with the payload	Analysis	<TBD>

B

Task Division

This task division is included for the purposes of grading by the tutor and coaches.

Table B.1: Distribution of the workload

Chapter	Task	Work by	Written by
	Executive overview	Everyone	Luciano, Alessandro, Tamim, Simon, Kyoungeun, Juan, Timo
1	Introduction	Kyoungeun, Timo, Luciano	Kyoungeun, Timo
2	Market Analysis	Tamim	Tamim
3	Concept of Operations	Alessandro, Tamim, Jeremy	Alessandro, Tamim, Jeremy
4	Functional Analysis	Alessandro, Tamim, Luciano	Alessandro, Tamim
5	Sustainability Strategy	Joao, Jeremy	Joao, Jeremy
6	Risk Analysis	Kyoungeun, Simon, Timo	Kyoungeun
7	Trajectory Optimisation	Siddharth, Alessandro, Tamim	Siddharth, Alessandro, Tamim
8	Propulsion	Siddharth, Alessandro, Tamim, Luciano	Siddharth, Alessandro, Tamim, Luciano
9	Electrical Power System	Siddharth, Timo	Siddharth, Timo
10	Structures	Joao	Joao, Alessandro (SHEPHERD BUS, TRIAD delpoyer), Tamim (SHEPHERD BUS)
11	Thermal Control System	Simon, Kyoungeun	Simon, Kyoungeun
12	CDHS	Timo	Timo
13	Telecommunication System	Juan, Timo, Kyoungeun	Juan
14	ADCS	Jeremy	Jeremy
15	Navigation System	Luciano, Jeremy	Luciano, Jeremy(assumptions)
16	Payload	Timo, Luciano	Timo
17	Subsystems Integration	Joao	Joao
18	Performance Analysis	Timo, Simon (Cost)	Timo, Simon
19	Verification and Validation	Juan, Timo	Juan, Timo
20	Design Phase and Development Logic	Simon, Luciano	Simon, Luciano, Jeremy
21	Conclusion and Recommendations	Kyoungeun, Juan	Kyoungeun, Juan